UNIVERSITE DE STRASBOURG

ÉCOLE DOCTORALE 414

INSERM UMR_S1109 – Equipe Tumor Biomechanics

THÈSE présentée par :

Shima GHOROGHI

Soutenue le: **8 December 2020**

Pour obtenir le grade de: **Docteur de l'Université de Strasbourg**

Discipline: Sciences de la Vie et de la Santé

Spécialité: Aspects moléculaires et cellulaires de la biologie

STUDY OF THE ROLE OF RAL GTPASES IN EXOSOME SECRETION AND METASTATIC PROGRESSION

Supervisor: Jacky GOETZ	**Directeur de recherche, Unistra**
Co-supervisor: Vincent HYENNE	**Chargé de recherche, Unistra**
Rapporteur: Maria Carla PARRINI	**Ingénieur de recherche HDR, Institut Curie**
Rapporteurs Carmen GARRIDO	**Directeur de recherche, INSERM**
Examinateur Interne : Fabien ALPY	**Directeur de recherche IGBMC**

ACKNOWLEDGEMENTS

This note shall serve as a small tribute to all those who supported me through my PhD journey.

I would like to thank **my mother** and **my father**, to whom I owe my very existence. You are the ones who helped me internalize a moral compass, and taught me how to live life with integrity, passion and grace. I would also like to thank **my husband**, without whom it would have been difficult to embark on this journey. You left behind your whole business to move to Europe with me; you had to find a new job and step out of your comfort zone so I could pursue my dream—if these are not love from my family, then I don't know what is.

I would like to thank my **close friends** with whom I have shared my joys, stress, happiness and sadness no matter how far we are living from each other. Distance means nothing when my **best friends** mean a lot, so I would like to send my love to Tehran, London, New York, and Quebec.

I am indebted to the amazing team who acknowledged my hard work, provided me with guidance and of their good company (**Sebastien, Florent, Valentin, Benjamin, Ignacio, Nandini, Nael, Kelly, Maria, Nina, Cynthia, Luc, and Gautier**). In particular, I would like to thank:

Jacky for your fearless leadership and teaching me that there is always scope for improvement. Thanks for converting my mistakes into lessons, pressure into productivity, and skills into strengths.

Vincent for always believing in me and giving me your helpful guidance and advice every day. You have taught me **a lot** and helped me to become mature in this career. Thank you for being **awesome!**

Olivier for being super helpful all the time. Is there any problem in the lab you can't fix?! Thank you for being so caring and supportive throughout the entire time.

Isabell for your positive energy that alleviated so much of my stress, and

Annabel for helping with my experiments in the most perfect way possible!

I also thank **my committee** for their support and advice.

Merci beaucoup!

SUMMARY OF MY PROJECT:

According to statistics published by the World Health Organization, cancer is among the most common causes of morbidity and mortality worldwide, with an estimated 14.1 million new cases and 8.2 million deaths in 2012 (Ferlay et al. 2015). The most commonly diagnosed cancers were breast, lung, and colorectal, and more than 90% of cancer-related death is due to metastasis rather than primary tumors (Ferlay et al. 2015). However, the therapeutic limitations of metastasis require a deeper understanding of its molecular machinery to identify effective therapeutic targets to block metastasis (Hanahan and Weinberg 2000; Gupta and Massagué 2006). In October 2016, **as a PhD student, I joined Jacky Goetz's group, whose focus is on metastasis and the mechanisms of its formation.** Cell-to-cell communication is crucial in the formation of metastasis. Extracellular Vesicles (EVs) (Graça Raposo and Stahl 2019) have been considered as crucial players by mediating the communication between tumors cells and their microenvironment (Adem, Vieira, and Melo 2020). EVs are composed of different biomolecules including RNA, lipids, and proteins, and can be taken up by distant cells and deliver a functional message. Interestingly, tumor cells are known to secrete a lot of tumor EVs (tEVs), that are enriched in pro-tumoral factors (Hyenne, Lefebvre, and Goetz 2017). Indeed, they can transform stromal cells into tumor-associated cells (Chow et al. 2014; Gu et al. 2012). Moreover, tEVs contribute to metastatic organotropism, creating a so-called "pre-metastatic niche" in specific metastatic secondary sites before the arrival of tumor cells (Hoshino et al. 2015; Peinado et al. 2017). The functional impact of tEVs in promoting metastasis mainly depend on their levels and content. However, the molecular mechanisms coordinating these processes remain obscure. Therefore, **the goal of my PhD project was to understand the mechanisms by which two GTPases (RalA/B) control exosome secretion and to determine how this affects breast cancer progression and metastasis.**

I built my PhD project on top of the work carried out by Vincent Hyenne who already showed RalA and RalB are evolutionarily conserved regulators of exosome secretion (Hyenne et al. 2015). Exosomes are small vesicles originating from the endosomal compartments called multivesicular bodies (MVBs) (Colombo, Raposo, and Théry 2014). Hyenne, et al. originally observed that, in the nematode *C. elegans*, the Ral GTPase ortholog RAL-1 controls exosome secretion by acting

on the biogenesis of MVBs. They further showed that RalA/B control the levels of secreted EVs in relevant models to human breast cancer (Hyenne et al. 2015) suggesting that these GTPases could influence disease progression through EVs secretion. During my PhD project, using 4T1 aggressive mouse mammary carcinoma cells, we showed that two GTPases (RalA/B) control MVBs homeostasis through the phospholipase D1(PLD1), thus tune the biogenesis and secretion level of pro-metastatic EVs. We also found RalA and RalB promote lung metastasis in a syngeneic mouse model. Importantly, EVs from RalA or RalB depleted cells have limited organotropic capacities *in vivo* and, as a consequence, are less efficient in promoting lung metastasis. Thus, our work suggests that Ral GTPases control the pro-metastatic function of EVs, by tuning their levels and likely by modulating their content. Finally, we found that Ral GTPases promote the secretion of CD146-enriched EVs, whose lung tropism sustains efficient metastasis. **Altogether, our study identified for the first time a new molecular machinery from its function in EV biogenesis up to its pro-metastatic function in breast cancer. We found Ral GTPases as important molecules linking the mechanisms of EVs secretion, cargo loading to their capacity to distribute and induce pre-metastatic niches.** Recently, my work was selected as one of International Society for Extracellular Vesicles (ISEV) 2020's outstanding contributions to the advance of basic science.

This thesis will thoroughly provide a better understanding of the contribution of tumor exosome in metastasis and determine the role of Ral GTPases in this process. In **Chapter 1**, I first explain the invasion of **cancer cells** into the surrounding tissue and their metastatic spread through the body. Then I continue by including a detailed description of **Extracellular Vesicles (EVs)**, including exosomes as well as their contribution in metastasis formation. Finally, I highlight the importance of **Ral GTPase** in various aspects of cell biology. In **Chapter 2**, I provide my **main findings** on how Ral GTPases promote metastasis by controlling biogenesis and organ colonization of exosomes (Ghoroghi et al. eLife, accepted). Then, I continue by including my results on establishing the zebrafish embryo as a novel animal model to track circulating tEVs *in vivo* (Hyenne et al. 2019). The tools and methods developed in this novel animal model were also used in part of my Ral project. Finally, in **Chapter 3**, I will **discuss my main findings** on how they integrate into the current knowledge in this field, and how they open new research avenues for the future.

ABBREVIATIONS

APC	Antigen Presenting Cell
ARF6	ADP-ribosylation Factor 6
ARMMs	ARRDC1-mediated Microvesicles
BMDCs	Bone Marrow Derived Dendritic Cell
BBB	Blood–brain barrier
CD	Cluster of Differentiation
CAF	Cancer Associated Fibroblast
CAM	Cancer Associated Macrophage
CSC	Cancer Stem Cell
CTCs	Circulating Tumor Cells
DC	Dendritic Cell
DNA	Deoxyribonucleic acid
DLS	Dynamic Light Scattering
DCIS	Ductal carcinoma in situ
ECM	Extracellular Matrix
EGFR	Epidermal Growth Factor Receptor
ER	Endoplasmic Reticulum
ESCRT	Endosomal Sorting Complex Required for Transport
EV	Extracellular Vesicle
FBS	Fetal Bovine Serum
GFP	Green Fluorescent Protein
HDL	High-Density Lipoprotein
HER2	Human Epidermal Growth Factor Receptor 2
HSPG	Heparan Sulfate Proteoglycans
ICAM	Intercellular Adhesion Molecule
ILV	Intraluminal Vesicle
IFNγ	Interferon-γ
LAMP2b	Lysosome-associated Membrane Protein 2b
LMP-1	Latent Membrane Protein 1
MHC	Major Histocompatibility Complex
MVBs	Multivesiclular Bodies
miRNA	MicroRNA
mRNA	Messenger RNA
MMP	Metaloproteinases
MDSCs	Myeloid-derived Suppressor Cells
MSCs	Mesenchymal Stromal Cells
MV	Microvesicle
MVB	Multivesicular Body
nSMase2	neutral Sphyngomyelinase 2
NGS	Next Generation Sequencing
NK	Natural Killer
NTA	Nanoparticle Tracking Analysis

PBS	Phosphate Buffered Saline
PDGFs	Platelet-derived growth factors
piRNA	Piwi-like RNA
PA	Phosphatidic Acid
PD-1	Programmed death receptor 1
PD-L1	Programmed death ligand 1
PS	Phosphatidylserine
PTM	Post-Translational Modifications
PMN	Pre-Metastatic Niche
PLD	Phospholipase D
Ral GTPases	Ral guanosine triphosphatases
RBP	RNA Binding Protein
RhoA	Ras Homolog Gene Family, Member A
RISC	RNA-induced Silencing Complex
RNA	Ribonucleic acid
RNAi	RNA Interference
RNP	Ribonucleoprotein
rRNA	Ribosomal RNA
RT	Room Temperature
SEC	Size Exclusion Chromatography
SIMPLE	Small Integral Membrane Protein of the Lysosome/Late Endosome
siRNA	Small Interfering RNA
SNARE	Soluble NSF Attachment Protein Receptor
TIM4	T cell immunoglobulin and mucin domain containing
TLR2	Toll-like receptor 2
TGF-β	Transforming Growth Factor-β
TAM	Tumor Associated Macrophage
TEM	Transmission Electron Microscopy
TME	Tumor Microenvironment
TNF	Tumor Necrosis Factor
tEVs	Tumor-derived Extracellular Vesicles
TRAIL	TNF-related Apoptosis-inducing Ligand
Tsg101	Tumor Susceptibility Gene 101
UC	Ultracentrifugation
VAMP7	Vesicle-Associated Membrane Protein 7
VEGF	Vascular Endothelial Growth Factor
WB	Western Blot
YBX1	Y-Box Protein 1

Table of Contents

INTRODUCTION

1 Cancer

Cancer is the second leading cause of death worldwide, accounting for an estimated 9.6 million deaths, or one in six deaths, in 2018 (Bray et al. 2018). Cancer is a large group of diseases characterized by uncontrolled cell growth (Baylin and Jones 2016). There are more than a hundred distinct types of cancer, which can be classified by the type of cells and organ from which they originate. Depending on the tissue they have developed from, carcinomas, lymphomas, and sarcomas are examples of solid tumors. Leukemias on the other hand is an example of liquid cancers that arise from the blood-forming cells. In leukemia, tumor cells are systemically spread without the formation of a tumor mass (Sell 2005). However, most cancers (~85%) are of epithelial origin, referred to as carcinomas, such as breast cancer in which cancer cells spread from a primary tumor to distant sites through the vascular and lymphatic circulations to establish secondary tumors known as metastasis (Valastyan and Weinberg 2011).

Breast cancer is the most frequent cancer among women, impacting more than 2 million new cases worldwide in 2018 (Siegel, Miller, and Jemal 2018). According to the World Health Organization, it is estimated that 627,000 women died from breast cancer that is approximately 15% of all cancer-related deaths among women in 2018 (Siegel, Miller, and Jemal 2018). Since the late 1980s, in many highly developed countries, mortality rates have declined due to improved detection, earlier diagnosis, and more effective treatments (Siegel, Miller, and Jemal 2018). Well-established risk factors for breast cancer in women include reproductive factors such as early age at menarche, late age at first childbirth, nulliparity, and late age at menopause, family history of breast cancer, alcohol consumption, exposure to ionizing radiation, prior hormone replacement therapy, use of oral contraceptives, lack of physical activity, increased age and obesity (Colditz and Bohlke 2014). Overall, 5–10% of breast cancers are inherited, and the risk is linked to two tumor suppressor genes: BRCA1(17q21) and BRCA2(13q12) that are involved in double-strand break DNA repair (Rebbeck et al. 2016). Breast cancer is a clinically, genetically and histologically heterogeneous disease. Malignancies of the breast can begin in different areas of the breast and depending on which cell type is affected, breast cancers can be divided into carcinomas and sarcomas (Polyak 2007; Allison 2012). Carcinomas are cancers arising from the epithelial component of the breast, they can be basal or luminal. The epithelium of the mammary gland

is composed of two main cellular lineages: luminal cells that surround a central lumen and highly elongated myoepithelial cells that are located in a basal position adjacent to the basement membrane. Alveoli sarcomas are a much rarer form of breast cancer (<1% of primary breast cancer) that arise from the stromal components of the breast including myofibroblasts and blood vessel cells (Figure.1) (Feng et al. 2018). In some cases, breast tumor could be the combination of different cell types. Histologically, breast cancer is broadly categorized into in situ carcinoma and invasive carcinoma, and most breast cancers are invasive. More details regarding the histological subtypes have been summarized in table 1(Feng et al. 2018). Approximately 30% of women with early-stage breast cancer will experience distant metastases which is the primary cause of cancer morbidity and mortality. The stage of breast cancer can be determined, ranging from stage 0 to stage IV, based on the size of the primary tumor, the involvement of lymph nodes, and the presence of distant metastasis (Allison 2012; Polyak 2007). However, studies have shown that histological differences along with biological markers, which have been summarized in table 2, are sufficient prognostic markers for metastasis risk (Harbeck et al. 2019). Throughout my PhD project, we mainly focused on **breast cancer** and a murine mammary tumor cell line, 4T1, was used as a model of aggressive cancer mimicking human triple-negative breast cancer (P. Kaur et al. 2012).

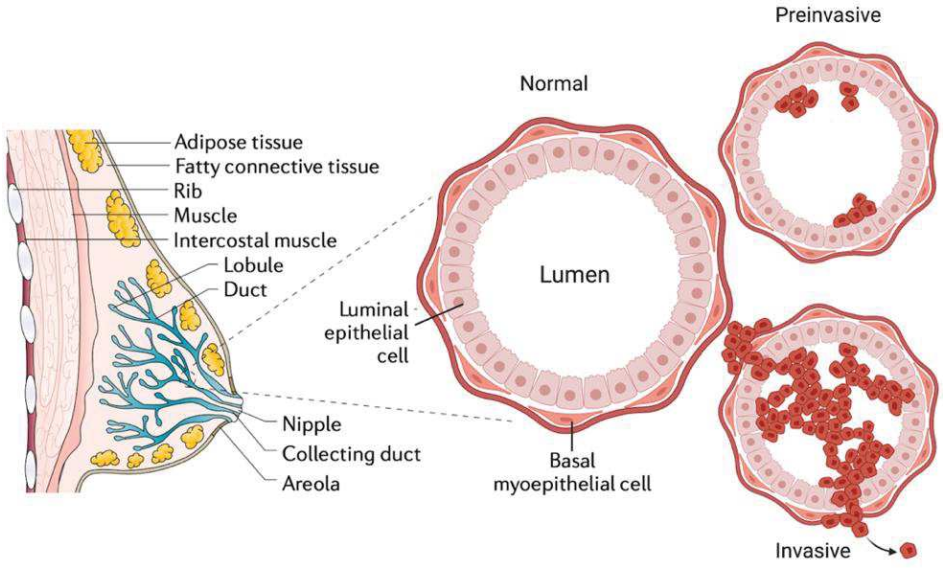

Figure 1. Anatomical and histologic origins of breast tumor cells.
Adapted from (Harbeck et al. 2019)**.** Created with BioRender.com

Histological subtypes	Ductal	Lobular
Preinvasive Cells limited to basement membrane	**Ductal carcinoma in situ (DCIS)** Spreads through ducts and distorts ductal architecture; can progress to invasive cancer; unilateral	**Lobular carcinoma in situ (LCIS)** Does not distort ductal architecture; can be bilateral Risk factor rather than precursor
Invasive Extension beyond the basement membrane	**Invasive ductal carcinoma (IDC)** Develops from DCIS; fibrous response to produce a mass; metastasizes via lymphatics and blood	**Invasive lobular carcinoma (ILC)** Isolated tumor cells (CDH1 mutations) minimal fibrous response; metastasizes preferentially via viscera

Table 1. Histological subtypes of breast cancer, (Harbeck et al. 2019).

Molecular/intrinsic subtypes of breast cancer		
Subtype	**Molecular Signatures**	**Characteristics**
Luminal A	ER+, PR±, HER2-, Low Ki67	~70%, Most common, Best prognosis
Luminal B	ER+, PR±, HER2±, High Ki67	10%-20% Lower survival than Luminal A
HER2	ER-, PR-, HER2±	5%-15%
Triple Negative	ER-, PR-, HER2-	15%-20% More common in black women Diagnosed at younger age Worst prognosis
Normal-like	ER+, PR±, HER2-, Low Ki67	Rare; Low proliferation gene cluster expression Low proliferation gene cluster expression

Table 2. Molecular/intrinsic subtypes of breast cancers, Breast cancers that have estrogen receptors are called ER-positive (or ER+) cancers, with progesterone receptors are called PR-positive (or PR+) cancers. HER2-positive breast cancer is a breast cancer that tests positive for a protein called human epidermal growth factor receptor 2 (HER2). Ki67 is cell proliferation marker (Feng et al. 2018).

In **section 1.1**, I will start by outlining common features of cancer that have been highlighted in "Hallmarks of Cancer"(Hanahan and Weinberg 2011), and briefly presenting a unified set of distinctive and complementary capabilities that enable tumor growth and metastatic dissemination. Since most of the hallmarks of cancer are related to the notion of tumor microenvironment (TME), in **section 1.2** I describe the crucial role of TME in tumor development and metastasis. In **section 1.3**, I proceed by describing tissue invasion and metastasis. Since successful metastatic

colonization occurs with a non-random pattern only at certain organ site, in **section 1.4** I highlight the concept of organotropism. Then in **section 1.5,** I take a close look at the development of a supportive microenvironment at the metastatic site taking place before the arrival of tumor cells and later promoting their survival and outgrowth.

1.1 General hallmarks of cancer

The originally proposed hallmarks of cancer by Hanahan and Weinberg pointedly linked six essential alterations in cell physiology to malignant growths (Hanahan and Weinberg 2000). In Hallmarks II, Hanahan and Weinberg re-evaluated and expanded their 2000 assessment with emerging hallmarks and enabling characteristics (Hanahan and Weinberg 2011) (Figure.2). Briefly, the characteristics that cancer cells acquire to survive and form a primary tumor mainly depend on one of these hallmarks called **genome instability and mutation** of neoplastic cells which is considered as an enabling characteristic of cancer cells. Then cancer cells form the primary tumor through some of these hallmarks listed below along with few examples of each:

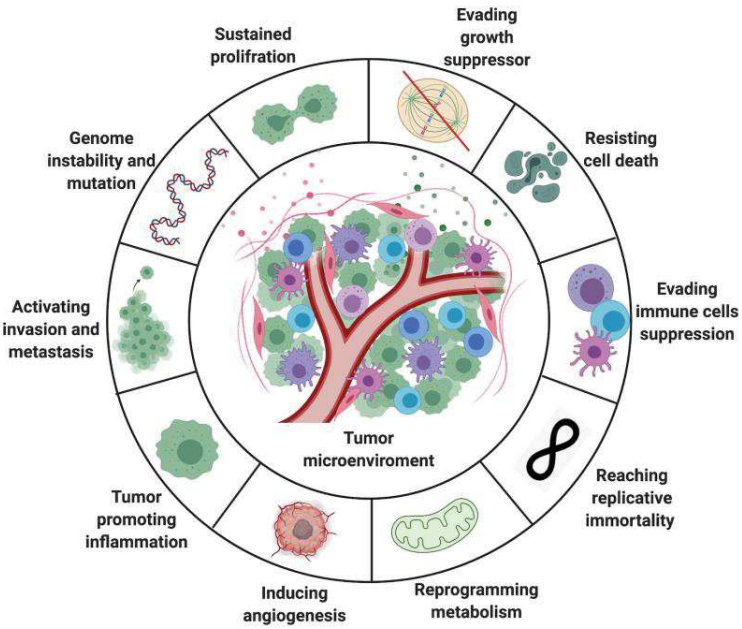

Figure 2. Cancer Hallmarks. **Inspired by** (Hanahan and Weinberg 2011). Created with BioRender.com

Sustained proliferation which is the main feature of cancer cells and is achieved in several ways. Normal cells control the production of their growth signals to maintain homeostasis of cell number, but cancer cells deregulate this control system (Hanahan and Weinberg 2011).

Evading growth suppressor which negatively regulate cells proliferation. Tumors often display mutations in Retinoblastoma (Rb) and p53 genes which lead to uncontrolled proliferation. Rb and p53 are central anti-proliferative protein and central cell cycle blocker, respectively (Hanahan and Weinberg 2011).

Resisting cell death, which is achieved through loss of p53, overexpression of anti-apoptotic factors such as B-cell leukaemia/lymphoma 2 (Bcl-2) or down-regulation of pro-apoptotic factors such as Bax or Bim (White and DiPaola 2009).

Evading immune cells suppression, which is related to resisting apoptosis from cytotoxic T lymphocytes (CTL) and natural killer (NK) cells. Several studies demonstrated that tumors with high infiltration of CTLs and NK cells had better prognosis (Shields et al. 2010).

Reaching replicative immortality, which means tumor cells acquire a state of immortality by passing through an unlimited number of growth/division cycle. The immortalization capability is attributed to the activation of the DNA polymerase telomerase that is responsible for the regeneration of telomeres adding segments of nucleotides (Raynaud et al. 2010).

Reprogramming metabolism, which is the deregulating cell energy pathways and provide tumor cells with not only necessary energy but also nutrients to fuel their excessive growth, survival, invasion, metastasis and resistance to anti-cancer therapies. Reprogramming metabolism also activates oncogenes such as RAS and MYC linking metabolism to the other hallmarks(DeBerardinis et al. 2008).

Inducing angiogenesis which refers to new blood vessel formation from the existing ones for providing oxygen and nutrients for the growth of tumors. The resulting vasculature is highly abnormal with enlarged vessels, leakiness and over-branching (Hanahan and Weinberg 2000; Baeriswyl and Christofori 2009).

Tumor-promoting inflammation, which is driven by the immune system and contribute to the growth of a primary tumor in its surrounding stroma. Inflammatory environments can modify extracellular matrix (ECM), and contribute to many hallmarks capabilities by supplying bioactive molecules to the tumor microenvironment (Hanahan and Weinberg 2011).

Activating invasion and metastasis which occurs due to all the above-mentioned characteristic. This hallmark is at the center of the focus in this thesis and will be discussed thoroughly. (Hanahan and Weinberg 2011). **Many of the above-mentioned hallmarks are related to the notion of tumor microenvironment (TME).**

1.2 Tumor Microenvironment

TME refers to the area surrounding the tumor, progressive formation of which relies on cell-cell communication, and ultimately favors the growth of the tumor in its surrounding stroma (Joyce and Pollard 2009). TME includes many types of cells, among which the different tumor cells recruited stromal, endothelial, and immune cells in a modified extracellular matrix (ECM) (Figure.3). Cell-to-cell communication has a critical role during tumor progression by profound influence on proliferation and dissemination of tumor cells. Intercellular communication between cancer cells and the TME can be direct by cell-to-cell contact (e.g., adhesion molecules) or indirect through signaling by cytokines, growth factors, and extracellular vesicles (EVs) (Dominiak et al. 2020; Galdiero, Marone, and Mantovani 2018; Thomas, Lee, and Beatty 2020). The noteworthy way of cell-cell communication between tumor cells and the TME is represented by EVs which will be discussed deeply in section 2.7. However, to better understand the mechanism of cell–cell communication between a tumor and its microenvironment it is necessary to study the main cellular players and ECM in the TME which have been summarized below.

Vascular and Lymphatic endothelial cells: In TME, tumor growth depends on angiogenesis, which provides oxygen and nutrients through the formation of new blood vessels, and lymphangiogenesis, which facilitates removal of excessive fluids and drainage of tumor cells and tumor-secreted factors from the tumor (Follain et al. 2020). Angiogenic factors present in the TME, such as VEGFs, FGFs, platelet-derived growth factors (PDGFs) and chemokines stimulate sprouting of endothelial cells that is needed for cancer growth. VEGF (also known as VEGFA) is the main angiogenic factor in the TME and is produced by both malignant cells and inflammatory

leukocytes (Carmeliet and Jain 2011). The tumor vasculature is abnormal in its structure and function. For example, blood vessels are leaky with chaotic branching structures and an uneven vessel lumen. Increased permeability of vessels raises the interstitial fluid pressure in the tumor tissue (Stylianopoulos et al. 2012). High interstitial fluid pressure (Swartz and Fleury, 2007) induces a convective flow from blood vessels towards the lymphatic vessels (Cornelison et al. 2018). Therefore, it could be suggested such convection forces along with blood and lymphatic circulations, relocate tumor cells as well as tumor-derived soluble factors or EVs to promote their dissemination towards the vascular systems or the ECM at the periphery (Follain et al. 2020). Tumor cells are able to invade existing lymphatic vessels or stimulate lymphatic vessel spouting through production of VEGFC or VEGFD (Pereira et al. 2018). Lymphatic vessels are also important in cancer progression by altering the host immune response to the tumor (Swartz and Lund 2012).

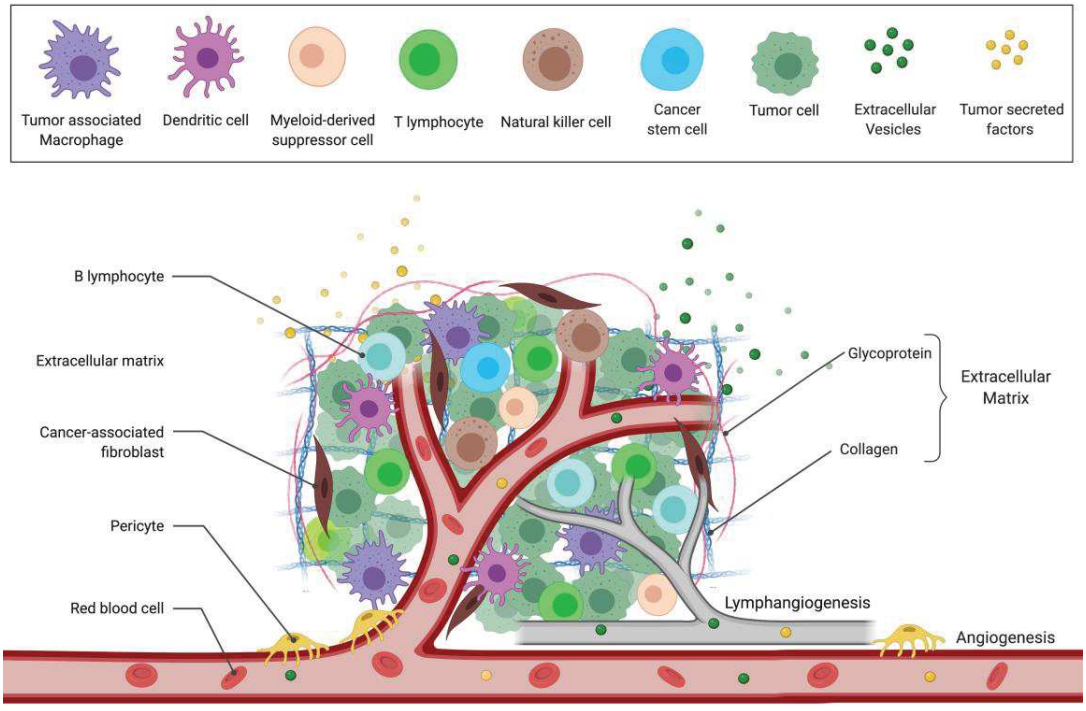

Figure 3. Typical tumor microenvironment. A schematic view of the tumor microenvironment components. The tumour mass consists not only of a heterogeneous population of cancer cells but also a variety of stromal, endothelial, and immune cells in a modified extracellular matrix. They form a complex regulatory network that supports tumor growth. **Inspired by** (Joyce and Pollard 2009). Created with BioRender.com

Pericytes: In addition, perivascular stromal cells called "pericytes" support the structure of blood vessels in the TME. They are also important cellular components of the TME, which contribute to tumor angiogenesis, growth, metastasis, and evasion of immune destruction (Armulik, Genové, and Betsholtz 2011; Cooke et al. 2012).

Immune cells: The crucial role of the immune system in the protection against cancer is well supported (Schreiber, Old, and Smyth 2011). However, the immune system consists of various different cell types which have a different interaction with tumor cells and other cells in the TME and promote tumor growth. Therefore, immune cells have a complex and ambiguous role in TME. Below I provide a rapid and simplified summary of the role of each cell type on TME.

T lymphocytes can be found within and surrounding the tumor mass as well as in draining lymphoid organs (Fridman et al. 2012). The phenotype of pro- and anti-tumor T cells can vary with disease type and stage. For instance, cytotoxic CD8+ memory T cells, and CD4+ Th1 helper cells normally destroy tumor cells. However, CD4+ Th2 helper T cells and FOXP3+ T regulatory cells are immunosuppressive, thus tumor promoting and associated with poor prognosis (Fridman et al. 2012; Hsieh et al. 2004). **B lymphocytes** sometimes can be found at the invasive margin of some tumors but are more often present in draining lymph nodes and lymphoid structures adjacent to the TME. B cell infiltration into the TME is associated with good prognosis in some breast and ovarian cancers(Milne et al. 2009; Coronella et al. 2001). However, immunosuppressive IL-10 producing subtypes of B cells, B10 or B reg cells also associated with tumor-promoting activity in mouse models (Mauri and Bosma 2012). Whether B cells and B regs in particular have similar roles in human cancers remains unknown. **Innate cytotoxic lymphocytes, natural killer (NK) cells and natural killer T (NKT) cells** are usually found outside of tumor area, and in many cancers appear to predict a good prognosis (Mauri and Bosma 2012). Recently, Glasner et al. reported a new anti-tumor role of NK cells by promoting the production of the ECM protein fibronectin 1 (FN1) from melanoma cells, thus ECM stiffening and preventing metastatic spread (Glasner et al. 2018). However, some tumor-related soluble factors (i.e. IL-10, IDO, PGE2, TGF-β1) produced by different tumor-infiltrating immune cells (i.e. M2-macrophages, MDSC, DC, Treg), may negatively impact NK cell activity (Sungur and Murphy 2014).

Myeloid cells are a variety of cells belonging to the innate immune system and tend to adapt their phenotype to their tissue of residence (Gabrilovich, Ostrand-Rosenberg, and Bronte 2012). Thus, in cancer, myeloid cells present in different states and perform a series of different functions. In the last decades, among those myeloid cells, macrophages, dendritic cells (DCs), and myeloid-derived suppressor cells (MDSCs) have received great attention because of their ability to initiate or suppress an anti-tumor immune response (Engblom et al. 2017). Here, I will briefly focus on these myeloid cells and their roles as cancer buddies or foes: In tumors, ***tumor associated macrophage (TAM)*** are derived from circulating monocytes that are recruited from the bone marrow or spleen. Macrophages also originate from embryonic precursors and develop into tissue-resident macrophages, such as macrophages in the lung, or Kupffer cells in the liver (Epelman et al. 2014; Lahmar et al. 2016). Due to their substantial heterogeneity, TAMs are commonly divided into M1 referring to anti-tumorigenic (arise in response to TLR ligands and IFN) and M2 to pro-tumorigenic macrophages (expand in response to IL4, IL13, and TGFβ) (Mosser and Zhang 2008; Lawrence and Natoli 2011). For example, TAMs with anti-tumorigenic potential enhance NK cell responses by producing IL18 and IL22 (Poh et al. 2019; Engblom et al. 2017). On the other hand, in growing tumors TAMs often accumulate in hypoxic areas, where the hypoxic conditions may induce a switch to a pro-angiogenic, invasive phenotype through multiple angiogenic factors, such as TGFβ, VEGF, PDGF, and fibrin (Quail and Joyce 2013; Kzhyshkowska, Ovsiy, and Gratchev 2014). ***Myeloid-derived suppressor cells (MDSCs)*** which are inhibitory immune cells producing a large amount of Il-10, inhibit cytotoxic T cells and polarized TAM to a tumor promoting phenotype (Gabrilovich, Ostrand-Rosenberg, and Bronte 2012; Sica and Bronte 2007). ***Terminally differentiated myeloid dendritic cells*** might be detective in the TME and cannot sufficiently stimulate an immune response to tumor-associated antigen (Meredith et al. 2012; Satpathy et al. 2012).

Fibroblasts:

On the other hand, Cancer-associated fibroblast (CAF) could serve as an important player in TME by producing growth factors and proinflammatory cytokines, such as transforming growth factor-β (TGF-β), vascular endothelial growth factor (VEGF), interleukin-6 (IL-6), and CXC-chemokine ligand (CXCL12), to promote angiogenesis and recruit immunosuppressive cells into the TME to

assist in immune evasion (Orimo et al. 2005; Erez et al. 2010; Sugimoto et al. 2006). CAF are also spindle-shaped cells that build up and remodel the ECM structure through the secretion of MMPs, ECM components and other enzymes (Erez et al. 2010). Below I will discuss the importance of ECM in TME.

The ECM of the tumor microenvironment:

As I mentioned TME is a complex structure composed of different cell types embedded in a modified ECM, where the ECM macromolecules determine tumor progression and metastatic dissemination (Henke, Nandigama, and Ergün 2020). The ECM is the noncellular component of tissue, consisting of various macromolecules including collagens, glycoproteins (fibronectin and laminins), proteoglycans, and polysaccharides with different physical and biological properties (Brassart-Pasco et al. 2012). In normal tissue, ECM's composition is regulated to control cell behaviors, but dysregulation of ECM leads to the development of cancer (Walker, Mojares, and del Río Hernández 2018). For example, Collagens is the most significant component of the ECM. In cancer cells, matrix stiffening via collagen deposit and crosslinking has been associated with tumor malignancy(Paszek et al. 2005). However, the exact role of collagen deposition in tumor progression is not very well known. Recent studies have shown that enhanced collagen crosslinking and deposition result in tumor progression via an enhanced integrin signaling (Levental et al. 2009). On the other hand, Glycoproteins including fibronectin and laminins, are mainly known as ECM connectors. Glycoproteins support ECM networks by linking cell surface receptors to other ECM components and growth factors (McKee et al. 2007). In normal tissue, laminin are the main components of the basement membranes, however in tumors laminin gets distorted or appears distributed in the stromal parts of the tumors which lead to invasiveness (Gusterson et al. 1982; Hand et al. 1985; Qiu et al. 2018). On the other hand, fibronectin has been shown to be highly stretched and considerably remodeled in the tumor stroma (Chandler et al. 2011; K. Wang et al. 2016). However, how these changes in fibronectin structure impact cancer progression is not well understood.

Tumor cells:

In addition to the above-mentioned characteristic of TME, cancer cells themselves acquire new and different mutations as the tumor develops, leading to intratumor heterogeneity (ITH) as

various subpopulations of cancer cells can be identified, including rare cancer stem cells (CSCs) (McGranahan and Swanton 2017). CSCs have the ability of self-renewal cloning and giving rise to heterogeneous cell populations with a high plasticity potential and resistance to stressful factors within the TME such as low level of oxygen or nutrient (Visvader and Stingl 2014; Aponte and Caicedo 2017). **Altogether, the above-mentioned cells and component of TME communicate with each other and with cancer cells. This communication allows the cancer cell to modify not only the surrounding tumor microenvironment but also cells located at distant sites leading to a stepwise progression from the primary tumor to the formation of metastasis.**

1.3 Metastasis

At the cellular level, metastasis represents the end product of a multistep cascade (Figure.4) starting with **Invasion.** Formation of successful tumor microenvironment along with the proliferation of tumor cells turn benign tumor mass to invasive (malignant) cancer when cancer cells are invading the tissue surrounding the primary tumor.

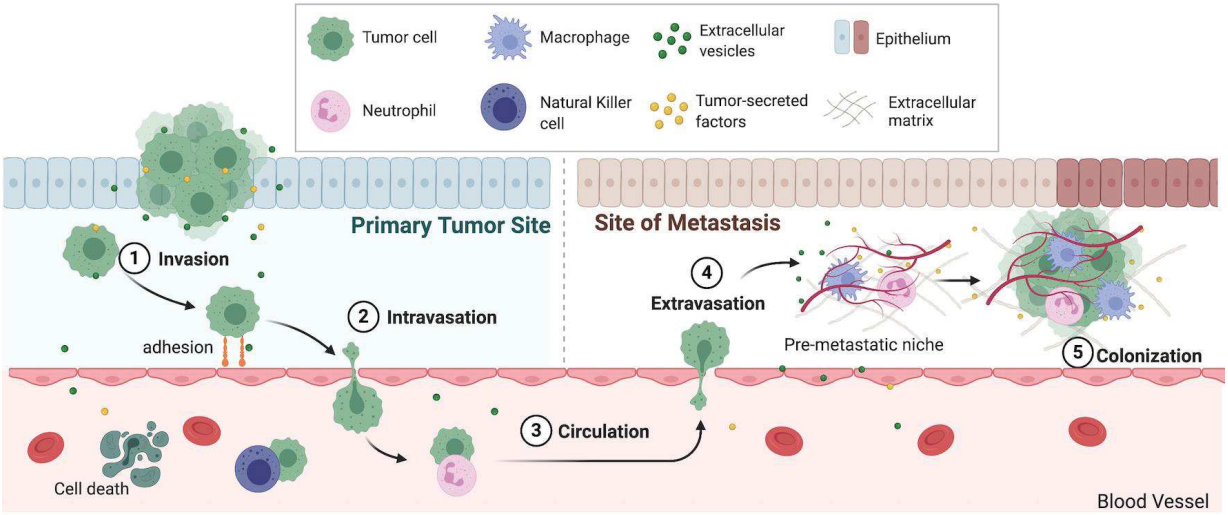

Figure 4. Overview of metastatic cascade. Metastasis is a multistep process, in which tumor cells invade their stroma towards the blood and lymphatic vessels and by entering these vessels (process called intravasation), they travel to distant organs by the flows. Survived cells in the circulation, adhere the vessels wall and extravasate (cross the endothelial barrier to reach the stroma), they might colonize and reactivate the growth of a new tumor called metastasis. **Inspired by** (Fares et al. 2020). Created with BioRender.com

In the most common type of cancers, as for instance in breast carcinoma, tumor cells must destroy their first barrier called basal lamina to move from being in situ (Spaderna et al. 2006; Nguyen-

Ngoc et al. 2012). The minimal pore size that a cell can go through is ~7 μm (E. J. Wolf et al. 2013). When the space is small like in basal lamina, cells will start expressing metalloproteinases (MMPs) and degrade the matrix first. MMPs are either transmembrane or secreted by tumor and stromal cells eventually through EVs (Lee 2004). Along with chemically degrading of the ECM using MMPs, cells mechanically remodel ECM through a complex intercoupling between intracellular forces (such as cell contractility) and extracellular forces (adhesions and protrusions) that depend on the stiffness of the surrounding stroma and the alignment of matrix fibers(Wisdom et al. 2018; Paz and Sánchez 2015).

All the above-mentioned process will promote invasion, through which some tumor cells are able to reach the vessels and cross the endothelial barrier, a process called **intravasation.** Due to constant rearrangement, lack of perivascular coverage and basement membrane, the vasculature of the primary tumor is immature and hyperpermeable causing leakage of plasma proteins that further facilitate new vessel formation and tumor cell intravasation(Lambert, Pattabiraman, and Weinberg 2017). After intravasation, cells surviving in the **circulation** will arrest, adhere and **extravasate** to escape the circulation. These last steps are one of the major focus in my lab. Although few cancer cells intravasate into the vasculature, even fewer survive the physical stresses, including hydrodynamic flow, loss of attachment to a substrate and shear stress(Rankin and Giaccia 2016; Follain et al. 2020). Other obstacles involve the human immune system—in particular, natural killer (NK) cells, which kill some of the cancer cells in the bloodstream—as well as anoikis, programmed cell death induced by lack of appropriate attachment to the ECM. These factors lead to a significant decrease in the number of cancer cells that reach the metastatic site from the primary tumor (Strilic and Offermanns 2017). However, a recent study in our team demonstrated that blood flow forces tune both the arrest and extravasation of circulating tumor cells (CTCs), suggesting that the success rate of CTC extravasation is increased when CTCs become arrested (trapped) in vessels with reduced blood flow dynamics and/or get engulfed due to endothelial remodeling (Follain et al. 2018).

In Addition, the process of adhesion and extravasation can be further aided by inflammatory cells, such as monocytes and neutrophils, which would form complexes with CTC and mediate their adhesion and translocation throughout the vessel wall, as well as establishing and maintaining the

metastatic niche (Headley et al. 2016). After extravasation, cancer cells have one final task to complete known as **colonization** of secondary sites. Colonization includes the capacity of arriving cells to survive and start proliferating or enter dormancy. **Successful metastatic colonization could occur with its non-random patterns only at certain organ site, highlighting the concept of organotropism (Fidler,1973).**

1.4Organotropism

Cancers metastasize to through a distinct metastatic route and follow a non-random distribution among distant organs, known as ‘‘organotropism’’ or ‘‘organ-specific metastasis” (Y. Gao et al. 2019). In both clinical and animal models, usually based on the histological origin of cancer, there will be a predictable pattern of organ-specific metastasis, as each cancer types are predicted to metastasize to specific secondary organs (Obenauf and Massagué 2015; Valastyan and Weinberg 2011; Wan, Pantel, and Kang 2013). The most common sites for cancers to metastasize are the brain, bones, lungs and liver, and the least metastatic sites are pancreas, skin, ovary, thyroid, muscle and spleen. Different cancer subtypes also correlated with distinct tendencies to metastasize to specific organs (Voduc et al. 2010).

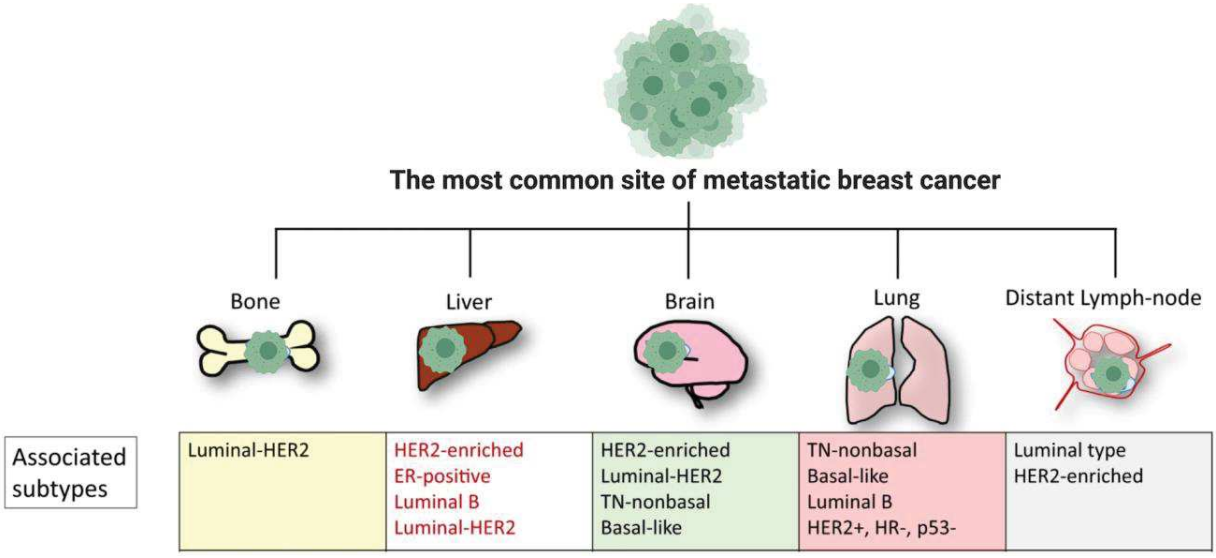

Figure 5. Summary of breast cancer organotropic metastases. The site-specific organotropic metastasis is regulated by the breast cancer subtypes Bone is the most common site of metastatic breast cancer patients, with the second most common site is brain, and liver and lungs are the next. **Adapted from** (W. Chen et al. 2018).

For instance, breast cancer tends to metastasize distantly to the bone, lung, liver, brain, and distant lymph node. However, the luminal subtype has a higher propensity to metastasize to the bone, whereas both basal-like and TN subtypes have a high rate of metastases to lung, distant lymph node and brain (Figure 5). Therefore, each cancer types and subtypes display distinct organotropisms (W. Chen et al. 2018). There are different factors explaining why certain organs are more prone to be a host than others which will be briefly listed below.

Blood flow patterns and vascular architecture are important factors in organotropism. In his -the hemodynamic hypothesis-, James Ewing explains organotropism based on the blood flow and anatomy of vascular connection between the primary tumor and the secondary organ (Ewing 1928). Basically, flow rates, vessel size and shear stress can all influence the survival of cancer cells in the circulation and control organotropic seeding patterns (Azevedo et al. 2015; Chambers, Groom, and MacDonald 2002; Baccelli et al. 2013). Distinct blood flow pattern may also lead to entrapment of tumor cells in capillary vessels or their attachment to adhesion molecules on the endothelium (Aceto et al. 2014). For instance, the venous blood that circulates through most organs is directed to the liver and lungs before reaching other organs, which may explain why these organs are such a common site of metastasis (Denève et al. 2013). However, blood flow pattern and capillary entrapment are not the only influencing factors and cannot sufficiently explain all the clinical observations of metastatic organotropism. For instance, organs with an equal volume of blood flow (kidney, liver, brain) still have very different metastatic patterns. Another factor that can facilitate extravasation and colonization is the architecture of blood vessel walls and endothelial cell morphology which also differ among organs (Budczies et al. 2014). In contrast to the vessels in the brain and lungs, which have more tight junctions between endothelial cells and a basement membrane, sinusoid vessels in the liver and the bone marrow are fenestrated, or lined, with a discontinuous layer of endothelial cells that provides greater permeability. Therefore, transendothelial migration is less restricted in the liver and bone marrow than it is in the brain or the lungs, as shown in quantitative cell-tracking studies in mice (Aird 2007). However, as explained before the vasculature of target organs can be impaired before the arrival of tumor cells. For instance, in breast cancer and melanoma tumor cell-derived SPARC, and

ANGPTL4 disrupts vascular endothelial cell-cell junctions, and increases the permeability of lung capillaries(P.-H. Huang et al. 2009; Padua et al. 2008; Tichet et al. 2015). Additionally, tumor cells can cross blood-brain barrier (BBB) by upregulating the expression level of COX2, HBEGF, MMP2, miR-105, and ST6GalNac5, which increase vascular permeability in the brain(Bos et al. 2009; Sevenich and Joyce 2014; Z. Zhou et al. 2017). The adhesion molecules on endothelial cells also vary by organ environment which may be related to metastatic tropism. For example, expression of induced E-selectin in the liver by inflammatory cytokines, such as TNF-α secretion by tumor-recruited macrophages and Kupffer cells, promote adhesion and liver metastasis (Auguste et al. 2007; Eichbaum et al. 2011). Moreover, E-selectin expression on endothelial cells in the bone marrow contribute to CTC adhesion and metastasis to the bone (Barthel et al. 2013). The presence of different adhesion molecules in distinct organs may enhance metastatic seeding, such as N-cadherin (Qi et al. 2005) and ICAM1 (intracellular adhesion molecule 1) (Rahn et al. 2005), which enhance transendothelial migration. Although there are even more known adhesion molecules whose contribution to colonization in specific tissues is still unclear. Another factor which has been shown in many studies is **the genetic adaptation of tumor cells during organ-specific colonization.** Different gene signatures enriched in metastatic cells promote CTCs survival in the vasculature, capillary adhesion, extravasation, migration, angiogenesis, and the mobilization of stromal components that can promote organotropism (Piskounova et al. 2015; Tabariès et al. 2012). For instance, clonal enrichment for preexisting mutations present in primary tumors, was shown to be upregulated in metastasis models and may lead to the survival of metastatic cells in specific organs (Jacob and Prekeris 2015). **Organotropic cancer cells also possess distinct metabolic features**. Considering the difference in oxygen levels, acidity, and metabolite profiles of host organs, it is expected to find distinct tumor characteristics matching organ-specific metabolic environments (Y. Gao et al. 2019). For example, the brain and lungs have high levels of glucose and oxygen, which may facilitate colonization of metastatic cells using aerobic glycolysis or oxidative phosphorylation (Y. Gao et al. 2019). **Finally and very importantly, many studies demonstrating the importance of secreted factors such as growth factors (e.g., VEGF), cytokines (e.g., TNF-b, TGF-b), matrisome proteins (e.g., LOX, versican) as well as EVs in metastatic tropism by preparing a Pre-Metastatic Niche (PMN) in specific organs before the arrival of tumor cell (Gao,2019).**

1.5 Pre-Metastatic Niche

In 1889, Steven Paget "seed and soil" theory proposed metastasis will succeed in organs where the local microenvironment (the soil) is favorable for tumor cells invasion and growth (the seed) (Paget 1989). This theory still stands over 100 years later, emphasizing the requirement for a supportive microenvironment, in metastatic outgrowth. Additionally, a similar model has been suggested in 2005 by David Lyden and his team, in which they explained that a favorable microenvironment must develop in order for tumor cells to be able to engraft and proliferate at secondary sites. These tumor growth-favoring microenvironments are termed 'pre-metastatic niches' (PMNs) which are formed before the arrival of the tumor cell (Kaplan et al. 2005). In ecology, a niche is a term describing the relational position of a species or population within a specific ecosystem. Similarly, Raymond Schofield postulated the concept of the stem cell niche as a specialized microenvironment that provides stem cell maintenance and regulates cell function and proliferation (Psaila and Lyden 2009). The PMN can be **primed and established** through a complex interplay among primary tumor-derived factors including EVs, tumor-mobilized bone marrow-derived cells, and local stromal components (Sleeman 2012; Yang Liu and Cao 2016). Many aspects of PMN are still unknown, below what is currently known about the constitution of the PMN will be discussed (Figure 6).

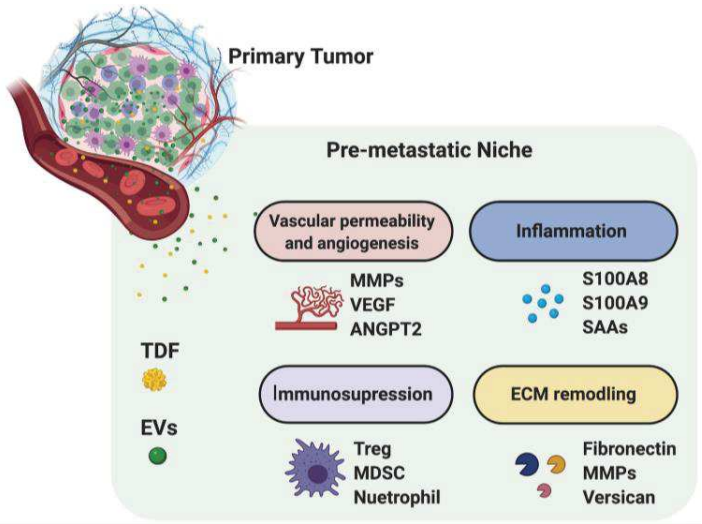

Figure 6. Characteristics of the pre-metastatic niche. TDSFs and EVs induce the mobilization and recruitment of several cell populations to secondary organ sites, creating a suitable niche microenvironment for metastatic tumor cell colonization. **Inspired by** (Yang Liu and Cao 2016). Created with BioRender.com

The vasculature at PMNs is remodeled by primary tumor-secreted factors (Psaila and Lyden 2009). For instance, MMP9, as a member of the MMP family, is also involved in regulating vascular integrity in PMNs (Kaplan et al. 2005). Hyperpermeability and breakdown of the vascular basement membrane result in altered vascular integrity in the pre-metastatic lungs of melanoma (P.-H. Huang et al. 2009) and breast cancer(H. H. Yan et al. 2010). For example, TGFβ in the breast tumor primes cancer cells for metastasis to the lungs by inducing angiopoietin-like 4 (ANGPTL4). Tumor cell-derived Angptl4 disrupts vascular endothelial cell-cell junctions, increases the permeability of lung capillaries, and facilitates the trans-endothelial passage of tumor cells (Padua et al. 2008). A landmark study, performed in patients/mice with melanoma showed that primary tumor-secreted factors upregulated angiopoietin 2 (ANGPT2), MMP3 and MMP10 in the pre-metastatic lung, and thereby disrupted blood vessels. However, identities of the cells expressing these molecules and the tumor-secreted factors that induce their expression are not known yet (P.-H. Huang et al. 2009). Moreover, CCL2 secretion by breast tumor cells and the stroma result in the recruitment of monocytes expressing C-C chemokine receptor type 2 (CCR2), that, in turn, secrete VEGFA (Qian et al. 2011). Formation of blood clots is another PMN-associated change at the vascular level and could be considered as one of the important causes of mortality in cancer patients (Kuderer, Ortel, and Francis 2009), however its mechanism, and biological relevance for cancer progression is not known. It has been shown, CD11b+CD68+F4/80+ myeloid cells are recruited to the lung by primary tumor-induced fibrin clots during PMN formation, thus enhancing CTC homing and survival (Gil-Bernabé et al. 2012). Interestingly, recruitment of CD11b+MMP9+Ly6G+ granulocytic cells by the platelet-secreted CXCR2 ligands, CXCL5 and CXCL7 chemokines, upon platelet contact with tumor cells is an essential mechanism for the guidance of granulocytes to form “early metastatic niches” (Labelle, Begum, and Hynes 2014).

Disruption of endothelial cell function is just one of the first modifications during PMN formation, as other stromal cell types are activated by primary tumors derived-secreted factors and contribute to the establishment of PMN (Yang Liu and Cao 2016). Tissue-resident macrophages are an example of stromal cells activated during PMN formation. For instance, pulmonary alveolar macrophages contribute to the lung PMN of breast cancer (P. Sharma and Allison 2015). Liver

Kupffer cells, also facilitate the recruitment of BMDCs to PMNs via exosome (discussed later) (Peinado et al. 2017). **Inflammation is another contributor to PMN formation** (Yang Liu and Cao 2016) . A common denominator of inflammatory responses within the PMN is the S100 protein that is essential in intercellular crosstalk between tumor cells and stromal cells during PMN formation (Peinado et al. 2017). Importantly, depending on the tumor type, exosomal cargo induces the upregulation of specific S100 family members in stromal cells which will be discussed later in section 2.7. It has been shown, mice injected subcutaneously with lung cancer cells, then treated with monoclonal antibodies against S100A8 and S100A9, displayed less accumulation of CD11b+ myeloid cells in lung PMN leading to reduced lung metastasis (Hiratsuka et al. 2011). Moreover, serum amyloid A1 (SAA1) and serum amyloid A3 (SAA3) can be induced by a breast cancer-derived S100A4 via TLR4 and NF-kB signaling in an organ-specific manner and may serve as a connection between inflammation and tumor metastasis in the PMN (Hansen et al. 2015). Moreover, SAA1 and SAA3 upregulation by S100A4 increased BMDC recruitment to metastatic organs and tumor cell adhesion to fibronectin (Lukanidin and Sleeman 2012). Thus, S100A4 acts similar to S100A8 and S100A9 to regulate the PMNs formation by promoting pro-inflammatory microenvironments both in the primary tumor and in PMNs (Mauti et al. 2011).

In addition, the **ECM undergoes remarkable remodeling** at PMN organ sites in response to systemic factors released from the primary tumor, recruited BMDCs or activated stromal cells (Sleeman 2012). The remodeling to ECM happens through two mechanisms including deposition of new ECM components and changing the physical properties of pre-existing ECM at PMNs. Some important ECM components are fibronectin, MMPs, versican, periostin, and tenascin-C (Ghajar et al. 2013; S. Kim et al. 2009). For example, before the arrival of tumor cells, carcinoma cells upregulate fibronectin at PMN in lung, which promotes BMDC through α4β1 integrin. These BMDCs are recruited to the metastatic site by tumor-derived factors and express MMP9 to facilitate the breakdown of the basement membrane (Kaplan et al. 2005). In addition to fibronectin, other components of ECM support the PMN. Tenascin C, which is initially expressed by breast cancer cells and later by stromal cells promote survival and outgrowth of lung metastases (Oskarsson et al. 2011). Secretion and incorporation of periostin into ECM is another important factor in the establishment of PMN. For example, tumor-derived factors, such as TGFβ, induce the expression and secretion of periostin from stromal fibroblasts expressing α-smooth muscle actin

and vimentin in the lung PMN of breast cancer (Malanchi et al. 2012). Furthermore, versican, an ECM proteoglycan, is upregulated by many tumors in human. Tumor-derived versican activates macrophages through Toll-like receptor 2 (TLR2) to produce interleukin-6 (IL-6) and tumor necrosis factor (TNF), thereby establishing a pro-inflammatory microenvironment in the pre-metastatic lung (S. Kim et al. 2009). All the above-mentioned study supports the ECM remodeling, however, the specific functional consequences of ECM remodeling at the PMN on metastasis is not fully understood.

Establishing **an immunosuppressive PMN** is another important strategy for tumors and their metastatic derivatives (Yang Liu and Cao 2016). Natural killer (NK) cells, non-classical ‘‘patrolling’’ monocytes and CD8+ T cells contribute to preventing tumor metastasis without affecting primary tumor growth (Bidwell et al. 2012; Hanna et al. 2015). However, immunosuppressive cells within the PMN, such as MDSCs, macrophages, and Treg cells potentially suppress anti-tumor immune responses (Yang Liu and Cao 2016; McAllister and Weinberg 2014). For example, T cell-expressed prolyl- hydroxylase proteins which are proposed to create an immunosuppressive PMN in the lung by prompting pulmonary Treg cells and restraining CD4+ and CD8+ T cell responses (Clever et al. 2016). MDSCs can either develop from tissue-resident myeloid populations or they may be recruited to PMNs (Peinado et al. 2017). MDSCs in the lung also convert the niche site into a pro- inflammatory, immunosuppressive PMN by suppressing interferon-γ (IFNγ)-mediated immune responses while inducing the expression of pro-inflammatory cytokines, interleukins and SDF1 (H. H. Yan et al. 2010). Other tissue-resident cells, such as pulmonary alveolar macrophages also participate in the lung PMN in breast cancer and reported to create an immunosuppressive niche by suppressing anti-tumor T cell responses (P. Sharma and Allison 2015). Neutrophils were also shown to support the formation of lung PMNs in breast cancer. Recently it has been demonstrated that, besides neutrophils, there could be active, EV-mediated communication between tumor cells and other innate immune cells during PMN formation which will be discussed later in section 2.7.

Altogether, the combined systemic effects of tumor-secreted factors and tumor-shed EVs lead to PMN formation. The fundamental role of EVs in mediating communication between tumor cells and cells of the microenvironment for PMN formation was a great discovery by Lyden’s group in

2012 (Peinado et al. 2012). **It has been followed by subsequent studies, showing tumor EVs contribute to metastatic organotropism, creating a so-called PMN in specific metastatic secondary sites before the arrival of tumor cells (Peinado et al. 2017). However, the exact mechanisms by which tEVs contribute to PMN formation are still unknown and the subject of current investigations.**

2 Extracellular Vesicles (EVs)

EVs comprise a heterogeneous population of membrane vesicles secreted by all cell types, and present in all body fluids. EVs contain RNA, lipids, proteins and possibly DNA, which can be taken up by distant cells and deliver a message. Size of EVs may vary (typically between 50 nm and 500 nm)(Mathieu et al. 2019). Based on the current knowledge of their biogenesis, EVs can be broadly divided into two main categories: exosomes and microvesicles (van Niel, D'Angelo, and Raposo 2018). I will start this part with **section 2.1** by briefly explaining the history and terminology of EVs. In **section 2.2**, I describe the most common methods of isolation and characterization of EVs, which are the essential and challenging steps before subsequent analysis and functional studies of EVs. In **section 2.3**, I proceed by describing the EVs composition, since understanding the EV content is very important for understanding their biological functions as well as their roles in cancer development. In **section 2.4,** I explain the mechanisms of EVs biogenesis and secretion; many aspects of which remain unknown. In addition to EV biogenesis and secretion, other essential aspects of EVs such as uptake mechanisms are still unknown and still important for understanding the progression in cancer specially organ-specific metastasis. Therefore, in **section 2.5** I describe the mechanisms of EV uptake. Then in **section 2.6**, I talk about the biological and pathological role of EVs. Finally, in **section 2.7** I take a close look at the important role of EVs in different facets of cancer progression and metastasis including their function in PMN.

2. 1 History and Terminology:

The discovery of vesicles around cells in mammalian tissues or fluid dates back to the late 1960s, and until the 1980s, these cell-derived vesicles were considered as platelet "dust" or cellular debris

that directly budded from the plasma membrane(P. Wolf 1967). In 1971, the term "extracellular vesicle" was used for the first time in the title of a scientific publication that showed electron microscopy evidence for EV biogenesis from *O. danica*, a flagellated alga (Aaronson et al. 1971). Around this time, EVs were referred to by several names by groups working in different fields, without knowing clearly what these particles were (Witwer and Théry 2019). The most critical finding came later in 1983 when two papers published almost at the same time in JCB and Cell reported that in reticulocytes, transferrin receptors at the surface of small ~50 nm vesicles were released from maturing blood reticulocytes into the extracellular space (Harding, Heuser, and Stahl 1983; Pan and Johnstone 1983). A few years later, Johnstone used the term "exosomes", with regards to the vesicle structures that are released into the extracellular space (Johnstone et al. 1987). Although the term "exosome" had in fact been used a few years earlier, when referring to other membrane fragments isolated from biological fluids, ranged in size from 40 to 1000 nm (Trams et al. 1981).

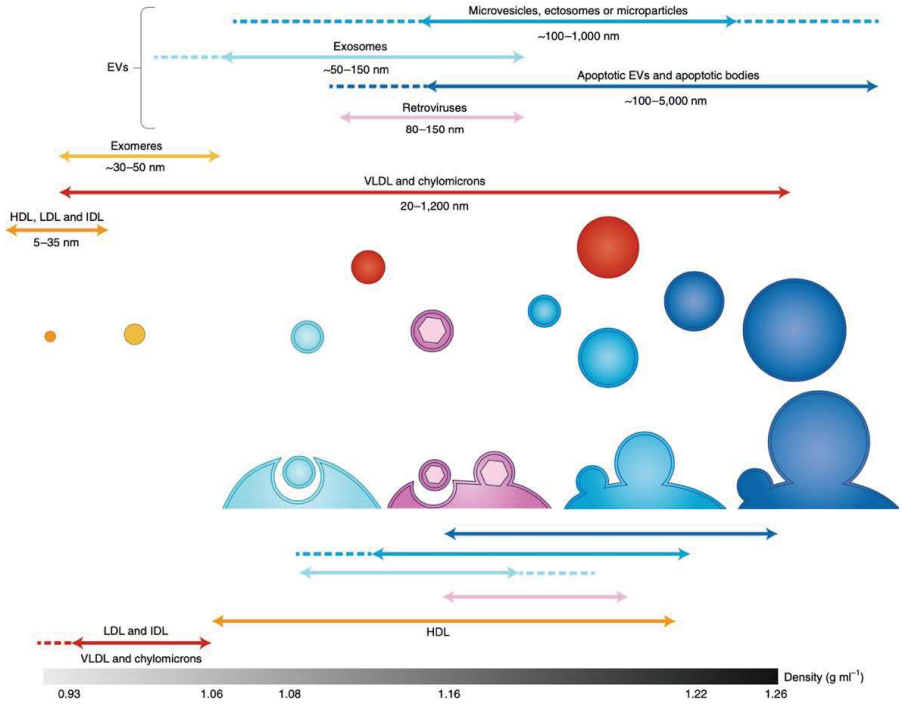

Figure 7. Physical characteristics of the different EV subtypes: Exosomes (indicated as water blue vesicles) originate from the endosomal pathway and are secreted upon fusion of MVBs with the cell plasma membrane. Apoptotic EVs or apoptotic bodies (dark blue) and microvesicles, ectosome or micropartcile (blue) buds directly from the plasma membrane. Others are co-isolated particles together with EVs. **Extracted from** (Mathieu et al. 2019).

The term “exosome” has also been employed with a completely different meaning, by Mitchell and colleagues to name the intracellular particle involved in RNA editing (Mitchell et al. 1997). These preliminary reports helped to develop the field as we know it now, where many studies described the relevance of heterogeneous EVs population. Novel isolation and characterization methods over the last two decades allowed great progress defining major EV populations including exosomes and microvesicles based on their underlying biogenesis, and content (van Niel, D’Angelo, and Raposo 2018). The main classes of EVs, exosomes are the smallest among EVs categories (~50–150 nm) and generated by an intracellular endocytic trafficking pathway involving the fusion of multivesicular late endocytic compartments (multivesicular bodies (MVBs)) with the plasma membrane(Mathieu et al. 2019). On the other hand, microvesicles (100-1000 nm) and apoptotic bodies (100-5000nm) that are generated by the outward budding and fission of the plasma membrane of healthy and apoptotic cells, respectively (Mathieu et al. 2019). Despite this classification, and regardless of the secretion mechanisms, there is still a grey zone where the overlapping range of size or density, similar morphology and variable composition have made it challenging to create a precise nomenclature for EVs (Willms et al. 2016; 2018). For instance, there is a size overlap between small microvesicles, exosomes and enveloped viruses (50-150nm). In addition, apoptotic bodies or small apoptotic vesicles might be undistinguishable from the other EVs .Other secreted particles such as exomeres(∼35 nm)(H. Zhang et al. 2018) and different types of lipoproteins can be co-isolated with EVs as well (Figure 7) (Mathieu et al. 2019). Therefore, referring the literature on EVs-specific population nomenclature may generate confusion, because the results are not always informative and consistent (Witwer and Théry 2019). To avoid this confusion, it is critical to refer to the International Society for Extracellular Vesicles (ISEV) guidelines on minimal information for studies of extracellular vesicles (MISEV)(Witwer and Théry 2019). According to the MISEV, the commonly used term of “exosome” and “microvesicle” should be replaced with EV as the generic term for particles released from the cell that is delimited by a double-leaflet membrane and cannot replicate, i.e., do not contain a functional nucleus (Théry et al. 2018). For clarity, in this thesis, I will use the term exosomes for studies directly addressing the mechanisms of exosome biogenesis in MVBs or the term EVs for experiments concerning general populations of vesicles (exosomes and microvesicles).

Altogether, due to heterogeneity in EV population, it is very challenging to purify EV subtypes to 100% homogeneity. However, effective isolation and characterization shedding light on EV heterogeneity will advance our understanding of their critical roles in health and disease, ultimately accelerating the development of EVs as therapeutics and diagnostics, especially since they have been considered as a novel biomarker in various pathologies such as cancer. Selecting appropriate isolation and characterization method is therefore a critical step in all areas of EV research.

2.2 EV isolation, and characterization

2.2.1 EV isolation

EVs are generally purified from conditioned cell culture media or various body fluids such as blood plasma (Caby et al. 2005), urine (Pisitkun, Shen, and Knepper 2004), saliva(Houali et al. 2007), breast milk (Admyre et al. 2007), semen (Poliakov et al. 2009), and other biofluids (Asea et al. 2008). Culture media and body fluid contain a complex mixture of EVs and other components of the extracellular space such as cell debris, protein, lipoproteins, and nucleic acids. Therefore, EV isolation is still challenging, and a perfect standardization in isolation methods does not exist, but progress has been made to develop improved isolation techniques (Théry et al. 2006). In my PhD project I used two different methods of EV isolation including **differential ultracentrifugation**, and **size exclusion chromatography (SEC)** (Stranska et al. 2018). **Other EV isolation methods** have been developed including density gradient, other size-based techniques, immune affinity, precipitation, and microfluidic (D. Yang et al. 2020). These alternative methods have been developed based on a particular feature of EVs, such as their density, shape, size, and surface proteins to aid their isolation, however, each of these methods has a unique set of advantages and disadvantages (D. Yang et al. 2020). Below I will briefly explain the most-commonly used isolation methods used during my PhD as well as the advantages and shortcomings associated with these methods.

Differential Ultracentrifugation (UC) is the most widely used primary isolation method for EVs (Gardiner et al. 2016). With the high capacity of centrifugal force, ranging from ~100,000 to 120,000 × g, ultracentrifugation isolates EVs based on their density and size differences from other components in a sample (Théry et al. 2006). F**or all my experiments (mainly *in vitro*) I used this**

method dues to its advantages including versatile, cost-effective, and provide vesicle enrichment as a pellet. However, this method is time-consuming and leads to low purity and in some cases aggregation with "contaminating" protein complexes (Zarovni et al. 2015).

Size exclusion chromatography (SEC) is another size-based separation method for EV isolation (Nordin et al. 2015). In SEC, porous materials such as polymer beads are utilized to separates macromolecules by differences in size as they pass through the column (Gámez-Valero et al. 2016). In the past few years, companies such as qEV (iZON) have developed different commercial SEC kits to isolate EVs from <150 µL up to 10 mL volume of starting material with porous resins of 35 nm or 75 nm for optimal EV isolation (Vogel et al. 2016). **For my *in vivo* (mice) experiments,** I used SEC method since it doesn't affect EV structure, preserve its integrity, and prevent aggregation, all of which are important for safe injection of EVs into mice. However, in this method, there is still possible sample contamination with proteins (D. Yang et al. 2020). **Characterization of EVs after isolation is very important to have pure isolation and absence of contamination.**

2.2.2 EV characterization

EVs characterization is essential, not only to confirm the presence, size and concentration of EVs in the preparation (physical characterization) but also to assess EV-content (molecular characterization) (Lötvall et al. 2014). Below, the most common techniques for EVs characterization will be discussed briefly (Rebbeck et al. 2016; Doyle and Wang 2019). However, the small size, the heterogeneity, the presence of contaminants and the poor sensitivity of the current technologies, make the EV characterization still relatively challenging.

Physical characterization is a great way to measure the size and/or concentration of EVs in a sample through high-resolution imaging such as electron microscopy, or by using optical or electrical readouts such as nanoparticle tracking analysis (NTA), dynamic light scattering, and tunable resistive pulse sensing (Hartjes et al. 2019). Among these methods, NTA is one of the widely used EV analysis methods which is based on recording a time-lapse of particles undergoing Brownian motion when in solution. Particles are detected by either scattered light or emitted

fluorescence. The software simultaneously records the Brownian motion of diffuse particles and based on these motions calculate the size of the particles(Dragovic et al. 2011).On the other hand, electron microscopy including transmission electron microscopy (TEM) and scanning electron microscopy (SEM) are common approaches to produce high-resolution image demonstrating the morphology of EVs using a beam of electrons (Wu, Deng, and Klinke 2015).

Molecular characterization is a good way to study the content of the isolated EVs and is usually done through different approaches, some of which have been mentioned below (Webber and Clayton 2013). The proteomic approach is being used to identify as many proteins as possible within relatively high amounts of EV sample. This method is being used to discover novel EV markers, as well as comparing the EV proteome between EV subpopulations (Schey, Luther, and Rose 2015). According to MISEV 2018, to validate the purity of EV preparation the presence of at least three positive protein markers of EVs, including at least one transmembrane/lipid-bound protein (e.g. CD9, CD81, CD63) and one cytosolic protein (e.g. Alix, Syntenin, HSC-70, Tsg101) and the absence of at least one negative protein marker (e.g., IMMT, GM130) should be confirmed (Lötvall et al. 2014; Théry et al. 2018; Kowal et al. 2016). Similar to proteomics, recently lipidomics has been also known to study the lipid component of EVs however, the limitations in lipidomic analyses need to be improved (Skotland et al. 2019). Next generation sequencing (NGS) or microarrays are also a great tool for RNA characterization of EVs. Due to lipoproteins or ribonucleoproteins (RNPs) contaminants coming from the cell culture media, it is recommended to treat the EV with proteinase, RNase or DNase prior to analysis (Mateescu et al. 2017).

Even though the isolation and characterization of EVs are challenging, a careful selection of methods (or a combination of methods) leads to a better understating of EV composition as well as biogenesis and function.

2.3 EV Composition

Study of EV composition revealed that they contain proteins, lipids and nucleic acids, and this composition can differ between secreting cell types and culture conditions. The specific composition of EVs affect their fate and function, underlying the importance of selective cargo-

sorting mechanism (Kalra et al. 2012; Simpson, Kalra, and Mathivanan 2012; Haraszti et al. 2016). Type and abundance of EV cargoes depend on cell type and are often influenced by the physiological or pathological state of the donor cell, the stimuli that modulate their molecular mechanisms that lead to their biogenesis (Minciacchi, Freeman, and Di Vizio 2015). Within the past few years, many studies on the composition of EVs using various omics approaches have been performed and complied in databases such as EVpedia (http://evpedia.info), Vesiclepedia (http://www.microvesicles.org), and Exocarta (http://www.exocarta.org). Below the composition of EVs will be described and in a global scheme of EVs (Figure 8) more detail will be given on various type of transmembrane and cytosolic protein as well as other lipids and nucleic acids.

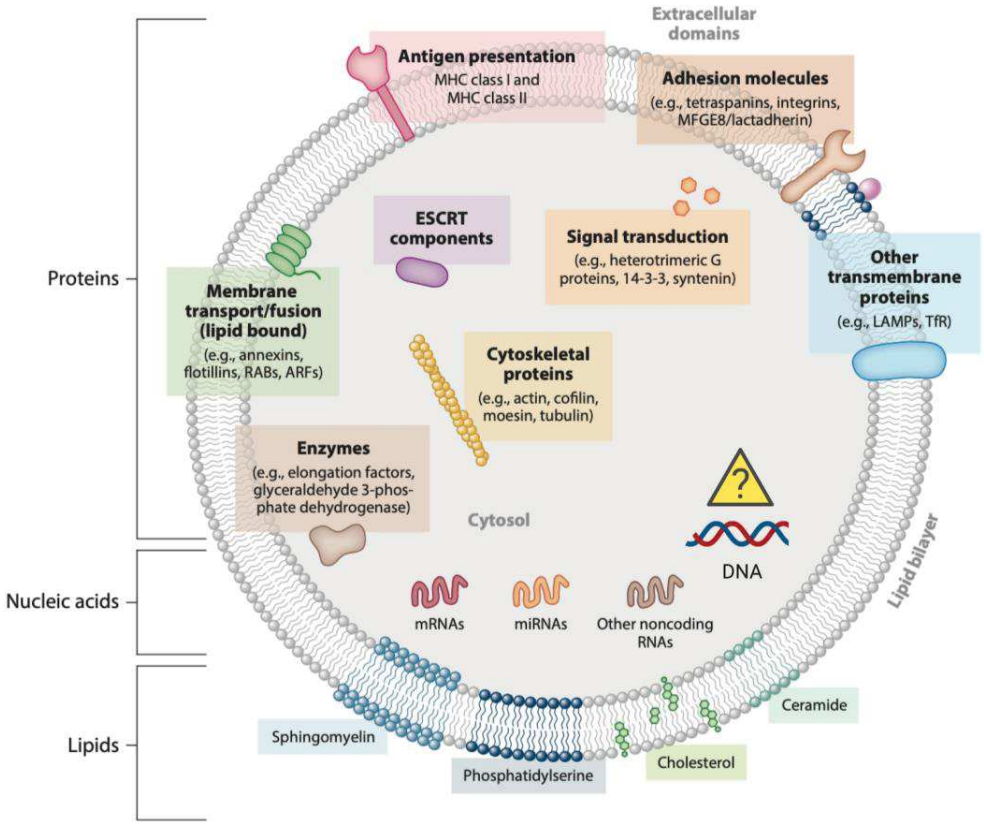

Figure 8. Overall composition of Extracellular Vesicles. Schematic representation of EV composition including families of proteins, lipids, and nucleic acids. Please note that each listed component may be present in some subtypes of EVs and not in others. For example, tetraspanins (CD63, CD81, and CD9) are commonly found in small EVs. However, DNAs are probably secreted in large plasma membrane derived EVs and/or apoptotic vesicles rather than exosomes. Abbreviations: ARF, ADP ribosylation factor; ESCRT, endosomal sorting complex required for transport; LAMP, lysosome-associated membrane protein; MHC, major histocompatibility complex; MFGE8, milk fat globule–epidermal growth factor-factor VIII; RAB, Ras-related proteins in brain; TfR, transferrin receptor. **Adapted from** (Colombo, Raposo, and Théry 2014).

2.3.1 Protein Composition and Sorting Mechanisms

Proteins are a major component of the EV cargo, and their expression is commonly used for characterization purposes. Many proteomic studies have also been employed to discover novel EV markers (Kowal et al. 2016), compare the EV proteome upon different isolation methods (Nordin et al. 2015) or classify between EV subpopulations (Willms et al. 2016). A compilation of 16 proteomic data sets has identified common vesicular markers, accepted across the EV community, however careful characterization of these protein has been recommended by International Society for Extracellular Vesicles (ISEV) (Lötvall et al. 2014; Théry et al. 2018). Many of these EV-associated proteins are regulators of the EV biogenesis. However, no general agreement has yet emerged on specific markers of EV subtypes, such as endosome-origin "exosomes" and plasma membrane-derived "ectosomes" (microparticles/microvesicles) (Théry et al. 2018). While no specific protein markers have been identified for different EVs subtypes, MVs, exosomes, and apoptotic bodies have different protein profiles due to their different routes of formation (Jeppesen et al. 2019).

Tetraspanin (CD9, CD63 and CD81), the family of proteins with four transmembrane domains, are highly enriched exosomes, but not exclusive to exosomes as they are also detected on bigger vesicles (van Niel, D'Angelo, and Raposo 2018; Verweij et al. 2011; Kowal et al. 2016). The presence of the tetraspanins on EVs is due to the formation of clustered microdomains together with other partners such as integrins (Yáñez-Mó, Gutiérrez-López, and Cabañas 2011; Berditchevski, Zutter, and Hemler 1996) and syntenin (Latysheva et al. 2006), that promote the budding of the membrane either towards the extracellular environment or toward the lumen of the MVBs(Andreu and Yáñez-Mó 2014; Hemler 2005). In addition, exosomes are also enriched with proteins of the Endosomal Sorting Complex Required for Transport (ESCRT) such as Alix that was shown to interact with syndecan through syntenin, supporting exosome biogenesis and ensuring cargo loading into the vesicles (Baietti et al. 2012).

Diverse post-translational modifications (PTM) of proteins are also known to participate in the selective mechanism of protein cargo sorting into EVs, which could explain the enrichment of specific proteins in EVs compared to the global cellular level (Moreno-Gonzalo, Villarroya-Beltri, and Sánchez-Madrid 2014). SUMOylation, phosphorylation, ubiquitylation, and glycosylation, are

some of the common mechanisms of PTMs that regulate cargo sorting (Anand et al. 2019). For instance, the recognition of the ubiquitinated epidermal growth factor receptor (EGFR) by the ESCRT complex, promotes the invagination of the endosomal membrane and thus the recruitment of EGFR into EVs (Trajkovic et al. 2008). On the contrary, secretion of small integral membrane protein of the lysosome/late endosome (SIMPLE) into exosomes is enhanced by mutations in its PPXY motif, which mediates its binding to E3 ubiquitin ligases, suggesting that ubiquitination negatively regulates SIMPLE secretion on exosomes (Zhu et al. 2013). Ubiquitination is also not required for the packaging of major histocompatibility complex II (MHC-II) into exosomes (Gauvreau et al. 2009). The phosphorylation of some proteins such as Annexin A2 has been also shown to influence their sorting in EVs, by protecting them from endosomal degradation (Valapala and Vishwanatha 2011). Considering EVs are molecularly reflective of their tissue of origin, EVs are also enriched with particular transmembrane protein receptors (e.g., epidermal growth factor receptors/EGFRs) and adhesion proteins (e.g., epithelial cell adhesion molecule/EpCAM), some of which could be considered as important pathophysiological EV biomarkers (Al-Nedawi et al. 2008; Tauro et al. 2013). Therefore, understanding the protein composition of EVs is crucial for biomarker research as well.

2.3.2 Nucleic Acid Composition and Sorting Mechanisms

In addition to protein cargoes, different forms of RNA and DNA are also possible EV cargoes. Recent studies have shown that certain EVs may contain **DNA** fragments such as single-stranded DNA, double-stranded DNA, genomic DNA, mitochondrial DNA, and even reverse-transcribed complementary DNAs (Balaj et al. 2011; Sansone et al. 2017). However, unlike other EVs cargoes, selective sorting of specific DNA fragments into EVs is disputable (Kahlert et al. 2014; Thakur et al. 2014). Recently, the secretion of DNA and histones was shown to be an autophagy/amphisome-dependent mechanism and no association with exosomes was shown (Jeppesen et al. 2019). Since it is also not clear how much of the EV-associated DNA is inside and how much is bound to the surface, DNA is still often considered a contaminant from improper EV isolation (Mateescu et al. 2017; Jeppesen et al. 2019).

RNAs represent the main nucleic acid cargo of EVs (Valadi et al. 2007). EVs are heterogeneous populations with different types and proportions of RNA cargo within them and shown to deliver functional mRNA and miRNA to recipient cells (Bellingham et al. 2012; S. Kaur et al. 2018; Shurtleff et al. 2017; Mateescu et al. 2017). Functionally, these RNAs can be divided into those with known functions, such as some mRNA, microRNA (miRNA) and small interfering RNA, those with predicted functions, for example, some transfer RNA, small nucleolar RNA, small nuclear RNA, Y RNA and vault RNA and those with unknown functions, such as fragmented and degraded (methylated and uridylidated) RNA species(O'Brien et al. 2020). Quantification analysis of EV cargo is difficult due to low numbers of cargo molecules per vesicle. On average, only one microRNA per EVs (M. Li et al. 2014) to one microRNA per 100 EVs (Chevillet et al. 2014) and one intact long RNA molecule (e.g. a full-length mRNA) per 1,000 extracellular vesicles (Wei et al. 2017) were reported. However, the repertoire of RNAs cargo of EVs is different from the cells which they were derived, indicating an active RNA sorting into the EVs (Leidal and Debnath 2020). Even though, the exact mechanism of RNA sorting into EVs is still unclear four potential mechanisms have been described so far. These include: 1) Kosaka et al. found that in HEK293 cells overexpression of nSMase2 leads to an increased number of miRNAs loaded into EVs, thus suggesting nSMase2-dependent pathway is associated with the sorting of miRNAs into EVs (Kosaka, Yoshioka, et al. 2013) 2)Villarroya-Beltri et al. discovered that the in T-cells interaction between four nucleotide motif (GGAG) and the ribonucleoprotein (hnRNPA2B1) is necessary for loading miRNAs into EVs (Villarroya-Beltri et al. 2013). Similarly, Shurtleff and colleagues demonstrated in HEK293 cells RNA-binding protein YBX1 has been implicated in sorting miRNAs into EVs (Shurtleff et al. 2017). 3) It has also been proposed that a sequence motif within the 3'UTR of a number of mRNAs enriched in glioblastoma-derived EVs may act as a ''zip code'' that targets mRNAs into EVs. This zip code consists of a 25-nucleotide sequence which contains a short CTGCC core sequence on a stem-loop structure (Bolukbasi et al. 2012). 4) Finally, studies have also revealed the direct role of Ras-MEK network in regulating the RNA-induced silencing complex (RISC) component Argonaute 2 (Ago2) proteins (functional carriers of miRNAs), thereby controlling the loading of miRNA into EVs. Knocking out AGO2 reduces the number of specific miRNAs in colon cancer-derived EVs (McKenzie et al. 2016).

2.3.3 Lipids

The interest in studying EV lipids has been growing within the past few years. According to these findings, the EV membrane contains phosphatidylcholine (PC), phosphatidylserine (PS), phosphatidylethanolamine (PE), phosphatidylinositols (PIs), phosphatidic acid (PA), cholesterol, ceramides (GM3), sphingomyelin, glycosphingolipids, as well as some other lower abundance lipids (Skotland et al. 2020). These lipids could contribute to the structure of vesicles, exosome formation, membrane trafficking, and dynamics of release (Skotland et al. 2019). For example, despite its simple structure and relatively low abundance, PA is also important for membrane dynamics (Egea-Jimenez and Zimmermann 2018). PA might be key at several stages of exosome formation, due to its ability to induce a negative membrane curvature because of its small headgroup (forming a 'cone' that might favor endosomal intraluminal budding) (Kooijman et al. 2005). One study indicates that PA is 1.8-fold enriched in exosome enriched EVs versus lysates from PC-3 cells (Llorente et al. 2013, 3). On the other hand, there is a two to three times enrichment from cells to exosomes of cholesterol, and PS, a similar mole percent of PE in cells and exosomes, and a lower mole percent of PC and PI in exosomes than in their parent cells (Skotland et al. 2020). What might explain this difference is not very well known. **Altogether, understanding the EVs composition is crucial not only for selecting an accurate method for EV characterization, isolation and biomarker research but also because it can give an indication on 1) mechanism of biogenesis 2) their spreading and uptake and 3) their function.**

2.4 Biogenesis of EVs

Since EVs have been classified based on differences in biogenesis, below I will discuss the different molecular mechanisms resulting in the release of MVs or release of exosomes (Figure 9). As a first regulator for EV biogenesis, cargoes destined for secretion within EVs must be targeted to the site of production, either at the plasma membrane (for MV) or at the limiting membrane of the MVB (for exosomes). Second, cargoes are enriched in the forming vesicles by stepwise mechanisms which ultimately lead to vesicle release (van Niel, D'Angelo, and Raposo 2018). Below, I briefly explain the biogenesis of MVs and exosomes, even though the exosome biogenesis is more complicated than biogenesis of MV and is better studied.

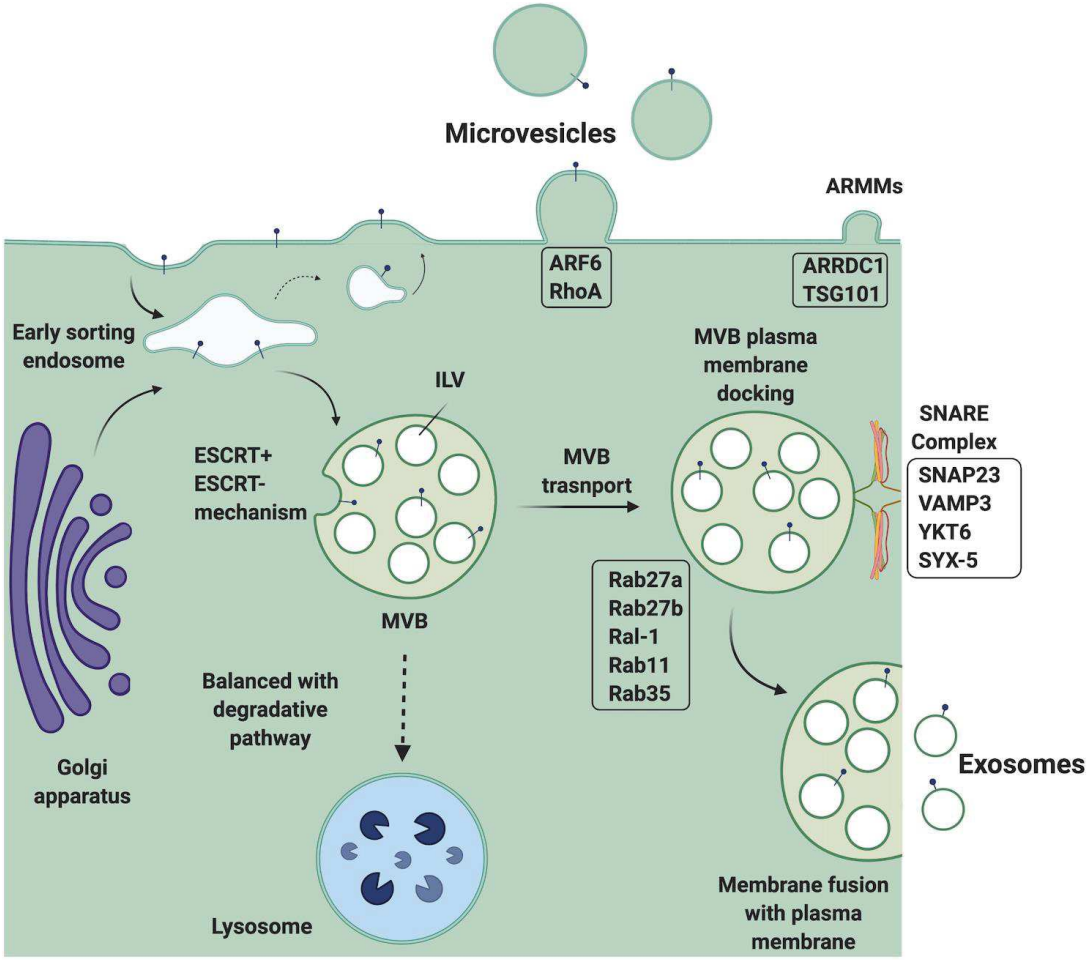

Figure 9. Biogenesis of exosomes and microvesicles. The budding of microvesicles from the plasma membrane is regulated by ARF6 and RhoA proteins. Other type of microvesicle (ARMMs) were also shown to directly originate from the plasma membrane by ARRDC1 and Tsg101 intervention. In exosome biogenesis, the internalization of the cell plasma membrane form an early sorting endosome. The cargo contained in the early endosome can be recycled back to the cell plasma membrane or directed to the MVB. The MVBs are filled with ILVs formed by invagination of the MVB membrane via ESCRT- dependent and -independent mechanisms. MVBs can either degrade their content by fusing with the lysosome or be transported directly to and fuse with the plasma membrane. The docking and fusion to the plasma membrane are regulated by Ral-1, Rab and SNARE proteins. **Adapted from** (van Niel, D'Angelo, and Raposo 2018). Created with BioRender.com

2.4.1 Biogenesis of Microvesicles

The biogenesis and release of MVs from cells may be controlled by several mechanisms (Figure.9). MVs are generated from sites of high membrane blebbing, and their biogenesis is regulated by lipid composition and organization of the peripheral cytoskeleton, both of which are able to change membrane fluidity and deformability (Muralidharan-Chari et al. 2010). Lipid rafts,

specific lipid microdomains enriched with cholesterol and glycosphingolipids, are essential to the budding of the cell membrane and cholesterol is thought to play a key role in MV formation, as its depletion reduces MV formation (Skotland et al. 2019; Lingwood and Simons 2010; del Conde et al. 2005; Haraszti et al. 2016). Scramblases, flippases and floppases, three different types of enzymatic groups of phospholipid transportation enzymes, contribute to the translocation of phospholipids between the two membrane leaflets and are crucial during MVs formation (Minciacchi, Freeman, and Di Vizio 2015; Clark et al. 2009; Maas, Breakefield, and Weaver 2017). Also, the activity of acidic sphingomyelinases and the conversion of sphingomyelin to ceramide (a cone-shaped lipid) lead to membrane bending, and regulation of MV formation (Lingwood and Simons 2010). In addition to lipid rearrangement, cytoskeletal rearrangements of actin and myosin mediate the fission and release of the MVs from the cell. This process is regulated by a signaling cascade initiated with ARF6 and RhoA GTPase mediators(Tricarico, Clancy, and D'Souza-Schorey 2016; Muralidharan-Chari et al. 2010). Recently, Qian Lu's lab discovered an arrestin domain containing protein 1 [ARRDC1]-mediated microvesicles (ARMMs) which were shown to contain plasma membrane associated ARRDC1 and Tsg101 driving their direct secretion but lack of late endosomal markers, and reported to selectively recruit, package and deliver active siRNAs into recipient cells (J. Wang et al. 2018; Nabhan et al. 2012). Among the above mentioned molecules, TSG 101, and Arf6 not only regulate shedding of MVs biogenesis (Muralidharan-Chari et al. 2010), but also control the biogenesis of exosomes via the syndecan–syntenin–ALIX pathway (Ghossoub et al. 2014), thus it may control the balance between the generation of both subpopulations of EVs.

2.4.2 Biogenesis of Exosomes

The biogenesis of exosomes is closely related to the endosomal pathway. Exosomal membrane cargoes reach endosomes from the Golgi apparatus or are internalized from the plasma membrane before being sorted to ILVs during endosome maturation (Klumperman and Raposo 2014). Proteins that are destined for recycling are translocated back to the plasma membrane and will therefore not end up in ILVs unless their endosomal recycling is impaired as for the transferrin receptor in reticulocytes (Vidal, Mangeat, and Hoekstra 1997). Exosomes are generated as ILVs within the lumen of endosomes during their maturation into MVBs. Several molecules, including

a number of small GTPases, have been shown to affect exosome biogenesis by acting at different levels. Our team recently found that the small GTPase RAL-1 modulates exosome secretion by controlling ILV formation and the attachment and fusion of MVBs to the plasma membrane (Hyenne et al. 2015), which is the center of my PhD. The formation of the ILVs is the beginning of the biogenesis of exosomes which happen through different mechanisms which will be discussed shortly below (Figure.9)**.**

One of this mechanism depends on **Endosomal Sorting Complex Required for Transport (ESCRT) composed of four different subcomplexes (ESCRT-0, -I, -II, -III) and associated proteins (Alix, VPS4 and VTA-1)** (Hurley 2015). The formation of ILVs requires four complexes, ESCRT-0, -I, -II, and -III, with ESCRT-0, -I, and -II presumably involved in cargo sorting and ESCRT-III in membrane deformation and fission(Remec Pavlin and Hurley 2020). These subunits orchestrate the ILVs formation in a stepwise process, starting with ESCRT-0 that binds ubiquitin residues attached to the cytoplasmic domain of the transmembrane cargo proteins that have to be sorted. ESCRT-0 also recruit ESCRT-I and then ESCRT-II (Schöneberg et al. 2017). When ESCRT-0 disconnect, ESCRT-I and ESCRT-II recruit and activate ESCRT-III which forms spiral-shaped structures that act as molecular springs (Chiaruttini et al. 2015). These can store mechanical energy that is proposed to play a role in all membrane remodeling functions of ESCRT-III (Chiaruttini et al. 2015). ESCRT-III functions may also depend on the turnover of individual subunits via the triple A ATPase vacuolar protein sorting-associated protein (VPS4) (Lata et al. 2008; Mierzwa et al. 2017). ESCRT-0 and -I show gradual and linear recruitment and dissociation, whereas ESCRT-III and its regulatory ATPase VPS4 show fast and transient dynamics (Wenzel et al. 2018). Moreover, ESCRT-III recruits deubiquitinating enzymes that remove the ubiquitin on cargo proteins before the ILVs are released into the endosomal lumen. However, this step is not critical in exosome biogenesis, as ubiquitinated proteins can be still found in exosomes (Buschow et al. 2005). The role of the ESCRT complex has been deeply investigated by Colombo et al. using an RNA-interference screening, that targets 23 ESCRT and ESCRT-associated proteins in HeLa cells, they identified 7 proteins that influence exosome biogenesis in these cells. Depletion of proteins of ESCRT-0 or -I components STAM, HRS or TSG101 reduced exosome secretion, whereas depletion of ESCRT-III CHMP4C, VPS4 and

accessory molecules VTA1 or ALIX resulted in an increased exosome secretion(Colombo et al. 2013).

The ESCRT mechanism can be partially activated via ALIX for ILV formation. In recent works, the syntenin-ALIX pathway has emerged as a major player controlling ILV formation. It has been recently shown in HeLa cells that ALIX- can directly recruit ESCRT-III–to promotes ILV budding and the sorting and delivery of tetraspanins to exosomes (Larios et al. 2020). To identify ESCRT components involved in syndecan–syntenin–ALIX exosome biogenesis, using RNA-interference screening Baietti et al. showed depletion of TSG101 (ESCRT-I), VPS22 (ESCRT-II), CHMP4 (ESCRT-III) or VPS4 on MCF-7 cells reduced exosomal release of syndecans, syntenin and CD63, suggesting that these components are involved in this pathway (Baietti et al. 2012). It should be noted that this study mostly analyzed the specific syndecan–syntenin exosome subpopulation in MCF-7 which would explain the inconsistencies with other reports. In fact, syntenin plays a dual role and could be considered as a mediator that make a balance by recycling syndecan to the plasma membrane through phosphoinositide PIP2 and the small GTPase Arf6 (Zimmermann et al. 2005) or by dispatching syndecans to ILVs via the ESCRT accessory protein Alix (Baietti et al. 2012). Therefore, a special mechanism for biogenesis can differ based on the cell type and the cargo proteins enriched in specific subpopulations of exosomes or other unknown reasons.

The involvement **of tetraspanins in ESCRT-independent biogenesis of ILVs** was revealed upon depletion of components of the four ESCRT complexes, ILVs are still formed in an ESCRT independent manner (Stuffers et al. 2009). EM analyses have shown that ESCRT-independent ILVs are loaded with tetraspanin CD63 in HEp-2(Stuffers et al. 2009) and HeLa cells(Edgar, Eden, and Futter 2014). In melanocytes, CD63 is also required for the sorting of the melanosomal protein PMEL to ILVs (van Niel et al. 2011). Other tetraspanins have been also shown to have a role in ILV formation. For example, BMDCs from CD9 knockout mice secrete less exosomes, while expression of CD9 and CD82 promotes the release of β-catenin in exosomes (Chairoungdua et al. 2010). In a mouse model of breast cancer, the release of Wnt11 on exosomes from cancer-associated fibroblasts has been shown to depends on the tetraspanin CD81 (Luga et al. 2012).

In addition to proteins, lipids are also major actors in ILV formation. The first ESCRT-independent mechanism reported for exosome biogenesis was from Trajkovic and colleagues who reported that in oligodendrocyte precursor cells, inhibition of neural sphingomyelinase 2 (nSMase2) (enzymes that hydrolyze sphingomyelin to ceramide) decreased vesicle budding (Trajkovic et al. 2008). Ceramide could create specific lipid microdomains and induce negative membrane curvature, which gives rise to ILVs and exosomes enriched in ceramide (Kajimoto et al. 2013). Lipid rafts on exosomal membranes can also contribute to ILV formation and sorting of raft-associated molecules such as GPI-anchored proteins (Valapala and Vishwanatha 2011). Phospholipase D (PLD) has also been involved in the generation of exosomes via the syntenin–ALIX pathway (Ghossoub et al. 2014). PLD is a ubiquitously expressed enzyme that catalyzes the hydrolysis of phosphatidylcholine (PC), the most abundant membrane phospholipid, to generate phosphatidic acid (PA) and choline. PA is considered as the simplest phospholipid. Due to its small headgroup, PA is able to induce a negative membrane curvature that might also favor endosomal intraluminal budding (Jenkins and Frohman 2005). Therefore, PA might be key at several stages of exosome formation. However, the role of PA for budding in endosomes and for MVB formation has not been directly investigated (Egea-Jimenez and Zimmermann 2018). Lipids, therefore, play a crucial role in exosome biogenesis; however further investigation will be needed to fully understand their contribution.

Altogether, different subpopulations of exosomes can be secreted by one cell type. These different populations of exosomes could arise from different populations of MVBs that co-exist within the same cell. Alternatively, a single MVB could contain distinct populations of ILVs, which could thus lead to the secretion of different exosomes. Whether ESCRT-independent, semi-dependent (such as the syntenin–ALIX pathway) and ESCRT-dependent mechanisms each act in different MVBs, or if they can simultaneously act on the same MVB, is not very well known. ESCRT-dependent and -independent sorting pathways could act together on the same MVB, and the abundance of a given cargo protein or its PTM will determine the recruitment of one sorting mechanism over another and dictate the destiny of the MVB (Palmulli and van Niel 2018).The main fate of an MVB is to fuse with lysosomes in order to degrade their content (Scott, Vacca, and Gruenberg 2014). However, mechanisms that prevent lysosomal degradation and promote ILVs secretion exist, but they still remain poorly understood. Several studies have supported the

hypothesis of a balance between lysosomal degradation and exosome secretion (Villarroya-Beltri et al. 2013; Edgar et al. 2016). For example, in certain diseases impairment of lysosome function lead to endosomal accumulation of proteins or lipids which provoke their extracellular secretion via EVs (Eitan et al. 2016; Strauss et al. 2010; Rajendran et al. 2006). **Thus, the balance between degradation and secretion of MVBs is a very important step before MVBs release their ILVs as exosomes.**

2.4.3 Regulators of Exosome Secretion

The transport and fusion of the MVBs towards the plasma membrane is promoted and regulated by association with the cytoskeleton, together with the action of molecular motors and small GTPases, and their fusion involves soluble NSF attachment protein receptor (SNARE) proteins (Granger et al. 2014; Jahn and Scheller 2006) (Figure 9). Members of the Rab family of small GTPases have been involved in transferring vesicles between intracellular compartments and play a role in MVB trafficking to the plasma membrane for exosome release. In an shRNA screening targeting 59 Rab GTPases in HeLa cells, of RAB2B, RAB5A, RAB9A, RAB27A and RAB27B were found to be involved in exosome secretion (Ostrowski et al. 2010). In the same study, RAB27B and RAB27A were shown to allow mobility and docking of MVBs to the PM, respectively. Several other studies have confirmed the reduction of exosome release upon Rab27a silencing in different cell lines, which has become a common strategy of modulating exosome secretion (Ostrowski et al. 2010). Moreover, in K562 cells RAB11 has been mostly known for its role in recycling cargo proteins from early endosomes to the plasma membrane (Savina et al. 2005) and RAB35 seems to have a role in the docking and tethering of MVBs to the PM in oligodendroglial cells (Hsu et al. 2010).

The final step of exosome release requires the fusion of MVBs with the plasma membrane which is mediated by SNARE (soluble N-ethylmaleimide-sensitive fusion attachment protein receptor) complex. The members of this protein family are classified as either R- or Q-SNAREs. Commonly, fusion is mediated by one R-SNARE and three Q-SNAREs. An R-SNARE on the MVB membrane comes together with a Q-SNARE complex, containing two to three Q-SNAREs, on the plasma membrane to form a trans-SNARE complex. This creates close proximity for the two membranes

leading to the formation of a fusion pore allowing the release of ILVs (Pfeffer 2010; Js and Bs 2004; Murray and Stow 2014). The SNARE proteins VAMP7 , YKT6 and SNAP23 were identified as key players in the secretion of exosomes in K562, HEK293 and HeLa cells, respectively (Palmulli and van Niel 2018). As mentioned earlier, in our team, Hyenne, et al. showed in *C. elegans*, the Ras-related GTPase homologue Ral-1 is involved in MVB biogenesis and fusion with the plasma membranes together with the Q-SNARE syntaxin 5 (Hyenne et al. 2015). In addition, actin cytoskeleton mediates the docking and fusion of MVBs with the PM, thus affecting exosome release. The actin regulatory protein cortactin has been shown to regulate exosome secretion by mediating both trafficking and docking of MVBs to the PM via the interaction with the small Rab GTPase, RAB27A and coronin1b (Sinha et al. 2016). The microtubule network which contributes to the overall intracellular organization is probably required for the transport of MVBs to the plasma membrane (Tuanlao Wang et al. 2011, 7). **In addition to the molecular mechanisms of EV secretion by donor cells, it is also important to understand the processes by which they are taken up by their target cells.**

2.5 EVs & recipient cells

The uptake of EVs by their target cells dependent on the type of the target cell, its physiological state, and whether ligands on the surface of the EV recognize receptors on the surface of the cell or vice versa (Mulcahy, Pink, and Carter 2014). In this process, **the first step is the binding of EVs to the surface of the target cells** which is likely to be mediated by specific interactions between proteins enriched at the surface of extracellular vesicles and receptors at the plasma membrane of the recipient cells (Morelli et al. 2004; Nazarenko et al. 2010). The exact cellular and molecular basis for the specific targeting to acceptor cells is still unclear. Several mediators of these interactions are known, such as tetraspanins, integrins, lipids, lectins, heparan sulfate proteoglycans and ECM components, and some data are available. For example, integrins on EVs can interact with adhesion molecules such as intercellular adhesion molecules (ICAMs) at the surface of recipient cells (Morelli et al. 2004). In addition, the interaction of integrins with EMC proteins, mostly fibronectin and laminin, has been shown to have important roles in exosome, and microvesicle binding to recipient cells (Sung et al. 2015; Purushothaman et al. 2016; Leiss et al. 2008). Exosomal tetraspanins can also mediate the binding process via interaction with integrins

and ultimately promote exosome docking and uptake by selected recipient cells (Mulcahy, Pink, and Carter 2014). Other molecules such as heparan sulfate proteoglycans and lectins, both present in EVs and at the plasma membrane, mediate the binding of these vesicles to recipient cells. For example, Glypican 1, a cell surface proteoglycan that bears heparan sulfate, and CD44, a cell surface glycoprotein involved in cell–cell interactions, are mediating exosome and microvesicle docking, respectively (Melo et al. 2015; Bruno et al. 2009). Lipid composition of EVs could also regulate cell targeting. For example, phosphatidylserine can recruit specific lipid binding proteins such as galectin 5 or annexin 5 that then induce docking of vesicles to the target cell membrane(van Niel, D'Angelo, and Raposo 2018). **After binding to the target cells, EVs may remain at the plasma membrane or may internalize** by clathrin-mediated or clathrin independent endocytosis, such as macropinocytosis and phagocytosis as well as through endocytosis via caveolae and lipid rafts (Figure.10) (Mulcahy, Pink, and Carter 2014).All these processes have specific characteristics with some functional overlap between them. Phagocytosis depends on specific receptors and mechanisms that are present primarily in specialized cells, which envelope EVs in phagosomes, eventually directing the cargo toward the lysosome (Gonda et al. 2019).

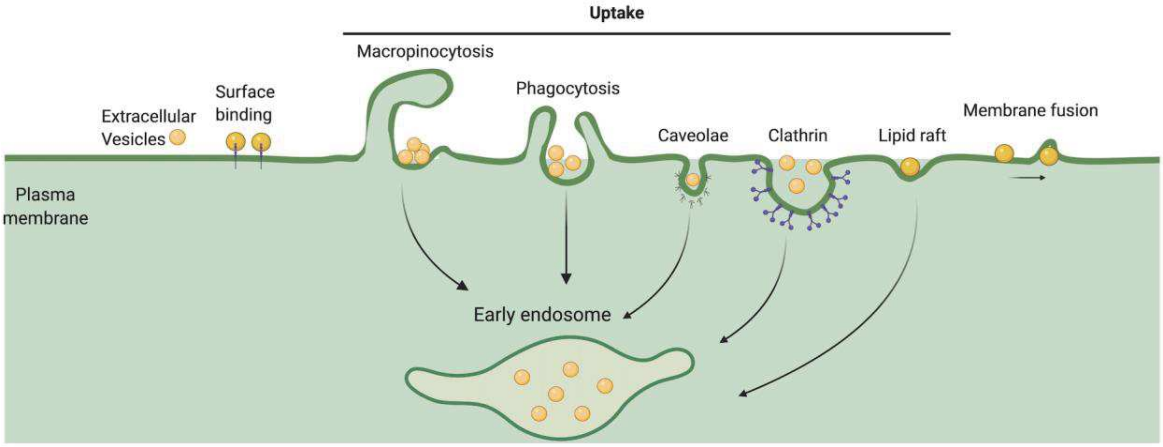

Figure 10. The uptake of EVs by their target cells. In the recipient cell (which can be the producing cell itself), exogenous EVs will bind to the cell surface and can undergo several internalizations including clathrin-mediated or clathrin independent endocytosis, such as macropinocytosis and phagocytosis as well as through membrane fusion or endocytosis via caveolae and lipid rafts. **Adapted from** (van Niel, D'Angelo, and Raposo 2018). Created with BioRender.com

Macropinocytosis on the other hand consists of membrane ruffles in which molecules are internalized unselectively from the extracellular space (Lim, 2011). However, it has been shown

that some exosomes induce macropinocytosis internalization and increase uptake by selectively activate this mechanism (Nakase et al. 2016; Costa Verdera et al. 2017). Other endocytosis focuses on specific cellular proteins such as clathrin and caveolin (cytosolic proteins) that form specific pits to internalize substances (Conner and Schmid 2003). Particle size and cell type seem to play a role on why and when a cell uses clathrin, caveolin, or neither however, the exact mechanism is still incompletely understood (Gonda et al. 2019). **Once docked at the plasma membrane, EVs can provoke functional responses** through binding to and activating receptors expressed on the recipient cells. For examples, EVs from B cells and dendritic cells induce a specific antigenic response by presenting antigens to T cells (Zitvogel et al. 1998; Graca Raposo 1996).

After internalization, cargo delivered by EVs can also activate many responses and processes in the recipient cell. For example, in dendritic cells, protein cargoes of EVs from intestinal epithelial cells (Mallegol et al. 2007) or other dendritic cells (Morelli et al. 2004) are processed in the endocytic compartment similarly to antigens and then used in antigen presentation, thus regulate the immune response. EVs could also fuse directly with the plasma membrane of recipient cells and ultimately release intraluminal content in the cytoplasm of recipient cells, a key step to support the release of miRNA and mRNA from EVs into recipient cells to regulate gene expression. The direct fusion of EVs with the membrane of recipient cells also enables the exchange of trans membrane proteins and lipids (Figure.10) (van Niel, D'Angelo, and Raposo 2018). **Altogether, we have discussed most of the important aspects of EVs from their composition to their biogenesis and uptake. Each of this aspect is crucial in understanding the biological and pathological roles of EVs.**

2.6 Biological, pathological, and clinical aspects of EVs

In this part, I quickly overview the biological, pathological, and clinical aspects of EVs in a non-exhaustive manner. Despite most of the literature mainly focusing on the roles of EVs in pathological conditions, there are evidence on the role of **EVs are also known as natural vehicles of biological cargo** with a crucial role in tissue homeostasis and repair (Roefs, Sluijter, and Vader 2020). EVs are able to **prevent cell death**. For example, EVs from bone marrow stem cells or cardiac progenitor cells can reduce apoptosis in myocardial cells after ischemia and reperfusion

injury(R. C. Lai et al. 2010). In addition, EVs have a role in **immune modulation**. For example, EVs derived from several immune cells, contain molecules typical of the immune system such as MHC-II molecules (Graca Raposo 1996), interleukin 15 receptor α-chain (Viaud et al. 2009), CD86 and ICAM-1(Segura et al. 2005). All these molecules have an impact on different immunological functions including induction of antigen-specific T cells response (Segura et al. 2005; Admyre et al. 2007; Théry, Zitvogel, and Amigorena 2002) promotion of NK cell proliferation (Viaud et al. 2009) and DCs maturation (D et al. 2001). Another role of EVs is **neovascularization** during recovery after ischemia/reperfusion injury and cutaneous wound healing. It has been shown neovascularization can be stimulated by the administration of EVs released from the different stem and progenitor cells 9/9/2021 6:47:00 PM. Furthermore, in response to stress or injury, healthy cells can release EVs containing bioactive proteins that **promote cell proliferation and migration** (Roefs, Sluijter, and Vader 2020). For example, in joint regeneration, CD73 present on EVs from embryonic stem cell-derived MSCs contribute to chondrocyte proliferation, migration, and ECM(S. Zhang et al. 2018). In addition, in neuronal communication (J et al. 2006) EVs promote axonal regeneration upon sciatic nerve injury (Lopez-Verrilli, Picou, and Court 2013). In addition to their biological role, **EVs are involved in the pathological** development and progression of many diseases. For example, EVs are associated with the generation and progression of **neurodegenerative diseases.** Increasing evidence indicates that EVs are potential carriers of misfolded proteins, whose accumulation cause neurodegenerative disorder (Kalani, Tyagi, and Tyagi 2014; Russo, Bubacco, and Greggio 2012). In **alzheimer's disease,** for instance, EVs containing β-amyloid, the toxic protein responsible for the formation of amyloid plaques, enhanced its deposition in various part of the brain (Rajendran et al. 2006). Moreover, the role of EVs in tumor biology have been extensively investigated which will be carefully reviewed later in this part (Hyenne, Lefebvre, and Goetz 2017). There has been also significant progress in the **potential clinical applications of EVs**. EVs are now being considered as an important tool for **drug delivery cargos**. For example, EVs from MSCs have been tested as the vehicle to package and transport active drugs such as paclitaxel with increased anti-tumor effects (Pascucci et al. 2014). The utilization of exosomes as drug delivery vehicles offers important advantages compared to other nanoparticulate drug delivery systems such as being non-immunogenic in nature due to similar composition as body′s own cells (Cordonnier et al. 2017).

Furthermore, publication frequencies of studies investigating different contents of EVs as **biomarkers** for disease diagnosis over the past 10 years attracted the greatest interest in EVs research (B. Zhou et al. 2020). Moreover, EVs has been also considered as major candidates for **non-invasive diagnosis** in cancer with significant superiority over other sources of liquid biopsy due to their presence in almost all body fluids and possessing high stability by encapsulating with lipid bilayers (Melo et al. 2015; Hoshino et al. 2015; B. Zhou et al. 2020). For example, it has been shown that circulating exosomes derived from melanoma patients express PD-L1 on their surface which could be considered as a better marker than PD-L1 expression in tumour biopsies and a good way to predict the tumour response to treatment (more explanation regarding PD-L1 will be provided in section 2.7.2)(Cordonnier et al. 2020). It has been also demonstrated that exosomal Hsp70 is a valuable biomarker of tumor presence, progression or recurrence (Chanteloup et al. 2020). Very recently, in a most complete proteomic study, several EV associated proteins have been identified were tumor type-specific (breast, colorectal, lung, and pancreatic cancer) regardless of disease stage (Hoshino et al. 2020). Lyden's group provided proof-of-principle that tumor EVs signature, which they refer to as extracellular vesicles and particles (EVPs), can be considered as cancer biomarkers. They identified protein signatures that not only distinguish between tumour and nonmalignant EVPs in plasma but also distinguish EVPs obtained from different human tumour types (Hoshino et al. 2020). **Since the center of my focus in my PhD is understanding the role of EVs in cancer metastasis, in the next part I will discuss the role of EVs in cancer.**

2.7 Role of EVs in cancer

EVs play a crucial role in cancer. Initially, tumor EVs were shown to induce an antitumoral immune response through the activation of dendritic cells and T lymphocytes (Zitvogel et al. 1998). However, since this initial discovery, most of the studies have established pro-tumoral roles for tumor EVs including promoting tumor growth and metastasis (Möller and Lobb 2020). Tumor cells release large amounts of EVs bearing tumoral markers, which can subsequently disseminate at distance(Hoshino et al. 2020). Despite their striking importance in tumor progression, the exact contribution of tEVs in local and distant modifications of the microenvironment *in vivo* remains to be fully deciphered. **In this part, I'm focusing on EVs**

secreted by tumor cells and will describe their involvement in primary tumor microenvironment and metastasis.

2.7.1 Involvement of EVs in the primary tumor microenvironment

As I have mentioned in the cancer part, EVs are an important part of TME. Both tumor EV (tEVs) and non-tumor EVs act as effective signaling molecules between cancer cells and the surrounding cells that make up TME and mediators of cancer therapy resistance (I. Li and Nabet 2019).

Role of non-tumor EVs in the primary tumor microenvironment

As cargo carriers, **EVs are also involved in the maintenance of cancer stem cells (CSC)** homeostasis and its mechanism as well as the transformation between non- CSC and CSC (Dai et al. 2020). EVs are also important participants in the resistance of CSCs, which involving multiple mechanisms, such as enhanced DNA repair efficiency and anti-apoptotic capacity (K. Wang et al. 2016). For example, in breast cancer, RAB27B promoted exosomes transfer from stromal cells to the breast cancer cell. These exosome contain 5′-triphosphates which activate the RIG-I (retinoic acid-induced gene 1 enzyme) signal in target cells, thus activating IRDS (Interferon-Related DNA Damage Resistance Signature) genes, in parallel to the NOTCH3 pathway activation to regulate the expansion of CSCs which are therapy-resistant tumor-initiating cells (Boelens et al. 2014). **EVs released by MSCs in the TME facilitate the alteration of non-CSC to CSC** and promote tumor progression by transporting special miRNA cargo to neighboring cells. For example, EVs from bone marrow-derived MSCs containing miR-214 inhibit oxidative stress injury in CSC, thus helping tumor progression (A. Sharma 2018). **Cancer-associated fibroblast (CAF)-derived EVs are also one of the key factors of oncogenic transformation (Zhao et al. 2016)**. CAF-derived EVs not only promotes the growth of cancer cells, but also promote drug resistance and tumor metastasis (Zhao et al. 2016; T.-X. Huang, Guan, and Fu 2019). For example, CAF-derived EVs promote angiogenesis and tumor development in colorectal cancer and also induce the dedifferentiation of cancer cells through the Wnt pathway, which leads to the chemical resistance of CRC (Hu et al. 2019; Savardashtaki et al. 2019).

Role of tumor EVs in the primary tumor microenvironment

In the primary TME, due to heterogeneity of cancer cells, there are different genetically and phenotypically subclones which can **transfer oncogenic traits via tEVs to neighboring cancer cells** to modify their biological phenotypes. For example, glioma cells transferred EVs with the oncogenic receptor EGFRvIII to neighboring glioma cells lacking this receptor, thereby enhancing tumorigenesis of these cells by activating the AKT pathway in them (Al-Nedawi et al. 2008). Similarly, Mutant KRAS, along with other oncogenes such as EGFR and SRC, can also be transferred via exosomes to recipient colon cancer cells of wild-type KRAS, promoting tumor invasion (Becker et al. 2016). Importantly, a recent study shows that Apoptotic glioblastoma cells release apoptotic extracellular vesicles that transfer various components of spliceosomes to change the mRNA splicing in recipient cells and promote their drug resistance as well as migration capacity(Pavlyukov et al. 2018). **tEVs not only transfer oncogenic traits between cancer cells but also transfer between cancer cells and stromal cells**. For instance, it has been shown MVs from MDA-MB-231 breast cancer cells confer normal fibroblasts and epithelial cells with transformed characteristics of cancer cells such as increased proliferation, survival, and anchorage-independent growth of immortalized fibroblasts and normal mammary epithelial cells(Antonyak and Cerione 2014). These effects were shown to be mediated by a cross-linked form of fibronectin present on the surface of MVs, which engaged integrins expressed on the recipient fibroblasts and mammary epithelial cells thus stimulated signaling events that promoted their growth under anchorage-free conditions (Antonyak and Cerione 2014). **Moreover, in TME, the tEVs cargoes stimulate the immune response** through alarmins (mRNA, transmembrane proteins including CD9, CD63, and CD81, HSPs, major histocompatibility complex I molecules) and tumor-associated antigens (Ramos-Zayas et al. 2019). The antigen-presenting and immune-stimulating properties of tEVs allow them to trigger anti-tumor responses and contribute to the recruitment and reconstruction of TME components (Jan et al. 2019). Many findings also support a key **role of tEVs between cancer cells and the surrounding vasculature by eliciting pro-angiogenic responses** (Groza et al. 2020). For example, exosomes were shown to reflect the hypoxic status of glioma cells by inducing microvasculature sprouting and vascularization during tumor formation in xenografts models (Kucharzewska et al. 2013). Under hypoxia conditions, multiple myeloma cells and 4T1 breast cancer cell line also increase the secretion of exosomes enriched in

miR-210 and miR-135b respectively, which increases endothelial tube formation to promote angiogenesis (King, Michael, and Gleadle 2012; Umezu et al. 2014). In further support of the EVs role during angiogenesis, Grange et al. have reported that CD105-positive renal carcinoma cells secrete EVs, which induce proliferation of HUVECs *in vitro* and *in vivo* (Grange et al. 2011). Exosomal Annexin A2 is found in greater amount in EVs from a malignant breast cell line, compare to the normal breast epithelial cells and promote the migration of endothelial cells in a tissue plasminogen activator tPA-dependent manner thus leading to angiogenesis (Chaudhary et al. 2020). In addition, it has been reported neutral sphingomyelinase 2 (nSMase2) affect exosomal miRNA secretion in metastatic breast cancer cells. Specifically, exosomal angiogenic miRNAs such as miR-210 that is transferred to endothelial cells, where it enhances the capillary formation and migration capability. Exosomal miR-210 might be one of the key factors for tumor angiogenesis and its high expression predict poor survival in breast cancer patients (King, Michael, and Gleadle 2012; Kosaka, Yoshioka, et al. 2013). **Altogether, tEVs not only alter the cellular physiology of the surrounding cells but also has an impact on distant non-tumor cells to allow dissemination and growth of cancer cells which ultimately lead to metastasis.**

2.7.2 Involvement of EVs in metastasis

The initiation of metastasis includes the local invasion of primary tumor cells into the surrounding tissues through the remodeling of the extracellular matrix (ECM) and the gaining migratory behavior (Figure 11). The contribution of EVs in all these steps has been summarized below: **First, tumor EVs are capable of carrying important ECM molecules thus controlling cell polarity and directional cell movement** (Adem, Vieira, and Melo 2020). Sung et al. reported that exosomal fibronectin bound with cellular integrin receptors form a strong adhesion at the leading edge to promote cell migration (Sung et al. 2015). The same group later showed that **tumor EVs not only increase cell migration speed but also promote directional movement towards a chemotactic gradient**, although the exact mechanisms are unknown (Sung and Weaver 2017). Luga and colleagues showed that EVs from cancer-associated fibroblasts also stimulate protrusive activity and motility in recipient breast cancer cells by activating autocrine WNT-planar cell polarity signaling (Luga et al. 2012). **Second, tumor EVs can directly degrade ECM which lead**

to an enhanced cell invasion and metastasis. For example, Hendrix et al. (2010) demonstrated that Rab27b-mediated exocytic release of HSP90 EVs from metastatic breast cancer cells activates matrix metallopeptidase 2, a protease that degrades the ECM (Hendrix et al. 2010). **Third, tumor EVs could promote recipient cells' epithelial-mesenchymal transition (EMT)**, during which ECM is degraded and tumor cells lose their epithelial features and gain mesenchymal properties by losing E-Cadherin and cell polarity while gaining N-cadherin, twist, snail, and vimentin to become more invasive. Several proteins, signaling molecules and miRNAs, regulating EMT, have been identified in the cargos of EVs such as HIF1α, matrix metalloproteinase 13, casein kinase II α, annexin A2, and latent membrane protein 1, TGF-β, β-catenin, IL-6, caveolin-1 or vimentin and nucleic acids like EMT-inducer miRNAs (Aga et al. 2014; Jeppesen et al. 2014; Yoshizaki et al. 2013).

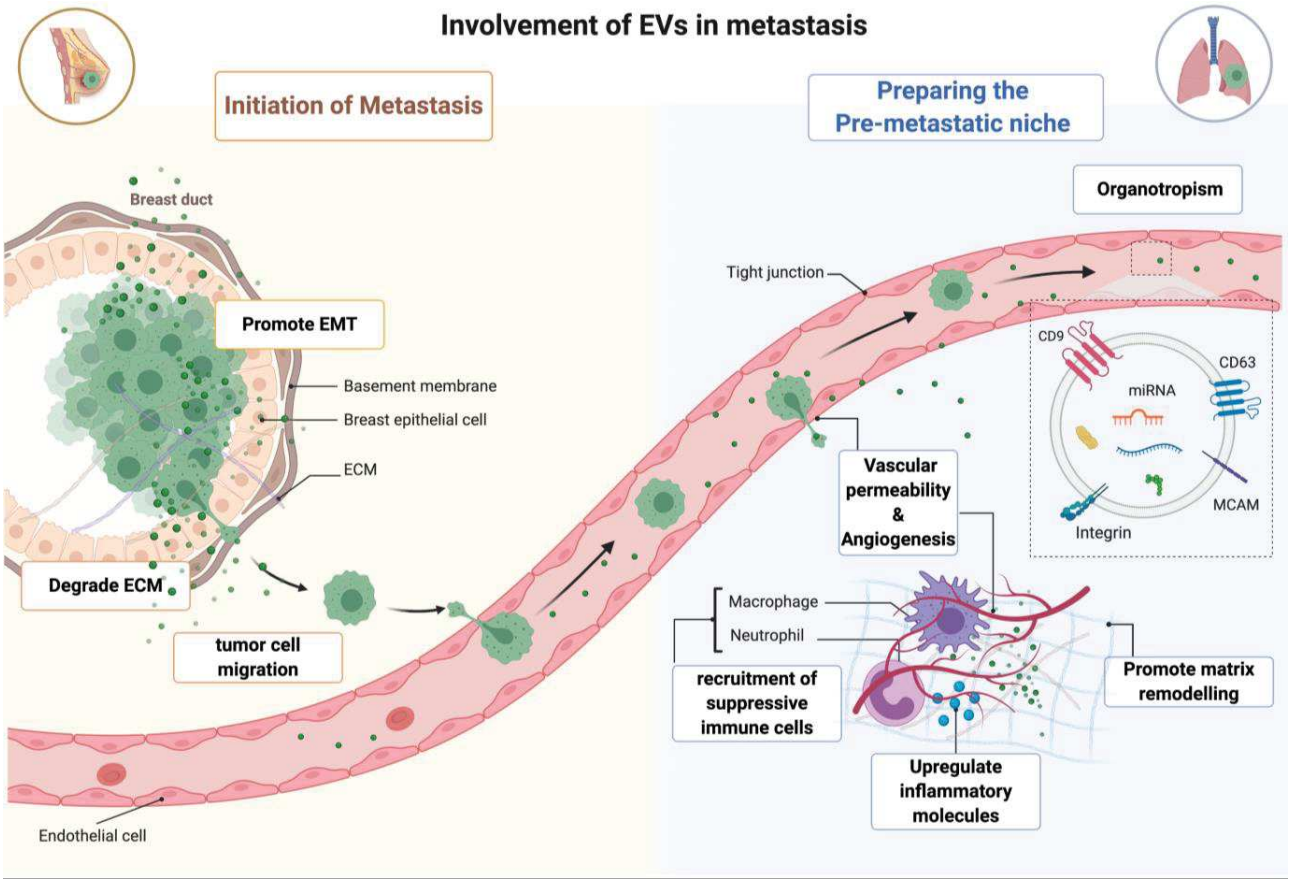

Figure 11. **EV-mediated metastasis**. EVs are involved in the initiation of metastasis, which lead to invasiveness and motility of tumor cell and clearance of natural barriers against metastases. EVs are also involved in the preparation of a pre-metastatic niche, via the recruitment of BMDCs and induction of ECM remodelling and angiogenic processes. **Inspired by** (Syn et al. 2016). Created with BioRender.com

Finally, tumor EVs influence the processes of intravasation and extravasation. EVs are able to unlock the tight junctions and increase the endothelial permeability to enhance tumor cells intravasation via miR-105 which reduce the expression of ZO-1 in recipient endothelial cells (W. Zhou et al. 2014). Recently, it has been demonstrated that exosomal Met (oncoprotein)contributes to a leaky vasculature and, ultimately promotes the intravasation and extravasation of cancer cells. This study further showed that Met-high subpopulations in melanoma cells develop vascular structures lacking pericytes (Adachi et al. 2016). However, how tEV pass the endothelial barrier is not very well known yet. Recently, it has been shown that tEVs can directly breach the blood–brain barrier (BBB) via transcytosis (Morad et al. 2019). Other mechanisms could also help EVs to pass through the endothelium such as a direct transition between endothelial cells through gap junctions or pores, or even the involvement of immune cells such as monocyte (Adem, Vieira, and Melo 2020).

In addition to the above-mentioned factors, several publications indicate the essential role of EVs in the **preparation of the pre-metastatic niche** and establishment of the tumor (Figure 11). If tumor cells are seeds and the pre-metastasis niche is the soil, then circulating EVs released from tumor cells can be seen as fertilizers, which can make the barren land fertile and facilitate the colonization of tumor cells. Recent work by Lyden and colleagues on exosome-mediated metastasis has partially supported this hypothesis. According to their findings, tumor EVs expressing specific integrins on their surface including α6β1, α6β4, αvβ5, and αvβ3 which are associated with ECM molecules, such as laminin and fibronectin, and certain cell types in target organs, partially dictated future PMNs at lung, liver, and brain **organotropic sites**, respectively (Hoshino et al. 2015). Moreover, using reporter systems under the control of the CRE recombinase demonstrated that vesicle enclosed CRE mRNA can be transferred and translated into functional protein *in vivo*. Using this methodology together with intravital imaging provided direct proof for the ability of tumor derived EVs to signal over long ranges (Zomer et al. 2015). **EVs also upregulate inflammatory molecules.** As it has been mentioned previously chronic inflammation is an essential factor for tumor development and metastasis. Thus, the local inflammatory microenvironment is important for pre-metastatic niche formation. Lyden and colleagues showed exosomal integrins upregulate the expression of proinflammatory S100 molecules in the distant tissue microenvironment via activating Src phosphorylation(Hoshino et al. 2015). **Moreover, EVs**

promote matrix remodeling. Several kinds of BMDCs have been shown to stimulate matrix remodeling in the PMN, and upregulation of fibronectin(Y. Gao et al. 2019; Kaplan et al. 2005). For example, Costa-Silva showed exosomes from pancreatic cancer cells contribute to the establishment of PMN in the liver by transferring macrophage migration inhibitory factor (MIF) to Kupffer cells. MIF induces the release of TGF-β from Kupffer cells, which in turn promotes the production of fibronectin and recruits bone marrow-derived macrophages for liver pre-metastatic niche formation (Costa-Silva et al. 2015). Another study from the same group also showed that the uptake of breast cancer exosome by lung fibroblasts stimulates their activation and fibronectin secretion (Hoshino et al. 2015). Additionally, Toll-like receptor3 (TLR3) activation in lung epithelial cells by non-coding small nuclear RNAs transferred by tEVs promote expression of S100A8, S100A9, MMP9 and fibronectin, which, in turn, contributes to lung PMN formation. Upregulation of TLR3 also promotes secretion of chemokines that mobilize neutrophils (CD45+CD11b+Ly6G+Ly6Cint c-Kit+ VEGFR1+), as well as macrophages (F4/80+) and monocytes (VEGFR1+Ly6G−Ly6C+) that further support PMN formation(Yanfang Liu et al. 2016). In a rat pancreatic adenocarcinoma model, exosomal CD151 and Tetraspanin 8 (Tspan8) enhance PMN formation and promote metastases in lungs and bone marrow, most likely through extracellular matrix remodeling. Interestingly, EVs deprived of Tspan8 have a reduced capacity to cross the blood-brain barrier *in vivo*(Yue et al. 2014). Increased **angiogenesis and vascular permeability** by EVs are other factors that promote the formation of PMN. Here I will mention a few examples. It has been reported EVs derived from hypoxic tumors have more potential to promote angiogenesis and vascular leakage (Kucharzewska et al. 2013). Grange et al. found that human kidney cancer stem cell-derived CD105-positive MVs induce angiogenesis and facilitate the metastatic niche formation (Grange et al. 2011). In mice, exosomal miR-181c from breast cancer metastatic cell lines disrupted cell-cell contact in the BBB by downregulating the actin regulator, PDPK1, leading to an increased brain metastatic burden (Tominaga et al. 2015). Furthermore, exosomal miR-25-3p from colorectal cancer cells promote angiogenesis and disrupt the tight junctions of vascular endothelial cells by targeting KLF2 and KLF4. The miR-25-3p further induce vascular leakiness and facilitate the PMN formation in the liver and lung of mice (Zeng 2018). EVs can also induce the **recruitment of suppressive immune cells** to the PMN. For example, the recruitment of BMDCs to lung PMNs is being induced by EVs (Peinado et al. 2012).

Wen, et al. found that EVs also promoted the accumulation of myeloid-derived suppressor cells and directly inhibiting T-cell growth and decreasing Natural killer (NK) cell cytotoxicity (Wen et al. 2016). Mature DCs also played important roles in antitumor immunity by presenting tumor antigens, but four known immunomodulatory proteins have been identified in melanoma EVs, the combination of which reduces DC maturation in the lymph node. This study shows the importance of exosome-mediated immune suppression since LN metastasis is critical for the progression of melanoma to metastasis (Maus et al. 2017).

EVs also serves as a vehicle for transport of programmed death-ligand 1 (PD-L1) into receptor cells. PDL1 is a membrane-bound ligand found on the cell surface of many tumor cells and binds programmed cell death protein-1 (PD-1) on T cells to suppress their activation (Tang et al. 2020). One study showed the presence of glioblastoma-derived EVs carrying PD-L1 in the plasma of glioblastoma patients were positively correlated with tumor burden (Ricklefs et al. 2018). Another study reported in breast cancer exosomal PD-L1 promote tumor evasion of immune surveillance by transferring PDL-1 to other cancer cells with low- or no- PD-L1(Y. Yang et al. 2018). The third study reported an increased circulating exosomal PD-L1 from human melanoma, breast cancer, or lung cancer. Thus, when the EVs containing PD-L1 reach the PMN, the immune system could be inhibited leading to the promotion of PMN formation(G. Chen et al. 2018). Additionally, it was reported that B16F10 melanoma exosomes contained small nuclear RNA from lung cancer or melanoma promoted lung PMN by activating TLR3 and releasing cytokines which recruited neutrophils to the lung (Yanfang Liu et al. 2016, 3). In contrast, EVs derived from non-metastatic melanoma cancer cells are not capable to generate PMN in the bone. However, these EVs promoted the expansion, recruitment, and differentiation of TRAIL-positive tumor-reactive macrophages, which kill and phagocytize tumor cells, contributing to cancer cell clearance at PMN (Plebanek 2017). In another study, tEVs derived from parental lung cancer cells contained miR-192, which inhibited interleukin 8 (IL8), intercellular adhesion molecules, and CXCL1 in the endothelial precursor cells of the bone microenvironment, thus decreasing tumor-induced angiogenesis *in vivo*. However, the EVs from metastatic cells with less miR-192, promoted bone-metastasis niches formation (Valencia et al. 2014).

In conclusion, all these studies on the role of EVs in cancer show that both the levels and the content of secreted tumor EVs are crucial in promoting metastasis. There also studies on how the

EV secretion machinery controls the pro-metastatic properties of tEVs. For example, as I have discussed earlier **Rab27A** that control exosome secretion(Ostrowski et al. 2010), also promotes breast and melanoma tumor growth and metastasis in mice(Bobrie et al. 2012; Peinado et al. 2012) and predicts poor survival in human pancreatic cancer (Q. Wang et al. 2015).These studies allowed the identification of Rab27A as a key driver of EV biogenesis and tumorigenesis. Two other RAB GTPases **RAB22A and RAB3D** known to regulate EV formation have been similarly used in breast cancer cells to determine the role of EVs in tumor progression(Ting Wang et al. 2014; J. Yang et al. 2015). Depletion of RAB22A decreased their capacity to secrete EVs under hypoxia *in vitro* and impairs their ability to form lung metastasis in mice(Ting Wang et al. 2014). Similarly, downregulation of RAB3D decreased EVs secretion in breast cancer cells *in vitro*, and in parallel reduced breast cancer cell invasion and lung metastasis in mice (J. Yang et al. 2015). Moreover, overexpression of **Sphingomyelinase nSMase2** breast cancer cells leads to more EVs secretion *in vitro* and promote lung metastasis through an increase in angiogenesis once injected in mice(Kosaka et al. 2010; Kosaka, Iguchi, et al. 2013). Altogether, these studies generally correlate the levels of secreted EVs by tumor cells and the capacity of these cells to form tumors and metastasis in mice. Along this line, **in my PhD project, we identified Ral GTPase from its function in EV biogenesis up to its pro-metastatic function in breast cancer.**

3 Ral GTPases

I established my PhD project on top of the study by Vincent Hyenne who already showed Ral GTPase are evolutionarily conserved regulators of exosome secretion (Hyenne et al. 2015). We originally observed that, in the nematode *C. elegans*, the Ral GTPase ortholog RAL-1 controls exosome secretion by acting on the biogenesis of MVBs. Although Ral genes and proteins are highly conserved across species, invertebrates, such as the fruit fly Drosophila melanogaster and the nematode *Caenorhabditis elegans* only possess a single Ral gene (Gentry et al. 2014). Importantly, Ral-1 has 2 orthologs in mammals (RalA and RalB), which function downstream of RAS (Chien and White 2003). RalA and RalB have been known as closest relatives of the classical Ras proteins and share a high structural similarity with RAS. In this section, I will discuss Ral GTPase in more details by focusing on its regulator in **section 3.1**. Then I continue in **section 3.2** by including the important effectors of Ral and their function. In **section 3.3** I will talk about

the role of Ral GTPase in normal physiology. Finally, in **section 3.4** I discuss the contribution of Ral GTPase in cancer.

3.1 Ral Regulators

Ral GTPases share general structural and biochemical features with Ras and other small GTPases, consisting of six b-sheets connected by loops and five a-helices, which form the highly flexible switch I and switch II regions (Gentry et al. 2015). Like Ras, Ral proteins terminate in carboxyl terminal CAAX tetrapeptide motifs (C = cysteine, A = aliphatic amino acid, and X = terminal amino acid; Ral amino acids), which signal for a series of posttranslational modifications that facilitate intracellular trafficking and are critical for the membrane association of RAL. The tertiary protein structure of both RALA and RALB proteins is very similar; containing a free-floating N-terminal 11-amino acid sequence, followed by the G-domain, involved in GDP/GTP binding, and the C-terminal membrane targeting sequence (Cox et al. 2014). Although RalA and RalB share more than 82% identical sequence, they have distinct C-terminal sequences, which can influence subcellular membrane localizations as well as effector interactions(C. Yan and Theodorescu 2018).

GTP-GDP Cycling

The specific set of guanine nucleotide exchange factors (GEFs) promote GDP to GTP exchange on Ral proteins to activate them in response to specific signals. Activated GTP-bound Ral proteins then bind to and modify the activity of a unique set of downstream target proteins that mediate their functions in cells. In addition, specific GTPase-activating proteins (GAPs) promote GTP to GDP hydrolysis on Ral family members to deactivate them. Seven GEFs and two GAPs have been identified as regulating Ral GTPases (Figure.12). Seven known RALGEFs can be divided into two groups. The first group (RALGDS, RGL1, RGL2, RGL3) directly bind to the effector binding region of activated RAS thus relies on RAS activation, while the other group (RALGPS1, RALGPS2, RGL4) can be activated through RAS-independent mechanisms (Gentry et al. 2014). However, RAL specific GAP proteins (RALGAP1 and RALGAP2) are not very well known.

RALGAPs are supporting an inhibitory role on RAL activity (Shirakawa et al. 2009; X.-W. Chen et al. 2010, 20).

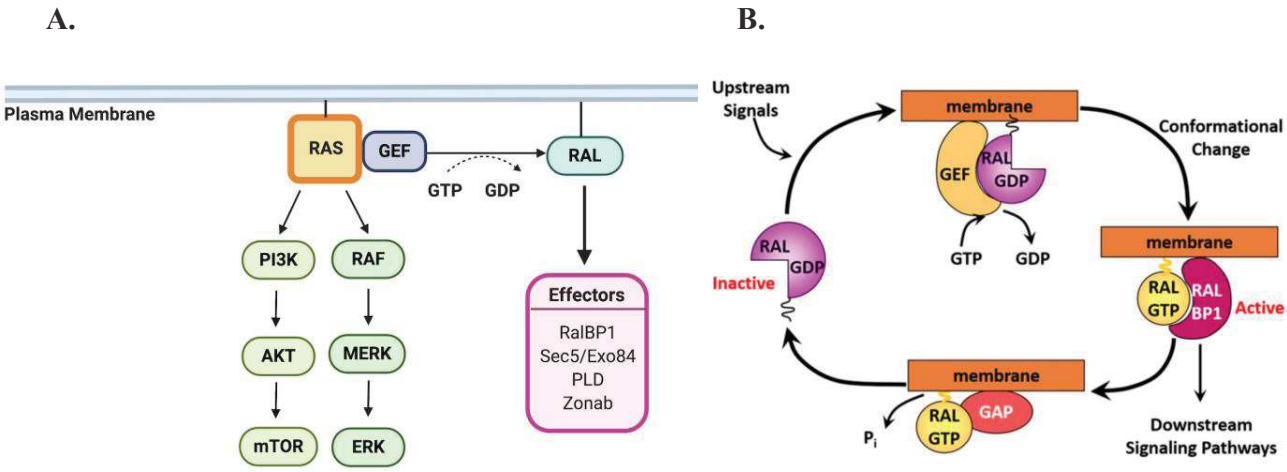

Figure 12. A. The three most characterized effector signaling pathways downstream of RAS, Adapted from (C. Yan and Theodorescu 2018)**B. The GDP-GTP cycle of Ral GTPases.** Upstream signals stimulate binding of RALGEF that triggers GDP-GTP exchange, leading to Ral activation. Then, RAL-GTP can bind to its downstream effector proteins (e.g. RALBP1). Ultimately, RALGAPs bind to RAL-GTP and hydrolyze GTP to GDP, cycling RAL back to its inactive GDP-bound form, **Extracted from** (C. Yan and Theodorescu 2018). Created with BioRender.com

Posttranslational Modifications

Prenylation of the CAAX motif was shown to be essential for Ral membrane association and subcellular localization (Gentry et al. 2015). Similar to Ras, Ral GTPases terminate in a CAAX motif which signals for post-translational modifications and membrane addressing. The CAAX-signaled modifications are critical for Ral function. The crucial step of the posttranslational modifications is the covalent addition of an isoprenoid lipid to the first cysteine residue by the geranylgeranyl- transferase-I (GGTase-I). The AAX residues were then cleaved and the terminal lipid-modified cysteine methylated (Bodemann and White 2008).

Phosphorylation of RAL at the C-terminal region also plays an important role in the regulation of RAL activity. Phosphorylation of RALA by Aurora A relocates RALA from plasma membrane

to endomembranes where RALA interacts with RALBP1 mediating RALA anchorage-independent growth (Lim et al. 2010). Phosphorylation of RALB by protein kinase C translocated RALB from plasma membrane to the perinuclear region of the cell which is required for RALB-mediated migration and metastasis(Martin et al. 2012).

3.2 Ral Effector Proteins

Like RAS, after activation, RAL exerts its biologic function via interaction with various effector protein and regulate different downstream pathways. A number of effector proteins have been identified that bind to Ral proteins, but it has been a challenge to determine the differences between RalA and RalB in effector engagement and how those differences are regulated(Moghadam et al. 2017). Furthermore, there is a lack of knowledge on which effectors preferentially engage Ral proteins under different physiological conditions and how these dynamics are regulated. Below I have summarized some effectors and how each of these effector pathways contributes to cellular physiology.

RAL Binding Protein 1/RLIP76: RAL binding protein 1 (RALBP1, also known as RLIP or RLIP76) was the first identified Ral binding partner was (synonyms: RLIP76 and Rip1) with a RAL binding domain that binds to both switch I and II regions of RAL-GTP (Fenwick et al. 2010). The binding surfaces on RalBP1 that contact RalA and RalB are not identical, even though RalA and RalB are 100% identical in their contact sites for binding RalBP1 (Campbell et al. 2015). RalBP1 is a large protein (76 kDa) and has a vast array of functions ranging from receptor mediated endocytosis to facilitating mitochondrial fission during mitosis (Jullien-Flores et al. 2000; Kashatus et al. 2011). RalBP1-Ral interaction also involves Ral in regulating actin cytoskeleton changes. For example, RalBP1 exhibits GAP activity toward CDC42 and Rac1, which stimulates filopodia and lamellipodia formation, respectively. In addition, the Ral-RalBP1 interaction involve in receptor-mediated endocytosis where RalBP1 binds two Eps homology (EH) domain-containing proteins: POB1 and Reps15. Moreover, RalBP1 also binds to the m2 subunit of AP2, which recruits clathrin to the sites of endocytosis (Jullien-Flores et al. 2000; Nakashima et al. 1999). However, whether Ral promotes or inhibits endocytosis is not well known and additional studies will be required to determine the exact role of the Ral-RalBP1 interaction in endocytosis

SEC5/EXOcyst Complex 84: Octameric protein complex termed the exocyst is the major effector of Ral proteins. The exocyst complex is composed of Sec3, Sec5, Sec6, Sec8, Sec10, Sec15, Exo70 and Exo84, among which Sec5 and Exo84 are critical components and responsible for targeting various secretory vesicles to specific regions of the cellular membrane (Fukai et al. 2003). Active GTP-bound Ral proteins directly interact with the exocyst subunits to regulate both localization and assembly of exocyst, but it is unclear how exactly Ral controls exocyst functions(Zago et al. 2019). The exocyst directly interacts with several important regulators of protrusion formation, front-rear polarity and extra-cellular matrix degradation or deformation, to mediate cell migration and invasion(Zago et al. 2019).

Phospholipase D (PLD):

PLD is a lipase that catalyzes the hydrolysis of phosphatidylcholine into choline and phosphatidic acid (PA). The product of PLD, PA, acts as a second messenger to facilitate vesicle budding and transport. Six different isoforms of PLD (PLDs) have been identified however, most of the knowledge about PLD biology relates to the PLD1 and PLD2 isoenzymes (Yao et al. 2020). Unlike other effectors, association with Ral is not GTP-dependent (J. H. Kim et al. 1998). Ral interacts with PLD1 in a nucleotide independent manner, but how Ral binds PLD2 is not known. The Ral-PLD1 complex is associated with a small GTPase, Arf, which in turn promotes PLD1 activity (Luo et al. 1998). Arf-induced PLD1 activation is involved in receptor-mediated endocytosis and exocytosis (Shen, Xu, and Foster 2001; Vitale et al. 2002). Moreover, both RalA and RalB interaction with PLD1 has been shown to be essential for HeLa cell cytokinesis (Cascone et al. 2008).

ZONAB: RalA interacts with the Y-box transcription factor, ZO-1-associated nucleic-acid-binding protein (ZONAB) in a GTP and cell-density-dependent manner. Moreover, an active RalA activates the ZONAB transcription factor to regulate the cell density in MDCK cells (Frankel et al. 2005).

3.3 Function of Ral GTPase

Ral GTPase regulates different mechanisms in the biology of cells such as **cell migration.** It has been shown RalB, but not RalA is important in cell migration (Rossé et al. 2006). They showed RalB expression is essential for promoting both exocyst assembly (Sec5 and Exo84) and localization at the leading edge of moving cells (Rossé et al. 2006). It has been also shown that activation of RalB by RGL2 at plasma-membrane promotes protrusions formation and invasion (Zago et al. 2019). Another publication from the same team also established a link between the Ral/Exocyst and the Rac, the two motility driving pathways. They showed, RalB controls the association of the subunits of its effector the exocyst complex and stimulates localization of the exocyst at the leading edge in motile cells. The exocyst localizes together with the GAP protein SH3BP1 to the leading edge of motile cells, which stimulates the hydrolysis of bound GTP to GDP on Rac1 (Parrini et al. 2011). In 2003, Chien and White revealed that RalA was dispensable for the proliferation of both normal and tumour-derived cell lines in adherent cultures but that RalA is required for **anchorage-independent proliferation** of transformed cells, while RalB is required for survival of transformed cells (Chien and White 2003). Another role of Ral GTPase is in **apoptosis.** For example, in Drosophila melanogaster Ral via the exocyst complex acts as a negative regulator of JNK-dependent apoptotic signaling (Balakireva et al. 2006). JNKs belong to the superfamily of MAP-kinases involved in the regulation of cell proliferation, differentiation, and apoptosis (Dhanasekaran and Reddy 2008). **Autophagy,** a multi-step process that enables cells to survive by removing unnecessary or dysfunctional components, is another role of Ral GTPase. For example, that RalB and the exocyst subunit Exo84 are required for autophagosome formation during nutrient starvation (Bodemann et al., 2011). RalA and RalB also play distinct roles in **cytokinesis.** RalA is required to tether the exocyst to the cytokinetic furrow in early cytokinesis and RalB is required for recruitment of the exocyst to the midbody of this bridge to initiate abscission and complete cytokinesis (Cascone et al. 2008). The role of both RalA and RalB in **vesicle trafficking and cell polarity** has been also demonstrated. For example, Ral is required for the maintenance of apical-basal polarity of post-mitotic epithelial cells during tissue remodeling and lack of Ral activity lead to a defect in subcellular localization of proteins implicated in apical-basal polarity (Belaiche 2014). Moreover, phosphorylation by protein kinase Cα (PKCα) is critical for RalB-mediated vesicle trafficking and exocytosis. For example, RalB

phosphorylation regulates vesicular trafficking and membrane fusion by regulating v- and t-SNARE interactions (Martin et al. 2012). There also other roles of Ral GTPase, such as regulation of **mitochondrial fission** at mitosis through RALA and RALBP1(Kashatus et al. 2011). Moreover, RalGPS2, an independent GEF for the Ral GTPase, was also shown to promote the **tunnelling nanotube formation** via actin cytoskeleton rearrangement in bladder cancer(D'Aloia et al. 2018).

3.4 Ral GTPase and cancers

To date, the most effective strategy to target RAS oncogenic signaling has been inhibiting the downstream RAF-MEK-ERK and PI3K- AKT-mTOR effector pathways. In the last decade, the **RALGEF-RAL signaling pathway** has emerged as a third important effector signaling axis downstream of RAS (Figure.12) (Roberts and Der 2007; Yap et al. 2008). RalGEFs participate in downstream signaling from activated Ras proteins. However, early studies in mouse fibroblast cells found other pathways rather than RALGEF-RAL pathway to be sufficient in mediating RAS-driven tumor transformation (Urano, Emkey, and Feig 1996). Thus, the role of RALGEF-RAL signaling in RAS-driven tumorigenesis was initially unnoticed.

Later, Counter and colleagues later report that unlike murine fibroblasts, signaling from H-Ras through the RalGEF-Ral pathway was sufficient for RAS transformation in immortalized human HEK cells (Hamad et al. 2002). Further, it was demonstrated that RalA but not RalB is the RALGEF effector protein that plays a critical role in RAS-mediated tumor transformation (Lim et al. 2005). RalB seems to be more potent than RalA in the regulation of cell invasion and migration (Lim et al. 2006). Additional support for a role of Ral signaling in human cancer was found by White and colleagues who showed RalB was critical for human tumor cells survival while RalA was necessary for the anchorage-independent growth of cancer cells (Chien and White 2003).

Pancreatic cancer is a very good model for studying the role of RAL in human cancer due to its high frequency of KRAS mutations. Counter group studied the activation status of the three known effector pathways in human pancreatic cancer cell lines (Lim et al. 2005) and tumor samples (Lim et al. 2006). Both studies showed an increased level of activated RalA and RalB in all samples. In addition, both RalA and RalB were found to be more activated compared to other RAS effector

pathways PI3K and RAF, showing the significant role of Ral signaling in KRAS driven pancreatic cancer. RalA and RalB were found to play distinct roles in pancreatic cancer, where RALB but not RALA knockdown impaired *in vitro* invasion of these cell lines and metastatic colonization *in vivo* (Lim et al. 2006).

Bladder cancer cell lines with RAS mutation status, and RalA/B overexpression and overactivation showed RalA and RalB have similar functions in tumor growth but opposite roles in motility (Oxford et al. 2005). Using a Ral transcriptional signature, the role of Ral signaling in patient bladder tumor samples was found to correlate with disease stage, progression to strength invasion, and survival(Smith et al. 2007; 2012). In addition, overexpression of Ral activators like RGL2 and Aurora A kinase, as well as Ral effectors like RALBP1 were also found in human bladder tumor samples (Smith et al. 2007)

Colorectal cancer cell lines and patient samples were shown to have upregulated RALA and RALB activation (Martin et al. 2011). However, RalA and RalB play antagonistic roles in colon cancer. Stable RNAi suppression of RalA reduced anchorage-independent growth of cancer cells, whereas stable suppression of RalB enhanced such growth. Different function of these isoforms was partially related to their distinct usage of effector proteins. Both RalA and RalB need to intract with RALBP1 but through different components of the exocyst complex. RALA interacts with EXO84, whereas RALB interacts with SEC5 to mediate their effect on anchorage-independent growth in colorectal cancer cells (Martin et al. 2011). This antagonistic role of RalA and RalB in colorectal cancer determined cancer cell type differences in RAL function thus the requirement of selective targeting of each RAL isoform in colorectal cancer.

In lung cancer, the requirement of RAL tumorigenesis was also established in a genetic knockout mouse model(Peschard et al. 2012). Deletion of both RALA and RALB genes but not either one alone blocked KRAS-driven lung tumor development, suggesting that RalA and RalB have redundant functions in tumorigenesis in a mouse model of lung cancer. The Farassati group (Male et al. 2012) showed that transient knockdown of RalA reduced the proliferation and invasiveness of NSCLC cell line A549 *in vitro* and tumorigenesis *in vivo*. More recently, a panel of 14 human NSCLC cell lines showed although both RalA and RalB had higher expression in KRAS mutant

cell lines, only RalA activity was high (Guin et al. 2013), suggesting RalA promote the tumor growth in NSCLC cell lines.

In melanoma, approximately one-third have activating NRAS mutations and about 60% have BRAF mutations. A role for RALGEF-RAL signaling in NRAS-driven melanoma tumorigenesis was found to have a major contribution to anchorage-independent growth in an immortalized mouse melanocyte model, where the transforming activities of the three NRAS downstream effectors, RAF, PI3K, and RALGEF were evaluated (Mishra et al. 2010). Moreover, findings of Zipfel et al. demonstrated that the Ral signaling pathway can be activated in melanoma in the absence of an oncogenic Ras mutation (Zipfel et al. 2010). Stable knockdown of RALA, and to a lesser extent of RALB, inhibited the tumorigenic growth of melanoma cell lines both *in vitro* and *in vivo* (Zipfel et al. 2010).

In **breast cancer** cells (MCF-7), EGF stimulated Ral activation, and RalA was shown to be critical for EGFR promotion of estrogen-independent proliferation (Yu and Feig 2002). Later Li et al. also showed lysophosphatidic acid-induced MDA-MB-231 breast cancer cell (associated with malignant behaviors including tumor invasion and metastasis) was linked to Ral activation, and their invasion was dependent on RalA/B expression (T. T. Li et al. 2009).

Altogether, with all these studies further research is required to understand why RalA and RalB have the same effectors and yet function differently. It remains also unclear how exactly RalA and RalB contribute to tumor growth downstream of Ras activation. According to the above-mentioned studies, it seems that the role of different Ral proteins is tumor-type specific, but then what lead to this preference for one Ral protein over another is unclear. Recent advancements in Ral inhibition and genetic modification such as CRISPR will help to further address these questions.

RESULTS

Study of the role of Ral GTPases in exosome secretion and metastatic progression

Growing evidence suggests that tumor derived EVs participate in crucial steps of metastatic spread of a primary tumor mainly by exerting pro-tumoral functions and changing the phenotypes of stromal cells to the benefit of tumor growth and metastasis(Becker et al. 2016). They shuttle to distant organs and promote metastasis by conditioning the pre-metastatic niche(Peinado et al. 2017). The levels of tumor EVs secretion correlate with tumor aggressiveness, however, the link between the mechanisms of EV secretion and their capacity to form pre-metastatic niches remains obscure. During my PhD the goal of my project was to understand the mechanisms by which two GTPases (RalA/B) recently identified in our laboratory control exosome secretion and to determine how this affects breast cancer progression and metastasis. My main finding first demonstrated a detailed dissection of the impact of the Ral GTPases on EV secretion levels. We showed GTPases of the Ral family control, through the phospholipase D1, multivesicular bodies (MVBs) homeostasis and thereby tune the biogenesis and secretion of EVs. We further demonstrated that RalA and RalB promote lung metastasis in a syngeneic mouse model without affecting the invasive potential of breast carcinoma. Another important finding was EVs from RalA or RalB depleted cells have limited organotropic capacities *in vivo* and, as a consequence, are less efficient in promoting lung metastasis. Finally, we identified the adhesion protein CD146/MCAM as a key EV cargo controlled by RalA and RalB and demonstrated that it conveys, in part, the pro-metastatic function to EVs by controlling the lung tropism of breast cancer EVs. Altogether, we identified RalA/B GTPases as a novel molecular machinery that regulates the formation and secretion of pro-metastatic EVs and unraveled RalA/B and CD146 as novel therapeutic targets for breast cancer metastasis-**see annex 1: Ral GTPases promote metastasis by controlling biogenesis and organ colonization of exosomes.**

RESEARCH ARTICLE

Ral GTPases promote breast cancer metastasis by controlling biogenesis and organ targeting of exosomes

Shima Ghoroghi[1,2,3], Benjamin Mary[1,2,3], Annabel Larnicol[1,2,3], Nandini Asokan[1,2,3], Annick Klein[1,2,3], Naël Osmani[1,2,3], Ignacio Busnelli[1,2,3], François Delalande[4], Nicodème Paul[1,2,3], Sébastien Halary[5], Frédéric Gros[1,2,3], Laetitia Fouillen[6], Anne-Marie Haeberle[7], Cathy Royer[8], Coralie Spiegelhalter[9], Gwennan André-Grégoire[10,11], Vincent Mittelheisser[1,2,3,12], Alexandre Detappe[12,13], Kendelle Murphy[14,15], Paul Timpson[14,15], Raphaël Carapito[1,2,3], Marcel Blot-Chabaud[16], Julie Gavard[10,11], Christine Carapito[4], Nicolas Vitale[7], Olivier Lefebvre[1,2,3], Jacky G Goetz[1,2,3†*], Vincent Hyenne[1,2,3,17†*]

[1]INSERM UMR_S1109, Tumor Biomechanics, Strasbourg, France; [2]Université de Strasbourg, Strasbourg, France; [3]Fédération de Médecine Translationnelle de Strasbourg (FMTS), Strasbourg, France; [4]Laboratoire de Spectrométrie de Masse BioOrganique (LSMBO), IPHC UMR 7178, CNRS, Université de Strasbourg, Strasbourg, France; [5]CNRS, UMR 7245 MCAM, Muséum National d'Histoire Naturelle de Paris, Paris, France; [6]Université de Bordeaux, CNRS, Laboratoire de Biogenèse Membranaire, UMR 5200, Villenave d'Ornon, France; [7]Centre National de la Recherche Scientifique, Université de Strasbourg, Institut des Neurosciences Cellulaires et Intégratives, Strasbourg, France; [8]Plateforme Imagerie In Vitro, CNRS UPS 3156, Strasbourg, France; [9]IGBMC Imaging Center CNRS (UMR7104)/ INSERM (U1258)/ Université de Strasbourg, Illkirch, France; [10]Team SOAP, CRCINA, INSERM, CNRS, Université de Nantes, Université d'Angers, Nantes, France; [11]Integrated Center for Oncology, ICO, St-Herblain, France; [12]Nanotranslational laboratory, Institut de Cancérologie Strasbourg Europe, Strasbourg, France; [13]Équipe de synthèse pour l'analyse (SynPA), Institut Pluridisciplinaire Hubert Curien (IPHC), UMR7178, CNRS/Université de Strasbourg, Strasbourg, France; [14]Vincent's Clinical School, Faculty of Medicine, University of New South Wales, Sydney, Australia; [15]The Kinghorn Cancer Centre, Garvan Institute of Medical Research, Sydney, Australia; [16]C2VN, INSERM 1263, Inrae 1260, Aix-Marseille Université, Marseille, France; [17]CNRS SNC5055, Strasbourg, France

***For correspondence:**
jacky.goetz@inserm.fr (JGG);
hyenne@unistra.fr (VH)

[†]These authors contributed equally to this work

Competing interests: The authors declare that no competing interests exist.

Funding: See page 23

Received: 28 July 2020
Accepted: 05 January 2021
Published: 06 January 2021

Reviewing editor: Erica A Golemis, Fox Chase Cancer Center, United States

Abstract Cancer extracellular vesicles (EVs) shuttle at distance and fertilize pre-metastatic niches facilitating subsequent seeding by tumor cells. However, the link between EV secretion mechanisms and their capacity to form pre-metastatic niches remains obscure. Using mouse models, we show that GTPases of the Ral family control, through the phospholipase D1, multivesicular bodies homeostasis and tune the biogenesis and secretion of pro-metastatic EVs. Importantly, EVs from RalA or RalB depleted cells have limited organotropic capacities in vivo and are less efficient in promoting metastasis. RalA and RalB reduce the EV levels of the adhesion molecule MCAM/CD146, which favors EV-mediated metastasis by allowing EVs targeting to the lungs. Finally, RalA, RalB, and MCAM/CD146, are factors of poor prognosis in breast cancer patients. Altogether, our study identifies RalGTPases as central molecules linking the mechanisms

of EVs secretion and cargo loading to their capacity to disseminate and induce pre-metastatic niches in a CD146-dependent manner.

Introduction

The communication between tumor cells and their neighboring stromal cells is essential to sustain tumor growth and promote invasion and metastasis (**Becker et al., 2016**; **Follain et al., 2020**). Notably, this communication allows tumors to indoctrinate their microenvironment and switch the phenotypes of various cell types, such as endothelial cells, fibroblasts, or immune cells to the benefit of tumor growth, invasion, immune escape and metastasis. Such communication occurs with organs distant of the primary tumors and favors the formation of pre-metastatic niches where the modified microenvironment can help settling metastatic tumor cells (**Peinado et al., 2017**). Seeding of this favorable metastatic environment can be mediated by soluble molecules (**Kaplan et al., 2005**; **Wang et al., 2017**) or by extracellular vesicles (EVs) secreted by tumor cells (**Costa-Silva et al., 2015**; **Hoshino et al., 2015**; **Jung et al., 2009**; **Peinado et al., 2012**). EVs are lipid bilayered vesicles of nanometric diameters containing a complex mixture of RNA and protein cargoes, including a repertoire of surface receptors (**Mathieu et al., 2019**). They can be directly secreted from the plasma membrane and called microvesicles or originate from an endosomal compartment, the multi-vesicular body (MVB), and then called exosomes (**van Niel et al., 2018**). The levels of circulating tumor EVs tend to correlate with tumor progression (**Baran et al., 2010**; **Galindo-Hernandez et al., 2013**; **Logozzi et al., 2009**). Accordingly, inhibition of key components of the EV secretion machinery often correlates with decreased metastasis (**Hyenne et al., 2017**). For instance, Rab27a, which directs exosome secretion by controlling the docking of MVBs to the plasma membrane (**Ostrowski et al., 2010**), promotes breast and melanoma tumor growth and metastasis in mice (**Bobrie et al., 2012**; **Peinado et al., 2012**) and predicts poor survival in human pancreatic cancer (**Wang et al., 2015**). In addition to the levels of secreted tumor EVs, their content, and in particular their set of surface adhesion proteins equally orchestrates metastasis formation. For instance, the presence of tetraspanins CD151 and Tspan8 on the surface of pancreatic adenocarcinoma EVs favors metastasis in rats by enhancing their adhesive capacities and controlling their biodistribution (**Yue et al., 2015**). Moreover, integrin receptors exposed by tumor EVs dictate their organotropism and thereby tune/control the seeding of a premetastatic niche in specific and distant organ (**Hoshino et al., 2015**). Therefore, accumulating evidence show that both the levels and the content of secreted tumor EVs are instrumental in promoting metastasis.

However, the molecular mechanisms coordinating these processes remain elusive. In particular, how the machinery governing EV secretion can impact the pro-metastatic properties of tumor EVs deserves in-depth characterization. To address this issue, we focused on the members of the Ral family, RalA and RalB (collectively referred to as RalA/B), acting downstream of RAS and promoting metastasis of different tumor types in both mice and human (**Gentry et al., 2014**; **Yan and Theodorescu, 2018**). We recently found that these versatile proteins are evolutionarily conserved regulators of exosome secretion (**Hyenne et al., 2015**). We originally observed that, in the nematode *C. elegans*, the Ral GTPase ortholog RAL-1 controls exosome secretion by acting on the biogenesis of MVBs. Importantly, we further showed that RalA/B modulate the levels of secreted EVs in models that are relevant to human breast cancer (**Hyenne et al., 2015**) suggesting that these GTPases could influence disease progression through EVs release. Here, we exploited 4T1 cells, an aggressive mammary tumor model that mimics human triple-negative breast cancer (**Kaur et al., 2012**) to further decipher how RalA/B tune EV secretion mechanisms and thereby control metastatic progression of the disease.

In this study, we first provide a detailed dissection of the impact of the Ral GTPases on EV secretion levels and unravel the mechanisms by which they control the homeostasis of MVBs. We have discovered that RalA/B directly acts through the phospholipase D1 (PLD1), which, as we show, also promotes EVs secretion, to favor the maturation of MVBs. We further demonstrate that RalA and RalB promote lung metastasis without affecting the invasive potential of breast carcinoma. Importantly, RalA/B are crucial for the organ targeting of tumor EVs, and, as a consequence, for the seeding of pre-metastatic niches. Finally, we identify the adhesion protein CD146/MCAM as a key EV

cargo controlled by RalA and RalB and demonstrate that it conveys, in part, the pro-metastatic function to EVs by controlling the lung tropism of breast cancer EVs.

Results

RalA and RalB control exosome secretion levels through the homeostasis of MVBs

We have previously shown that RalA and RalB control EV secretion in aggressive 4T1 mammary tumor cells (***Hyenne et al., 2015***) that reliably mimics the aggressive phenotype of human triple-negative breast cancer. We thus built on this relevant tumor model and decided to test the hypothesis that RalA and RalB could orchestrate pro-metastatic functions by tuning the molecular mechanisms driving the secretion levels and nature of EVs. We first confirmed our initial observations with the nanoparticle-tracking analysis (NTA) of EVs released by 4T1 cells and isolated by ultracentrifugation (100,000 g pellet). Stable depletion of RalA or RalB by shRNA reduces by 40% the amount of secreted EVs (***Figure 1a***, ***Figure 1—figure supplement 1a***), with no impact on their average size (***Figure 1—figure supplement 1b***). RBC8 and BQU57, two previously described specific chemical inhibitors of Ral GTPases (***Yan et al., 2014***) significantly reduced EV secretion levels in mouse and human mammary tumor cell lines (4T1, MDA-MB231, D2A1, and MCF7 cells) as well as in two other cancer cell lines, human melanoma (A375) and pancreatic carcinoma (Panc1) cells (***Figure 1b*** and ***Figure 1—figure supplement 1c***). Together with evidence previously obtained in *Caenorhabditis elegans* (***Hyenne et al., 2015***), this demonstrates that the mechanisms by which RalA/B GTPases tune EV secretion levels are conserved throughout evolution and are notably at play in various cancer cell lines.

To better understand how Ral GTPases could impact EVs secretion, we first characterized their intracellular distribution in 4T1 cells. Endogenous RalA and RalB localize mostly within CD63-positive endosomal compartments (MVBs and late endosomes), as well as at the plasma membrane (***Figure 1c***). Similarly, GFP-tagged RalA and RalB localize both in late endosomal compartments positive for Lysotracker and at the plasma membrane (***Figure 1c***). Therefore, in 4T1 cells, Ral GTPases localize both at biogenesis sites of microvesicles (plasma membrane) and exosomes (MVBs). To further determine whether Ral GTPases affect MVBs as previously observed in *C. elegans*, we performed thorough electron microscopy (EM) analysis of endosomal compartments in 4T1 cells. In a first analysis of cells that were processed upon chemical fixation, we quantified the densities of (i) MVBs and (ii) endolysosomes, as well as (iii) the diameter of MVBs, (iv) the number and (v) the diameter of intraluminal vesicles (ILVs) per MVB. Strikingly, we found RalA or RalB depletion leads to a 40% decrease in the number of MVB per cytoplasmic surface in 4T1 cells (***Figure 1d*** and ***Figure 1—figure supplement 2a***), with no impact on the density of endolysosomes (***Figure 1—figure supplement 2b***). Further analysis of Lysotracker-positive compartments using FACS confirmed that RalA/B depletion has no significant effect on the late endosome-lysosome pathway (***Figure 1—figure supplement 2c***). Besides, EM analysis revealed no differences in ILV numbers per MVB surface (***Figure 1—figure supplement 2d***), nor in MVB diameters (***Figure 1—figure supplement 2e***). However, since chemical fixation is known to affect the morphology of endosomal compartments, we took our EM analysis one step forward by implementing high-pressure freezing (HPF) of cells, which better preserves the ultrastructure of endosomes (***Klumperman and Raposo, 2014***). A similar decrease in the number of MVBs per cytoplasmic surface in RalA and RalB knockdown cells was observed in these conditions (***Figure 1—figure supplement 2a***). Upon HPF, we further observed a slight decrease in the number of ILVs per MVB surface (***Figure 1—figure supplement 2d***) that could be, in part, explained by a slight increase in MVB diameters (***Figure 1—figure supplement 2e***). In conclusion, depletion of either RalA or RalB significantly reduces MVB number, while the remaining MVBs are slightly bigger. Overall, thorough EM analysis of intracellular compartments using both chemical fixation and HPF clearly demonstrates that both RalA and RalB control MVB homeostasis in breast mammary tumor cells.

A RalA/B-PLD1-PA axis governs exosome biogenesis

We further investigated the molecular mechanisms controlling MVB homeostasis downstream of RalA/B GTPases. We decided to focus on phospholipases D (PLDs), which catalyzes the hydrolysis of

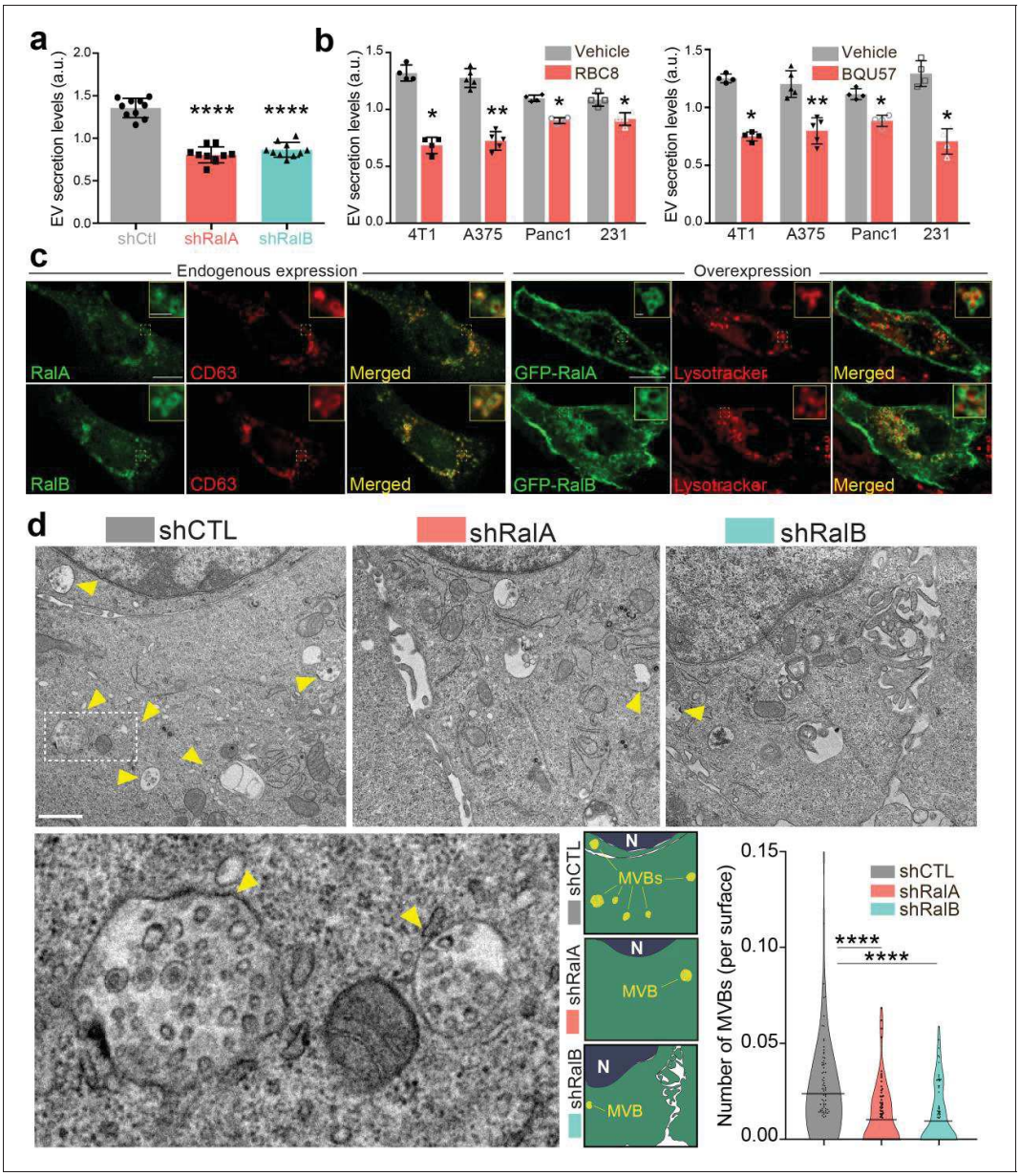

Figure 1. RalA and RalB control exosome secretion and multi-vesicular body (MVB) homeostasis. (**a–b**) Nanoparticle tracking analysis of extracellular vesicles (EVs) isolated by ultracentrifugation (100,000 g pellet) from the supernatant of shCtl, shRalA, or shRalB 4T1 cells (**a**) or from various cell types treated with Ral inhibitors RBC8 (**b**, left) or BQU57 (**b**, right). 231: MDA-MB-231 cells. Each dot represents one experiment (a: 10 independent

Figure 1 continued on next page

Figure 1 continued

experiments; One-Way Anova followed by Bonferroni's Multiple Comparison Test; b: four to five independent experiments, Mann Whitney test). (**c**) Representative confocal images of 4T1 cells showing endogenous expression of RalA, RalB, and CD63 by immunofluorescence (left) and overexpression of GFP-RalA and GFP-RalB in cells incubated with Lysotracker (right). Scale bar: 10 µm; zoom: 2 µm. (**d**) Representative electron micrographs of 4T1 shCtl, shRalA and shRalB cells, with zoom on MVBs; Scale bar: 1 µm; zoom: 200 nm. Violin plots show quantification of the number of MVB per cytoplasm surface. Each dot represents one field of view; horizontal bars represent the average (76–88 fields of view; Kruskal-Wallis test followed by Dunn's Multiple Comparison Test).

The online version of this article includes the following figure supplement(s) for figure 1:

Figure supplement 1. (**a**) Representative western blots showing tubulin, RalA (left) and RalB (right) expressions in 4T1 shControl, shRalA, and shRalB cells. (**b**) Graph showing the average diameter of the extracellular vesicles (EVs) isolated from 4T1 shControl, shRalA, and shRalB cells measured by nanoparticle-tracking analysis. Each dot represents one experiment (12 independent experiments; One-Way Anova followed by Bonferroni's Multiple Comparison Test). (**c**) Nanoparticle-tracking analysis of EVs isolated by ultracentrifugation (100,000 g pellet) from the supernatant of various breast cancer cell lines treated with the Ral inhibitor RBC8. Each dot represents one experiment (four independent experiments, Mann Whitney test, p value indicated on the graph).

Figure supplement 2. Electron microscopy analysis of endosomes in the absence of RalA or RalB (**a-b**).

phosphatidylcholine (PC) into phosphatidic acid (PA), for three reasons: (1) PLD1 and PLD2 are two well-known targets of RalA and RalB (***Jiang et al., 1995***; ***Luo et al., 1998***; ***Vitale et al., 2005***), (2) PLD2 controls exosome secretion in breast cancer cells (***Ghossoub et al., 2014***), and (3) PLDs impact cancer progression (***Bruntz et al., 2014***). We first verified that both PLD1 and PLD2 are expressed in 4T1 cells by RT-qPCR (***Figure 2—figure supplement 1a***). In the absence of efficient anti-PLD antibody for immunofluorescence, we decided to assess the subcellular localization of PLD-GFP fusion proteins. PLD1 mostly localizes to endosomal compartments positive for RalA, RalB, and lysotracker, whereas PLD2 mostly localizes to the plasma membrane (***Figure 2a*** and ***Figure 2—figure supplement 1b***). Therefore, we tested whether PLDs could function downstream of RalA/B to control MVBs homeostasis and exosome secretion using two chemical inhibitors, CAY10593 for PLD1 and CAY10594 for PLD2 (***Lewis et al., 2009***; ***Scott et al., 2009***). EM analysis of 4T1 cells revealed that inhibition of PLD1, but not of PLD2, induces a 40% decrease in the number of MVBs per cytoplasmic surface (***Figure 2b***). This phenotype is consistent with PLDs respective localizations and suggests that PLD1 functions in the RalA/B exosome secretion pathway. Further NTA analysis of treated cells showed that both inhibitors reduce EV secretion levels in 4T1 cells (***Figure 2c***), suggesting that both PLD isoforms regulate EV secretion potentially through distinct mechanisms. Importantly, PLD1 inhibition fully phenocopies the effect of RalA/B GTPases depletion, both on the cellular density of MVBs and on the level of EV secretion. To determine whether PLD1 acts downstream of RalA/B, we looked at its localization in the absence of RalA or RalB. Confocal analysis revealed that in 40% of shRalA or shRalB cells, PLD1 is uniformly cytoplasmic instead of being endosomal (***Figure 2d***). By contrast, RalA/B depletion had no major impact on PLD2 localization at the plasma membrane (also its trafficking might be altered) (***Figure 2—figure supplement 1c***). This shows that RalA/B GTPases are required for PLD1 localization on endosomes. To further investigate if PLD activity is involved in Ral GTPases-dependent EV secretion, we performed a lipidomic analysis of secreted EVs. As PLD converts PC into PA, we focused on these two lipid species. Importantly, RalA/B depletion significantly reduces the PA/PC ratio of secreted EVs (***Figure 2e***). In particular, the PA/PC ratio made of mono- and di-unsaturated lipid species (36:1, 36:2, 38:1, and 38:2), known to be PLD product/target, respectively, showed a tendency to be decreased although not reaching statistical significance (***Figure 2—figure supplement 1d***). This further implies that PLD's main product, PA, plays a crucial role in MVB homeostasis. Altogether, these results suggest that Ral GTPases control PLD1 localization on MVBs, which is required for local PA accumulation and ultimately for MVB homeostasis and exosome secretion (***Figure 2f***).

RalA and RalB promote metastasis non-cell autonomously

Having identified RalA and RalB as important regulators of EV secretion in breast cancer cells, we next investigated whether such a function could impact metastasis. At first, we analyzed public databases to interrogate a potential correlation between RalA/B expression levels and metastatic progression. Using a large cohort of breast cancer patients with metastatic progression from the Cancer Genome Atlas (TCGA), we found that high expression of either RalA or RalB is significantly

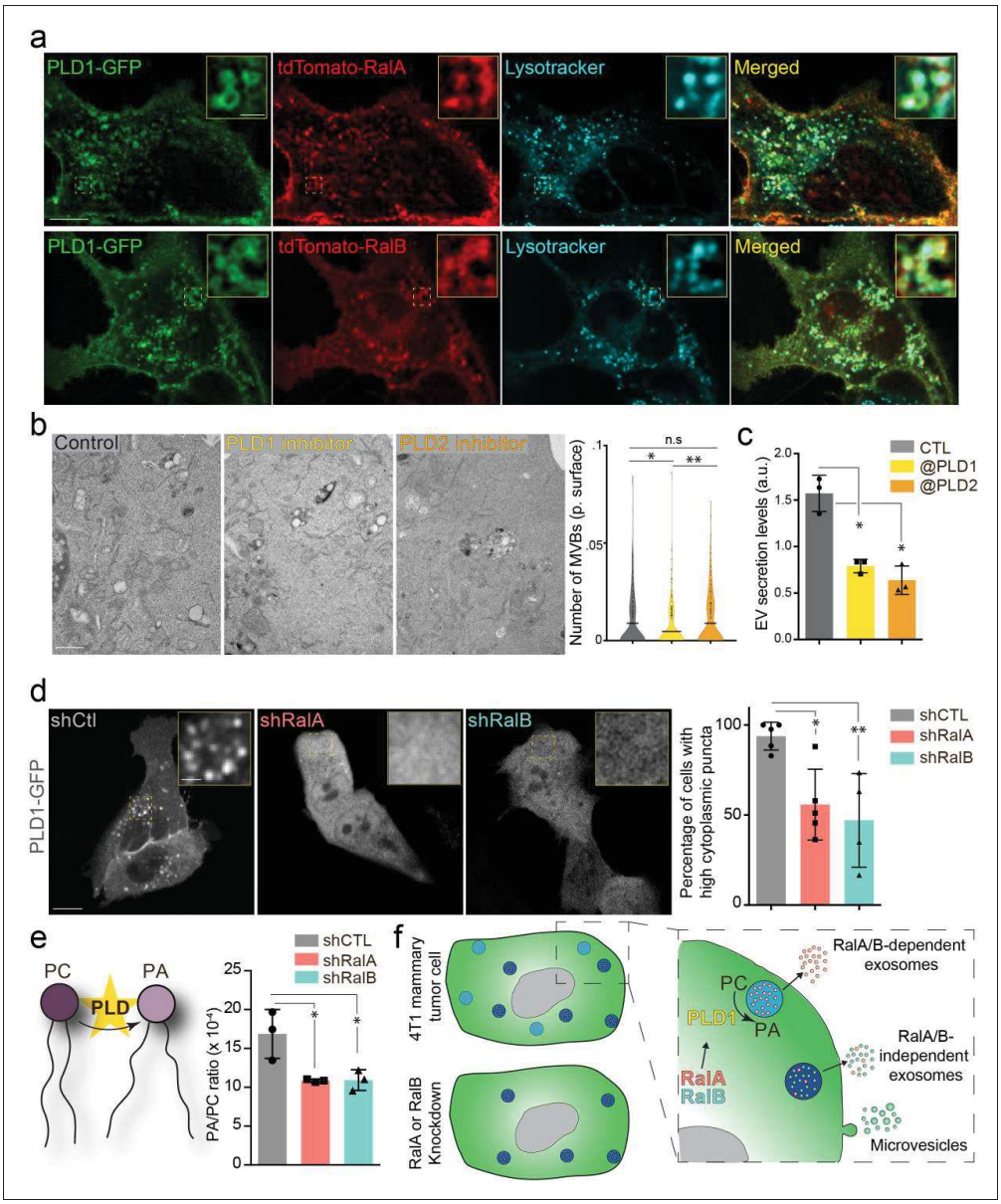

Figure 2. The RalA/B-PLD1-PA axis governs exosome secretion. (**a**) Representative confocal images of 4T1 cells co-transfected with PLD1-GFP and tdTomato-RalA (upper panels) or tdTomato-RalB (lower panels) and incubated with Lysotracker. Scale bar: 10 µm; zoom: 2 µm. (**b**) Electron microscopy analysis of 4T1 cells treated with PLD1 or PLD2 inhibitor. Scale bar: 1 µm. Violin plots show quantification of the number of multi-vesicular body (MVB) per cytoplasmic surface. Each dot represents one field of view; horizontal bar represents the average (180–194 fields of view; Kruskal-Wallis test

Figure 2 continued on next page

Figure 2 continued

followed by Dunn's Multiple Comparison Test). (**c**) Nanoparticle tracking analysis of extracellular vesicles (EVs) isolated by ultracentrifugation (100,000 g pellet) from the supernatant of 4T1 cells treated with PLD1 (CAY10593) or PLD2 (CAY10594) inhibitor. Each dot represents one experiment (three independent experiments; One-Way Anova permutation test followed by fdr multi-comparison permutation test). (**d**) Representative confocal images of shControl, shRalA and shRalB 4T1 cells transfected with PLD1-GFP. Scale bar: 10 µm; zoom: 2 µm. Graph shows the percentage of cells with high (>5) number of PLD1-GFP cytoplasmic puncta. (Each dot represents one experiment. Five independent experiments; Number of cells analyzed: shCtl (136), shRalA (170), shRalB (244); Kruskal-Wallis test followed by Dunn's Multiple Comparison Test). (**e**) Quantification of the Phosphatidic Acid (PA) / PhosphatidylCholine (PC) ratio in EVs isolated from shControl, shRalA, and shRalB cells (each dot represents one experiment; three independent experiments; One-Way Anova permutation test followed by fdr multi-comparison permutation test; fdr <0,1). (**f**) Model showing how RalA and RalB could control PLD1 localization on MVBs, thereby inducing the PA accumulation on MVBs, promoting MVB homeostasis and controlling exosome secretion.

The online version of this article includes the following figure supplement(s) for figure 2:

Figure supplement 1. PLD1 and PLD2 in 4T1 cells.

correlated with reduced survival (***Figure 3a***). Automated quantification of RalA/B expression levels by immunohistochemistry in primary tumors of breast cancer patients unraveled overexpression of both proteins in tumors from patients with metastasis (***Figure 3b***). These results prompted us to investigate in depth the role of RalA/B in a syngeneic mouse model of aggressive breast cancer, which is highly relevant to the human pathology.

Therefore, we conducted a careful and exhaustive longitudinal analysis of metastatic progression of mammary tumors in syngeneic Balb/c mice. Briefly, 4T1 cells depleted or not for RalA or RalB were orthotopically grafted in mammary ducts, and several criteria were tracked over time. First, RalA and RalB have antagonist effects on tumor growth measured in vivo over time and ex vivo after 41 days: while RalA depletion significantly increased tumors growth, RalB depletion induced the opposite effect when compared to control tumors (***Figure 3c***). Neither RalA, nor RalB affected apoptosis, using caspase3 as a read-out (***Figure 3—figure supplement 1a–b***). In contrast, 4T1 cells depleted of RalA and RalB show increased growth rate in vitro and a decreased proportion of cells in sub-G1 phase of the cell cycle (***Figure 3—figure supplement 1c–d***). A similar increase in proliferation rates was observed in vivo in the absence of RalA (***Figure 3d***). Therefore, while depletion of RalA favors in vivo tumor growth by enhancing 4T1 proliferation potential, it is likely that additional non-cell autonomous factors are responsible for the decreased tumor growth observed upon RalB depletion.

We obtained the most striking result when carefully assessing the lung metastasis burden of these mice after 41 days. We measured the number and the surface covered by metastatic foci in serial lung sections and observed that RalA or RalB depletion in mammary tumors drastically reduced their metastatic potency (***Figure 3e***). When compared to the tumor growth rate, the most dramatic reduction of metastasis was observed in the case of RalA depletion. These experiments show that although RalA and RalB have antagonist effects on primary tumors, they both promote metastasis. To dissect this phenotype, we tested whether RalA or RalB could impact inherent cell migration and invasion potential of 4T1 cells, as it had been reported for RalB (***Oxford et al., 2005***; ***Zago et al., 2018***). We performed 2D (***Figure 3f***) and 3D (***Figure 3g***) in vitro invasion assays and observed no effect of RalA or RalB expression levels on motility potential of 4T1 cells. Therefore, RalA/B seem to promote metastasis independently of cell invasion and are likely to promote metastasis of aggressive breast cancer cells non-cell autonomously by inducing pro-metastatic micro-environmental changes.

RalA- and RalB-dependent EVs induce endothelial permeability

Since RalA and RalB promote metastasis independently of their cell-intrinsic properties, we wondered whether they could control secreted factors that are likely to induce micro-environmental alterations. In addition to EVs, tumor cells secreted soluble factors can promote metastasis by modulating the microenvironment, notably by promoting the formation of a metastatic niche (***Ombrato et al., 2019***). To test this possibility, we examined the impact of RalA and RalB on the soluble secretome of 4T1 cells. Depletion of RalA or RalB had no drastic effect on the soluble factors secreted by 4T1 cells (***Figure 3—figure supplement 2***). However, the secretion of one protein known to promote metastasis (***Ombrato et al., 2019***), WISP1/CCN4, is significantly decreased in shRalA/B cells (***Figure 3—figure supplement 2***). Thus, RalA and RalB are likely to enhance

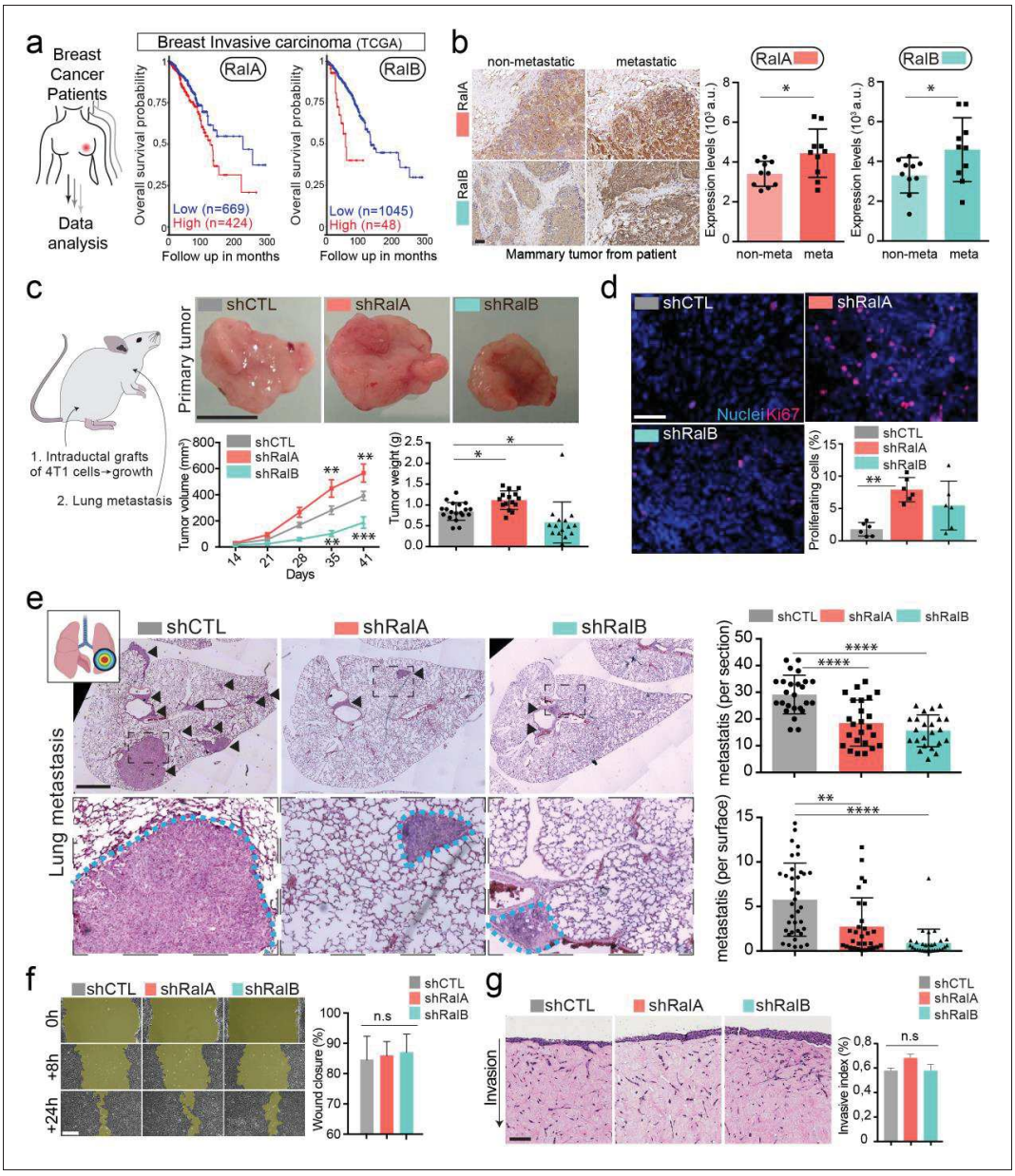

Figure 3. RalA and RalB promote lung metastasis in a non-cell autonomous fashion. (**a**) Kaplan-Meier curve, obtained from TCGA 1097 cohort, showing the survival probability of patients with tumor breast invasive carcinoma having high or low RalA (pvalue: 5.15 e-03; pAdj: 1.35e-01) or RalB (pvalue: 1.77 e-05; pAdj: 5.99e-03) expression levels. (**b**) Representative images of immunohistochemistry against RalA or RalB performed on mammary primary

Figure 3 continued on next page

Figure 3 continued

tumors from patients with or without metastasis. Scale bar: 500 µm Graphs represent automated scoring of DAB staining. Each dot represents one patient; 10 patients per group; Student t-test. (**c**) Orthotopic injection of shControl, shRalA, and shRalB 4T1 cells in syngenic mice. Representative images of primary tumors at day 41. Scale bar: 1 cm. Graphs showing the primary tumor growth over time (Left) and the primary tumor weight at day 41. Each dot represents one mouse. (Two independent experiments; Left: Two-way Anova followed by Bonferonni post-test, Right: Kruskal-Wallis test followed by Dunn's Multiple Comparison Test). (**d**) Representative confocal images of primary tumors stained with anti-Ki67 antibody. Scale bar: 50 µm. Graph indicates the % of Ki67-positive nuclei. Each dot represents one mouse. (six mice taken from two independent experiments; Kruskal-Wallis test followed by Dunn's Multiple Comparison Test. (**e**) Analysis of lung metastasis in mice from the orthotopic experiment presented in (**c**). Representative images of lung sections (Day 41) stained with hematoxilin eosin. Scale bar: 1 mm. Graphs show the number of metastatic foci per section (upper, One-Way Anova followed by Bonferroni's Multiple Comparison Test) and the metastatic surface per lung surface (lower; Kruskal-Wallis test followed by Dunn's Multiple Comparison Test). Each dot represents one section **f**) Pictures of wound healing closure at different time points. Scale bar: 150 µm. Graph represents the percentage of wound closure at 16 hr (three independent experiments; Kruskal-wallis test followed by Dunn's multiple comparison test). (**g**) Pictures of 3D invasion assay after 15 days. Graph represents the invasive index. Scale bar: 100 µm.
The online version of this article includes the following figure supplement(s) for figure 3:

Figure supplement 1. Proliferation and apoptosis of 4T1 cells and tumors.
Figure supplement 2. Soluble secretome of 4T1 shControl cells compared to 4T1 shRalA or 4T1 shRalB cells (three independent experiments; One-Way Anova permutation test followed with pairwise permutation test with fdr correction).

metastatic potency by promoting the secretion of EVs and possibly as well through WISP1/CCN4. Furthermore, in addition to enhancing the levels of secreted EVs, RalA/B could alter their functionality. To test this possibility, we challenged the pro-tumoral function of RalA/B EVs in an in vitro functional assay.

Since tumor EVs are known to induce vascular permeability in the vicinity of tumors as well as in distant organs (***Tominaga et al., 2015***; ***Treps et al., 2016***; ***Zhou et al., 2014***), we tested the capacity of RalA/B dependent EVs to promote endothelial permeability in vitro. When added to a monolayer of endothelial cells, 4T1 EVs increased its permeability in a dose-dependent manner (***Figure 3—figure supplement 1e***). We then tested the impact of EV content on vascular permeability by subjecting endothelial cells to similar amounts of EVs derived from 4T1 cells expressing or not RalA/B. Interestingly, endothelial monolayers became less permeable when treated with a similar amount of EVs derived from shRalA or shRalB cells. Similarly, such EVs fail to disrupt adherent and tight junctions by contrast to EVs derived from 4T1 control cells (***Figure 4b***) suggesting that EVs from RalA/B knockdown cells have reduced pro-permeability abilities. Therefore, depletion of RalA/B reduces secretion levels of EVs and leads to the secretion of EVs whose effect on vascular leakiness is hampered. The important observation that vascular permeability could be reduced upon depletion of RalA or RalB, and with a similar amount of EVs, prompted us to further dissect whether RalA or RalB could tune the priming of pre-metastatic niches.

RalA and RalB dependent EVs are pro-metastatic and lung tropic

Here, we thus explored whether RalA and RalB synergistically impact the pro-metastatic functions of EVs by tuning their secretion levels as well as their content. Since on one hand RalA and RalB positively control the levels and the functionality of secreted tumor EVs (***Figures 1*** and ***4a***), and on the other hand they promote metastasis (***Figure 3***), we tested a direct impact of RalA/B-dependent EVs on the promotion of lung metastasis. For this, we decided to directly assess the role of 4T1 EVs in priming lung metastatic niches in vivo, as previously described for other tumor EVs (***Costa-Silva et al., 2015***; ***Hoshino et al., 2015***; ***Peinado et al., 2012***; ***Zhou et al., 2014***). Priming of lungs with control EVs significantly enhances lung metastasis over 14 days when compared to PBS (***Figure 4c***). In striking contrast, priming of mouse lungs with a similar number of EVs derived from Ral-depleted cells did not promote metastasis. This key experiment demonstrates that RalA/B confer pro-metastatic functions to EVs, in addition to controlling their secretion levels. Indeed, the decreased metastasis observed in absence of RalA/B can result from either drastically reduced EVs secretion or diminished pro-metastatic potential of EVs. To unravel why EVs from RalA/B-depleted cells are unable to promote metastasis, we first determined their capacity to efficiently reach the lungs and prime pre-metastatic niches by tracking the dissemination of fluorescently labeled EVs that were injected in the blood circulation of Balb/c mice. We found that 1 hr after injection 4T1 EVs mostly accumulate in the lungs, as well as the liver and brain (***Figure 4d*** and ***Figure 4—figure***

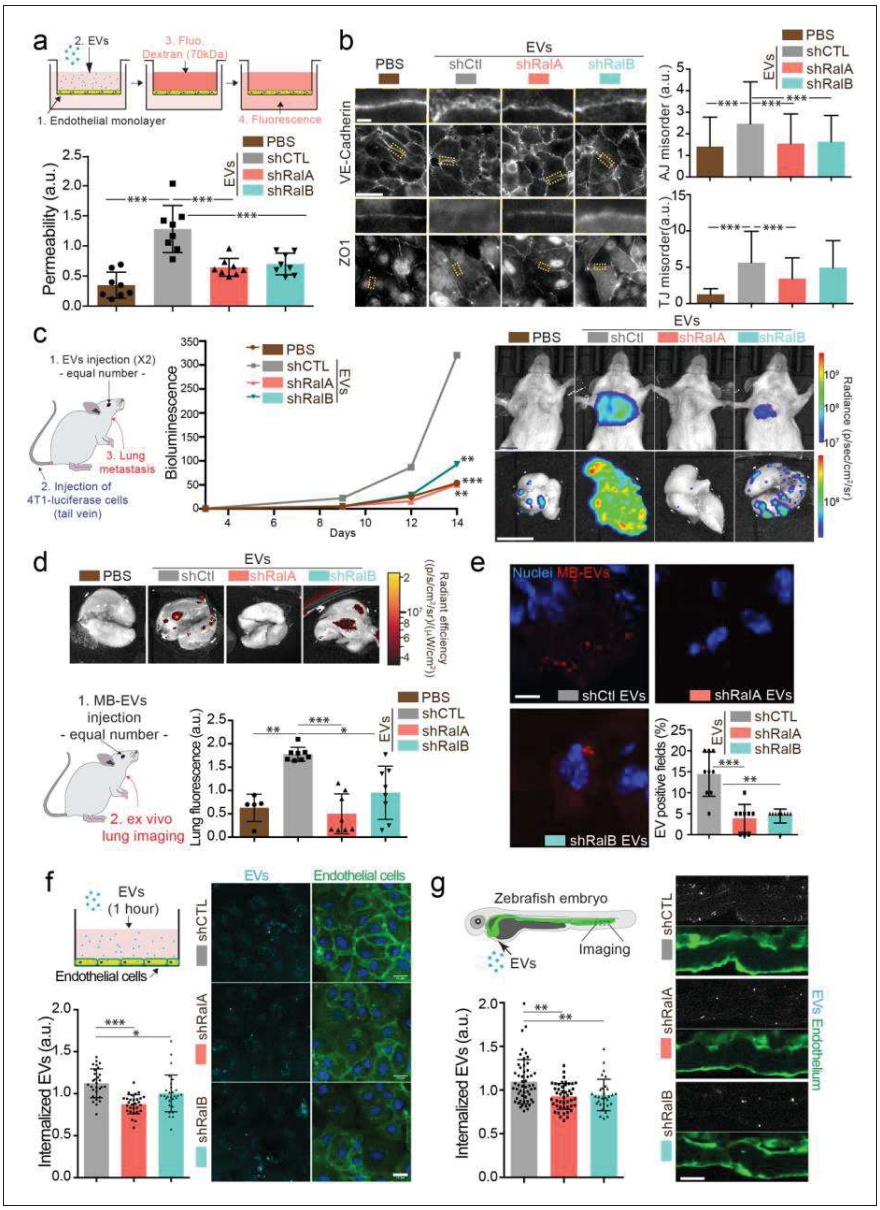

Figure 4. RalA and RalB control lung tropism of pro-metastatic tumor extracellular vesicles (EVs). (**a**) Effect of a similar amount of EVs on HUVEC monolayer permeability in vitro. The graph represents the normalized amount of fluorescent dextran that crossed the endothelial barrier. Each dot represents one experiment (eight independent experiments; One-Way Anova followed by Bonferroni's Multiple Comparison Test). (**b**) Representative epifluorescence images of VE-cadherin (upper panels) and ZO1 (Lower panel) stainings on HUVECS cells treated with similar amounts of EVs. Scale bar:

Figure 4 continued on next page

Figure 4 continued

20 µm; zoom: 2 µm. Graphs represent the disorganization of adherent (up) and tight (low) junctions (Three independent experiments; up; Kruskal-Wallis test followed by Dunn's Multiple Comparison Test). (**c**) Metastasis priming experiment, Balb/c mice are first injected twice with tumor equal number of EVs (1.5×10^8 EVs), then intravenously with 4T1 luciferase cells and metastasis is then followed over time. Graph shows metastasis progression over time in mice pre-injected with PBS, or with equal number of EVs from shControl, shRalA or shRalB cells (7–10 mice per group; merge of two independent experiments; Two-way Anova followed by Bonferonni multiple comparison post test; stars indicate statistically significant differences at day 14). Right: In vivo and ex vivo representative images of mice and lungs at day 14. Scale bars: 1 cm. (**d–e**) Lung accumulation of equal number of fluorescent-labeled EVs ($3\ 10^8$ EVs), from shControl, shRalA or shRalB cells injected intravenously. (**d**) Representative ex vivo images and graph showing the total lung fluorescence 1 hr post-injection. Each dot represents one mouse. (Eight mice taken from two independent experiments; Kruskal-Wallis test followed by Dunn's Multiple Comparison Test). (**e**) Representative confocal lung sections images and graph showing the percentage of EVs-positive fields. Each dot represents one section (three mice; Kruskal-Wallis test followed by Dunn's Multiple Comparison Test). Scale bar: 5 µm. (**f–g**) Arrest and internalization of equal number of EVs from shControl, shRalA, and shRalB cells on endothelial cells in vitro and in vivo. (**f**) Representative confocal Z-stacks of equal number of EVs after 1 hr or incubation with HUVEC monolayer. Scale bar: 25 µm. Each dot represents one field of view (each dot represents one field of view from three independent experiments; Kruskal-Wallis test followed by Dunn's Multiple Comparison Test). (**g**) Representative confocal Z-stacks the caudal plexus of Tg(Fli1:GFP) zebrafish embryos, where GFP is expressed in the endothelium, injected with similar number of EVs and imaged right after injection. Each dot represents one zebrafish (31–53 embryos from four independent experiments; Kruskal-Wallis test followed by Dunn's Multiple Comparison Test). Scale bar: 20 µm.

The online version of this article includes the following figure supplement(s) for figure 4:

Figure supplement 1. 4T1 extracellular vesicles (EVs) organotropism.

supplement 1a). These three organs are the main metastatic organs of 4T1 cells, and breast carcinoma, showing that the organotropism of 4T1 EVs mirrors the metastatic organotropism of their parental cells and further validates the relevance of our model to human pathology (***Kaur et al., 2012***; ***Lou et al., 2008***). Through a careful analysis of cell types that internalize EVs in these conditions, we observed that 4T1 EVs mostly accumulate in endothelial cells, macrophages, and fibroblasts of the lung parenchyma (***Figure 4—figure supplement 1b***). Importantly, EVs derived from RalA- or RalB-depleted cells failed to efficiently reach the lungs, even though similar amounts were injected in all conditions (***Figure 4d,e***). Similar results were observed for EVs reaching the liver (***Figure 4—figure supplement 1c***). Hence, we can conclude at this stage that RalA/B control the pro-metastatic properties of EVs by tuning their ability to reach vascular regions and local parenchyma and efficiently reach metastatic organs, thereby modulating the formation of a pre-metastatic niche.

The latter results raised the exciting hypothesis that metastasis impairment could be, in part, explained by a general defect in adhesion of circulating EVs at the vascular wall. We recently showed that EVs target specific vascular regions by first arresting at the surface of endothelial cells (***Hyenne et al., 2019***). We used two complementary models that allow careful tracking of single EVs and assessed early events of EVs internalization in endothelial cells. Using microfluidics, we found that internalization of 4T1 EVs within endothelial cells is decreased after 1 hr when they originate from RalA/B-depleted cells (***Figure 4f***). Similarly, upon tracking of fluorescent EVs injected in the circulation of zebrafish embryos, we observed that endothelial arrest/internalization of EVs from RalA/B knockdown cells is significantly hampered (***Figure 4g***). Altogether, these experiments suggest that RalA/B knockdown significantly reduced the adhesive properties of EVs to the endothelium, establishing a potential link with their failure to accumulate in mice lungs. Furthermore, our results support a model in which RalA/B GTPases, in addition to promoting EV secretion, also control the pro-metastatic function of these EVs, likely by modulating their content.

RalA/B promote CD146 EV loading for efficient lung targeting and pre-metastatic niche priming

These functional experiments (***Figure 4***) suggest that the content of EVs can directly influence metastasis formation and that such content is likely to be impacted by RalA/B. Therefore, we carried out a careful and thorough molecular comparison of the cargo content of EVs derived from RalA/B-tuned cells. We first analyzed the RNA content of EVs using RNAseq and found that a large proportion of the RNAs present in EVs from shRal cells were different from the control (30–50%) (***Figure 5a***; ***Supplementary file 1***). Accordingly, GO terms associated with mRNA enriched in each EV type showed important differences in biological processes, molecular function, or cellular components (***Figure 5—figure supplement 1***). In addition, EVs from shRalA cells differed from control or

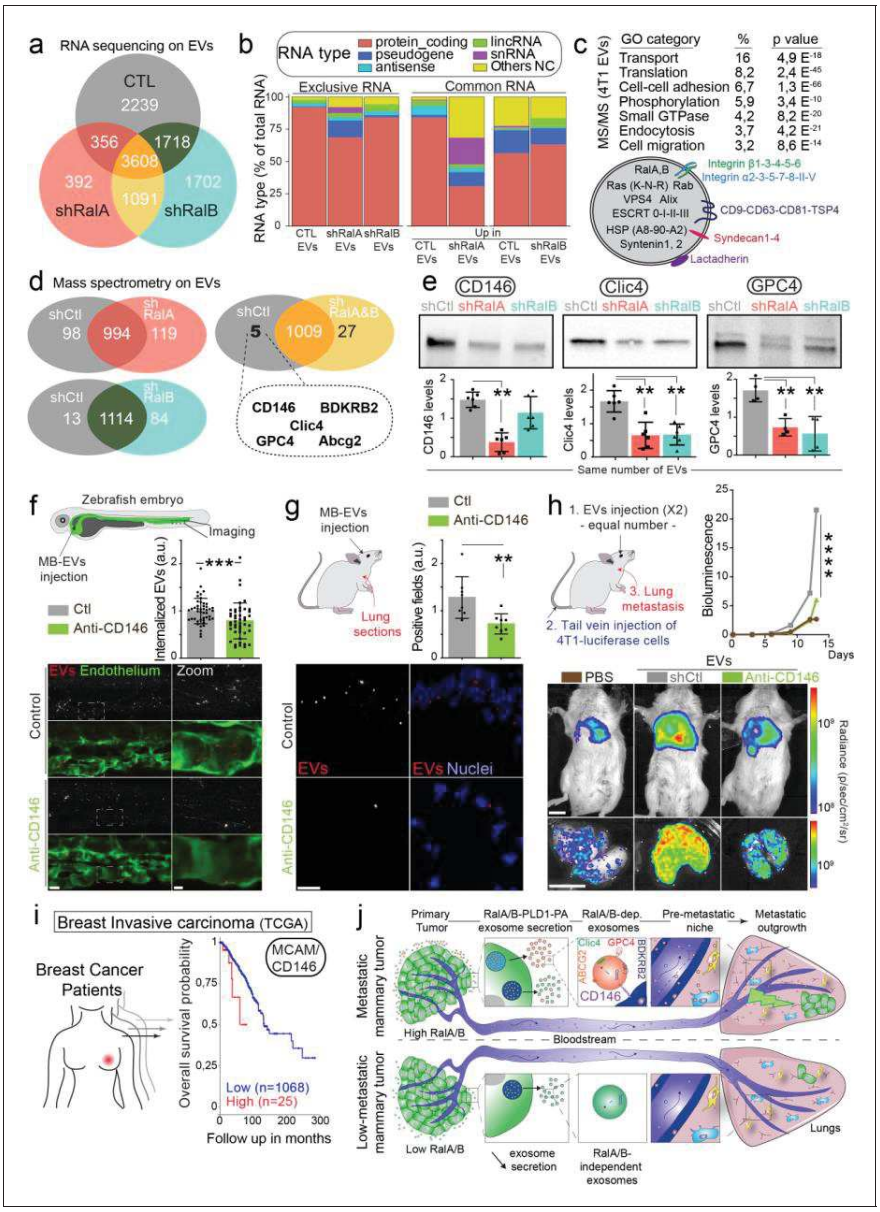

Figure 5. CD146/MCAM is under-expressed in RalA/B knockdown extracellular vesicles (EVs) and mediates their lung tropism. (**a**) Venn diagram representing the RNA present in the EVs isolated from shControl, shRalA or shRalB cells (with a minimum of 10 reads per sample; RNA sequencing performed in triplicate). (**b**) Type of RNA associated identified in EVs isolated from shControl, shRalA, or shRalB cells. Left: RNA exclusively present in one type of EVs. Right: enriched RNAs (log2 fold change >2; p(adj.)<0,05). (**c**) GO terms of the proteins identified in EVs isolated from 4T1 cells by

Figure 5 continued on next page

Figure 5 continued

ultracentrifugation (100,000 g pellet) and illustration of some proteins known to be present in EVs. (**d**) Comparison of the protein content of EVs isolated from shControl, shRalA, and shRalB cells. The venn diagram represents proteins having different expression levels (Mass spectrometry performed in triplicate; FDR < 1%). (**e**) Analysis of the expression of CD146/MCAM, Clic4, and Glypican four in EVs isolated from shControl, shRalA and shRalB cells by western blots. Each dot represents one experiment (four to six independent experiments; Kruskal-Wallis test followed by Dunn's Multiple Comparison Test). (**f–g**) Arrest, internalization, and organotropism of EVs treated with an anti-CD146 antibody and injected in the circulation of zebrafish embryos (**f**) or mouse (**g**). (**f**) Representative confocal Z-stacks the caudal plexus of Tg(Fli1:GFP) zebrafish embryos, where GFP is expressed in the endothelium, injected with equal number of EVs and imaged right after injection. Scale bar: 20 µm; Zoom scale bar: 5 µm. Each dot represents one zebrafish (46 embryos from four independent experiments; Mann Whitney test). (**g**) Representative confocal images of lung sections and graph showing the percentage of EVs-positive fields. Scale bar: 10 µm. Each dot represents one mouse (eight mice from two independent experiments; Mann Whitney test). (**h**) Metastasis priming experiment, Balb/c mice are injected twice with tumor equal number of EVs (1.5×10^8 EVs), pre-incubated with CD146 blocking antibody or isotype control, and then intravenously injected with 4T1 luciferase cells and metastasis is followed over time. Graph shows metastasis progression over time (14 mice per group; merge of two independent experiments; Two-Way Anova followed by Bonferonni multiple comparison post test; stars indicate statistically significant differences at day 14). In vivo and ex vivo representative images of mice and lungs at day 14. Scale bars: 1 cm. (**i**) Kaplan-Meier curve, obtained from TCGA 1097 cohort, showing the survival probability of patients with tumor breast invasive carcinoma having high or low MCAM/CD146 expression levels (pvalue: 3.42 e-02; pAdj: 5.67e-01). (**j**) Model describing the role of RalA/B-dependent EVs in metastatic formation.

The online version of this article includes the following figure supplement(s) for figure 5:

Figure supplement 1. RNA content of extracellular vesicles (EVs) from shControl, shRalA, and shRalB cells.

Figure supplement 2. 4T1 cells and extracellular vesicles (EVs) express CD146/MCAM long isoform.

shRalB EVs in the nature of the RNA they contain, as shRalA EVs showed an important increase in non-coding RNA (***Figure 5b***). Overall, this experiment reveals that RalA/B have a profound impact on the content of RNA in 4T1 EVs.

We further analyzed the protein content of 4T1 EVs by mass spectrometry. As shown in ***Figure 5c*** and 4T1 EVs contain a large number of proteins usually found in small EVs (77 of the top 100 proteins from Exocarta are found in 4T1 EVs; ***Supplementary file 2***), such as tetraspanins, integrins, ESCRT proteins or small GTPases, such as RalA/B themselves. Importantly, many of these proteins are known to localize to endosomes, suggesting that some of these EVs are bona fide exosomes. Unexpectedly, comparison of the proteome of EVs secreted by RalA or RalB knockdown cells did not reveal major differences, as no protein is exclusive to one type of EVs. Instead, a small proportion of proteins showed differential expression levels (***Figure 5d***; ***Supplementary file 2***). Regarding their protein content, we noted that EVs from control cells are closer to EVs from shRalB cells (97 proteins with differential expression) than to EVs from shRalA cells (217 proteins with differential expression). We then focused on the five proteins over-expressed in EVs from shCtl cells compared to both EVs from shRalA and EVs from shRalB cells. These proteins are CD146/MCAM, Clic4, Glypican 4, BDKRB2, and Abcg2. We verified the expression levels of CD146/MCAM, Clic4 and Glypican four by western blot of identical number of EVs (***Figure 5e***). While Clic4 and Glypican four are significantly under-expressed in EVs from shRalA or shRalB cells, the long isoform of CD146/MCAM (***Figure 5—figure supplement 2a***) showed a significant decrease in EVs from shRalA cells, and a tendency to decrease in EVs from shRalB cells, which was confirmed by anti-CD146 ELISA (***Figure 5—figure supplement 2b***). The hypothesis that Ral GTPases could control CD146 EV loading is further sustained by colocalization analysis. Indeed, by immunofluorescence, we observed that CD146 localizes both at the plasma membrane and in CD63-positive MVB/late endosomes in 4T1 cells, similarly to Ral GTPases (***Figure 5—figure supplement 2c***). Altogether, content analysis reveals that depletion of either RalA or RalB deeply affects the EV RNA loading and changes the levels of several key proteins.

We next interrogated whether the impact of RalA/B on the lung targeting and priming potential of EVs could be explained by its effect on the EV levels of MCAM/CD146. MCAM/CD146 (also known as Mel-CAM, Muc18, S-endo1, Gicerin) is an adhesion receptor overexpressed in various cancer types, including breast cancer, where it was shown to promote invasion and tumor progression (***Garcia et al., 2007***; ***Zeng et al., 2011***; ***Zeng et al., 2012***). In addition, MCAM/CD146 is present on endothelial cells where it mediates the adhesion of several cell types, including the transendothelial migration of monocytes (***Bardin et al., 2009***). Given, the known function of MCAM/CD146 in cell adhesion (***Wang and Yan, 2013***), we hypothesized that it may, at least in part, be responsible for

the lung tropism defects observed with EVs derived from RalA/B-depleted cells. To test the involvement of MCAM/CD146 in EVs adhesion, we treated 4T1 EVs with an anti-mouse MCAM/CD146 blocking antibody before injection in zebrafish or mouse circulation. EVs pretreated with MCAM/CD146 blocking antibody failed to successfully arrest on endothelial walls of zebrafish embryos (***Figure 5f***) and inefficiently reached the lungs in our mouse model (***Figure 5g***). Finally, we assessed the functional role of EV-bound CD146 in priming of pre-metastatic niches. To do this, 4T1 EVs were pre-treated with MCAM/CD146 blocking antibody (or with an isotype control) and injected intravenously, preceding tail-vein injection of 4T1 luciferase cells. Blocking CD146 on EVs significantly reduced their pro-metastatic potential. Therefore, inhibition of MCAM/CD146 precludes their lung accumulation and the subsequent formation of metastasis and thereby phenocopies RalA/B knockdown. These results demonstrate that MCAM/CD146, whose presence at the surface of EVs is tuned by RalA/B, is, at least partly responsible of the adhesion and lung tropism of 4T1 EVs. It further explains why EVs from RalA knockdown cells, which have reduced levels of MCAM/CD146, fail to reach the lungs efficiently. The pro-metastatic role of MCAM/CD146 is further confirmed by the analysis of a human cohort of breast cancer showing that its high expression is associated with worsened prognosis (***Figure 5h***). Altogether, our work demonstrates that RalA/B, by controlling MVB homeostasis, promote the secretion CD146-enriched EVs, whose lung tropism sustains efficient metastasis (***Figure 5i***).

Discussion

The therapeutic limitations of breast cancer metastasis warrant a deeper understanding of its molecular machinery. Our findings highlight the exosome-mediated priming of metastatic niches by Ral GTPases as a critical requisite for lung metastasis during breast cancer progression. We show that RalA and RalB promote the secretion of exosomes by maintaining a high number of multi-vesicular bodies, likely through the PLD1-PA axis. Furthermore, we demonstrate that RalGTPases favor the secretion of CD146-rich exosomes, which accumulate in metastatic organs, notably in lungs, where they establish premetastatic niches (***Figure 5i***). Finally, we show that high levels of RalA and RalB correlated with poor prognosis suggesting a unified mechanism for human breast cancer metastasis.

This work, together with our previous study of RAL-1 in *C. elegans* (***Hyenne et al., 2015***), establishes Ral GTPases as major evolutionarily conserved mediators of exosome secretion. Our experiments suggest that RalA/B contribute to exosome secretion in several tumor cell lines, of different origins, implying that they might function pleiotropically over various cancers. Our results suggest that RalA/B and their effector PLD1 affect the levels of secreted exosomes by tuning the levels of cytoplasmic MVBs. While Ral GTPases, partially localized at the plasma membrane, could also affect microvesicle secretion, our data indicate that they function in exosome biogenesis upstream of PLD1. Similarly, a direct correlation between MVB density and levels of secreted EVs was recently suggested by studies showing that chemical or electric stimulation of MVB biogenesis results in increased EV secretion (***Kanemoto et al., 2016***; ***Yang et al., 2020***). The formation of MVBs results from dramatic biochemical transformations of endosomes involving multiple protein and lipid switches (***Huotari and Helenius, 2011***; ***Scott et al., 2014***). Understanding the steps at which RalA/B and PLD affect this endosome maturation program is critical and remains to be fully deciphered. Our results from mice and *C. elegans* suggest that biogenesis of ILVs, which is a key step in MVB maturation and the initial phase of the exosome secretion pathway, could as well be controlled by RalA/B. Our work further identifies PLD as an effector acting downstream of Ral to control exosome secretion. Whether other Ral effectors contribute to EV secretion remains to be addressed. Interestingly, while PLD2 was found to impact exosome secretion by governing ILV biogenesis in a different breast carcinoma cell line (***Ghossoub et al., 2014***), our data rather suggest that PLD1 controls exosome biogenesis in 4T1 cells. Indeed, PLD1 localizes on MVBs and its inhibition, but not the inhibition of PLD2, decreases MVB density. Nevertheless, it should be noted that we measured EV secretion levels and MVB density based on PLD inhibition at previously-published high concentrations of the inhibitors (compared to their respective IC50) and that off-target effect can not be ruled out. By contrast, PLD2 is essentially localized at the plasma membrane of 4T1 cells and its inhibition reduces EV secretion suggesting that PLD2 could rather promote microvesicle secretion in 4T1 cells. Therefore, we speculate that RalA/B-PLD1 control ILV biogenesis in 4T1 cells, possibly through the

regulation of PA levels. Alternatively, they could impact the homeostasis of a subclass of MVBs, for instance by controlling their stability or their degradation.

Priming of metastatic niches by (soluble or) EV-mediated factors takes central stages in cancer progression (**Gao et al., 2019**; **Peinado et al., 2017**) and identification of molecular machineries that underlie this condition could point to new therapeutic or diagnostic targets. Our study demonstrates that Ral GTPases enhance the formation of lung metastasis in mouse models, by promoting the secretion of exosomes within primary tumors, while RalA/B expression levels correlates with metastasis in human breast cancer. While the pro-tumoral activity of Ral GTPases was so far mostly attributed to their capacity to promote anchorage-independent cell growth (for RalA) or cell invasion (for RalB) (**Yan and Theodorescu, 2018**), we now show that Ral GTPases have additional non-cell autonomous functions, and that these functions are important contributors to metastasis. Indeed, in 4T1 cells, depletion of either RalA or RalB alters the levels, content and functionality of secreted EVs, without decreasing cell migration or proliferation. Depending on the cell type or the biological process, RalA and RalB can display redundant, synergistic or even antagonist activities (**Gentry et al., 2014**). Since RalA and RalB mostly share similar phenotypes regarding EV secretion, content and function, they likely function in the same pathway. Interestingly, both Ral proteins appear to be essential for exosome secretion, revealing that their functions are not fully redundant. Therefore, both GTPases are required for the generation of a specific subpopulation of EVs with enhanced pro-metastatic properties and further work is needed to fully unravel the downstream molecular pathways. With this work, RalA and RalB add to the list of proteins known to control exosome secretion and to affect tumor progression, such as Rab27a (**Bobrie et al., 2012**; **Kren et al., 2020**; **Peinado et al., 2012**), Alix (**Monypenny et al., 2018**), syntenin (**Das et al., 2019**), and components of the ESCRT machinery (**Mattissek and Teis, 2014**). These studies demonstrate that the number of EVs secreted by a primary tumor is an essential element determining the efficiency of metastasis. However, it is important to keep in mind that all these proteins regulating EV trafficking, including RalA/B, contribute to tumor progression through both exosome dependent and exosome independent functions. Altogether, despite pointing to additional functions of RAL GTPases, our study is the first to identify new molecular machinery from its function in EV biogenesis up to its pro-metastatic function in breast cancer lung metastasis.

Priming of metastatic niches by EVs has, so far, mostly been attributed to increased levels of pro-metastatic EVs with pro-metastatic functions (**Becker et al., 2016**; **Bobrie et al., 2012**; **Peinado et al., 2012**). In addition to controlling the levels of secreted EVs, we show that RalA/B affect their function by enhancing their capacity to induce endothelial permeability in vitro and pre-metastatic niches in vivo. These two observations could be linked, as RalA/B-dependent EVs could promote endothelial permeability locally in the primary tumor or at distance in lungs, thereby favoring both tumor intravasation and extravasation. Content analysis revealed that RalA/B control the identity and levels of RNAs and proteins present in secreted EVs. Interestingly, Ras, which is known to activate RalA/B (**Gentry et al., 2014**), also controls the protein and RNA cargo of tumor EVs (**Cha et al., 2015**; **Demory Beckler et al., 2013**; **McKenzie et al., 2016**), although its effect on the levels of secreted EVs is unclear (**Demory Beckler et al., 2013**; **McKenzie et al., 2016**). As McKenzie and collaborators identified a MEK-ERK-Ago2 pathway downstream of Ras (**McKenzie et al., 2016**), it would be interesting to determine how this pathway connects with the Ral-PLD-PA axis described in our study. Among the few proteins significantly enriched in RalA/B-dependent EVs, we identified CD146, a molecule known to modulate cell-cell adhesion (**Wang and Yan, 2013**). We showed, using functional inhibition, that CD146 present on pro-metastatic EVs controls their lung targeting efficiency thereby impacting their biodistribution and niche-promoting function. Accordingly, we and others show that high expression of CD146 correlates with poor prognosis in human breast carcinoma (**Garcia et al., 2007**; **Zeng et al., 2012**). CD146 functions as an adhesion molecule involved in homophilic and heterophilic interactions (**Wang and Yan, 2013**), promoting for instance monocyte transmigration (**Bardin et al., 2009**). CD146 can perform trans-homophilic interactions via its immunoglobulin-like extracellular domain (**Taira et al., 1994**; **Taira et al., 2005**). It also binds to extracellular matrix proteins or other transmembrane proteins, such as VEGFR2 (**Wang and Yan, 2013**). Therefore, it is tempting to speculate that CD146 affects the biodistribution and organ targeting efficiency of circulating tumor EVs by mediating their interaction with specific ligands present on the luminal side of endothelial cells of metastatic organs. Other adhesion molecules, such as integrins and tetraspanins were shown to affect the biodistribution of tumor EVs and ultimately the formation

of metastasis (**Hoshino et al., 2015**; **Yue et al., 2015**). Therefore, it is likely that the combination of these receptors at the surface of tumor EVs, combined with the differential expression of their ligands on endothelial cells throughout the organism will dictate their homing. More work will be needed to characterize this organ specific EV zip code and to identify relevant endothelial ligands for circulating EVs and develop inhibitory strategies to impair their arrest and uptake at metastatic sites. In addition, the presence of other cell types in the circulation, such as patrolling monocytes, which take up large amounts of circulating EVs, could also contribute to the accumulation of tumor EVs in specific organs (**Hyenne et al., 2019**; **Plebanek et al., 2017**). Finally, other factors, such as the vascular architecture and hemodynamic patterns could be involved (**Follain et al., 2020**; **Hyenne et al., 2019**) and the interplay between these mechanical cues and the surface repertoire of metastatic EVs should be a fertile ground for future research. Precisely dissecting the mechanisms by which tumor EVs reach specific organs would allow to understand the priming of premetastatic niches.

Overall, our study identifies RalA/B GTPases as a novel molecular machinery that regulates the formation and shedding of pro-metastatic EVs. We also discovered CD146 as an EV cargo whose targeting could inspire new therapeutic strategies to impact the progression of metastatic breast cancer.

Materials and methods

Cell culture

The establishment of 4T1 cell lines stably expressing shRNA against RalA, RalB, or a scramble sequence has been described previously (**Hyenne et al., 2015**). 4T1-Luciferase (RedLuc) cells were purchased from Perkin-Elmer. All 4T1 cell lines were cultured in RPMI-1640 medium, completed with 10% fetal bovine serum (FBS, Hyclone) and 1% penicillin-streptomycin (PS) (GIBCO). 4T1 shRNA cell lines were maintained in medium containing 1 µg/ml puromycin, except during experiments, and regularly checked for the stability of knockdown by western blots. Human Umbilical Vein Endothelial Cells (HUVEC) (PromoCell) were grown in ECGM (PromoCell) supplemented with a supplemental mix (PromoCell C-39215) and 1% PS. Human A375 melanoma and human MDA-MB-231, MCF7 and SKBR3 breast cancer (ATCC) cell lines were grown in high-glucose Dulbecco's modified Eagle's Medium (DMEM, Gibco Invitrogen Corporation) supplemented with 10% (FBS) and 1% PS. D2A1 cell were grown in high-glucose Dulbecco's modified Eagle's Medium (DMEM, Gibco Invitrogen Corporation) supplemented with 5% (FBS), 5% new born calf serum, 1% non-essential amino acids, and 1% PS. Human Panc-1 pancreatic adenocarcinoma cell line was grown in RPMI-1640 supplemented with 10% FBS, and 50 µg/ml gentamicin sulfate (Gibco/Life Technologies). All cell lines were cultured in a humidified atmosphere containing 5% CO_2 at 37˚C and checked regularly for absence of mycoplasma by PCR (VenorGeM, Clinisciences).

Plasmid transfections

Cells at 50–70% confluency were transfected with 1 µg of plasmid using JetPRIME (PolyPlus, Illkirch, France) according to the manufacturer's instructions. The following plasmids were used: pGFP-PLD1, pGFP-PLD2 (**Corrotte et al., 2006**), pLenti CMV:tdtomato-RalA, and pLenti CMV:tdtomato-RalB.

Drug treatment

Cells were incubated with the following drugs in the appropriate medium: RalA/B inhibitors BQU57 (10 µM; Sigma) and RBC8 (10 µM; Sigma), PLD1 inhibitor CAY10593 (10 µM; Santa Cruz Biotechnology) or PLD2 inhibitor CAY10594 (10 µM; Santa Cruz Biotechnology). Cells were treated for 18 hr before processing for EV isolation or cell analysis.

qRT-PCR analysis

Total RNA was extracted from cells using TRI Reagent (Molecular Research Center) according to the manufacturer's instructions. For qRT-PCR, RNA was treated with DNase I and reverse transcribed using the High-Capacity cDNA RT Kit. qRT-PCR was performed using the Power SYBR Green PCR Master Mix or TaqMan Gene Expression Master Mix using a 7500 Real-Time PCR machine (Applied Biosystems). All compounds were purchased from Life Technologies (St Aubin, France). Data were

normalized using a Taqman mouse probe against GADPH as endogenous control (4333764T, Life Technology) and fold induction was calculated using the comparative Ct method (-ddCt).

Western blot

Cell or EV extracts were denatured in Laemmli buffer and incubated at 95˚C for 10 min. 10 µg of protein extract (for cell lysates) or equal number of EVs (8.50 × 10^8 EVs per lane, measured by NTA) were loaded on 4–20% polyacrylamide gels (Bio-Rad Laboratories, Inc). The following antibodies were used: CD9 (Rat, 553758; BD Biosciences), RalA (mouse, 610221; BD Biosciences), RalB (mouse, 04037; Millipore), Glypican 4 (Rabbit, PA5-97801; Thermo Fisher Scientific), antibodies specifically recognizing the short and long isoforms of CD146 were previously described (***Kebir et al., 2010***), Clic4 (mouse, 135739; Santa Cruz Biotechnology), α-tubulin (mouse, CP06; Millipore) and Secondary horseradish peroxidase-linked antibodies: anti-Rat (GE healthcare; NA935), anti-Mouse (GE healthcare; NA 931) and anti-rabbit (GE healthcare; NA934). Acquisitions were performed using a PXi system (Syngene). Intensities were measured using the Fiji software.

Elisa

Elisa was performed according to the manufacture's instruction (RayBiotech) by loading equal number of EVs (7 × 10^8 - 9.5 × 10^9) per well (two experiments in triplicate).

Electron microscopy

Chemical fixation

Cells were fixed with 2.5% glutaraldehyde/2.0% paraformaldehyde (PFA) (Electron Microscopy Sciences) in 0.1M Cacodylate buffer at room temperature for 2 hr, then rinsed in 0.1M Cacodylate buffer (Electron Microscopy Sciences) and post-fixed with 1% OsO4 (Electron Microscopy Sciences) and 0.8% $K_3Fe(CN)_6$ (Sigma-Aldrich) for 1 hr at 4˚C. Then, samples were rinsed in 0.1M Cacodylate buffer followed by a water rinse and stained with 1% uranyl acetate, overnight at 4˚C. The samples were stepwise dehydrated in Ethanol (50%, 70% 2 × 10 min, 95% 2 × 15 min and 100% 3 × 15 min), infiltrated in a graded series of Epon (Ethanol100%/Epon 3/1, 1/1, 1 hr) and kept in Ethanol100%/Epon 1/3 overnight. The following day, samples were placed in pure Epon and polymerized at 60˚C. One hundred nm thin sections were collected in 200 copper mesh grids and imaged with a Philips CM12 transmission electron microscope operated at 80 kV and equipped with an Orius 1000 CCD camera (Gatan).

High-pressure freezing

HPF was performed using an HPF COMPACT 03 high pressure freezing machine (Wohlwend), using 3 mm diameter Aclar film disks (199 um thickness), as cell carriers. Subsequent freeze substitution in acetone was performed using an automatic FS unit (Leica AFS), including 0.25% OsO4 staining, and Epon embedding. Sections were contrasted on grids with 1% uranyl acetate followed with 0,4% lead citrate (Sigma-Aldrich). Imaging was performed similarly to chemical fixation.

The number of MVBs and lysosomes per surface of cytoplasm were quantified using the Fiji software. MVBs and lysosomes were distinguished based on their morphology: MVBs have one or more ILVs and lysosomes contain ILVs but are also electron dense and contain irregular membrane curls.

FACS analysis

For cell cycle analysis, 10^6 cells were fixed using the FoxP3 Staining Kit (00-5523-00 eBioscience) for 30 min at toomr temperature in the dark. Samples were then resuspended in permeabilization buffer containing 20 µg of RNase A (R6513 Sigma) and 1 µg of propidium iodide (PI) (130-093-233 Miltenyi Biotech) for 30 min. PI fluorescence was analyzed using a BD Accuri C6 cell analyzer with BD CSampler Analysis Software. Results were analyzed with FlowJo software version 10 (TreeStar).

For lysosomal analysis, confluent cells were incubated with 1 µM Lysotracker Green DND 26 (L7526-Thermo Fischer) diluted in complete RPMI medium for 30 min at 37˚C. Cells were then detached by addition of TrypLE (12604021, ThermoFischer), washed in PBS 2% (v/v) FCS, and stained with 0.1 µM DAPI in PBS 2% (v/v) FCS immediately before analysis. Samples were processed on a Gallios Flow Cytometer (Beckman Coulter). Dead cells and doublets were excluded from analysis respectively by the selection of DAPI negative cells and co-analysis of integral vs time-of-flight

side scatter signals. Data were analyzed on FlowJo software (BD Bioscience). Mean Fluorescence intensities (MFI) of lysotracker in each condition were normalized by performing a ratio with MFI of an unstained condition in the same channel.

Migration assays

For 2D migration assays, 4T1 mammary tumor cells were plated on 35 mm plastic dishes (six-well plates) and grown for 2 days until reaching 90% confluence. The cells were then grown for 16 hr in serum-free medium before wounding of the monolayer by scraping from the middle of the plate. Cells were incubated in complete RPMI medium and sequential images of the wound were collected with a ×10 objective at 0, 8, and 24 hr after wounding. Percentage of wound closure over time was analyzed and quantified using the Fiji software.

3D Organotypic invasion assays were conducted as previously described (***Timpson et al., 2011***; ***Vennin et al., 2017***). Briefly, rat tail tendon collagen was extracted with 0.5 mol/L acetic acid to a concentration of 2.5 mg/ml. A total of 8.4×10^4 telomerase immortalized fibroblasts (TIFs) were embedded into the neutralized collagen in the presence of 1 x MEM and 8.8% FBS. Matrices were allowed to contract over a 12-day period in DMEM (1% P/S, 10% FBS). Following contraction TIFs were removed with puromycin (2 µg/ml) for 72 hr before 8×10^4 4T1 cells were seeded on the contracted matrices and allowed to grow to confluence for 48 hr in RPMI (1% P/S, 10% FBS). The matrices were then transferred to an air-liquid interface on a metal grid and cells allowed to invade for 15 days with media changes every 2 days. Following the invasion, organotypic matrices were fixed in 10% buffered formalin and processed for histochemical analysis. The invasive index was measured in three representative fields of view per matrix with three matrices per replicate for three replicates.

$$\text{Invasive Index} = \frac{\text{Number of cells}>200\ \mu\text{m depth}}{\text{Cells on top of the matrix}}$$

In vitro permeability assay

Transwell filter inserts (pore size 1.0 µm, 12 mm diameter, polyester membrane, Corning, New York, USA) were coated with fibronectin (10 µg/ml; Sigma). Then, HUVECs were seeded (0.3×10^6 cells/well) and grown on transwell filters for 48 hr until reaching confluency. Confluent monolayers of HUVEC cells were treated with similar amounts (10–100 µg) of 4T1-EVs, PBS (as a negative control) or with 100 ng/ml TNF-α (as a positive control) overnight. FITC-dextran (MW ~70,000; Sigma) was added to the top well at 25 mg/ml for 20 min at 37˚C, and fluorescence was measured in the bottom well using a fluorescence plate reader (Berthold Tris Star 2; 485 nm excitation and 520 nm emission). Cells were washed for three times and were fixed for immunofluorescence (described below).

Secretome analysis

Cell culture supernatants were collected and centrifuged for 15 min at 300 g. Supernatants were incubated with Mouse XL Cytokine Array membranes (R and D Systems) according to the manufacturers' instructions. Three independent experiments were performed. Intensities were measured using the Fiji software.

In vitro proliferation assay

Briefly, cells were seeded in 96-well plates at the density of 2000 cells per well with 200 µl of complete culture medium and cultured for 24, 48, and 72 hr at 37˚C. Culture medium without cells was used as the blank control group. To avoid the edge effect, the peripheral wells were filled with sterile PBS. For the proliferation test, a total of 20 µl MTS solution was added to each well, followed by incubation for 2 hr at 37˚C. Optical density was measured at 490 nm using a Berthold Tristar device.

EVs isolation and characterization

Cells were cultured in EV-depleted medium (obtained by overnight ultracentrifugation at 100,000 g, using a Beckman, XL-70 centrifuge with a 70Ti rotor) for 24 hr before supernatant collection. The extracellular medium was concentrated using a Centricon Plus-70 centrifugal filter (10 k; Millipore) and EVs were isolated by successive centrifugation at 4˚C: 15 min at 300 g, 10 min at 2000 g, 30 min at 10,000 g and 70 min at 100,000 g (using a Beckman XL-70 centrifuge with a SW28 rotor). EVs pellets were washed in PBS, centrifuged again at 100,000 g for 70 min, resuspended in PBS and stored

at 4˚C. For all functional experiments, EVs were used immediately after isolation or stored overnight at 4˚C and injected the next day. For content analysis, EVs were frozen at −80˚C. After EV isolation, EVs numbers and size distribution were measured by NTA using a ZetaView (Particle Metrix, Meerbusch, Germany).

For in vivo mouse experiments, EVs were isolated the using the iZON qEV2 size exclusion column (Izon science, Cambridge MA) according to the manufacturer's instructions. After rinsing the columns with PBS, 2 ml of concentrated extracellular medium were applied on top of a qEV column (Izon Science) and 6 ml fractions were collected. For organotropism experiments, four EV-rich fractions (F2, F4, F6, and F8) were pooled, then ultracentrifuged for 1 hr at 100,000 ×g, 4˚C with a SW28 rotor in a Beckman XL-70 centrifuge or concentrated using an Amicon Ultra-4 10 kDa centrifugal filter device (Merck Millipore). Pellets were resuspended in 500 µl PBS. For priming experiment, the most EV-rich fraction was used (F4).

For fluorescent labeling, isolated EVs were incubated with MemBright-Cy3 or Cy5 (***Collot et al., 2018***) at 200 nM (zebrafish) and 500 nM (mice) (final concentration) in PBS for 30 min at room temperature in the dark. Labeled EVs were then rinsed in 15 ml of PBS, centrifuged at 100,000 g with a SW28 rotor in a Beckman XL-70 centrifuge and pellets were resuspended in 50 µl PBS. EVs were used immediately after isolation or stored for a maximum of one night at 4˚C before use.

Mass spectrometry-based proteomics experiments

Sample preparation of EVs Proteins. A total of 20 mg samples were denatured at 95˚C for 5 min in Laemmli buffer and concentrated in one stacking band using a 5% SDS-PAGE gel. The gel was fixed with 50% ethanol/3% phosphoric acid and stained with colloidal Coomassie Brilliant Blue. The gel bands were cut, washed with ammonium hydrogen carbonate and acetonitrile, reduced and alkylated before trypsin digestion (Promega). The generated peptides were extracted with 60% acetonitrile in 0.1% formic acid followed by a second extraction with 100% acetonitrile. Acetonitrile was evaporated under vacuum and the peptides were resuspended in 10 µl of H20% and 0.1% formic acid before nanoLC-MS/MS analysis.

NanoLC-MS/MS analysis. NanoLC-MS/MS analyses were performed on a nanoACQUITY Ultra-Performance LC system (Waters, Milford, MA) coupled to a Q-Exactive Plus Orbitrap mass spectrometer (ThermoFisher Scientific) equipped with a nanoelectrospray ion source. The solvent system consisted of 0.1% formic acid in water (solvent A) and 0.1% formic acid in acetonitrile (solvent B). Samples were loaded into a Symmetry C18 precolumn (0.18 × 20 mm, 5 µm particle size; Waters) over 3 min in 1% solvent B at a flow rate of 5 µl/min followed by reverse-phase separation (ACQUITY UPLC BEH130 C18, 200 mm x 75 µm id, 1.7 µm particle size; Waters) using a linear gradient ranging from 1% to 35% of solvent B at a flow rate of 450 nl/min. The mass spectrometer was operated in data-dependent acquisition mode by automatically switching between full MS and consecutive MS/MS acquisitions. Survey full scan MS spectra (mass range 300–1800) were acquired in the Orbitrap at a resolution of 70K at 200 m/z with an automatic gain control (AGC) fixed at 3.10^6 and a maximal injection time set to 50 ms. The 10 most intense peptide ions in each survey scan with a charge state ≥2 were selected for fragmentation. MS/MS spectra were acquired at a resolution of 17.5K at 200 m/z, with a fixed first mass at 100 m/z, AGC was set to 1.10^5, and the maximal injection time was set to 100 ms. Peptides were fragmented by higher energy collisional dissociation with a normalized collision energy set to 27. Peaks selected for fragmentation were automatically included in a dynamic exclusion list for 60 s. All samples were injected using a randomized and blocked injection sequence (one biological replicate of each group plus pool in each block). To minimize carry-over, a solvent blank injection was performed after each sample. EVs mass spectrometry was performed in triplicate.

Data interpretation. Raw MS data processing was performed using MaxQuant software1 v1.6.7.0 (***Cox et al., 2014***). Peak lists were searched against a database including *Mus musculus* protein sequences extracted from SwissProt (09-10-2019; 17 007 sequences, Taxonomy ID = 10 090). MaxQuant parameters were set as follows: MS tolerance set to 20 ppm for the first search and five ppm for the main search, MS/MS tolerance set to 40 ppm, maximum number of missed cleavages set to 1, Carbamidomethyl (C) set as a fixed modification, Oxidation (M) and Acetyl (Protein N-term) set as variable modifications. False discovery rates (FDR) were estimated based on the number of hits after searching a reverse database and were set to 1% for both peptide spectrum matches (with a minimum length of seven amino acids) and proteins. All other MaxQuant parameters were set as default.

Protein intensities were used for label-free quantification. The imputation of the missing values (DetQuantile imputation) and differential data analysis were performed using the open-source ProStaR software (**Wieczorek et al., 2017**). A Limma moderated t-test was applied on the dataset to perform differential analysis. The adaptive Benjamini-Hochberg procedure was applied to adjust the p-values and FDR values under 1% were achieved.

Complete dataset has been deposited to the ProteomeXchange Consortium via the PRIDE partner repository5 with the dataset identifier PXD020180 (**Deutsch et al., 2020**).

RNA sequencing

EV pellets were treated with proteinase K (0.05 µg/µl) for 10 min at 37˚C. Roche Cocktail Inhibitor was then added to the sample for 10 min at room temperature followed by incubation at 85˚C for 5 min. Samples were then incubated with RNase A (0.5 µg/µl) for 20 min at 37˚C to degrade unprotected RNA. Total RNAs of isolated EVs was extracted using TRI Reagent (Molecular Research Center). Total RNA Sequencing libraries were prepared with SMARTer Stranded Total RNA-Seq Kit v2 - Pico Input Mammalian (TaKaRa) according to the manufacturer's instructions. Libraries were pooled and sequenced (paired-end 2*75 bp) on a NextSeq500 using the NextSeq 500/550 High Output Kit v2 according to the manufacturer's instructions (Illumina, San Diego, CA, USA). Raw sequencing data generated by the Illumina NextSeq500 instrument were mapped to the mouse reference genome using the hisat2 software (**Kim et al., 2015**). For every sample, quality control was carried out and assessed with the NGS Core Tools FastQC (http://www.bioinformatics.babraham.ac.uk/projects/fastqc/). Read counts were generated with the htseq-count tool of the Python package HTSeq (**Anders et al., 2015**). Differential analysis was performed by the DESEQ2 (**Love et al., 2014**) package of the Bioconductor framework. Detection of significantly up- and down-regulated genes between pairs of conditions based on their log2FC and functional enrichment analyses were performed using STRING v11 (**Szklarczyk et al., 2019**). EVs RNA sequencing was performed in triplicate.

Lipidomics

EVs were extracted with 2 ml of chloroform/methanol 2/1 v/v and 1 ml water, sonicated for 30 s, vortexed, and centrifuged. Lower organic phase was transferred to a new tube, the upper aqueous phase was re-extracted with 2 ml chloroform. Organic phases were combined and evaporated to dry. Lipid extracts were resuspended in 50 µl of eluent A. Synthetics internals lipid standards (PA 14:1/17:0, PC 17:0/14:1 and PS 17:0/17:0) from Avanti Polar Lipids was added. LC-MS/MS (MRM mode) analyses were performed with a MS model QTRAP 6500 (ABSciex) coupled to an LC system (1290 Infinity II, Agilent). Analyses were achieved in the negative (PA) and in positive (PC) mode; nitrogen was used for the curtain gas (set to 20), gas 1 (set to 20) and gas 2 (set to 10). Needle voltage was at − 4500 or 5500 V without needle heating; the declustering potential was adjusted set at − 172 V or + 40 V. The collision gas was also nitrogen; collision energy is set to − 46 or + 47 eV. The dwell time was set to 30 ms. Reversed phase separations were carried out at 50˚C on a Luna C8 150 × 1 mm column, with 100 Å pore size, 5 µm particles (Phenomenex). Eluent A was isopropanol/CH_3OH/H_2O (5/1/4) +0.2% formic acid+0.028% NH_3 and eluent B was isopropanol+0.2% formic acid+0.028% NH_3. The gradient elution program was as follows: 0–5 min, 30–50% B; 5–30 min, 50–80% B; 31–41 min, 95% B; 42–52 min, 30% B. The flow rate was set at 40 µl/min; 15 µl sample volumes were injected. The areas of LC peaks were determined using MultiQuant software (v3.0, ABSciex) for PA and PC quantification. EVs lipid analysis was performed in triplicate.

Animal experiments

All animals were housed and handled according to the guidelines of INSERM and the ethical committee of Alsace, France (CREMEAS) (Directive 2010/63/EU on the protection of animals used for scientific purposes). Animal facility agreement number: #C67-482-33. Experimental license for mice: Apafis #4707–20 I6032416407780; experimental license for zebrafish: Apafis #16862–2018121914292754.

Mouse experiments

Six- to 8-week-old female BalB/c mice (Charles River) were used in all experiments.

Orthotopic breast tumor experiments: Syngenic BalB/c mice were injected in the left fourth mammary gland with 250,000 4T1 mammary tumor cells stably expressing either scramble control shRNA, RalA shRNA, or RalB shRNA and diluted in 50 µl PBS. When tumors became palpable, tumor volume was assessed by caliper measurements using the formula (width^2 × length)/2 (mm^3) twice a week for 41 days. At the endpoint of the experiment, tumors and lungs were harvested, weighted, and fixed in formaldehyde. Alternatively, organs were embedded in OCT and frozen at −80˚C. In this case, lungs were inflated with OCT before dissection.

Priming experiments

Mice were injected retro-orbitally with 1.5 × 10^8 EVs isolated from 4T1-shControl, shRalA and shRalB cells. Two injections of EVs were performed 2 days apart. PBS was used as a negative control. Subsequently, 4T1-luciferase cells (90.000) were injected via tail vein one day after EV pre-conditioning. After cells injection, the extent of lung metastasis was measured every 3 days for 12 days using non-invasive imaging with IVIS Lumina III (Perkin Elmer). In brief, a D-luciferin solution (purchased from Perkin Elmer and used at 150 mg/kg, according to manufacturer's instructions) was injected intraperitoneally to the isofluorane (Zoetis) anesthetized mice. 5 min after luciferin injection, a bioluminescence image was acquired with an IVIS Lumina III (Perkin Elmer) imaging system and then analyzed using the Living Image software (Perkin Elmer). The rate of total light emission of the lung metastatic area was calculated and expressed as radiance photons counted during the whole acquisition time (5 min) and normalized to the initial radiance photon (photon/second/cm^2/sr) measured immediately after 4T1- luciferase cells injection for each mouse (t0).

EV biodistribution

Mice were injected via retro-orbital venous sinus with 1–4 × 10^8 MenBright-Cy3-labeled EVs freshly isolated from 4T1-shControl, shRalA, and shRalB cells. PBS was used as a negative control. Mice were sacrificed 1 hr post-injection to quantify the fluorescence intensity of the organs ex vivo with IVIS Lumina III (Perkin Elmer). Average of fluorescent photons per lung were quantify as radiant efficiency [photon/second/cm^2/sr] / [µW/cm^2]. For experiment testing the role of CD146 in EV biodistribution, isolated EVs were incubated with CD146 blocking antibody (EPR3208; Abcam; 12 µg/ml) for 30 min at room temperature before injection. For metastasis priming experiments, CD146 was blocked similarly and a rabbit IgG isotype was used as control (Abcam) at an equivalent concentration.

Zebrafish experiments

At 48 hr post-fertilization (hpf), Tg(Fli1 :GFP) zebrafish embryos were dechorionated and mounted in 0.8% low melting point agarose pad containing 650 mM of tricaine (ethyl-3-aminobenzoate-methanesulfonate). Embryos were injected in the duct of Cuvier with 27.6 nl of Membright Cy5-labeled EVs (at 10^{10} EVs/ml) freshly isolated from 4T1-shControl, shRalA, and shRalB cells with a Nanoject microinjector 2 (Drummond) under a M205 FA stereomicroscope (Leica), using microforged glass capillaries (25–30 mm inner diameter) filled with mineral oil (Sigma). Embryos were imaged with confocal right after injection. For experiment testing the role of CD146, 4T1-isolated EVs were incubated with CD146 blocking antibody (12 µg/ml) for 30 min at room temperature before injection.

Tissue section and staining

Mouse lungs were incubated overnight in 4% PFA, dehydrated in 100% ethanol for 24 hr, embedded in paraffin, cut in 7-µm-thick sections, dewaxed and rehydrated with 100% Toluene (two washes of 15 min) then incubated in 100–70% alcohol solutions (10 min each) followed by final staining with hematoxylin (Surgipath) for 5 min and washing with tap water. Sections were further processed with differentiation solution (1% HCl in absolute ethanol, for 7 s), followed by washing under tap water for 10 min. Sections were then incubated in eosin (Harris) for 10 s, rinsed and dehydrated in 70–100% alcohol baths with rapid dips in each bath before a final wash in toluene for 15 min and embedded in Eukitt solution (Sigma). Two random distanced sections taken in each of the five lung were analyzed for each mouse. Stitching imaging was performed using an AxioImager (Zeiss) with a ×10 objective. Metastatic surfaces and whole lung surfaces were measured using the Fiji software.

Caspase 3/7 assay

Mouse tumor samples stored at −80˚C are disrupted in a buffer containing Tris HCl pH 7.5, 50 mM, NaCl 150 mM, NP40 1% + Protease Inhibitors cocktail (Complete from Roche) in the presence of 4 zirconium beads, using the Precellis system (Bertin instruments) with two pulses (10'') at 5000 rpm. Protein concentration was measured using Bradford kit (BioRad) and 5 µg was analyzed using the Caspase 3/7 glo kit (Promega) according to manufacturer's instructions. Photons production generated by the luciferase was measured using a luminometer (Berthold Tris Star 2).

Immunofluorescence

For immunofluorescence on cultured cells, cells were fixed with 4% PFA for 15 min, permeabilized in PBS-Triton 0.1% (Sigma) for 10 min and incubated in 5% normal goat serum for 1 hr. The following primary antibodies were used: ZO-1 (Rabbit, 61–7300; Thermo Fisher Scientific), VE-Cadherin (mouse, 348502; BioLegend), CD63 (rat, D623-3; MBL), RalA (mouse, 610221; BD), RalB (mouse, 04037; Millipore), CD146 (Mouse, P1H12, Thermofisher). The following secondary antibodies were used: goat anti-mouse/rat/rabbit coupled with Alexa Fluor 488, Alexa 555, or Alexa 647 (Invitrogen). Cells were mounted with DAPI-containing Vectashield (Vector Laboratories).

For immunofluorescence on tissue sections, tissues were cut in 7-µm-thick sections, dewaxed for paraffin-embedded tissues and air-dried for frozen tissues. Sections were incubated first in 5% normal goat serum for 2 hr in a humidified container. The following antibodies were used: CD31 (Mouse, 37–0700; Thermo Fisher Scientific), S100A4 A gift from Nona Ambartsumian (Institut for Cancer Biology, Copenhagen, DK-2100, Denmark.), F4/80 (Rat, ab6640; abcam), rabbit monoclonal antibody against Ki67 (Rabbit, RM-9106-S0; Thermo Fisher Scientific), and caspase-3 (Mouse, 966S1; Cell Signaling Technology). Secondary antibodies were similar to the ones used with cells. Nuclei were stained with DAPI (Sigma).

Imaging and analysis

Imaging on fixed samples. Tissue and cell sections were imaged with a Zeiss Imager Z2 with a ×40 objective (N.A. 1.4) or with an SP5 confocal (Leica) with a ×63 objective (N.A. 1.25). Image analysis and processing were performed using the Fiji software. For endothelial adherent and tight junction analysis, 10 random junctions were analyzed per image (five images per sample) measuring junction width. For Ki67 and Caspase three imaging, 15 random fields of view were quantified per sample. For EVs imaging, 40–60 random fields of view were imaged on three to four sections per mouse.

Live-cell imaging. For live-cell imaging, cells were seeded on 3.5 cm diameter glass-bottom dishes (MatTek Corporation, Ashland, MA) pre-coated with fibronectin (10 µg/ml; Sigma). Nuclei were labeled with NucBlue Live Ready Probe (Life Technologies, Grand Island, NY). In some experiments, cells were incubated with Lysotracker Deep Red (Thermo Fisher Scientific) at 1 µM for 30 min before imaging. Cells were imaged by confocal microscopy (SP5, Leica) equipped with a thermostated chamber at 37˚C with 5% CO_2. Image analysis and processing were performed using the Fiji software.

HUVEC cells were seeded in fibronectin (10 µg/ml; Sigma) pre-coated glass bottom culture chambers (LabTek I, Dutscher 055082). Confluent cells were incubated with 2×10^8 MemBright-labeled EVs in ECGM EV-free medium for 1 hr. Nucleus were labeled using NucBlue (Life Technologies, Grand Island, NY). Cells were imaged by confocal microscopy (SP5 Leica) in a thermostated chamber at 37˚C with 5% CO_2.

Zebrafish imaging: Confocal imaging was performed on the caudal plexus of zebrafish embryos right after injection with an inverted TCS SP5 with HC PL APO 20X/0,7 IMM Corr CS objective (Leica). Image analysis and processing were performed using the Fiji software.

Human samples

Human databases: Kaplan-Meier survival curves and statistical analysis of overall survival and gene expression was assessed on the TCGA breast invasive carcinoma cohort (1097 patients) using data generated by the TCGA Research Network: https://www.cancer.gov/tcga.

Immunohistochemistry

Paraffin sections of 4 µm from metastasic and non-metastasic breast tumours were obtained from CRB-Tumorothèque of the Institut de Cancérologie de l'Ouest (ICO, Saint-Herblain, France) (***Heymann et al., 2020***). Immunohistochemsitry was performed using RalA (BD Transduction #610222, 1/100) and RalB (Sigma WH0005899, 1/400) antibodies on MicroPICell facility (Nantes, France) Citrate buffer pH6 was used for antigen retrieval 20 min a 96˚C (Target Retrieval solution low pH, Dako) and DAB and Hematoxylin staining were revealed using ImPath detection kit (DAB OB Sensitive Detection Kit, ImPath). Whole slides were scanned on Hamamatsu scanner using Nanozoomer Digital Pathology software. Automated computer quantification of DAB staining in perinuclear zones (brown intensity measurement) after automatic nuclei detection with hematoxylin staining in the whole biopsies was performed using Qupath open source software for digital pathology image analysis (***Bankhead et al., 2017***) on MicroPICell platform (Nantes, France). Quantification was further confirmed by manual blinded arbitrary scoring of DAB brown intensity in tumoral zones was performed using a score of 1 for low staining to score of 3 for intense staining.

Statistical analyses

All results were confirmed in at least two independent experiments. Statistical significance of results was analyzed using the GraphPad Prism program version 5.04. The Shapiro-Wilk normality test was used to confirm the normality of the data. The statistical difference of Gaussian data sets was analyzed using the Student unpaired two-tailed t test, with Welch's correction in case of unequal variances and the one-way ANOVA test followed by a Bonferonni multiple comparison post-test was used for multiple data comparison. For data not following a Gaussian distribution, the Mann-Whitney test was used, and the Kruskal-Wallis test followed by Dunn's Multiple Comparison post-test was used for multiple data comparison. Two Way Anova was used to compare more than one parameters followed by Bonferonni post-test. For analyzing data containing only three measurements, One-Way Anova permutation test followed pairwise permutation test with false detection rate (fdr) correction, using R software (version 3.6.2) was used. Illustrations of these statistical analyses are displayed as the mean +/- standard deviation (SD). p-Values smaller than 0.05 were considered as significant. *, $p<0.05$, **, $p<0.01$, ***, $p<0.001$, ****, $p<0.0001$.

Acknowledgements

We thank all members of the Goetz Lab for helpful discussions, in particular Florent Colin for careful reading, as well as Gregory Khelifi and Camille Hergott for animal care. We thank the CRB-Tumorothèque of the Institut de Cancérologie de l'Ouest (ICO, Saint-Herblain, France) and the Cellular and Tissular Imaging Core Facility of Nantes University MicroPICell (SFR-Santé, Nantes, France). We thank Mayeul Collot and Andrey Klymchenko (UMR 7021) for providing the MemBright dye. We thank Monique Dontenwill (CNRS 7213) for her help. This work was supported by a fellowship from IDEX (University of Strasbourg) and ARC (Association pour le Recherche sur le Cancer) to SG; by grants from La Ligue contre le Cancer, Canceropole Grand-Est, INCa (PLBIO19-291), Plan Cancer (Nanotumor) and Roche to JGG; and by institutional funds from University of Strasbourg and INSERM to JGG, and ANR (to CC, French Proteomics Infrastructure ProFI, ANR-10-INBS-08–03; to NV, ANR-19-CE44-0019). The Metabolome Bordeaux facility was supported by the grant Metabo-HUB-ANR-11-INBS-0010. PT and KM were supported by Suttons, Sydney Catalyst, NHMRC, Cancer Council NSW, Cancer Institute NSW and by an Avner Pancreatic Cancer Foundation and Len Ainsworth Pancreatic Research Funds. BM and VM are supported by fellowships from the French Ministry of Science (MESRI).

Additional information

Funding

Funder	Grant reference number	Author
Institut National Du Cancer	PLBIO19-291	Jacky G Goetz
La Ligue contre le cancer		Jacky G Goetz

Canceropole grand est		Jacky G Goetz
Plan Cancer		Jacky G Goetz
Roche		Jacky G Goetz
Agence Nationale de la Recherche	ANR-10-INBS-08-03	Christine Carapito
Agence Nationale de la Recherche	ANR-19-CE44-0019	Nicolas Vitale
Agence Nationale de la Recherche	ANR-11-INBS- 0010	Laetitia Fouillen
University of Strasbourg		Shima Ghoroghi
Association pour la Recherche sur le Cancer		Shima Ghoroghi
Inserm		Jacky G Goetz
ANR		Jacky G Goetz
French ministry of science		Benjamin Mary Vincent Mittelheisser
Suttons		Kendelle Murphy Paul Timpson
Sydney catalyst		Kendelle Murphy Paul Timpson
NHMRC		Kendelle Murphy Paul Timpson
Cancer Council NSW		Kendelle Murphy Paul Timpson
Pancreatic Cancer Action		Kendelle Murphy Paul Timpson
pancreatic cancer resource		Kendelle Murphy Paul Timpson

The funders had no role in study design, data collection and interpretation, or the decision to submit the work for publication.

Author contributions

Shima Ghoroghi, Benjamin Mary, Formal analysis, Investigation, Methodology; Annabel Larnicol, Investigation, Methodology; Nandini Asokan, Annick Klein, Naël Osmani, Ignacio Busnelli, Anne-Marie Haeberle, Cathy Royer, Coralie Spiegelhalter, Vincent Mittelheisser, Investigation; François Delalande, Nicodème Paul, Frédéric Gros, Laetitia Fouillen, Gwennan André-Grégoire, Kendelle Murphy, Formal analysis, Investigation; Sébastien Halary, Data curation, Formal analysis; Alexandre Detappe, Paul Timpson, Supervision; Raphaël Carapito, Christine Carapito, Nicolas Vitale, Formal analysis, Supervision; Marcel Blot-Chabaud, Resources; Julie Gavard, Resources, Formal analysis, Supervision; Olivier Lefebvre, Data curation, Formal analysis, Supervision, Investigation; Jacky G Goetz, Conceptualization, Formal analysis, Supervision, Funding acquisition, Investigation, Writing - original draft, Project administration, Writing - review and editing; Vincent Hyenne, Conceptualization, Data curation, Formal analysis, Supervision, Funding acquisition, Investigation, Methodology, Writing - original draft, Writing - review and editing

Author ORCIDs

Nicodème Paul http://orcid.org/0000-0003-4680-3012
Frédéric Gros http://orcid.org/0000-0002-6252-4323
Laetitia Fouillen http://orcid.org/0000-0002-1204-9296
Jacky G Goetz https://orcid.org/0000-0003-2842-8116

Ethics

Human subjects: Paraffin sections of 4 µm from metastasic and non-metastasic breast tumours were obtained from CRB-Tumorothèque of the Institut de Cancérologie de l'Ouest (ICO, Saint-Herblain, France) (Heymann et al., 2020). Patients were diagnosed and treated at ICO (Integrated Center for Oncology, St Herblain) for metastatic and non-metastatic breast cancers. Samples were processed and included in the CRB-Tumorothèque ICO upon donor agreement and informed consent. Samples and related information are destroyed at the request of the donor. The CRB-Tumorothèque ICO have been declared to and authorized by the French Research Ministry (Declaration Number: DC-2018-3321). This declaration includes approval by a research ethics committee (CPP "Comité de protection des personnes"), in accordance with the French legislation of the Public Health Code.
Animal experimentation: All animals were housed and han- dled according to the guidelines of INSERM and the eth- ical committee of Alsace, France (CREMEAS) (Direc- tive 2010/63/EU on the protection of animals used for scientific purposes). Animal facility agreement num- ber: C67-482-33. Experimental license for mice: Apafis 4707-20l6032416407780; experimental license for zebrafish: Apafis 16862-2018121914292754.

Decision letter and Author response

Decision letter https://doi.org/10.7554/eLife.61539.sa1
Author response https://doi.org/10.7554/eLife.61539.sa2

Additional files

Supplementary files

- Supplementary file 1. EVs RNA analysis. Sheet a: RNAs overexpressed in EVs from 4T1 shCtl cells Vs EVs from shRalA cells Sheet b: RNAs overexpressed in EVs from 4T1 shRalA cells Vs EVs from shCtl cells Sheet c: RNAs overexpressed in EVs from 4T1 shCtl cells Vs EVs from shRalB cells Sheet d: RNAs overexpressed in EVs from 4T1 shRalB cells Vs EVs from shCtl cells

- Supplementary file 2. EVs proteomic analysis. Sheet a: Proteins identified in EVs from 4T1 shCtl cells Sheet b: Proteins overexpressed in EVs from 4T1 shCtl cells Vs EVs from shRalA cells Sheet c: Proteins overexpressed in EVs from 4T1 shRalA cells Vs EVs from shCtl cells Sheet d: Proteins overexpressed in EVs from 4T1 shCtl cells Vs EVs from shRalB cells Sheet e: Proteins overexpressed in EVs from 4T1 shRalB cells Vs EVs from shCtl cells Sheet f: Proteins overexpressed in EVs from 4T1 shCtl cells Vs EVs from shRalA cells and EVs from shRalB cells

Data availability

Sequencing and mass spectrometry data have been deposited to EV-Track knowledgebase.

The following previously published dataset was used:

Author(s)	Year	Dataset title	Dataset URL	Database and Identifier
The Cancer Genome Atlas Network	2012	Comprehensive molecular portraits of human breast tumours	https://www.cancer.gov/tcga	TCGA breast invasive carcinoma cohort (1097 patients), accession, other

References

Anders S, Pyl PT, Huber W. 2015. HTSeq–a Python framework to work with high-throughput sequencing data. *Bioinformatics* **31**:166–169. DOI: https://doi.org/10.1093/bioinformatics/btu638, PMID: 25260700

Bankhead P, Loughrey MB, Fernández JA, Dombrowski Y, McArt DG, Dunne PD, McQuaid S, Gray RT, Murray LJ, Coleman HG, James JA, Salto-Tellez M, Hamilton PW. 2017. QuPath: open source software for digital pathology image analysis. *Scientific Reports* **7**:5. DOI: https://doi.org/10.1038/s41598-017-17204-5, PMID: 29203879

Baran J, Baj-Krzyworzeka M, Weglarczyk K, Szatanek R, Zembela M, Barbasz J, Czupryna A, Szczepanik A, Zembala M. 2010. Circulating tumour-derived microvesicles in plasma of gastric Cancer patients. Cancer immunology. *Immunotherapy* **59**:841–850. DOI: https://doi.org/10.1007/s00262-009-0808-2

Bardin N, Blot-Chabaud M, Despoix N, Kebir A, Harhouri K, Arsanto JP, Espinosa L, Perrin P, Robert S, Vely F, Sabatier F, Le Bivic A, Kaplanski G, Sampol J, Dignat-George F. 2009. CD146 and its soluble form regulate monocyte transendothelial migration. *Arteriosclerosis, Thrombosis, and Vascular Biology* **29**:746–753. DOI: https://doi.org/10.1161/ATVBAHA.108.183251, PMID: 19229070

Becker A, Thakur BK, Weiss JM, Kim HS, Peinado H, Lyden D. 2016. Extracellular vesicles in Cancer: cell-to-cell mediators of metastasis. *Cancer Cell* **30**:836–848. DOI: https://doi.org/10.1016/j.ccell.2016.10.009, PMID: 27960084

Bobrie A, Krumeich S, Reyal F, Recchi C, Moita LF, Seabra MC, Ostrowski M, Théry C. 2012. Rab27a supports exosome-dependent and -independent mechanisms that modify the tumor microenvironment and can promote tumor progression. *Cancer Research* **72**:4920–4930. DOI: https://doi.org/10.1158/0008-5472.CAN-12-0925, PMID: 22865453

Bruntz RC, Lindsley CW, Brown HA. 2014. Phospholipase D signaling pathways and phosphatidic acid as therapeutic targets in Cancer. *Pharmacological Reviews* **66**:1033–1079. DOI: https://doi.org/10.1124/pr.114.009217, PMID: 25244928

Cha DJ, Franklin JL, Dou Y, Liu Q, Higginbotham JN, Demory Beckler M, Weaver AM, Vickers K, Prasad N, Levy S, Zhang B, Coffey RJ, Patton JG. 2015. KRAS-dependent sorting of miRNA to exosomes. *eLife* **4**:e07197. DOI: https://doi.org/10.7554/eLife.07197, PMID: 26132860

Collot M, Ashokkumar P, Anton H, Boutant E, Faklaris O, Galli T, Mély Y, Danglot L, Klymchenko AS. 2018. MemBright: a family of fluorescent membrane probes for advanced cellular imaging and neuroscience. *Cell Chemical Biology* **26**:9. DOI: https://doi.org/10.1016/j.chembiol.2019.01.009

Corrotte M, Chasserot-Golaz S, Huang P, Du G, Ktistakis NT, Frohman MA, Vitale N, Bader MF, Grant NJ. 2006. Dynamics and function of phospholipase D and phosphatidic acid during phagocytosis. *Traffic* **7**:365–377. DOI: https://doi.org/10.1111/j.1600-0854.2006.00389.x, PMID: 16497229

Costa-Silva B, Aiello NM, Ocean AJ, Singh S, Zhang H, Thakur BK, Becker A, Hoshino A, Mark MT, Molina H, Xiang J, Zhang T, Theilen TM, García-Santos G, Williams C, Ararso Y, Huang Y, Rodrigues G, Shen TL, Labori KJ, et al. 2015. Pancreatic Cancer exosomes initiate pre-metastatic niche formation in the liver. *Nature Cell Biology* **17**:816–826. DOI: https://doi.org/10.1038/ncb3169, PMID: 25985394

Cox J, Hein MY, Luber CA, Paron I, Nagaraj N, Mann M. 2014. Accurate proteome-wide label-free quantification by delayed normalization and maximal peptide ratio extraction, termed MaxLFQ. *Molecular & Cellular Proteomics* **13**:2513–2526. DOI: https://doi.org/10.1074/mcp.M113.031591, PMID: 24942700

Das SK, Sarkar D, Emdad L, Fisher PB. 2019. *MDA-9/Syntenin: An Emerging Global Molecular Target Regulating Cancer Invasion and Metastasis*. Elsevier Inc.

Demory Beckler M, Higginbotham JN, Franklin JL, Ham AJ, Halvey PJ, Imasuen IE, Whitwell C, Li M, Liebler DC, Coffey RJ. 2013. Proteomic analysis of exosomes from mutant KRAS Colon cancer cells identifies intercellular transfer of mutant KRAS. *Molecular & Cellular Proteomics* **12**:343–355. DOI: https://doi.org/10.1074/mcp.M112.022806, PMID: 23161513

Deutsch EW, Bandeira N, Sharma V, Perez-Riverol Y, Carver JJ, Kundu DJ, García-Seisdedos D, Jarnuczak AF, Hewapathirana S, Pullman BS, Wertz J, Sun Z, Kawano S, Okuda S, Watanabe Y, Hermjakob H, MacLean B, MacCoss MJ, Zhu Y, Ishihama Y, et al. 2020. The ProteomeXchange consortium in 2020: enabling "big data" approaches in proteomics. *Nucleic Acids Research* **48**:gkz984. DOI: https://doi.org/10.1093/nar/gkz984

Follain G, Herrmann D, Harlepp S, Hyenne V, Osmani N, Warren SC, Timpson P, Goetz JG. 2020. Fluids and their mechanics in tumour transit: shaping metastasis. *Nature Reviews Cancer* **20**:107–124. DOI: https://doi.org/10.1038/s41568-019-0221-x, PMID: 31780785

Galindo-Hernandez O, Villegas-Comonfort S, Candanedo F, González-Vázquez MC, Chavez-Ocaña S, Jimenez-Villanueva X, Sierra-Martinez M, Salazar EP. 2013. Elevated concentration of microvesicles isolated from peripheral blood in breast Cancer patients. *Archives of Medical Research* **44**:208–214. DOI: https://doi.org/10.1016/j.arcmed.2013.03.002, PMID: 23506723

Gao Y, Bado I, Wang H, Zhang W, Rosen JM, Zhang XH. 2019. Metastasis organotropism: redefining the congenial soil. *Developmental Cell* **49**:375–391. DOI: https://doi.org/10.1016/j.devcel.2019.04.012, PMID: 31063756

Garcia S, Dalès JP, Charafe-Jauffret E, Carpentier-Meunier S, Andrac-Meyer L, Jacquemier J, Andonian C, Lavaut MN, Allasia C, Bonnier P, Charpin C. 2007. Poor prognosis in breast carcinomas correlates with increased expression of targetable CD146 and c-Met and with proteomic basal-like phenotype. *Human Pathology* **38**:830–841. DOI: https://doi.org/10.1016/j.humpath.2006.11.015, PMID: 17316758

Gentry LR, Martin TD, Reiner DJ, Der CJ. 2014. Ral small GTPase signaling and oncogenesis: more than just 15minutes of fame. *Biochimica Et Biophysica Acta (BBA) - Molecular Cell Research* **1843**:2976–2988. DOI: https://doi.org/10.1016/j.bbamcr.2014.09.004

Ghossoub R, Lembo F, Rubio A, Gaillard CB, Bouchet J, Vitale N, Slavík J, Machala M, Zimmermann P. 2014. Syntenin-ALIX exosome biogenesis and budding into multivesicular bodies are controlled by ARF6 and PLD2. *Nature Communications* **5**:3477. DOI: https://doi.org/10.1038/ncomms4477, PMID: 24637612

Heymann D, Kerdraon O, Verriele V, Verhille E, Veron V, Vitre M, Delmas F, Henry C, Gouy Y, Amiand M, Bard J-M. 2020. Centre de ressources Biologiques-Tumorothèque: bioresources and associated clinical data dedicated to translational research in oncology at the institut de cancérologie de l'Ouest, France. *Open Journal of Bioresources* **7**:62. DOI: https://doi.org/10.5334/ojb.62

Hoshino A, Costa-Silva B, Shen TL, Rodrigues G, Hashimoto A, Tesic Mark M, Molina H, Kohsaka S, Di Giannatale A, Ceder S, Singh S, Williams C, Soplop N, Uryu K, Pharmer L, King T, Bojmar L, Davies AE, Ararso

Y, Zhang T, et al. 2015. Tumour exosome integrins determine organotropic metastasis. *Nature* **527**:329–335. DOI: https://doi.org/10.1038/nature15756, PMID: 26524530

Huotari J, Helenius A. 2011. Endosome maturation. *The EMBO Journal* **30**:3481–3500. DOI: https://doi.org/10.1038/emboj.2011.286, PMID: 21878991

Hyenne V, Apaydin A, Rodriguez D, Spiegelhalter C, Hoff-Yoessle S, Diem M, Tak S, Lefebvre O, Schwab Y, Goetz JG, Labouesse M. 2015. RAL-1 controls multivesicular body biogenesis and exosome secretion. *Journal of Cell Biology* **211**:27–37. DOI: https://doi.org/10.1083/jcb.201504136

Hyenne V, Lefebvre O, Goetz JG. 2017. Going live with tumor exosomes and microvesicles. *Cell Adhesion & Migration* **11**:173–186. DOI: https://doi.org/10.1080/19336918.2016.1276694, PMID: 28135898

Hyenne V, Ghoroghi S, Collot M, Bons J, Follain G, Harlepp S, Mary B, Bauer J, Mercier L, Busnelli I, Lefebvre O, Fekonja N, Garcia-Leon MJ, Machado P, Delalande F, López AA, Silva SG, Verweij FJ, van Niel G, Djouad F, et al. 2019. Studying the fate of tumor extracellular vesicles at high spatiotemporal resolution using the zebrafish embryo. *Developmental Cell* **48**:554–572. DOI: https://doi.org/10.1016/j.devcel.2019.01.014, PMID: 30745140

Jiang H, Luo JQ, Urano T, Frankel P, Lu Z, Foster DA, Feig LA. 1995. Involvement of ral GTPase in v-Src-induced phospholipase D activation. *Nature* **378**:409–412. DOI: https://doi.org/10.1038/378409a0, PMID: 7477381

Jung T, Castellana D, Klingbeil P, Cuesta Hernández I, Vitacolonna M, Orlicky DJ, Roffler SR, Brodt P, Zöller M. 2009. CD44v6 dependence of premetastatic niche preparation by exosomes. *Neoplasia* **11**:1093–1105. DOI: https://doi.org/10.1593/neo.09822, PMID: 19794968

Kanemoto S, Nitani R, Murakami T, Kaneko M, Asada R, Matsuhisa K, Saito A, Imaizumi K. 2016. Multivesicular body formation enhancement and exosome release during endoplasmic reticulum stress. *Biochemical and Biophysical Research Communications* **480**:166–172. DOI: https://doi.org/10.1016/j.bbrc.2016.10.019, PMID: 27725157

Kaplan RN, Riba RD, Zacharoulis S, Bramley AH, Vincent L, Costa C, MacDonald DD, Jin DK, Shido K, Kerns SA, Zhu Z, Hicklin D, Wu Y, Port JL, Altorki N, Port ER, Ruggero D, Shmelkov SV, Jensen KK, Rafii S, et al. 2005. VEGFR1-positive haematopoietic bone marrow progenitors initiate the pre-metastatic niche. *Nature* **438**:820–827. DOI: https://doi.org/10.1038/nature04186, PMID: 16341007

Kaur P, Nagaraja GM, Zheng H, Gizachew D, Galukande M, Krishnan S, Asea A. 2012. A mouse model for triple-negative breast Cancer tumor-initiating cells (TNBC-TICs) exhibits similar aggressive phenotype to the human disease. *BMC Cancer* **12**:120. DOI: https://doi.org/10.1186/1471-2407-12-120

Kebir A, Harhouri K, Guillet B, Liu JW, Foucault-Bertaud A, Lamy E, Kaspi E, Elganfoud N, Vely F, Sabatier F, Sampol J, Pisano P, Kruithof EK, Bardin N, Dignat-George F, Blot-Chabaud M. 2010. CD146 short isoform increases the proangiogenic potential of endothelial progenitor cells in vitro and in vivo. *Circulation Research* **107**:66–75. DOI: https://doi.org/10.1161/CIRCRESAHA.109.213827, PMID: 20448216

Kim D, Langmead B, Salzberg SL. 2015. HISAT: a fast spliced aligner with low memory requirements. *Nature Methods* **12**:357–360. DOI: https://doi.org/10.1038/nmeth.3317, PMID: 25751142

Klumperman J, Raposo G. 2014. The complex ultrastructure of the endolysosomal system. *Cold Spring Harbor Perspectives in Biology* **6**:a016857. DOI: https://doi.org/10.1101/cshperspect.a016857, PMID: 24851870

Kren N, Michaud D, Bagchi S, Greene K, Pylayeva-Gupta Y. 2020. Rab27a plays a dual role in metastatic propensity of pancreatic Cancer. *Scientific Reports* **10**:e64248-1. DOI: https://doi.org/10.1038/s41598-020-64248-1

Lewis JA, Scott SA, Lavieri R, Buck JR, Selvy PE, Stoops SL, Armstrong MD, Brown HA, Lindsley CW. 2009. Design and synthesis of isoform-selective phospholipase D (PLD) inhibitors. part I: impact of alternative halogenated privileged structures for PLD1 specificity. *Bioorganic & Medicinal Chemistry Letters* **19**:1916–1920. DOI: https://doi.org/10.1016/j.bmcl.2009.02.057, PMID: 19268584

Logozzi M, De Milito A, Lugini L, Borghi M, Calabrò L, Spada M, Perdicchio M, Marino ML, Federici C, Iessi E, Brambilla D, Venturi G, Lozupone F, Santinami M, Huber V, Maio M, Rivoltini L, Fais S. 2009. High levels of exosomes expressing CD63 and caveolin-1 in plasma of melanoma patients. *PLOS ONE* **4**:e5219. DOI: https://doi.org/10.1371/journal.pone.0005219, PMID: 19381331

Lou Y, Preobrazhenska O, auf dem Keller U, Sutcliffe M, Barclay L, McDonald PC, Roskelley C, Overall CM, Dedhar S. 2008. Epithelial-mesenchymal transition (EMT) is not sufficient for spontaneous murine breast Cancer metastasis. *Developmental Dynamics* **237**:2755–2768. DOI: https://doi.org/10.1002/dvdy.21658, PMID: 18773493

Love MI, Huber W, Anders S. 2014. Moderated estimation of fold change and dispersion for RNA-seq data with DESeq2. *Genome Biology* **15**:550. DOI: https://doi.org/10.1186/s13059-014-0550-8, PMID: 25516281

Luo JQ, Liu X, Frankel P, Rotunda T, Ramos M, Flom J, Jiang H, Feig LA, Morris AJ, Kahn RA, Foster DA. 1998. Functional association between arf and RalA in active phospholipase D complex. *PNAS* **95**:3632–3637. DOI: https://doi.org/10.1073/pnas.95.7.3632, PMID: 9520417

Mathieu M, Martin-Jaular L, Lavieu G, Théry C. 2019. Specificities of secretion and uptake of exosomes and other extracellular vesicles for cell-to-cell communication. *Nature Cell Biology* **21**:9–17. DOI: https://doi.org/10.1038/s41556-018-0250-9, PMID: 30602770

Mattissek C, Teis D. 2014. The role of the endosomal sorting complexes required for transport (ESCRT) in tumorigenesis. *Molecular Membrane Biology* **31**:111–119. DOI: https://doi.org/10.3109/09687688.2014.894210, PMID: 24641493

McKenzie AJ, Hoshino D, Hong NH, Cha DJ, Franklin JL, Coffey RJ, Patton JG, Weaver AM. 2016. KRAS-MEK Signaling Controls Ago2 Sorting into Exosomes. *Cell Reports* **15**:978–987. DOI: https://doi.org/10.1016/j.celrep.2016.03.085

Monypenny J, Milewicz H, Flores-Borja F, Weitsman G, Cheung A, Chowdhury R, Burgoyne T, Arulappu A, Lawler K, Barber PR, Vicencio JM, Keppler M, Wulaningsih W, Davidson SM, Fraternali F, Woodman N, Turmaine M, Gillett C, Franz D, Quezada SA, et al. 2018. ALIX regulates Tumor-Mediated immunosuppression by controlling EGFR activity and PD-L1 presentation. *Cell Reports* **24**:630–641. DOI: https://doi.org/10.1016/j.celrep.2018.06.066, PMID: 30021161

Ombrato L, Nolan E, Kurelac I, Mavousian A, Bridgeman VL, Heinze I, Chakravarty P, Horswell S, Gonzalez-Gualda E, Matacchione G, Weston A, Kirkpatrick J, Husain E, Speirs V, Collinson L, Ori A, Lee JH, Malanchi I. 2019. Metastatic-niche labelling reveals parenchymal cells with stem features. *Nature* **572**:603–608. DOI: https://doi.org/10.1038/s41586-019-1487-6, PMID: 31462798

Ostrowski M, Carmo NB, Krumeich S, Fanget I, Raposo G, Savina A, Moita CF, Schauer K, Hume AN, Freitas RP, Goud B, Benaroch P, Hacohen N, Fukuda M, Desnos C, Seabra MC, Darchen F, Amigorena S, Moita LF, Thery C. 2010. Rab27a and Rab27b control different steps of the exosome secretion pathway. *Nature Cell Biology* **12**:19–30. DOI: https://doi.org/10.1038/ncb2000, PMID: 19966785

Oxford G, Owens CR, Titus BJ, Foreman TL, Herlevsen MC, Smith SC, Theodorescu D. 2005. RalA and RalB: antagonistic relatives in Cancer cell migration. *Cancer Research* **65**:7111–7120. DOI: https://doi.org/10.1158/0008-5472.CAN-04-1957, PMID: 16103060

Peinado H, Alečković M, Lavotshkin S, Matei I, Costa-Silva B, Moreno-Bueno G, Hergueta-Redondo M, Williams C, García-Santos G, Ghajar C, Nitadori-Hoshino A, Hoffman C, Badal K, Garcia BA, Callahan MK, Yuan J, Martins VR, Skog J, Kaplan RN, Brady MS, et al. 2012. Melanoma exosomes educate bone marrow progenitor cells toward a pro-metastatic phenotype through MET. *Nature Medicine* **18**:883–891. DOI: https://doi.org/10.1038/nm.2753, PMID: 22635005

Peinado H, Zhang H, Matei IR, Costa-Silva B, Hoshino A, Rodrigues G, Psaila B, Kaplan RN, Bromberg JF, Kang Y, Bissell MJ, Cox TR, Giaccia AJ, Erler JT, Hiratsuka S, Ghajar CM, Lyden D. 2017. Pre-metastatic niches: organ-specific homes for metastases. *Nature Reviews Cancer* **17**:302–317. DOI: https://doi.org/10.1038/nrc.2017.6, PMID: 28303905

Plebanek MP, Angeloni NL, Vinokour E, Li J, Henkin A, Martinez-Marin D, Filleur S, Bhowmick R, Henkin J, Miller SD, Ifergan I, Lee Y, Osman I, Thaxton CS, Volpert OV. 2017. Pre-metastatic Cancer exosomes induce immune surveillance by patrolling monocytes at the metastatic niche. *Nature Communications* **8**:e01433-3. DOI: https://doi.org/10.1038/s41467-017-01433-3

Scott SA, Selvy PE, Buck JR, Cho HP, Criswell TL, Thomas AL, Armstrong MD, Arteaga CL, Lindsley CW, Brown HA. 2009. Design of isoform-selective phospholipase D inhibitors that modulate cancer cell invasiveness. *Nature Chemical Biology* **5**:108–117. DOI: https://doi.org/10.1038/nchembio.140

Scott CC, Vacca F, Gruenberg J. 2014. Endosome maturation, transport and functions. *Seminars in Cell & Developmental Biology* **31**:2–10. DOI: https://doi.org/10.1016/j.semcdb.2014.03.034

Szklarczyk D, Gable AL, Lyon D, Junge A, Wyder S, Huerta-Cepas J, Simonovic M, Doncheva NT, Morris JH, Bork P, Jensen LJ, Mering CV. 2019. STRING v11: protein-protein association networks with increased coverage, supporting functional discovery in genome-wide experimental datasets. *Nucleic Acids Research* **47**:D607–D613. DOI: https://doi.org/10.1093/nar/gky1131, PMID: 30476243

Taira E, Takaha N, Taniura H, Kim CH, Miki N. 1994. Molecular cloning and functional expression of Gicerin, a novel cell adhesion molecule that binds to neurite outgrowth factor. *Neuron* **12**:861–872. DOI: https://doi.org/10.1016/0896-6273(94)90338-7, PMID: 8161457

Taira E, Kohama K, Tsukamoto Y, Okumura S, Miki N. 2005. Gicerin/CD146 is involved in neurite extension of NGF-treated PC12 cells. *Journal of Cellular Physiology* **204**:632–637. DOI: https://doi.org/10.1002/jcp.20365, PMID: 15880440

Timpson P, Mcghee EJ, Erami Z, Nobis M, Quinn JA, Edward M, Anderson KI. 2011. Organotypic collagen I assay: a malleable platform to assess cell behaviour in a 3-Dimensional context. *Journal of Visualized Experiments* **13**:e3089. DOI: https://doi.org/10.3791/3089

Tominaga N, Kosaka N, Ono M, Katsuda T, Yoshioka Y, Tamura K, Lötvall J, Nakagama H, Ochiya T. 2015. Brain metastatic Cancer cells release microRNA-181c-containing extracellular vesicles capable of destructing blood-brain barrier. *Nature Communications* **6**:6716. DOI: https://doi.org/10.1038/ncomms7716, PMID: 25828099

Treps L, Edmond S, Harford-Wright E, Galan-Moya EM, Schmitt A, Azzi S, Citerne A, Bidère N, Ricard D, Gavard J. 2016. Extracellular vesicle-transported Semaphorin3A promotes vascular permeability in glioblastoma. *Oncogene* **35**:2615–2623. DOI: https://doi.org/10.1038/onc.2015.317, PMID: 26364614

van Niel G, D'Angelo G, Raposo G. 2018. Shedding light on the cell biology of extracellular vesicles. *Nature Reviews Molecular Cell Biology* **19**:213–228. DOI: https://doi.org/10.1038/nrm.2017.125, PMID: 29339798

Vennin C, Chin VT, Warren SC, Lucas MC, Herrmann D, Magenau A, Melenec P, Walters SN, Del Monte-Nieto G, Conway JR, Nobis M, Allam AH, McCloy RA, Currey N, Pinese M, Boulghourjian A, Zaratzian A, Adam AA, Heu C, Nagrial AM, et al. 2017. Transient tissue priming via ROCK inhibition uncouples pancreatic Cancer progression, sensitivity to chemotherapy, and metastasis. *Science Translational Medicine* **9**:eaai8504. DOI: https://doi.org/10.1126/scitranslmed.aai8504, PMID: 28381539

Vitale N, Mawet J, Camonis J, Regazzi R, Bader M-F, Chasserot-Golaz S. 2005. The small GTPase RalA controls exocytosis of large dense core secretory granules by interacting with ARF6-dependent phospholipase D1. *Journal of Biological Chemistry* **280**:29921–29928. DOI: https://doi.org/10.1074/jbc.M413748200

Wang Q, Ni Q, Wang X, Zhu H, Wang Z, Huang J. 2015. High expression of RAB27A and TP53 in pancreatic Cancer predicts poor survival. *Medical Oncology* **32**:372. DOI: https://doi.org/10.1007/s12032-014-0372-2, PMID: 25428385

Wang D, Sun H, Wei J, Cen B, DuBois RN. 2017. CXCL1 Is Critical for Premetastatic Niche Formation and Metastasis in Colorectal Cancer. *Cancer Research* **77**:3655–3665. DOI: https://doi.org/10.1158/0008-5472.CAN-16-3199

Wang Z, Yan X. 2013. CD146, a multi-functional molecule beyond adhesion. *Cancer Letters* **330**:150–162. DOI: https://doi.org/10.1016/j.canlet.2012.11.049

Wieczorek S, Combes F, Lazar C, Giai Gianetto Q, Gatto L, Dorffer A, Hesse A-M, Couté Y, Ferro M, Bruley C, Burger T. 2017. DAPAR & ProStaR: software to perform statistical analyses in quantitative discovery proteomics. *Bioinformatics* **33**:135–136. DOI: https://doi.org/10.1093/bioinformatics/btw580

Yan C, Liu D, Li L, Wempe MF, Guin S, Khanna M, Meier J, Hoffman B, Owens C, Wysoczynski CL, Nitz MD, Knabe WE, Ahmed M, Brautigan DL, Paschal BM, Schwartz MA, Jones DN, Ross D, Meroueh SO, Theodorescu D. 2014. Discovery and characterization of small molecules that target the GTPase ral. *Nature* **515**:443–447. DOI: https://doi.org/10.1038/nature13713, PMID: 25219851

Yan C, Theodorescu D. 2018. RAL GTPases: biology and potential as therapeutic targets in Cancer. *Pharmacological Reviews* **70**:1–11. DOI: https://doi.org/10.1124/pr.117.014415, PMID: 29196555

Yang Z, Shi J, Xie J, Wang Y, Sun J, Liu T, Zhao Y, Zhao X, Wang X, Ma Y, Malkoc V, Chiang C, Deng W, Chen Y, Fu Y, Kwak KJ, Fan Y, Kang C, Yin C, Rhee J, et al. 2020. Large-scale generation of functional mRNA-encapsulating exosomes via cellular nanoporation. *Nature Biomedical Engineering* **4**:69–83. DOI: https://doi.org/10.1038/s41551-019-0485-1

Yue S, Mu W, Erb U, Zöller M. 2015. The tetraspanins CD151 and Tspan8 are essential exosome components for the crosstalk between Cancer initiating cells and their surrounding. *Oncotarget* **6**:2366–2384. DOI: https://doi.org/10.18632/oncotarget.2958, PMID: 25544774

Zago G, Veith I, Singh MK, Fuhrmann L, De Beco S, Remorino A, Takaoka S, Palmeri M, Berger F, Brandon N, El Marjou A, Vincent-Salomon A, Camonis J, Coppey M, Parrini MC. 2018. RalB directly triggers invasion downstream ras by mobilizing the wave complex. *eLife* **7**:e40474. DOI: https://doi.org/10.7554/eLife.40474, PMID: 30320548

Zeng GF, Cai SX, Wu GJ. 2011. Up-regulation of METCAM/MUC18 promotes motility, invasion, and tumorigenesis of human breast Cancer cells. *BMC Cancer* **11**:113. DOI: https://doi.org/10.1186/1471-2407-11-113, PMID: 21450088

Zeng Q, Li W, Lu D, Wu Z, Duan H, Luo Y, Feng J, Yang D, Fu L, Yan X. 2012. CD146, an epithelial-mesenchymal transition inducer, is associated with triple-negative breast Cancer. *PNAS* **109**:1127–1332. DOI: https://doi.org/10.1073/pnas.1111053108, PMID: 22210108

Zhou W, Fong MY, Min Y, Somlo G, Liu L, Palomares MR, Yu Y, Chow A, O'Connor ST, Chin AR, Yen Y, Wang Y, Marcusson EG, Chu P, Wu J, Wu X, Li AX, Li Z, Gao H, Ren X, et al. 2014. Cancer-secreted miR-105 destroys vascular endothelial barriers to promote metastasis. *Cancer Cell* **25**:501–515. DOI: https://doi.org/10.1016/j.ccr.2014.03.007, PMID: 24735924

During my PhD, I contributed to establish the zebrafish embryo as a novel animal model to track circulating tEVs *in vivo* (Hyenne et al. 2019). The tools and methods developed in these studies were also used in part of my main project as well.

The zebrafish embryo as a model to track circulating EVs *in vivo*

In vivo, very few is known about the behavior of EVs in the circulation. One major limitation in the field is the ability to track such small particles *in vivo*. Microscopic visualization of circulating EVs *in vivo*, which depends both on subcellular resolution and brightness of the labeled EVs still faces major challenges (Verweij, Hyenne, et al. 2019). In addition, the appropriate models are crucial to have deep, non-invasive access to internal organs in order to identify EVs receiving cells and organs. In the mouse model, different strategies, based on bioluminescence, lipophilic dyes or transgenic expression of EVs fluorescent markers have been developed (Hyenne, Lefebvre, and Goetz 2017). However, these approaches often involve *ex vivo* imaging and do not allow to precisely follow EVs dynamics in body fluids. To overcome these limitations, several groups developed intravital imaging of EVs in mice however, due to the complexity of these procedures, high-throughput imaging and are often not compatible with a high sampling of EVs shuttling in body fluids (van der Vos et al. 2016; Zomer et al. 2015; C. P. Lai et al. 2015). Alternatively, the zebrafish embryo emerged as a unique animal model to study physiological and pathological circulating EVs at unprecedented spatiotemporal resolution (Verweij, Hyenne, et al. 2019). Zebrafish embryos offer several advantages for non-invasive analysis *in vivo* including a stereotype vasculature (and blood circulation), a maturing immune system within 48h, translucid body and easily amenable to all types of confocal and high-speed microscopy. Overall, zebrafish presents a high level of genetic and physiologic homology with humans and more particularly, it reproduces a relevant physiological environment for the study of circulating EVs (Verweij, Revenu, et al. 2019; Hyenne et al. 2019). Detection of fluorescent EVs, labelled with either lipophilic dyes or by transgenic expression of fluorescent markers within secreting cells is favored by transparent embryos. Zebrafish model also allows to perform an extensive analysis of circulating EVs and describe their hemodynamic behavior *in vivo* (Verweij, Revenu, et al. 2019; Hyenne et al. 2019). As an alternative strategy, EV proteins can be fused to fluorescent proteins and expressed in EV-producing cells (Corso et al. 2019; Görgens 2016). This allows to visualize unique subpopulations of EVs and can also be used to track EVs from the genetically engineered

cell (Verweij, Revenu, et al. 2019). In addition, MemBright is recently developed cyanine-based membrane probes (Cy3, Cy5 or Cy7) (Collot et al. 2019) with unique properties that provide high brightness and specificity to labeled-EVs as well as preventing fluorescent self-aggregation (Hyenne et al. 2019). MemBright can be also used to co-inject different types of EVs labeled with different colors (Cy3, Cy5), which allows us to compare different EV population (or origin) and track their specific behavior, fate and function. **In our project, we aimed to track and assess the function of circulating tumor EVs *in vivo* using the zebrafish embryo and provide a high-resolution description of their dissemination and uptake.** First, we injected membright labelled EVs from fish melanoma cells (zmel) (Heilmann et al. 2015) into the zebrafish embryos and tracked EVs in the blood flow. Then we characterized their uptake by endothelial cells and patrolling monocytes. In these cells, we demonstrated that the majority of the EVs concentrate in lysosomal compartments. We also performed a functional test on different transgenic embryos showing activation and production of TNF-a (Nguyen et al. 2015), which correspond to the M2-M1 transition, often associated with the transformation of normal macrophages (M2) to cancer associated macrophage (M1) (Biswas and Mantovani 2010). Finally, we performed pre-injection with EVs (called priming), followed by tumor cell injection demonstrate the induction of premetastatic niches by EVs. We showed that tumor cells invade more efficiently the fish stroma and develop bigger micro-metastasis in the case of EV priming (Hyenne et al. 2019) – **see annex 2: Study the fate of tumor extracellular vesicles at high spatiotemporal resolution using the zebrafish embryo.** On the other project, we mainly focused on the experimental details of zebrafish model and wrote a chapter on-**see annex 3: Live tracking of extracellular vesicles in larval zebrafish.**

Resource

Developmental Cell

Studying the Fate of Tumor Extracellular Vesicles at High Spatiotemporal Resolution Using the Zebrafish Embryo

Graphical Abstract

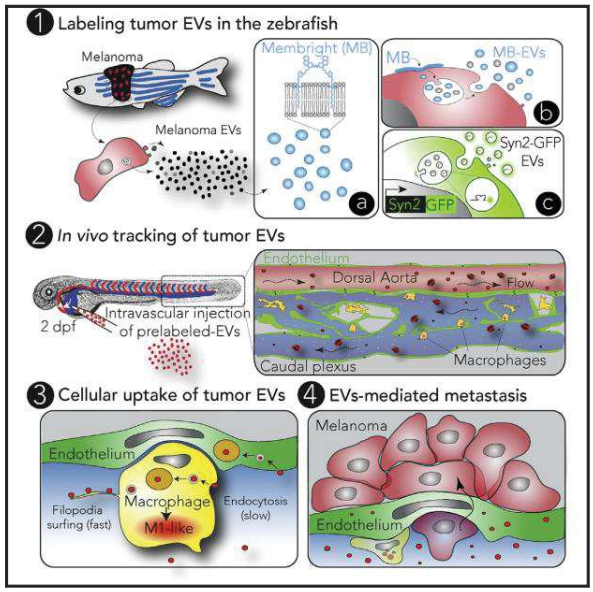

Highlights

- MemBright allows for bright and specific staining of EVs
- The zebrafish embryo allows tracking of tumor EVs at high spatiotemporal resolution
- Circulating tumor EVs are mostly taken up by endothelial cells and patrolling macrophages
- Zebrafish melanoma EVs favor metastatic outgrowth in zebrafish embryos

Authors

Vincent Hyenne, Shima Ghoroghi, Mayeul Collot, ..., Christine Carapito, Andrey S. Klymchenko, Jacky G. Goetz

Correspondence

hyenne@unistra.fr (V.H.), jacky.goetz@inserm.fr (J.G.G.)

In Brief

Tumor extracellular vesicles (EVs) promote tumor progression. However, their behavior in body fluids remains mysterious. Hyenne et al. show that the zebrafish embryo can be used to track and assess the function of circulating tumor EVs *in vivo* and provide a high-resolution description of their dissemination and uptake.

Hyenne et al., 2019, Developmental Cell *48*, 554–572
February 25, 2019
https://doi.org/10.1016/j.devcel.2019.01.014

CellPress

CellPress

Developmental Cell
Resource

Studying the Fate of Tumor Extracellular Vesicles at High Spatiotemporal Resolution Using the Zebrafish Embryo

Vincent Hyenne,[1,2,3,4,12,*] Shima Ghoroghi,[1,2,3] Mayeul Collot,[5] Joanna Bons,[6] Gautier Follain,[1,2,3] Sébastien Harlepp,[1,2,3] Benjamin Mary,[1,2,3] Jack Bauer,[1,2,3] Luc Mercier,[1,2,3] Ignacio Busnelli,[1,2,3] Olivier Lefebvre,[1,2,3] Nina Fekonja,[1,2,3] Maria J. Garcia-Leon,[1,2,3] Pedro Machado,[7] François Delalande,[6] Ana Amor López,[8] Susana Garcia Silva,[8] Frederik J. Verweij,[9,10] Guillaume van Niel,[9,10] Farida Djouad,[11] Héctor Peinado,[8] Christine Carapito,[6] Andrey S. Klymchenko,[5] and Jacky G. Goetz[1,2,3,*]

[1]INSERM UMR_S1109, Strasbourg 67200, France
[2]Université de Strasbourg, Strasbourg 67200, France
[3]Fédération de Médecine Translationnelle de Strasbourg, Strasbourg 67200, France
[4]CNRS SNC5055, Strasbourg 67200, France
[5]Laboratoire de Biophotonique et Pharmacologie, UMR CNRS 7213, Université de Strasbourg, Illkirch 67000, France
[6]CNRS, Laboratoire de Spectrométrie de Masse Bio-Organique (LSMBO), IPHC, UMR 7178, Université de Strasbourg, Strasbourg 67087, France
[7]Electron Microscopy Core Facility, European Molecular Biology Laboratory, Heidelberg 69117, Germany
[8]Microenvironment and metastasis group. Department of Molecular Oncology, Spanish National Cancer Research Center (CNIO), Madrid, Spain
[9]Institut Curie, PSL Research University, CNRS UMR144, Paris 75005, France
[10]Center for Psychiatry and Neuroscience, Hôpital Saint-Anne, Université Descartes, INSERM U894, Paris 75014, France
[11]IRMB, Université de Montpellier, INSERM, Montpellier, France
[12]Lead Contact
*Correspondence: hyenne@unistra.fr (V.H.), jacky.goetz@inserm.fr (J.G.G.)
https://doi.org/10.1016/j.devcel.2019.01.014

SUMMARY

Tumor extracellular vesicles (EVs) mediate the communication between tumor and stromal cells mostly to the benefit of tumor progression. Notably, tumor EVs travel in the bloodstream, reach distant organs, and locally modify the microenvironment. However, visualizing these events *in vivo* still faces major hurdles. Here, we describe an approach for tracking circulating tumor EVs in a living organism: we combine chemical and genetically encoded probes with the zebrafish embryo as an animal model. We provide a first description of tumor EVs' hemodynamic behavior and document their intravascular arrest. We show that circulating tumor EVs are rapidly taken up by endothelial cells and blood patrolling macrophages and subsequently stored in degradative compartments. Finally, we demonstrate that tumor EVs activate macrophages and promote metastatic outgrowth. Overall, our study proves the usefulness and prospects of zebrafish embryo to track tumor EVs and dissect their role in metastatic niches formation *in vivo*.

INTRODUCTION

Over the past two decades, extracellular vesicles (EVs) have emerged as novel mediators of cell-cell communication due to their capacity to carry functional molecules coupled with their ability to travel in biological fluids (Raposo and Stoorvogel, 2013). EVs are heterogeneous in content and origin, as they can either arise from plasma membrane budding (then called microvesicles) or originate from a late endosomal compartment, the multi-vesicular body (MVB) (i.e., exosomes) (van Niel et al., 2018). EVs are known to be important in tumor progression and metastasis, where the complex tumor microenvironment requires a permanent cross-communication between cells (Hyenne et al., 2017). EVs secreted by tumor cells are enriched in pro-tumoral and pro-metastatic factors (proteins, mRNAs, miRNAs, and other non-coding RNAs) and can modify the phenotype of both tumor and stromal cells, mostly to the benefit of tumor growth and metastasis formation (Hyenne et al., 2017). For instance, tumor EVs were shown to transfer oncogenic traits from more aggressive to less aggressive tumor cells (Al-Nedawi et al., 2008). Importantly, tumor EVs can differentiate macrophages or fibroblasts into tumor-associated macrophages or fibroblasts, thereby promoting tumor growth and invasion (Chow et al., 2014; Gu et al., 2012; Paggetti et al., 2015). This pro-metastatic EV-mediated communication can occur within the primary tumor or at distance in physically far-off organs (Peinado et al., 2017). Remarkably, repeated injection of EVs isolated from metastatic cells into the mouse blood circulation induces the formation of a pre-metastatic niche, even in the absence of tumor cells (Costa-Silva et al., 2015; Grange et al., 2011; Hoshino et al., 2015; Liu et al., 2016; Peinado et al., 2012). The ability of circulating tumor EVs to alter the microenvironment of a given organ is particularly relevant with regard to (1) the increased amounts of tumor EVs present in the blood circulation of patients with cancer (Baran et al., 2010; Galindo-Hernandez et al., 2013;

Logozzi et al., 2009), and (2) the fact that elevated levels of EV proteins have been associated with poor prognosis in metastatic melanoma patients (Peinado et al., 2012). Therefore, it is crucial to precisely understand the mechanisms governing tumor EV dispersion and uptake in the blood circulation.

However, local or distant dissemination of tumor EVs has only been sparsely characterized in living organisms (Hoshino et al., 2015; Lai et al., 2015; Pucci et al., 2016). In particular, how EVs circulate in the blood flow and how specifically they are internalized by stromal cells during the priming of pre-metastatic niches remain poorly understood. EVs are nanoscale objects and are thus difficult to track *in vivo*. Moreover, mouse models are not fully suited for real time and *in vivo* EV tracking. In mice, EVs can either be followed after bulk injections (Lai et al., 2014; Takahashi et al., 2013) or with increased resolution through intravital imaging procedures (Lai et al., 2015; Van Der Vos et al., 2016; Zomer et al., 2015). However, such approaches have not yet been able to describe the behavior of tumor EVs in the blood circulation. An ideal animal model suited to accurately dissect the behavior of tumor EVs *in vivo* would allow their tracking in the circulation and their uptake and, at the same time, be amenable for modeling tumor and metastasis progression.

Interestingly, the zebrafish embryo largely complies with all these needs. Indeed, zebrafish has recently emerged as a potent model in cancer biology (White et al., 2013). The molecular pathways driving cancer progression and the anatomo-pathological features of tumorigenesis are essentially conserved between human and fish. In addition, the zebrafish embryo is transparent, possesses a stereotyped vasculature, a maturating immune system and is therefore perfectly suited for intravital imaging with high spatial and temporal resolution. For these reasons, the zebrafish embryo appears as an adequate model to study tumor EVs *in vitro*.

Here, we show that zebrafish melanoma EVs are similar to human melanoma EVs and demonstrate how their fate can be tracked in the zebrafish embryo. For efficient staining of EVs, we used MemBright, a recently developed cyanine-based membrane probe with improved brightness and specificity (Collot et al., 2019). Using this tool, and EVs from genetically engineered cells in parallel, we provide the first description of EVs' dynamics in the blood circulation. We subsequently examined the transit routes and arrest sites of tumor EVs and identified endothelial cells and patrolling macrophages as major EVs-recipient cells. Importantly, these cells have also been identified in a parallel study describing endogenous EVs dispersion in the zebrafish embryo (Verweij et al., 2019). We further show that these cell types have increased uptake efficiency toward tumor EVs, and found that patrolling macrophages internalize tumor EVs through at least two distinct endocytic mechanisms, before storing them in acidic compartments. Using correlated light and electron microscopy (CLEM), we precisely identified the cells uptaking EVs and finely described their morphology as well as the storage or degradative compartments at the electron microscopy level. In addition, we demonstrate that it is possible to track naturally released EVs *in vivo* in the zebrafish embryo using either pre-labeling with MemBright or genetically engineered cells. Finally, we show that melanoma EVs activate macrophages and promote metastatic outgrowth in zebrafish.

RESULTS

Zebrafish Melanoma EVs Are Similar to Human and Mouse Melanoma EVs

To study tumor EVs in zebrafish, we first characterized EVs released by a melanoma cell line (Zmel1) derived from a transgenic mitfa-BRAF(V600E);p53(−/−) zebrafish line (Heilmann et al., 2015) (Figure 1A). EVs were isolated from a cell culture supernatant following an established protocol of differential centrifugation (Théry et al., 2006), and EVs present in the 100.000 g pellet were characterized by nanoparticle tracking analysis (NTA) and electron microscopy. We found that Zmel1 EVs have an average diameter of 150 nm in solution and 90 nm after chemical fixation (Figures 1B and 1C). Subsequently, we characterized the protein content of these EVs by mass spectrometry and identified 794 proteins present in Zmel1 EVs (Table S1A). This list includes several proteins typically found in extracellular vesicles, such as ALIX, CD81, Flotillin 1, TSG101, CD9, RalA, Hsc70, HSP90, syntenin 2, integrins α5 and β1, and others (of note, CD63 was absent from Zmel1 EVs) (Figure 1D; Table S1A). We then wondered whether the content of zebrafish melanoma EVs was comparable to the ones of human or mouse melanoma EVs. We compared proteins present in Zmel1 EVs with proteins identified in the EVs isolated from six human (451-LU, SK-Mel28, SK-Mel147, SK-Mel103, WM35, and WM164) (Tables S1B–S1G) and three mouse (B16-F0, B16-F1, and B16-F10) (Tables S1H–S1J) melanoma cell lines. Protein content comparison revealed that 65% and 40% of Zmel1 proteins were also identified in human or mouse melanoma EVs, respectively (Figure 1E). Zmel1 EVs are closer to human melanoma EVs than to mouse melanoma EVs. We identified a core list of 82 proteins found in melanoma EVs from either zebrafish, mice, or human (Table S1K). Altogether, these data demonstrate that Zmel1 EVs derived from an established zebrafish melanoma cell line are highly similar to mammalian melanoma EVs and therefore constitute a good model to study human melanoma EVs.

In addition, we compared proteins present in Zmel1 EVs with proteins present in two other types of zebrafish EVs identified in a parallel study (Verweij et al., 2019). First, 17% of Zmel1 EVs proteins are also present in EVs from AB9 fibroblastic cell line (Table S1L). Then, we compared Zmel1 EVs with CD63-positive EVs secreted by a zebrafish embryonic epithelium, the yolk syncytial layer (YSL), and isolated from zebrafish embryos (Verweij et al., 2019). Interestingly, we found a relatively low similarity between these two types of zebrafish EVs (1–2% of Zmel1 EV proteins are present in YSL CD63+EVs; 10% of YSL CD63+EV proteins are present in Zmel1 EVs) (Table S1M). This difference illustrates the cell-type specificity of EV cargo enrichment. However, the mechanism of biogenesis of these two EV types could be partially similar, as 5 of the 12 proteins common to Zmel1 EVs and YSL EVs have been shown to affect, positively or negatively, exosome secretion in mammalian cells: TSG101, ALIX, Syntenin 2, Flotillin 1, and Rab2 (Baietti et al., 2012; Colombo et al., 2013; Okabayashi and Kimura, 2010; Ostrowski et al., 2010).

The MemBright Dye Specifically and Brightly Labels Tumor EVs

In order to fluorescently label Zmel1 EVs and follow them *in vivo*, we used new membrane probes, MemBright (Collot et al., 2019).

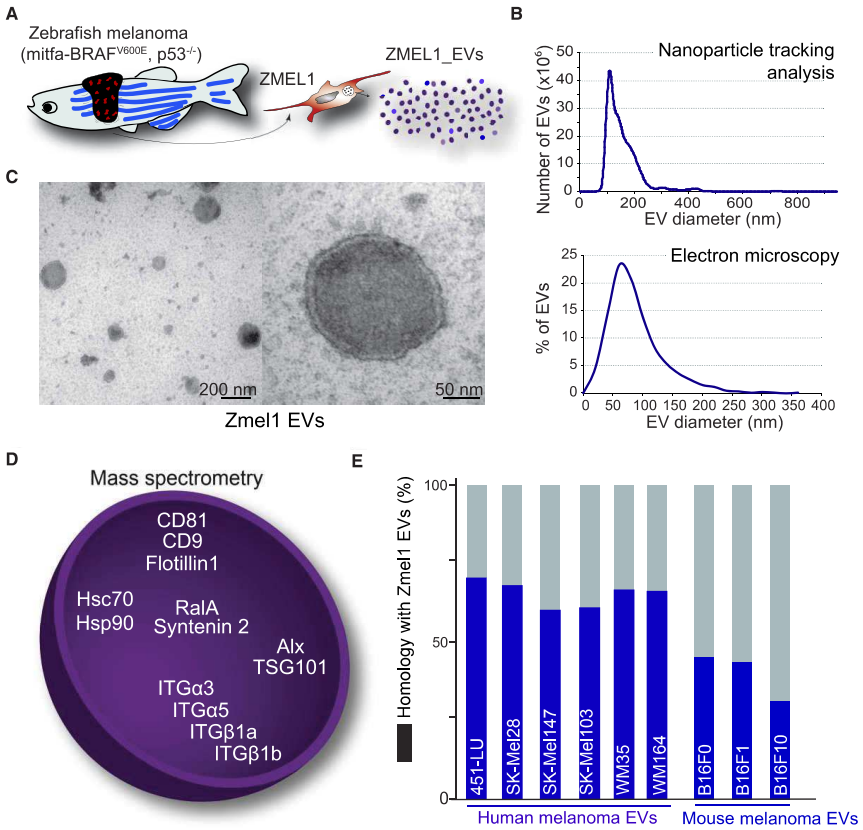

Figure 1. EVs Secreted by Zmel1 Zebrafish Melanoma Cells Are Similar to Mouse and Human Melanoma EVs

(A) Zebrafish melanoma EVs were isolated from Zmel1 cells by differential centrifugation (Heilmann et al., 2015).

(B) Histogram of a nanoparticle tracking analysis of Zmel1 EVs showing the number of EVs (y axis) versus their diameter (nm, x axis).

(C) Electron microscopy images of Zmel1 EVs and a histogram showing the percentage of total EVs (y axis) versus their diameter (nm, x axis).

(D) Illustration of some of the classical EV proteins present among the 794 proteins identified in ZMel1 EVs by mass spectrometry (see Table S1).

(E) Histogram showing the percentage of Zmel1 EVs proteins common with EV proteins from various human or mouse cell lines (using human orthologs).

They differ significantly from existing commercial dyes because they bear two amphiphilic groups composed of zwitterions and alkyl chains, which insert the dye into the membrane bilayer (Figure 2A). Moreover, MemBright is available in several colors, which therefore enables multi-color approach in EV imaging (Figures S2G–S2I). To assess the value of MemBright in EV labeling, we first globally compared the MemBright-labeled EVs to identical EVs labeled with PKH-26, a commercially available and widely used dye for EV labeling (Hoshino et al., 2015; Imai et al., 2015). Zmel1 EVs were incubated with MemBright-Cy3 (at 0.2 μM) or with PKH-26 (at 2 μM, according to manufacturer's instructions), washed and isolated by ultracentrifugation. Using fluorescence spectroscopy, we observed that PKH-labeled EVs display a broad absorption spectrum, with a blue shifted peak typically indicating the presence of H-aggregation (Figure 2B) (Würthner et al., 2011). By contrast, MemBright-labeled EVs show an absorption spectrum identical to the solubilized form of the probe (Figures 2B and S1A), revealing that the MemBright is efficiently embedded in EV membranes. MemBright-labeled EVs are as bright as PKH-labeled EVs even though the MemBright was 10-fold less concentrated than PKH (Figures 2B, 2C, and S1D). When both dyes were used at similar dilutions (0.2 μM), the MemBright labeled EVs were much brighter than the PKH ones (Figure S1E). Indeed, MemBright displays >20-fold higher quantum yield than the PKH: 0.42 versus 0.02 (Table S2). Since MemBright-Cy3 and

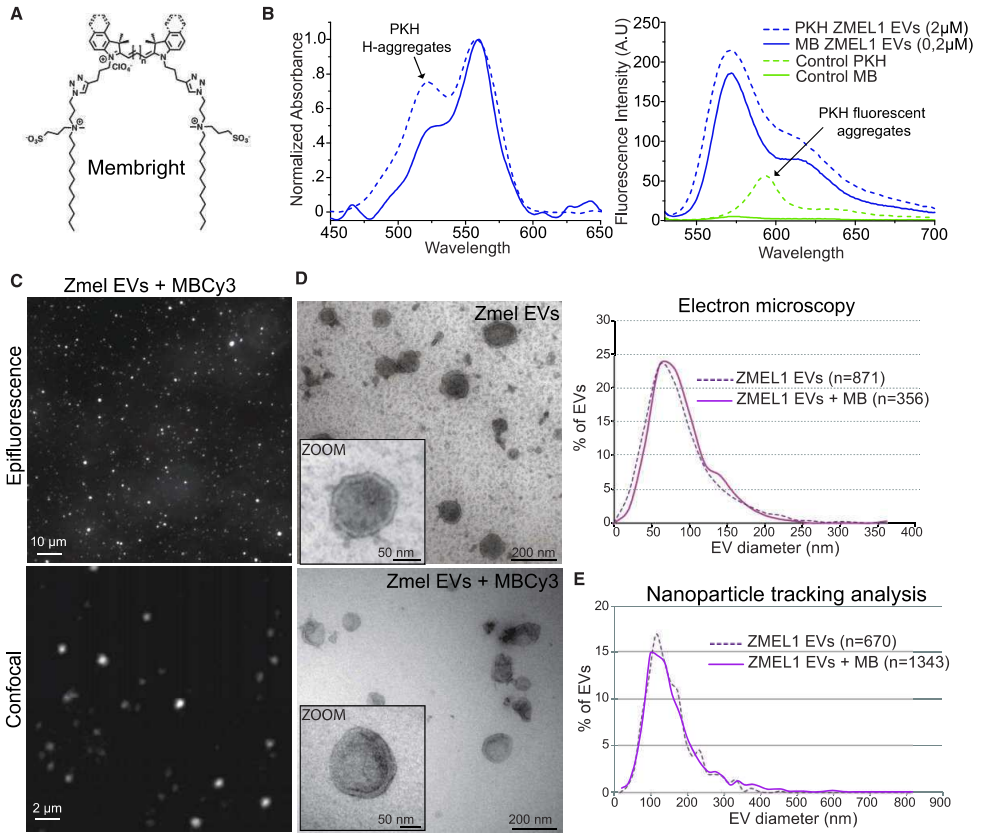

Figure 2. EVs Can Be Brightly and Specifically Labeled with MemBright

(A) Molecular structure of the membrane binding probe MemBright.

(B) Histograms showing a spectroscopy analysis of MemBright (MB) and PKH labeled Zmel1 EVs describing the absorbance (left histogram, y axis) and the fluorescence intensity (right histogram, y axis) versus the wavelength (nm, x axis). Arrows indicate the presence of PKH aggregates in labeled EVs (left) as well as in control PKH alone (right).

(C) Zmel1 EVs labeled with MemBright Cy3 (MBCy3) observed by Epifluorescence (upper) and confocal (lower).

(D) Electron microscopy of non-labeled (upper) and labeled (lower) Zmel1 EVs and histogram showing the percentage of labeled and non-labeled Zmel1 EVs (y axis) versus their diameter (x axis, nm) by electron microscopy (right graph).

(E) Nanoparticle tracking analysis of MemBright-labeled and non-labeled Zmel1 EVs showing the number of EVs (y axis) versus their diameter (nm, x axis).

PKH26 contain the same Cy3-based fluorophore, such remarkable difference in the quantum yield suggests inefficient partitioning of PKH into EV membranes. This poor partitioning probably arises from the aggregation of PKH in aqueous media, in line with characteristic short-wavelength shoulder in the absorption spectrum in the samples of EVs (Figure S1B). This is not the case for MemBright. Interestingly, a similar spectroscopic experiment conducted without EVs reveals the presence of a red-shifted fluorescence peak with PKH alone but not with MemBright alone (Figure S1C). These fluorescent PKH aggregates have an average diameter of 80 nm (± 10 nm), as analyzed by fluorescence correlation spectroscopy (FCS), which is in the range of EVs and therefore could lead to artifacts. To complement these studies, we analyzed MemBright-labeled EVs by electron microscopy and NTA and found that neither their morphology nor their size was affected, when compared to non-labeled EVs (Figure 2D). Importantly, no larger size aggregates were detected in MemBright-labeled EVs (Figure 2E). Finally, we demonstrated the versatility of MemBright by labeling EVs isolated from 4T1 mouse mammary carcinoma cells. Spectroscopy (Figure S1B; Table S2) and electron microscopy analysis (data not shown) confirmed the advantages of the

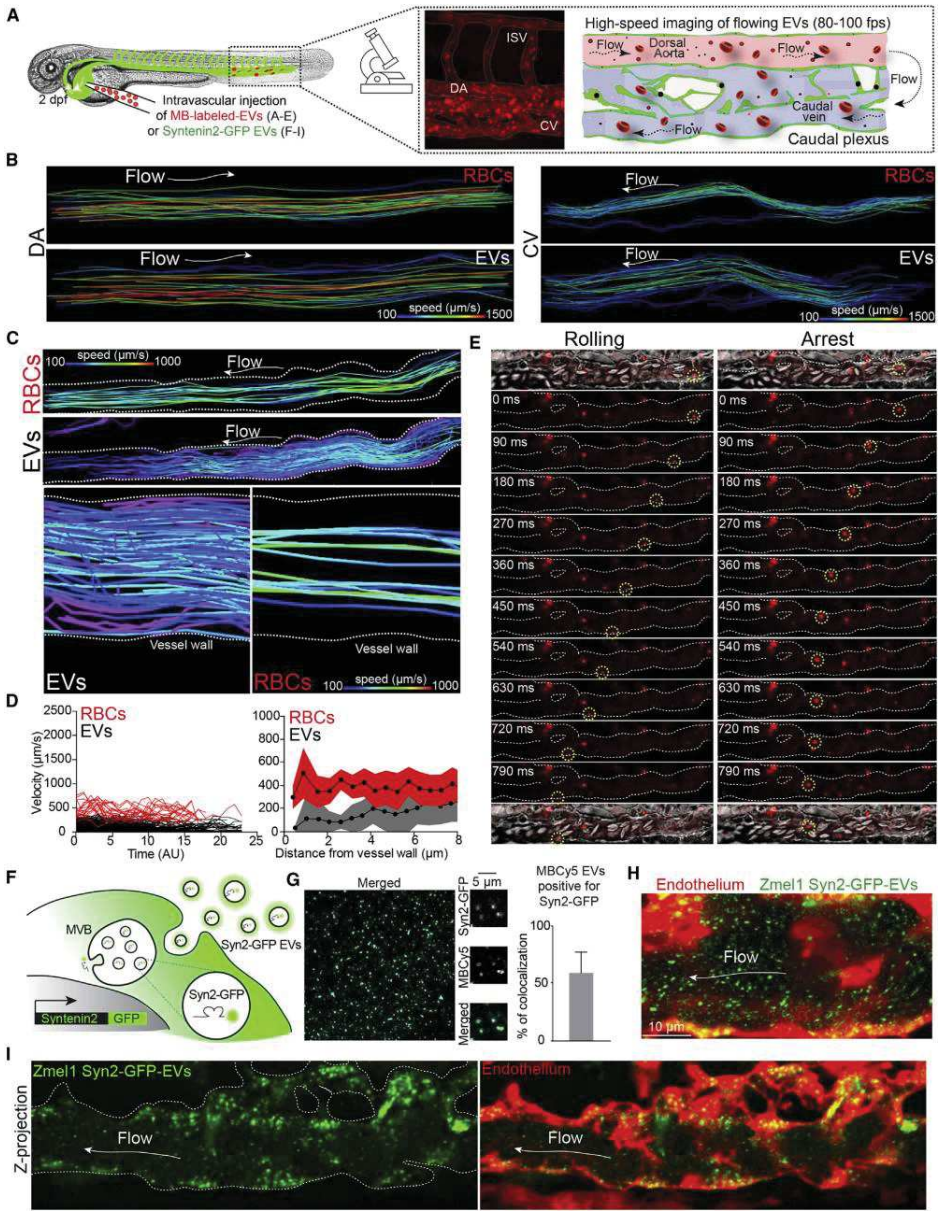

(legend on next page)

MemBright probes. Furthermore, separation of MemBright-labeled 4T1 EVs by density gradient revealed that the majority of the fluorescent MemBright is present in the fractions where most EVs are found, as confirmed by the presence of ALIX and TSG101 (Figure S1F). Altogether, these experiments prove that labeling EVs with MemBright does not lead to soluble fluorescent aggregates that can be confounded with labeled EVs. In addition, given its high quantum yield, MemBright can be used at a relatively low concentration to efficiently label isolated EVs.

Tumor EVs Can Be Individually Tracked in the Living Zebrafish Embryo

We next investigated whether MemBright labeling could be used for tracking tumor EVs *in vivo*. We injected zebrafish embryos at 2 days post-fertilization with MemBright-labeled EVs in the blood circulation. Fluorescent EVs were observed essentially in the tail region of the embryo, which is composed of the dorsal aorta and the venous caudal plexus (Figure 3A). Minutes following injection, we observed several fluorescent EVs that were either still flowing or that were already arrested along the endothelium (Figure 3A; Video S1A). We first assessed the apparent size of EVs by comparing them to 100 nm fluorescent polystyrene beads. *In vitro* and upon injection in the circulation of zebrafish embryos, we found that MemBright-labeled EVs and 100 nm fluorescent beads display similar apparent sizes, which correspond to the resolution limits of confocal microscopy (Figures S2A–S2D). Furthermore, MemBright-labeled EVs do not adhere to red blood cells (RBCs), and no leakage of MemBright from EVs to RBCs could be observed *in vitro* or *in vivo* (Figures S2E and S2F). These observations suggest that MemBright in combination with our microscopy set-up allow imaging of fluorescent objects of the size of an individual EV. At this stage, however, we cannot assess whether bigger spots result from bigger EVs or clusters of small EVs. In addition, MemBright can be used to co-inject different types of EVs labeled with different colors (Cy3, Cy5) and specifically track their fate. As a proof of concept, we co-injected Zmel1 tumor EVs (labeled with MemBright-Cy5) with 4T1 mouse tumor EVs (labeled with MemBright-Cy3) in zebrafish embryos and observed both specific localizations for each EVs population as well as a common uptake in isolated cells (Figures S2H and S2I). This suggests that MemBright could be used to follow specific internalization routes of distinct types of EVs that might be on the basis of their function and message delivery.

We then aimed to describe the over-looked behavior of tumor EVs in the blood circulation. To do that, we performed high-speed confocal acquisitions of flowing tumor EVs (and of co-flowing RBCs) in different regions of the vasculature of living zebrafish embryos (Figure 3A; Videos S1B and S1C). When tracking both tumor EVs and RBCs, we first found that EVs have a higher velocity in the aorta than in the caudal veins, in accordance with the hydrodynamic profiles previously described in this region of the zebrafish embryo vasculature (Figure 3B) (Follain et al., 2018a). Second, when analyzing co-motion of tumor EVs and RBCs in a single vessel, we noticed that EVs have a reduced velocity compared to RBCs. These observations are not restricted to Zmel1 EVs since 4T1 EVs display a higher velocity in the dorsal aorta than in the caudal veins but a slower velocity than RBCs (Figures 3C and 3D). Interestingly, we observed that the hemodynamic behavior of tumor EVs differs in regions close to the vessel wall, from which RBCs are mostly excluded. Indeed, when we plotted the velocity of tumor EVs as a function of their position with regards to vessel walls, we observed that tumor EVs explore the vicinity of vessel walls with a reduced velocity (Figures 3C and 3D). Thus, it seems that tumor EVs follow a Poiseuille flow, which predicts that objects displaced by a laminar flow would have a reduced velocity because of frictional forces, along the border of the vessel wall. Such a behavior, in addition to their potential adhesive capacity, could thus favor the arrest of tumor EVs. Indeed, individual inspection of EVs in close proximity to the vessel wall reveals that they are either flowing, rolling on the surface of the endothelium, or arresting (Figure 3E). We observed arrest of EVs following a rolling behavior, suggesting that it could be driven by progressive activation of adhesion molecules, as well as the sharp arrest of flowing EVs, without a rolling phase (Video S2). A very similar behavior was observed for endogenous EVs (Verweij et al., 2019). Altogether, we provide the first accurate description of circulating tumor EVs in the vasculature.

In addition, we used a complementary genetic approach. We expressed Syntenin2 (a major cargo detected in Zmel1 EVs by mass spectrometry, Figure 1D) fused to GFP in Zmel1 cells and showed that these cells secrete GFP-positive EVs (Figures 3F and 3G). Upon intravascular injection in zebrafish embryos, the Syntenin2-GFP EVs can be tracked in the circulation similar to MemBright-labeled EVs (Figures 3H and 3I). Altogether, we document that both genetically and chemically labeled tumor

Figure 3. Hemodynamic Characterization of Individual EVs Tracked in the Circulation of Zebrafish Embryo

(A) Experimental setup used to track circulating EVs: two days post-fertilization zebrafish embryos are injected in the duct of Cuvier with fluorescent EVs (left) and observed in the caudal plexus with high-speed confocal microscopy. Middle: *Z* projection of MemBright-Cy3 Zmel1 EVs in the caudal plexus right after injection. Right: schematic representation of the caudal plexus showing the direction of the blood flow in the dorsal aorta (pink) and the venous plexus (blue).

(B) Individual tracks of red blood cells (RBC) or Zmel1 EVs in the dorsal aorta (DA, left) and in the caudal vein (CV, right).

(C) Upper: Individual tracks of red blood cells (RBC) or 4T1 EVs in the CV. Lower: Zoom on individual tracks of red blood cells (RBC, right) or 4T1 EVs (left) in the CV in proximity of the vessel wall (white lines). (B) and (C): Color coding represents velocities.

(D) Left: histogram showing the velocity (y axis, μm/s) versus the time (x axis, AU) of RBCs (red) and EVs (black) in the CV. Right: histogram showing the velocity (y axis, μm/s) versus the distance to the vessel wall (x axis, μm) of RBCs (red) and EVs (gray) in the CV.

(E) Examples of individual EVs rolling (left) or arresting (right) in the circulation of the CV.

(F) Schematic representation of Zmel1 cells expressing Syntenin2-GFP.

(G) EVs isolated from Zmel1 Syntenin2-GFP cells and labeled with MemBright; the diagram indicates the colocalization between GFP and MemBright (mean and standard deviation).

(H) Temporal projection of a time-lapse of *Tg(Fli:Gal4, UAS:RFP)* embryos injected with Zme1 Syntenin2-GFP EVs imaged immediately after injection.

(I) *Z*-projection of *Tg(Fli:Gal4, UAS:RFP)* embryos injected with Zme1 Syntenin2-GFP EVs imaged 1h after injection.

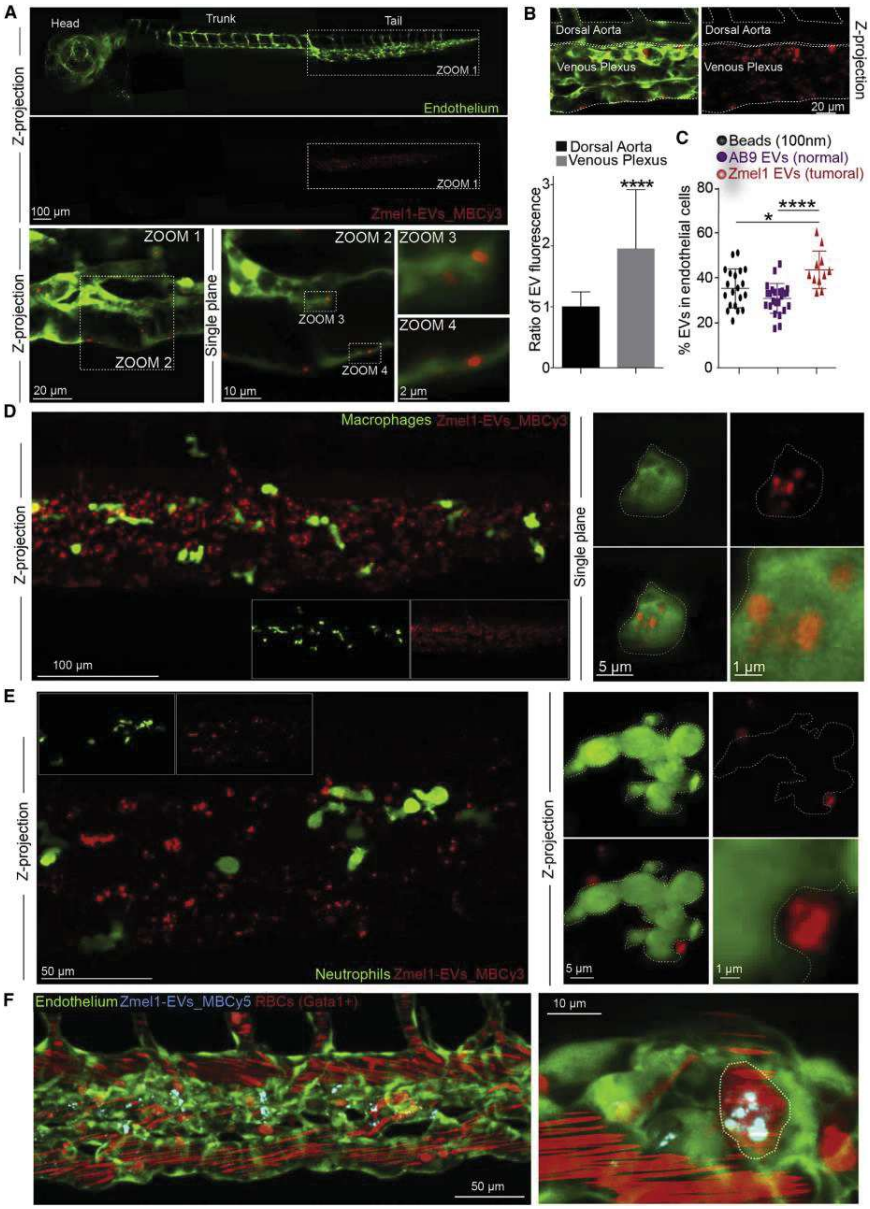

Figure 4. Zmel1 EVs Are Mainly Taken Up by Endothelial Cells, Macrophages, and Hematopoietic Stem Cells but Not by Neutrophils

(A) Confocal images of MemBright-Cy3 labeled Zmel1 EVs 3 h post-injection (hpi) in *Tg(Fli1:GFP)* embryos (endothelium specific expression). The upper panels were stitches from several individual images to allow a large region to be visualized.

(legend continued on next page)

EVs can be tracked in the bloodstream of zebrafish embryos, allowing the study of their hemodynamic behavior and intravascular arrest.

Circulating Tumor EVs Are Mostly Taken Up by Endothelial Cells and Patrolling Macrophages

How circulating tumor EVs target specific cell types at distance remains a mystery, mostly because this step could not be captured before. Here, most of the tumor EVs are found arrested, exclusively in the tail region of the fish, only 10 to 15 min following injection (Figure 4A). In addition, we found that most of the uptake by endothelial cells occurs in the venous region (Figure 4B), suggesting that the permissive flow profiles of this particular region favor arrest and uptake of tumor EVs, as they do for circulating tumor cells (Follain et al., 2018a). Syntenin2-GFP EVs arrest similarly in *Tg(Fli:Gal4, UAS:RFP)* embryos (Figure 3I) and similar observations have been done for endogenous EVs (Verweij et al., 2019). To assess which cell types could uptake tumor EVs, we used four transgenic zebrafish lines with different tissue-specific fluorescent expression *Tg(Fli1:GFP)* for the endothelium (Figure 4A), *Tg(mpeg1:GFP)* for macrophages (Figure 4D), *Tg(mpo:GFP)* for neutrophils (Figure 4E), and *Tg(gata1:dsRed)* for RBCs and putative hematopoietic stem cells (Figure 4F). We found that tumor EVs are rapidly taken up by endothelial cells, macrophages, and immobile Gata1-positive cells (putative hematopoietic stem cells) but not by neutrophils that are known to have a reduced phagocytic activity (Figures 4A, 4D, 4E, and 4F) (Le Guyader et al., 2008). Embryos injected with the MemBright dye alone do not show any signal that could arise from soluble fluorescent aggregates (Figure S3). In addition, endothelial cells and macrophages take up equivalent proportions of Zmel1 EVs, 43% (n = 19 fish) and 38% (n = 11) respectively. Together, this represents the large majority of arrested EVs in the zebrafish embryo at that stage. Importantly, a similar behavior is observed for endogenous CD63-positive EVs (Verweij et al., 2019), suggesting again that circulating EVs of different origins share common mechanisms of arrest *in vivo*. Interestingly, although inert polystyrene beads and non-tumoral EVs (from AB9 zebrafish fibroblasts) can be taken up by macrophages and endothelial cells, they show a reduced accumulation compared to Zmel1 EVs (Figures 4C and 5C). This suggests that both unspecific and specific uptake mechanisms co-exist *in vivo*.

In mice, tumor EVs are internalized by different types of monocytes and macrophages (Whiteside, 2016). In the zebrafish embryo, we noticed that tumor EVs are mostly taken up by small round mpeg1-positive cells (Figures 5A and 5B). In non-injected embryos, these round cells are in direct contact with the blood flow (Figure 5A), which they scan using long protrusions (Figure 5D; Video S3). They also display a reduced velocity (Figure 5E; Video S4). Therefore, the morphology, location, and dynamics of these cells are reminiscent of patrolling monocytes, which are known to play an important role in tumor progression and metastasis in mice and humans (Auffray et al., 2007; Carlin et al., 2013; Hanna et al., 2015). To confirm this observation and gain insight into the ultrastructure of these cells, we used our established CLEM procedure (Goetz et al., 2014; Karreman et al., 2016b) in *Tg(mpeg1:GFP)* embryos injected with tumor EVs labeled with MemBright-Cy3 (Figure 5F; Video S5). We targeted two typical mpeg1:GFP positive cells that have taken up circulating tumor EVs in the living zebrafish embryo (see STAR Methods; Figures S4A and S4B). Fine segmentation of EM images revealed that macrophages localize in a cavity of the lumen of the vessel, where they form tight contacts with the endothelium and extend wide protrusions in the lumen (Figure 5F; Video S5). Interestingly, the region of the endothelium that contacts the macrophages is enriched of endocytic structures, suggesting active exchange between those two cell types (Figure 5G). The macrophages that have taken up tumor EVs extend long and dynamic protrusions in the lumen of the vessel (Figures 5D and 5H), as shown for patrolling monocytes in mice (Carlin et al., 2013). Surprisingly, analysis of the serial sections reveals that their height can be >3 μm and that these protrusions are actually forming large flat sheets deployed in the lumen. Altogether, our data show that circulating tumor EVs are rapidly taken up by patrolling macrophages in the zebrafish embryo, which suggests that it can be used to track the mechanisms of delivery of tumor EVs at high spatiotemporal resolution.

Internalized Tumor EVs Are Targeted to Late Endosomal Compartments

To gain further insight into the mechanisms through which patrolling macrophages uptake tumor EVs, we then imaged the dynamics of circulating tumor EVs (Video S6A). On one hand, EVs arrest at the surface of the macrophage and undergo a slow internalization that can be tracked at optimal spatiotemporal resolution (Figures 6A and 6C; Video S6B). The timing of this uptake (∼ 30 s) is in the range of classical endocytosis (Figure 6A) (Idrissi and Geli, 2014; Taylor et al., 2011). On the other hand, tumor EVs are first caught by a protrusion extending from the macrophage, and then crawl back toward the cell center before being internalized at the basis of the protrusion (Figures 6B and 6C; Video S6C). This second mechanism of internalization is significantly faster (< 5 s) (Figure 6C).

Next, we wondered which intracellular compartments are targeted by uptaken EVs. For this, we incubated *Tg(mpeg1:GFP)* zebrafish embryos with the LysoTracker to label late endosome-lysosomes (LELs). Rapidly after injection, several Zmel1 EVs already colocalize with LysoTracker, although the majority does not (Figure 6D). This colocalization increases over time and 3 h post-injection (hpi), most EV signal is found in

(B) *Z*-projections showing the borders of the dorsal aorta (DA) and the venous plexus (VP), and a histogram showing the EV fluorescence per surface in DA and VP (mean and standard deviation; $p < 0.0001$; Mann-Whitney test).
(C) Quantification of the proportion of 100 nm polystyrene beads, fibroblasts AB9 Evs, or Zmel1 melanoma EVs taken up by endothelial cells 3 hpi (Zmel1 EVs Vs beads: $p = 0.015$, unpaired t test; Zmel1 EVs Vs AB9 EVs: $p < 0.0001$, unpaired t test).
(D) Confocal images of MemBright-Cy3 labeled Zmel1 EVs 3 hpi in *Tg(mpeg1:GFP)* (macrophage specific expression).
(E) Confocal images of MemBright-Cy3 labeled Zmel1 EVs 3 hpi in *Tg(mpo1:GFP)* (neutrophil-specific expression).
(F) Confocal images of MemBright-Cy5 labeled Zmel1 EVs 3 hpi in *Tg(Fli1:GFP; Gata1:RFP)* (GFP: endothelium; *Gata1*: red blood cells and hematopoietic stem cells).

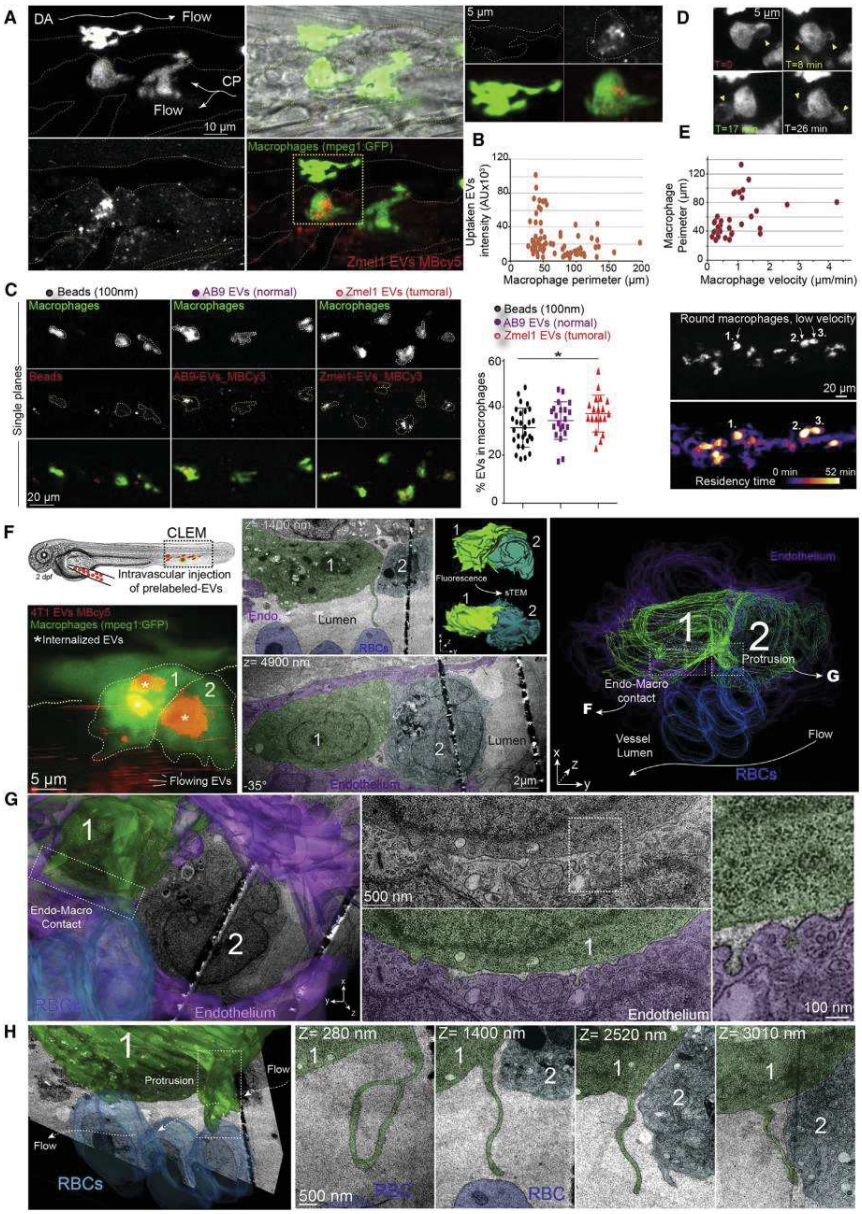

Figure 5. Circulating EVs Are Taken Up by Patrolling Macrophages

(A) Confocal Z projection images of MemBright-Cy3 labeled Zmel1 EVs injected in *Tg(mpeg1:GFP)* (left) with zoom on elongated macrophages devoid of EVs and round macrophages accumulating EVs (right).

(legend continued on next page)

endosome-lysosome compartments (Figure 6D). Of note, 24 hpi, the MemBright signal is still visible and fully colocalizes with LysoTracker (Figure 6D). Although this approach provides a dynamic view of EVs trafficking in zebrafish embryos, LysoTracker labeling does not distinguish between MVBs, late endosomes, and lysosomes. To complement this study, we again exploited our established CLEM procedure on *Tg(mpeg1:GFP)* embryos injected with tumor EVs (Figures 5F–5H and 6E). We generated a 3D model of MemBright-labeled EVs in each macrophage, based on the confocal fluorescent data (called fluorescent 3D model, Figure 6F, upper panel). In parallel, based on TEM serial sections of the same cells, we segmented all the MVBs, late endosomes, and lysosomes that we could locate, and generated a 3D model of these compartments (called TEM 3D model) (Figure 6F, lower panel; Video S5). When comparing the two models, we found that the 3D model created from the fluorescent tumor EVs overlaps with the model from serial TEM sections of LELs (Video S5). This suggests that the internalized tumor EVs are stored within these MVBs, LELs compartments that we imaged at high-resolution (Figure 6E, lower panels). Besides, close examination of the EM stack revealed EVs present in the lumen of the vessel, in close proximity of macrophage protrusions, as well as putative EVs present in endosomes (Figures S4C–S4E). Altogether, this demonstrates the power of the zebrafish embryo to track, at multiple scales, the fate of nanometer-sized objects such as tumor EVs.

Tracking the Release of EVs *In Vivo* Using MB and Genetically Engineered Cells

We focused so far on tumor EVs that were previously isolated and labeled *in vitro* and subsequently tracked *in vivo*. This strategy, however, does not allow tracking of tumor EVs shed from *in-vivo*-grown tumors. Interestingly, we noticed that EVs can be labeled by incubating the secreting cells with the MemBright dye. MemBright quickly and exclusively accumulates in late endosomal compartments of Zmel1 cells in culture (Figure 7A). Upon extensive washing, these cells release fluorescently labeled EVs (Figure 7B) whose morphologies and diameters are similar to EVs from non-labeled cells (Figure 7B). When this approach was used on 4T1 cells expressing CD63-GFP, we could detect EVs positive for both MemBright and CD63, proving that the MemBright can label exosomes (Figure S5). We observed puncta positive for CD63-GFP but not for MemBright and vice-versa. This suggests that the MemBright dye does not label all EVs equally and illustrates the heterogeneity of EVs, which has recently been described (Kowal et al., 2016). Altogether, these experiments suggest that the MemBright is rapidly endocytosed, targeted to MVBs, and incorporated into the membrane of intra-luminal vesicles before being subsequently released outside of the cells attached to the membrane of exosomes. Such a behavior is extremely useful since it allows labeling and tracking of naturally released EVs by pre-incubating cells with MemBright. To prove this, we co-cultured Zmel1 pre-labeled with MemBright-Cy5 with Zmel1 cells expressing cytoplasmic tdTomato. After a week, we observed several Cy5 fluorescent puncta accumulating in the cytoplasm of Zmel1 tdTomato cells, suggesting that indirectly labeled EVs successfully transferred between neighboring cells (Figure 7B). Such a result opens the door to *in vivo* experiments where pre-labeled tumor cells would be grafted in zebrafish embryos (Figures 7C and 7D). To test local EVs transfer, tdTomato Zmel1 cells were pre-labeled with MemBright-Cy5 and subsequently injected into the circulation of *Tg(mpeg1:GFP)* zebrafish embryos. We observed macrophages crawling around arrested Zmel1 tumor cells, and containing Cy5-positive fluorescent puncta (Figure 7C; Video S7), suggesting local EVs transfer between tumor cells and macrophages. These puncta are negative for tdTomato, revealing a different mechanism than the transfer of cytoplasmic material between melanoma cells and macrophages (Roh-Johnson et al., 2017). In addition, we tested the distant transfer of EVs by injecting tdTomato Zmel1 cells pre-labeled with MemBright-Cy5 in the yolk region and imaging macrophages present in the caudal plexus. Similar to the previous experiment, we detected Cy5 fluorescence in macrophages, suggesting the existence of a distant transfer of EVs that exploits the blood circulation for shedding and targeting at distance (Figure 7D). We further validated the ability to detect secreted EVs *in vivo* by intravascular injection of Syntenin2-GFP expressing Zmel1 cells. Upon injection of these cells in the bloodstream, we followed successful extravasation and metastatic outgrowth overtime, which was accompanied by an increased secretion of tumor EVs. While the release of fluorescent EVs was not observed around recently extravasated cells (4 hpi), growing metastatic foci gradually released increasing amounts of Syn2-GFP EVs, which were either mobile or immobile (Figure 7E). Altogether, these experiments demonstrate that the zebrafish embryo allows tracking of the release and transfer of chemically and genetically labeled EVs from tumor to stromal cells *in vivo*.

Tumor EVs Activate Macrophages and Promote Metastatic Growth in Zebrafish

In contrast to inert objects, tumor EVs are loaded with signaling molecules that are likely to affect the fate or behavior of cells that

(B) EVs are mostly taken up by small macrophages. Histogram showing the intensity of taken up EVs (y axis, arbitrary units) versus the perimeter of the macrophages (x axis, μm). Each dot represents one macrophage.
(C) Macrophages internalize tumor EVs more efficiently than 100 nm polystyrene beads (mean and standard deviation; p = 0.016, unpaired t test).
(D) Individual time points of single plane confocal images showing the dynamics of the protrusions in round macrophages.
(E) Histogram showing the perimeter of macrophages (y axis, μm) versus their velocity (x axis, μm/s) (left) and images at the beginning (T = 0) and the end (T = 60 min) of a representative time-lapse. Velocities of migration of *Tg(mpeg1:GFP)*-positive cells are represented with a color code. Three round *Tg(mpeg1:GFP)*-positive cells (1, 2, and 3) show very little displacement during one h.
(F) CLEM experiment on *Tg(mpeg1:GFP)* embryos injected with MemBright-Cy3 4T1 EVs imaged by confocal right after injection (left, *Z* projection). Middle: electron microscopy images on two different *Z* planes showing the same cells. Right: 3D model showing the two macrophages (green), the endothelium (purple), and three red blood cells (blue).
(G) Electron microscopy images of the contact between the endothelium and the macrophage, showing the accumulation of endocytic structures on the endothelium side.
(H) 3D model and electron microscopy images of one protrusion sent by the macrophage into the lumen. This protrusion is visible over several microns in Z.

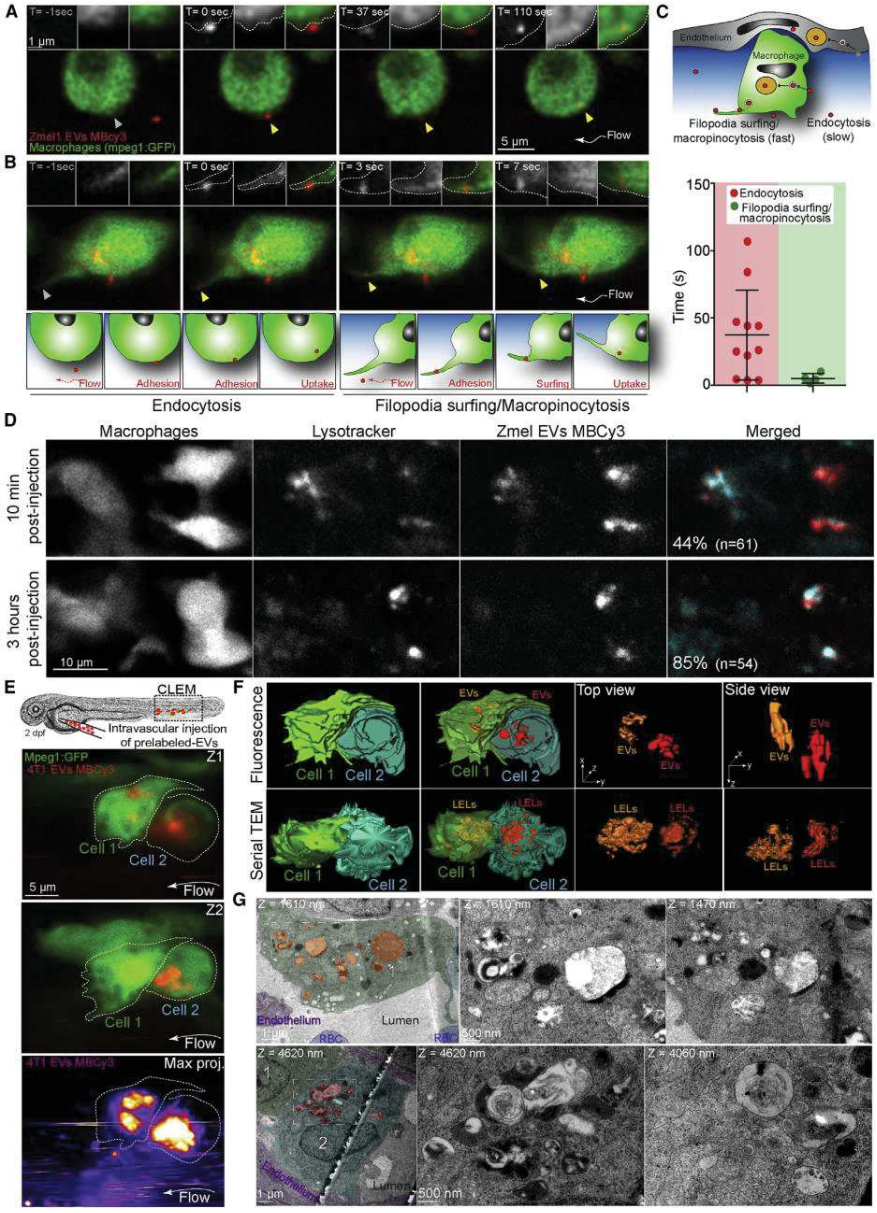

(legend on next page)

internalize them. We thus assessed whether Zmel1 EVs could modify the behavior of receiving cells. We focused on macrophages, which are taking up most of the circulating EVs, and first analyzed their velocities upon uptake. The uptake of tumor EVs by patrolling macrophages significantly reduced their motility when compared to macrophages that had internalized control beads (Figure 8A). Since macrophage velocity has been associated with their activation status *in vitro* (Vogel et al., 2014), we chose to evaluate the impact of Zmel1 EVs on macrophage activation. To do this, we used a recently described transgenic line that relies on the expression of TNF-α to discriminate between pro-inflammatory "M1-like" and "M2-like" polarized macrophages (Nguyen-Chi et al., 2015). Strikingly, most embryos injected with Zmel1 EVs showed M1 activated macrophages 20 hpi (Figures 8B and 8C). Such switches were rarely observed when embryos were injected with 100 nm control polystyrene beads, which clearly demonstrates that circulating Zmel1 EVs can modify the behavior of receiving cells at distance. Tumor EVs can educate receiving cells and confer them pro-metastatic characteristics (Peinado et al., 2017). Inspired by such experiments mostly performed in mice, we next assessed whether circulating tumor EVs could tune metastatic outgrowth. We first "primed" embryos with intravascular injection of either Zmel1 EVs (or 100 nm polystyrene beads). After 12 h, the same embryos were injected with Zmel1 cells in a classical experimental metastasis assay as previously performed (Follain et al., 2018a). Metastatic growth was assessed 7 days later by measuring fluorescence in the caudal plexus. We observed a marked and significant increase in metastatic outgrowth when embryos were primed with Zmel EVs, and not with inert beads (Figure 8D). Furthermore, metastatic foci of embryos primed with tumor Zmel EVs were strikingly more invasive and displayed colonization of the fin parenchyma (Figures 8D and 8E). Altogether, these experiments demonstrate that (1) tumor EVs transform the phenotypes of macrophages and (2) favor metastatic outgrowth and invasiveness by modifying the microenvironment. In addition to demonstrating that labeling EVs with MemBright does not perturb their function, this further validates the use of zebrafish embryos to dissect, with high spatiotemporal resolution, the cascade of events induced by circulating tumor EVs and leading to pre-metastatic niche formation *in vivo*.

DISCUSSION

The work presented here establishes the zebrafish embryo as a new animal model to study tumor EVs *in vivo*. It demonstrates the proximity of zebrafish melanoma EVs to human melanoma EVs and shows how a new membrane probe, the MemBright, specifically and brightly labels EVs. Using this probe, but also genetically labeled EVs, we were able to precisely track their fate and behavior at high spatiotemporal resolution *in vivo*. This allowed us to provide a description of the behavior of tumor EVs circulating in the blood flow and to track their fate upon arrest. We identify the three main cell types taking up circulating tumor EVs (endothelial cells, patrolling macrophages, and putative hematopoietic stem cells) and unravel their uptake mechanisms. Besides, we describe two complementary methods, a conventional genetic approach and the pre-labeling of secreting cells by MemBright, allowing to track the release and transfer of EVs *in vivo*. Finally, we provide evidence for a functional role of tumor EVs in altering the metastatic microenvironment and promoting metastatic outgrowth in zebrafish embryos.

In a parallel study, Verweij and colleagues examine the fate of CD63 positive EVs secreted by the YSL in zebrafish embryo (Verweij et al., 2019). They track endogenous EVs, genetically labeled and naturally secreted during zebrafish development, while we tracked exogenous MemBright-labeled injected tumor EVs. Yet, both studies reach similar conclusions. They both show that (1) endogenous and tumor EVs mainly arrest in the caudal plexus, in regions of low blood flow, (2) EVs are mostly taken up by endothelial cells and patrolling macrophages, and (3) EVs are stored in acidic compartments. Together, our reports establish the zebrafish embryo (*Danio rerio*) as a new model to study fundamental aspects of EVs biology *in vivo*. It thus represents a precious and complementary tool to invertebrate models *Drosophila* and *C. elegans*, which already contributed to better understand the mechanisms of EV secretion as well as their function (Beer and Wehman, 2017).

In addition, we propose the zebrafish embryo as a new and complementary model to murine and human cell culture systems for studying the fate and the function of tumor EVs during the priming of metastatic niches at distance. Compared to *in vitro* systems, zebrafish embryo offers an invaluable complex microenvironment, where different cell types known to contribute to tumor progression are present and can be tracked using established fluorescent transgenic lines. Its transparency allows visualization of individual tumor EVs dispersion and uptake in living zebrafish with unprecedented spatiotemporal resolution, which represents a major advantage over the mouse, where more complex intravital imaging procedures are required in order to visualize single EVs (Lai et al., 2015; Van Der Vos et al., 2016; Zomer et al., 2015). The zebrafish embryo is also amenable to CLEM,

Figure 6. EVs Are Taken Up through Different Mechanisms and Accumulate in Late Endosomal Compartments

(A and B) Single-plane confocal images of *Tg(mpeg1:GFP)* embryos injected with Zmel1 MemBright-Cy3 (MBCy3) EVs extracted from time-lapses generated immediately after injection and showing: (A) the attachment and uptake of EVs by endocytosis and (B) the sliding of EVs on the macrophage protrusion and its fast internalization.

(C) Schematic representation of the modes of uptake by macrophages (upper) and histogram showing the duration (y axis, s) of those two mechanisms (mean and standard deviation).

(D) Single plane confocal images of *Tg(mpeg1:GFP)* embryos injected with Zmel1 MBCy3 EVs and incubated with LysoTracker.

(E) CLEM experiment on *Tg(mpeg1:GFP)* embryos injected with MemBright-Cy3 4T1 EVs imaged by confocal (2 single confocal planes of the GFP and the MBCy3 channels and Z projection of the EV channel (lower)).

(F) 3D model of the two cells and the taken up EVs generated from the confocal data (upper panel, fluorescence), and 3D model of the two cells and the MVBs-late endosomes-lysosomes compartments (LELs) generated from the serial transmission electron microscopy data (lower panel, serial TEM).

(G) Global view of each macrophage highlighting the MVBs-late endosomes-lysosomes compartments (orange and red, left). Zooms of those compartments are shown on the right in two different *Z* positions of the same region.

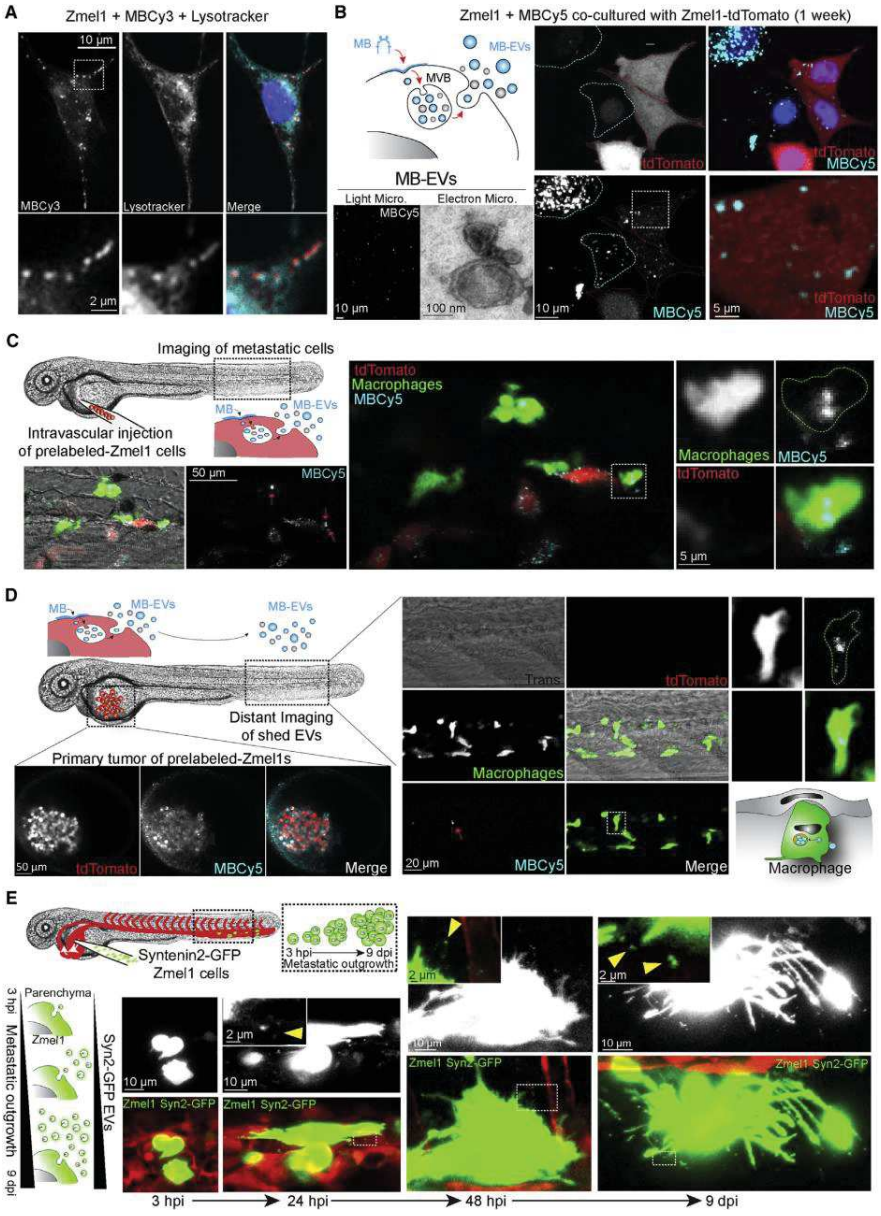

(legend on next page)

through procedures which are simplified compared to the mouse (Goetz et al., 2015; Karreman et al., 2016b). In the future, nanoscale imaging should unravel how tumor EVs secreted by a primary tumor reach the blood circulation before crossing the endothelium when reaching a given organ but also to grasp the details of their uptake and trafficking at a subcellular level.

Here, we show that most tumor EVs are internalized by a subset of macrophages. We consider these cells as functionally similar to murine and human patrolling monocytes for the following reasons: (1) they are positive for the mpeg1 promoter, which is expressed both by monocytes and macrophages in human (Spilsbury et al., 1995), (2) they are small, round and have a slow migration velocity when compared to elongated differentiated macrophages, and (3) they are sending highly dynamic protrusions toward the lumen of the vessels and show areas of direct cell-cell contacts with the endothelial wall, as previously shown (Murayama et al., 2006). These last two aspects match the main characteristics of human and mice patrolling monocytes (Auffray et al., 2007; Carlin et al., 2013). Notably, CLEM analysis reveals that the dynamic protrusions observed in live imaging are actually flat sheets of several microns that scan the vessel lumen and could function as butterfly nets to catch tumor EVs deep in the vessel lumen. Such structures are specific to macrophages, allowing them to internalize fluid-borne objects, unlike neutrophils that only phagocytose surface-bound ones (Colucci-Guyon et al., 2011). Once they have contacted the protrusion, the EVs quickly slide toward the cell body through unknown mechanisms, which could be similar to the filopodia surfing recently described (Heusermann et al., 2016). Those protrusions could also participate in macropinocytic uptake of EVs, similar to what has been observed by microglia (Fitzner et al., 2011). EVs are then internalized at the basis of the protrusions, probably in regions of active endocytosis. Interestingly, our EM data revealed several EVs present at the basis of protrusions (see Figure S4C). Alternatively, circulating EVs can directly bind to the macrophage surface before being endocytosed. The capacity of patrolling macrophages to rapidly uptake circulating EVs explains the very short half-life (10–20 min) of circulating EVs after their injection in the blood circulation of either mouse (Morishita et al., 2015; Saunderson et al., 2014; Takahashi et al., 2013) or zebrafish (our work). This is in agreement with the observation that chemical depletion of monocytes and macrophages in mice dramatically increases the stability of circulating EVs (Imai et al., 2015).

Tumor EVs are then rapidly stored in acidic degradative compartments, similar to what has been described for macrophages *in vitro* (Feng et al., 2010). Determining whether and how internalized EVs deliver signaling molecules to the receiving cell, although they are mostly targeted to degradative compartments, is a central question in the EV field. It will be particularly important to address it in the case of tumor EVs taken up by patrolling macrophages. It is interesting to note that uptake mechanisms and compartments are similar between exogenous tumor EVs (this study) and endogenous EVs (Verweij et al., 2019). This suggests that tumor EVs are internalized using universal mechanisms and further demonstrates that the zebrafish embryo is a perfect model for dissecting such behavior.

In addition, the zebrafish embryo allows a direct comparison of EVs with distinct sizes, contents, or origins. This will be essential to better understand the heterogeneity of EVs, as it is now clear that multiple sub-populations (or sizes) of EVs co-exist with different cargo contents and presumably different functions (Kowal et al., 2016). Co-injection of different types of EVs can, for instance, be used to precisely dissect the involvement of one given EV transmembrane or cargo protein, or to compare tumor EVs from patients at different stages of tumor progression. Using multi-color MemBright probes (Cy3, 5, or 7) to label EVs, it is possible to directly compare the behavior of co-injected populations of EVs. Labeling EVs with membrane probes after their isolation is fast and allows obtaining bright fluorescent EVs regardless of their origin. It is particularly relevant for EVs isolated from cell lines reluctant to gene expression manipulation, from animal body fluids, or, importantly, in the case of tumor EVs from samples of cancer patients. However, the use of membrane probes requires the assurance of labeling specificity. This is particularly essential for studies aiming to track EVs dispersion and uptake, as dye aggregates can easily be confounded with EVs, due to their small sizes (Lai et al., 2015; Takov et al., 2017). Here, using spectroscopic and microscopic approaches, we have shown that the MemBright does not form such fluorescent aggregates, in contrast to commonly used PKH. In addition, it is brighter and can therefore be used at reduced concentrations, minimizing again the risk of false-positive results. The key difference of MemBright from PKH is the presence of amphiphilic groups, which favor efficient transfer of the fluorophore from aqueous media to lipid membranes (Collot et al., 2015; Kucherak et al., 2010). Therefore, MemBright can be used to confidently track EV dispersion and uptake.

Finally, our work demonstrates that zebrafish can be used to dissect the causal relationship between circulating tumor EVs uptake and formation of metastatic niches. While most studies performed in mice demonstrate correlations between bulk injection of EVs and emergence of a pre-metastatic niche, the zebrafish embryo, by allowing continuous imaging, allows direct

Figure 7. Tracking EVs Released by Zebrafish Melanoma Cells

(A) Confocal images of Zmel1 cells incubated with MemBright-Cy3 and stained with LysoTracker.

(B) Schematic representation of the experimental procedure: MemBright added to cells in culture accumulates in MVBs and is subsequently released in exosomes. Such EVs can be observed by electron microscopy. Confocal images of Zmel1 cells pre-labeled with MemBright-Cy5 and co-cultured with Zmel1 tdTomato cells, showing the transfer of MemBright in *Z* projections (left) and single planes (right).

(C) Confocal images of tdTomato Zmel1 cells pre-labeled with MemBright-Cy5 injected in the circulation of *Tg(mpeg1:GFP)* embryos and imaged in the caudal plexus two days post-injection, showing the local transfer of MemBright-Cy5 to macrophages.

(D) Confocal images of tdTomato Zmel1 cells pre-labeled with MemBright Cy5 injected above the yolk of *Tg(mpeg1:GFP)* embryos and imaged in the yolk region (primary tumor, left) and in the caudal plexus (distant imaging of shed EVs, right) two days post-injection, showing the long distance transfer of MemBright-Cy5 to macrophages.

(E) *In vivo* release of Syntenin2-GFP EVs. Zmel1 Syntenin2-GFP cells injected in the circulation of *Tg(Fli:Gal4, UAS:RFP)* embryos and imaged by confocal in the following days.

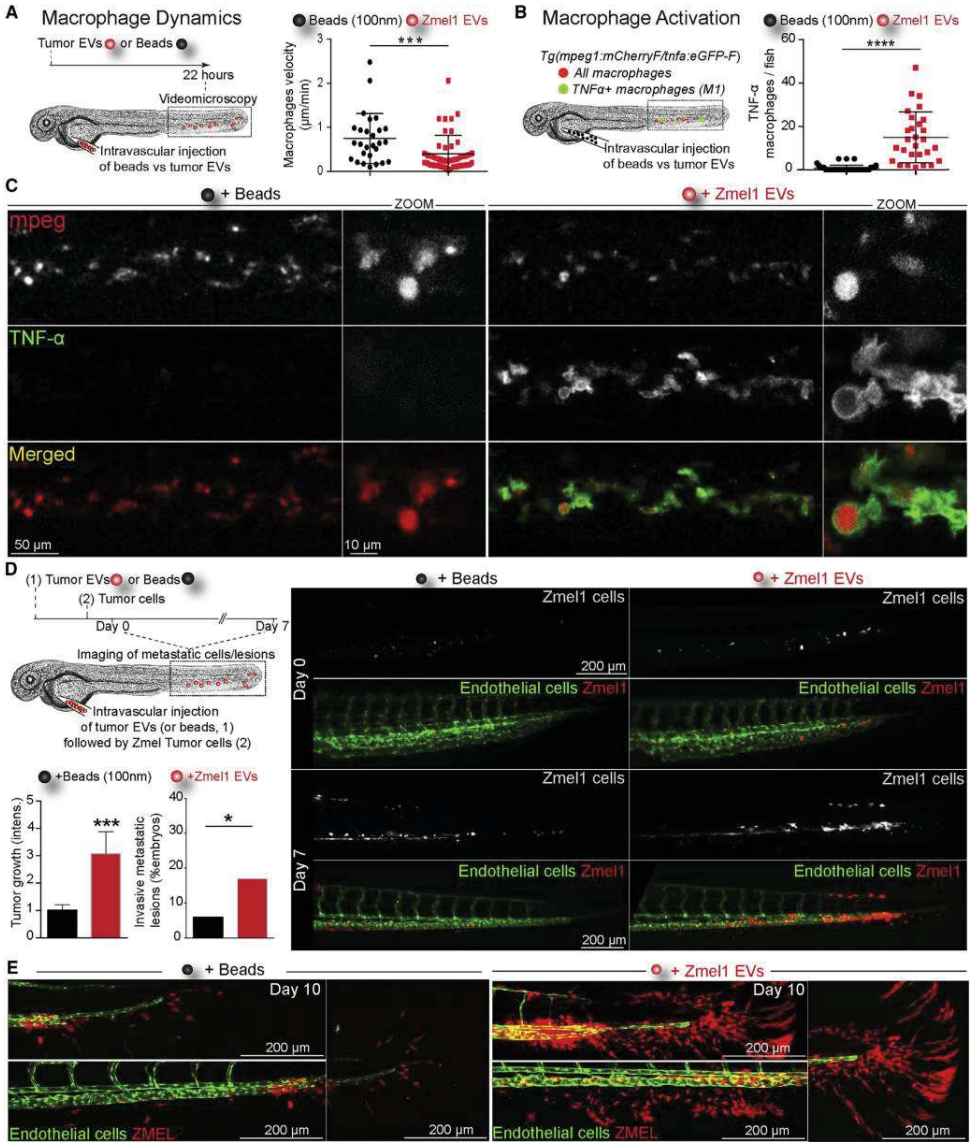

Figure 8. Melanoma EVs Activate Macrophages and Promote Tumor Growth in Zebrafish

(A) 22 h following injection of Zmel1 EVs or 100 nm beads, the dynamics of mpeg1:GFP macrophages was measured by time-lapse. Histogram showing that the velocity of macrophages 22 h after injection (one dot represents one macrophage; mean and standard deviation; $p = 0.0009$, Mann-Whitney test).

(B) *Tg(mpeg1:mCherry/TNFa:eGFP)* injected with Zmel1 EVs or 100 nm beads and imaged 20 h post-injection. Histogram showing the number of TNFa:GFP positive cells per fish caudal plexus (one dot represents one embryo; mean and standard deviation; $p < 0.0001$, Mann-Whitney test).

(C) Confocal images of *Tg(mpeg1:mCherry/TNFa:eGFP)* injected with Zmel1 EVs or 100 nm beads and imaged 20 h post-injection.

(legend continued on next page)

quantitative assessment of how metastatic niches are formed and how they can contribute to metastatic outgrowth. In this work, we show that injection of tumor EVs in the circulation is rapidly followed by expression of TNFα, reminiscent of their activation into a pro-inflammatory "M1-like" phenotype. These results are consistent with *in vitro* studies showing that EVs from breast cancer cells or oral squamous carcinoma cells stimulate an M1 macrophage inflammatory response (including TNF induction) (Xiao et al., 2018; Chow et al., 2014). Other studies, however, show that tumor EVs, for instance from prostate tumors, induce an M2 activation (Halin Bergström et al., 2016). Although the M1/M2 binary polarization model of macrophages has been challenged (Aras and Zaidi, 2017), pro-inflammatory macrophages have been reported to exert pro- or anti-tumoral effects depending on the context (Engblom et al., 2016). Further work is thus needed to better understand how tumor EVs tune macrophages' fate during metastatic progression. Here, the zebrafish model offers the opportunity to revisit the interactions between tumor EVs, macrophages and other immune cells (and their activation status), and tumor cells during extravasation and metastatic outgrowth. Recent work performed in mice, which exploited intravital imaging, revealed close interactions between tumor cells arrested in the circulation and myeloid cells and the exchange of microvesicles promoting extravasation (Headley et al., 2016). Complementary usage of these two models, based on intravital imaging, is thus likely to bring important insights into how tumor EVs can tune metastatic outgrowth.

Importantly, we show that pre-treatment of zebrafish with Zmel1 tumor EVs enhances metastatic outgrowth, leading to a more invasive phenotype. This phenotype is reminiscent of several mice studies showing that pre-injection of EVs from either melanoma, pancreatic ductal adenocarcinoma, or breast tumors promotes metastasis of their respective tumors cells injected in the circulation (Costa-Silva et al., 2015; Hoshino et al., 2015; Plebanek et al., 2017). In Zmel1 EVs pre-treated fish, we also observed that tumor cells were more efficient at actively invading the caudal fin. Such a phenotype could result from increased extravasation efficiency or from EV-mediated increased proliferation. Alternatively, it could arise from tumor EVs that can directly alter the extracellular matrix in pre-metastatic niches (Costa-Silva et al., 2015), or induce the secretion of pro-migratory factors by activated pro-inflammatory macrophages (Xiao et al., 2018).

Altogether, our work on the tracking of exogenous tumor EVs (this study) and of endogenous EVs (Verweij et al., 2019) set the zebrafish embryo as a new and highly attractive *in vivo* model to track EVs at the single EV scale. Interestingly, both studies identified similar mechanisms of transit and uptake for physiological and pathological extracellular vesicles, which further validate the zebrafish embryo as a reliable animal model for studying the biology of EVs. Finally, we believe that the zebrafish embryo will open new avenues for EV biology, as it offers adapted time and space scales to the study of small organelles *in vivo*.

STAR★METHODS

Detailed methods are provided in the online version of this paper and include the following:

SUPPLEMENTAL INFORMATION

Supplemental Information includes five figures, two tables, and seven videos and can be found with this article online at https://doi.org/10.1016/j.devcel.2019.01.014.

ACKNOWLEDGMENTS

We thank all members of the Goetz Lab for helpful discussions. We are indebted to K. Richter and F. Peri (EMBL, Heidelberg, Germany) as well as to P. Hanns and C. Lengerke (University Hospital Basel, Switzerland) for supplying zebrafish embryos. We are grateful to R. White (MSKCC, New York, USA) for the Zmel1 (native and tdTomato) cells, to Dr. D.C. Bennett (St. George's University of London, U.K.) and Dr. M. Soengas (CNIO, Madrid, Spain) for mammalian melanoma cells, and to P. Zimmerman (CRCM,

(D) Zmel1-tdTomato tumor growth is enhanced in *Tg(Fli1:GFP)* embryos that were pre-injected with Zmel1 EVs. Histograms showing tumor growth at 7 days (left; $p = 0.0004$, Mann-Whitney test) and invasive lesions at 10 days (right; $p < 0.05$; chi-squared test). Epifluorescent images of tumor growth in the caudal plexus, right panels.
(E) Confocal images of tumor cell invasion in embryos.

Marseille, France) for the Syntenin-2 construct. We thank A. Michel (EFS, Strasbourg, France) and C. Spiegelhalter (IGBMC, Illkirch, France) for EM assistance, Y.Schwab for advice during CLEM analysis (EMBL, Heidelberg), E. Guiot and Y. Lutz (IGBMC, Illkirch, France) for advice on confocal imaging, and A. Audfray (Malvern Instruments) for NTA. We thank the CNIO proteomics core for performing the mass spectrometry on mouse and human melanoma EVs. We thank P. Herbomel for critical reading of the manuscript. This work was supported by a fellowship from IDEX (University of Strasbourg) to S.G.; by grants from La Ligue contre le Cancer, Canceropole Grand-Est, INCa (MetaCLEM) and Roche to J.G.G.; and by institutional funds from University of Strasbourg, INSERM, and ANR (to CC, French Proteomics Infrastructure ProFI; ANR-10-INBS-08-03).

AUTHOR CONTRIBUTIONS

V.H. and J.G.G. planned the project. V.H. designed and conducted most of the experiments with contributions from S.G., B.M., G.F., M.J.G-L., and J.B. M.C. synthesized the MemBright and led the spectroscopy experiments, with A.S.K. S.H. designed the automated EV tracking and the EV colocalization analysis. O.L. engineered the fluorescent cell lines. F.De., J.B., and C.C. conducted the mass spectrometry on Zmel1 EVs. A.I.A., S.G.S., and H.P. lead the mass spectrometry analysis on human and mice melanoma EVs. F.V. and G.v.N. generated the mass spectrometry data on AB9 and endogenous zebrafish EVs. N.F. prepared the samples for CLEM and P.M. did the serial sectioning and the microCT. F.Dj. provided the *Tg(mpeg:mCherry,tnf:GFP)* zebrafish line and advised its use. L.M. and I.B. performed image analysis. V.H. and J.G.G. wrote the manuscript with insights from all authors.

DECLARATION OF INTERESTS

The authors declare no competing interests.

Received: March 15, 2018
Revised: October 19, 2018
Accepted: January 10, 2019
Published: February 7, 2019

REFERENCES

Al-Nedawi, K., Meehan, B., Micallef, J., Lhotak, V., May, L., Guha, A., and Rak, J. (2008). Intercellular transfer of the oncogenic receptor EGFRvIII by microvesicles derived from tumour cells. Nat. Cell Biol. *10*, 619–624.

Aras, S., and Zaidi, M.R. (2017). TAMeless traitors: macrophages in cancer progression and metastasis. Br. J. Cancer *117*, 1583–1591.

Auffray, C., Fogg, D., Garfa, M., Elain, G., Join-Lambert, O., Kayal, S., Sarnacki, S., Cumano, A., Lauvau, G., and Geissmann, F. (2007). Monitoring of blood vessels and tissues by a population of monocytes with patrolling behavior. Science *317*, 666–670.

Baietti, M.F., Zhang, Z., Mortier, E., Melchior, A., Degeest, G., Geeraerts, A., Ivarsson, Y., Depoortere, F., Coomans, C., Vermeiren, E., et al. (2012). Syndecan–syntenin–ALIX regulates the biogenesis of exosomes. Nat. Cell Biol. *14*, 677–685.

Baran, J., Baj-Krzyworzeka, M., Weglarczyk, K., Szatanek, R., Zembala, M., Barbasz, J., Czupryna, A., Szczepanik, A., and Zembala, M. (2010). Circulating tumour-derived microvesicles in plasma of gastric cancer patients. Cancer Immunol. Immunother. *59*, 841–850.

Beer, K.B., and Wehman, A.M. (2017). Mechanisms and functions of extracellular vesicle release in vivo-what we can learn from flies and worms. Cell Adh. Migr. *11*, 135–150.

Carapito, C., Burel, A., Guterl, P., Walter, A., Varrier, F., Bertile, F., and Van Dorsselaer, A. (2014). MSDA, a proteomics software suite for in-depth mass spectrometry Data Analysis using grid computing. Proteomics *14*, 1014–1019.

Cardona, A., Saalfeld, S., Schindelin, J., Arganda-Carreras, I., Preibisch, S., Longair, M., Tomancak, P., Hartenstein, V., and Douglas, R.J. (2012). TrakEM2 software for neural circuit reconstruction. PLoS One *7*, e38011.

Carlin, L.M., Stamatiades, E.G., Auffray, C., Hanna, R.N., Glover, L., Vizcay-Barrena, G., Hedrick, C.C., Cook, H.T., Diebold, S., and Geissmann, F. (2013). Nr4a1-dependent Ly6C(low) monocytes monitor endothelial cells and orchestrate their disposal. Cell *153*, 362–375.

Chow, A., Zhou, W., Liu, L., Fong, M.Y., Champer, J., Van Haute, D., Chin, A.R., Ren, X., Gugiu, B.G., Meng, Z., et al. (2014). Macrophage immunomodulation by breast cancer-derived exosomes requires Toll-like receptor 2-mediated activation of NF-κB. Sci. Rep. *4*, 5750.

Collot, M., Kreder, R., Tatarets, A.L., Patsenker, L.D., Mely, Y., and Klymchenko, A.S. (2015). Bright fluorogenic squaraines with tuned cell entry for selective imaging of plasma membrane vs. endoplasmic reticulum. Chem. Commun. *51*, 17136–17139.

Collot, M., Ashokkumar, P., Anton, H., Boutant, E., Faklaris, O., Galli, T., Mély, Y., Danglot, L., and Klymchenko, A.S. (2019). MemBright: a family of red to near-infrared fluorescent membrane probes for advanced cellular imaging and neuroscience. Cell Chem. Biol. *26*, https://doi.org/10.1016/j.chembiol.2019.01.009.

Colombo, M., Moita, C., van Niel, G., Kowal, J., Vigneron, J., Benaroch, P., Manel, N., Moita, L.F., Théry, C., and Raposo, G. (2013). Analysis of ESCRT functions in exosome biogenesis, composition and secretion highlights the heterogeneity of extracellular vesicles. J. Cell Sci. *126*, 5553–5565.

Colucci-Guyon, E., Tinevez, J.Y., Renshaw, S.A., and Herbomel, P. (2011). Strategies of professional phagocytes in vivo: unlike macrophages, neutrophils engulf only surface-associated microbes. J. Cell Sci. *124*, 3053–3059.

Costa-Silva, B., Aiello, N.M., Ocean, A.J., Singh, S., Zhang, H., Thakur, B.K., Becker, A., Hoshino, A., Mark, M.T., Molina, H., et al. (2015). Pancreatic cancer exosomes initiate pre-metastatic niche formation in the liver. Nat. Cell Biol. *17*, 816–826.

Cox, J., Hein, M.Y., Luber, C.A., Paron, I., Nagaraj, N., and Mann, M. (2014). Accurate Proteome-wide label-free quantification by delayed normalization and maximal peptide ratio extraction, termed MaxLFQ. Mol. Cell Proteomics *13*, 2513–2526.

Van Deun, J., Mestdagh, P., Sormunen, R., Cocquyt, V., Vermaelen, K., Vandesompele, J., Bracke, M., De Wever, O., and Hendrix, A. (2014). The impact of disparate isolation methods for extracellular vesicles on downstream RNA profiling. J. Extracell. Vesicles *3*, 1–14.

EV-TRACK Consortium, Van Deun, J., Mestdagh, P., Agostinis, P., Akay, Ö., Anand, S., Anckaert, J., Martinez, Z.A., Baetens, T., Beghein, E., et al. (2017). EV-TRACK: transparent reporting and centralizing knowledge in extracellular vesicle research. Nat. Methods *14*, 228–232.

Engblom, C., Pfirschke, C., and Pittet, M.J. (2016). The role of myeloid cells in cancer therapies. Nat. Rev. Cancer *16*, 447–462.

Feng, D., Zhao, W.L., Ye, Y.Y., Bai, X.C., Liu, R.Q., Chang, L.F., Zhou, Q., and Sui, S.F. (2010). Cellular internalization of exosomes occurs through phagocytosis. Traffic *11*, 675–687.

Fitzner, D., Schnaars, M., van Rossum, D., Krishnamoorthy, G., Dibaj, P., Bakhti, M., Regen, T., Hanisch, U.K., and Simons, M. (2011). Selective transfer of exosomes from oligodendrocytes to microglia by macropinocytosis. J. Cell Sci. *124*, 447–458.

Follain, G., Osmani, N., Azevedo, A.S., Allio, G., Mercier, L., Karreman, M.A., Solecki, G., Garcia Leòn, M.J., Lefebvre, O., Fekonja, N., et al. (2018a). Hemodynamic forces tune the arrest, adhesion, and extravasation of circulating tumor cells. Dev. Cell *45*, 33–52.

Follain, G., Osmani, N., Fuchs, C., Allio, G., Harlepp, S., and Goetz, J.G. (2018b). Using the zebrafish embryo to dissect the early steps of the metastatic cascade. Methods Mol. Biol. *1749*, 195–211.

Galindo-Hernandez, O., Villegas-Comonfort, S., Candanedo, F., González-Vázquez, M.C., Chavez-Ocaña, S., Jimenez-Villanueva, X., Sierra-Martinez, M., and Salazar, E.P. (2013). Elevated concentration of microvesicles isolated from peripheral blood in breast cancer patients. Arch. Med. Res. *44*, 208–214.

Goetz, J.G., Steed, E., Ferreira, R.R., Roth, S., Ramspacher, C., Boselli, F., Charvin, G., Liebling, M., Wyart, C., Schwab, Y., et al. (2014). Endothelial cilia mediate low flow sensing during zebrafish vascular development. Cell Rep. *6*, 799–808.

Goetz, J.G., Monduc, F., Schwab, Y., and Vermot, J. (2015). Using correlative light and electron microscopy to study zebrafish vascular morphogenesis. Methods Mol. Biol. *1189*, 31–46.

Grange, C., Tapparo, M., Collino, F., Vitillo, L., Damasco, C., Deregibus, M.C., Tetta, C., Bussolati, B., and Camussi, G. (2011). Microvesicles released from human renal cancer stem cells stimulate angiogenesis and formation of lung premetastatic niche. Cancer Res. *71*, 5346–5356.

Gu, J., Qian, H., Shen, L., Zhang, X., Zhu, W., Huang, L., Yan, Y., Mao, F., Zhao, C., Shi, Y., et al. (2012). Gastric cancer exosomes trigger differentiation of umbilical cord derived mesenchymal stem cells to carcinoma-associated fibroblasts through TGF-β/Smad pathway. PLoS One *7*, e52465.

Le Guyader, D., Redd, M.J., Colucci-Guyon, E., Murayama, E., Kissa, K., Briolat, V., Mordelet, E., Zapata, A., Shinomiya, H., and Herbomel, P. (2008). Origins and unconventional behavior of neutrophils in developing zebrafish. Blood *111*, 132–141.

Halin Bergström, S., Hägglöf, C., Thysell, E., Bergh, A., Wikström, P., and Lundholm, M. (2016). Extracellular vesicles from metastatic rat prostate tumors prime the normal prostate tissue to facilitate tumor growth. Sci. Rep. *6*, 31805.

Hanna, R.N., Cekic, C., Sag, D., Tacke, R., Thomas, G.D., Nowyhed, H., Herrley, E., Rasquinha, N., McArdle, S., Wu, R., et al. (2015). Patrolling monocytes control tumor metastasis to the lung. Science *350*, 985–990.

Headley, M.B., Bins, A., Nip, A., Roberts, E.W., Looney, M.R., Gerard, A., and Krummel, M.F. (2016). Visualization of immediate immune responses to pioneer metastatic cells in the lung. Nature *531*, 513–517.

Heilmann, S., Ratnakumar, K., Langdon, E.M., Kansler, E.R., Kim, I.S., Campbell, N.R., Perry, E.B., McMahon, A.J., Kaufman, C.K., Van Rooijen, E., et al. (2015). A quantitative system for studying metastasis using transparent zebrafish. Cancer Res. *75*, 4272–4282.

Heusermann, W., Hean, J., Trojer, D., Steib, E., von Bueren, S., Graff-Meyer, A., Genoud, C., Martin, K., Pizzato, N., Voshol, J., et al. (2016). Exosomes surf on filopodia to enter cells at endocytic hot spots and shuttle within endosomes to scan the ER. J. Cell Biol. *213*, 173–184.

Hoshino, A., Costa-Silva, B., Shen, T.L., Rodrigues, G., Hashimoto, A., Tesic Mark, M., Molina, H., Kohsaka, S., Di Giannatale, A., Ceder, S., et al. (2015). Tumour exosome integrins determine organotropic metastasis. Nature *527*, 329–335.

Hyenne, V., Lefebvre, O., and Goetz, J.G. (2017). Going live with tumor exosomes and microvesicles. Cell Adh. Migr. *11*, 173–186.

Idrissi, F.Z., and Geli, M.I. (2014). Zooming in on the molecular mechanisms of endocytic budding by time-resolved electron microscopy. Cell. Mol. Life Sci. *71*, 641–657.

Imai, T., Takahashi, Y., Nishikawa, M., Kato, K., Morishita, M., Yamashita, T., Matsumoto, A., Charoenviriyakul, C., and Takakura, Y. (2015). Macrophage-dependent clearance of systemically administered B16BL6-derived exosomes from the blood circulation in mice. J. Extracell. Vesicles *4*, 26238.

Karreman, M.A., Mercier, L., Schieber, N.L., Solecki, G., Allio, G., Winkler, F., Ruthensteiner, B., Goetz, J.G., and Schwab, Y. (2016a). Fast and precise targeting of single tumor cells in vivo by multimodal correlative microscopy. J. Cell Sci. *129*, 444–456.

Karreman, M.A., Hyenne, V., Schwab, Y., and Goetz, J.G. (2016b). Intravital correlative microscopy: imaging life at the nanoscale. Trends Cell Biol. *26*, 848–863.

Kowal, J., Arras, G., Colombo, M., Jouve, M., Morath, J.P., Primdal-Bengtson, B., Dingli, F., Loew, D., Tkach, M., and Théry, C. (2016). Proteomic comparison defines novel markers to characterize heterogeneous populations of extracellular vesicle subtypes. Proc. Natl. Acad. Sci. USA *113*, E968–E977.

Kucherak, O.A., Oncul, S., Darwich, Z., Yushchenko, D.A., Arntz, Y., Didier, P., Mély, Y., and Klymchenko, A.S. (2010). Switchable Nile red-based probe for cholesterol and lipid order at the outer leaflet of biomembranes. J. Am. Chem. Soc. *132*, 4907–4916.

Lai, C.P., Mardini, O., Ericsson, M., Prabhakar, S., Maguire, C.A., Chen, J.W., Tannous, B.A., and Breakefield, X.O. (2014). Dynamic biodistribution of extracellular vesicles in vivo using a multimodal imaging reporter. ACS Nano *8*, 483–494.

Lai, C.P., Kim, E.Y., Badr, C.E., Weissleder, R., Mempel, T.R., Tannous, B.A., and Breakefield, X.O. (2015). Visualization and tracking of tumour extracellular vesicle delivery and RNA translation using multiplexed reporters. Nat. Commun. *6*, 7029.

Liu, Y., Gu, Y., Han, Y., Zhang, Q., Jiang, Z., Zhang, X., Huang, B., Xu, X., Zheng, J., and Cao, X. (2016). Tumor exosomal RNAs promote lung pre-metastatic niche formation by activating alveolar epithelial TLR3 to recruit neutrophils. Cancer Cell *30*, 243–256.

Logozzi, M., De Milito, A., Lugini, L., Borghi, M., Calabrò, L., Spada, M., Perdicchio, M., Marino, M.L., Federici, C., Iessi, E., et al. (2009). High levels of exosomes expressing CD63 and caveolin-1 in plasma of melanoma patients. PLoS One *4*, e5219.

Magde, D., Rojas, G.E., and Seybold, P.G. (1999). Solvent dependence of the fluorescence lifetimes of xanthene dyes. Photochem. Photobiol. *70*, 737–744.

Morishita, M., Takahashi, Y., Nishikawa, M., Sano, K., Kato, K., Yamashita, T., Imai, T., Saji, H., and Takakura, Y. (2015). Quantitative analysis of tissue distribution of the B16BL6-derived exosomes using a streptavidin-lactadherin fusion protein and iodine-125-Labeled biotin derivative after intravenous injection in mice. J. Pharm. Sci. *104*, 705–713.

Müller, P., Schwille, P., and Weidemann, T. (2014). PyCorrFit - generic data evaluation for fluorescence correlation spectroscopy. Bioinformatics *30*, 2532–2533.

Murayama, E., Kissa, K., Zapata, A., Mordelet, E., Briolat, V., Lin, H.F., Handin, R.I., and Herbomel, P. (2006). Tracing hematopoietic precursor migration to successive hematopoietic organs during zebrafish development. Immunity *25*, 963–975.

Nguyen-Chi, M., Laplace-Builhe, B., Travnickova, J., Luz-Crawford, P., Tejedor, G., Phan, Q.T., Duroux-Richard, I., Levraud, J.P., Kissa, K., Lutfalla, G., et al. (2015). Identification of polarized macrophage subsets in zebrafish. Elife *4*, e07288.

van Niel, G., D'Angelo, G., and Raposo, G. (2018). Shedding light on the cell biology of extracellular vesicles. Nat. Rev. Mol. Cell Biol. *19*, 213–228.

Okabayashi, S., and Kimura, N. (2010). Lgl3 interacts with flotillin-1 to mediate APP trafficking and exosome formation. NeuroReport *21*, 606–610.

Oliveros, J.C. (2007). VENNY. An Interactive Tool for Comparing Lists with Venn Diagrams. BioinfoGP of CNB-CSIC, http://bioinfogp.cnb.csic.es/tools/venny/.

Ostrowski, M., Carmo, N.B., Krumeich, S., Fanget, I., Raposo, G., Savina, A., Moita, C.F., Schauer, K., Hume, A.N., Freitas, R.P., et al. (2010). Rab27a and Rab27b control different steps of the exosome secretion pathway. Nat. Cell Biol. *12*, 19–30.

Paggetti, J., Haderk, F., Seiffert, M., Janji, B., Distler, U., Ammerlaan, W., Kim, Y.J., Adam, J., Lichter, P., Solary, E., et al. (2015). Exosomes released by chronic lymphocytic leukemia cells induce the transition of stromal cells into cancer-associated fibroblasts. Blood *126*, 1106–1117.

Peinado, H., Alečković, M., Lavotshkin, S., Matei, I., Costa-Silva, B., Moreno-Bueno, G., Hergueta-Redondo, M., Williams, C., García-Santos, G., Ghajar, C.M., et al. (2012). Melanoma exosomes educate bone marrow progenitor cells toward a pro-metastatic phenotype through MET. Nat. Med. *18*, 883–891.

Peinado, H., Zhang, H., Matei, I.R., Costa-Silva, B., Hoshino, A., Rodrigues, G., Psaila, B., Kaplan, R.N., Bromberg, J.F., Kang, Y., et al. (2017). Pre-metastatic niches: organ-specific homes for metastases. Nat. Rev. Cancer *17*, 302–317.

Plebanek, M.P., Angeloni, N.L., Vinokour, E., Li, J., Henkin, A., Martinez-Marin, D., Filleur, S., Bhowmick, R., Henkin, J., Miller, S.D., et al. (2017). Pre-metastatic cancer exosomes induce immune surveillance by patrolling monocytes at the metastatic niche. Nat. Commun. *8*, 1319.

Pucci, F., Garris, C., Lai, C.P., Newton, A., Pfirschke, C., Engblom, C., Alvarez, D., Sprachman, M., Evavold, C., Magnuson, A., et al. (2016). SCS macrophages suppress melanoma by restricting tumor-derived vesicle-B cell interactions. Science *1328*, 242–246.

Raposo, G., and Stoorvogel, W. (2013). Extracellular vesicles: exosomes, microvesicles, and friends. J. Cell Biol. *200*, 373–383.

Roh-Johnson, M., Shah, A.N., Stonick, J.A., Poudel, K.R., Kargl, J., Yang, G.H., di Martino, J., Hernandez, R.E., Gast, C.E., Zarour, L.R., et al. (2017). Macrophage-dependent cytoplasmic transfer during melanoma invasion in vivo. Dev. Cell *43*, 549–562.e6.

Saunderson, S.C., Dunn, A.C., Crocker, P.R., and McLellan, A.D. (2014). CD169 mediates the capture of exosomes in spleen and lymph node. Blood *123*, 208–216.

Schindelin, J., Arganda-Carreras, I., Frise, E., Kaynig, V., Longair, M., Pietzsch, T., Preibisch, S., Rueden, C., Saalfeld, S., Schmid, B., et al. (2012). Fiji: an open-source platform for biological-image analysis. Nat. Methods *9*, 676–682.

Spilsbury, K., O'Mara, M.A., Wu, W.M., Rowe, P.B., Symonds, G., and Takayama, Y. (1995). Isolation of a novel macrophage-specific gene by differential cDNA analysis. Blood *85*, 1620–1629.

Stoletov, K., Kato, H., Zardouzian, E., Kelber, J., Yang, J., Shattil, S., and Klemke, R. (2010). Visualizing extravasation dynamics of metastatic tumor cells. J. Cell Sci. *123*, 2332–2341.

Takahashi, Y., Nishikawa, M., Shinotsuka, H., Matsui, Y., Ohara, S., Imai, T., and Takakura, Y. (2013). Visualization and in vivo tracking of the exosomes of murine melanoma B16-BL6 cells in mice after intravenous injection. J. Biotechnol. *165*, 77–84.

Takov, K., Yellon, D.M., and Davidson, S.M. (2017). Confounding factors in vesicle uptake studies using fluorescent lipophilic membrane dyes. J. Extracell. Vesicles *6*, 1388731.

Taylor, M.J., Perrais, D., and Merrifield, C.J. (2011). A high precision survey of the molecular dynamics of mammalian clathrin-mediated endocytosis. PLoS Biol. *9*, e1000604.

Théry, C., Amigorena, S., Raposo, G., and Clayton, A. (2006). Isolation and characterization of exosomes from cell culture supernatants. Curr. Protoc. Cell Biol. 3.22.1–3.22.29.

Thomas, P.D., Campbell, M.J., Kejariwal, A., Mi, H., Karlak, B., Daverman, R., Diemer, K., Muruganujan, A., and Narechania, A. (2003). PANTHER: A library of protein families and subfamilies indexed by function. Genome Res. *13*, 2129–2141.

Verweij, F., Revenu, C., Arras, G., Dingli, F., Loew, D., Pegtel, M., Follain, G., Allio, G., Goetz, J.G., Zimmermann, P., et al. (2019). Live tracking of inter-organ communication by endogenous exosomes in vivo. Dev. Cell *48*, this issue, 573–589.

Vogel, D.Y.S., Heijnen, P.D.A.M., Breur, M., de Vries, H.E., Tool, A.T.J., Amor, S., and Dijkstra, C.D. (2014). Macrophages migrate in an activation-dependent manner to chemokines involved in neuroinflammation. J. Neuroinflamm. *11*, 1–11.

Van Der Vos, K.E., Abels, E.R., Zhang, X., Lai, C., Carrizosa, E., Oakley, D., Prabhakar, S., Mardini, O., Crommentuijn, M.H.W., Skog, J., et al. (2016). Directly visualized glioblastoma-derived extracellular vesicles transfer RNA to microglia/macrophages in the brain. Neuro. Oncol. *18*, 58–69.

White, R., Rose, K., and Zon, L. (2013). Zebrafish cancer: the state of the art and the path forward. Nat. Rev. Cancer *13*, 624–636.

Whiteside, T.L. (2016). Exosomes and tumor-mediated immune suppression. J. Clin. Invest. *126*, 1216–1223.

Würthner, F., Kaiser, T.E., and Saha-Möller, C.R. (2011). J-aggregates: From serendipitous discovery to supramolecular engineering of functional dye materials. Angew. Chem. Int. Ed. *50*, 3376–3410.

Xiao, M., Zhang, J., and Chen, W., Chen W. (2018). M1-like tumor-associated macrophages activated by exosome-transferred THBS1 promote malignant migration in oral squamous cell carcinoma. J. Exp. Clin. Cancer Res. *37*, 1–15.

Zomer, A., Maynard, C., Verweij, F.J., Kamermans, A., Schäfer, R., Beerling, E., Schiffelers, R.M., De Wit, E., Berenguer, J., Ellenbroek, S.I.J., et al. (2015). In vivo imaging reveals extracellular vesicle-mediated phenocopying of metastatic behavior. Cell *161*, 1046–1057.

STAR★METHODS

KEY RESOURCES TABLE

REAGENT OR RESOURCE	SOURCE	IDENTIFIER
Chemicals, Peptides and Recombinant proteins		
MemBright	Collot et al. (2019)	N/A
PKH-26	Sigma-Aldrich	MINI26
100nm fluorescent beads	Phosphorex	2211
Antibodies		
Mouse monoclonal anti-Alix antibody	BD Biosciences	Cat# 611621; RRID: AB_2236941
Mouse monoclonal anti-TSG-101 antibody	GeneTex	Cat# GTX70255; RRID: AB373239
Anti-mouse IgG coupled to HRP	Fisher scientific	Cat# NC9491974
Deposited Data		
EV related experimental details	EV-track consortium	EV180078
EV proteomics	Exocarta	TBD
Experimental Models: Cell lines		
Zmel1	White lab (MSKCC)	N/A
Zmel1 tdTomato	White lab (MSKCC)	N/A
Zmel1 Syntenin2-GFP	This paper	N/A
AB9	ATCC	ATCC-CRL-2298
4T1		RRID: CVCL_0125
4T1 CD63-GFP	This paper	N/A
B16F0	ATCC	ATCC CRL-6322; RRID: CVCL_0604
B16F1	ATCC	ATCC CRL-6323; RRID: CVCL_0158
B16F10	ATCC	ATCC CRL-6475; RRID: CVCL_0159
451-LU	Soengas lab (CNIO)	RRID: CVCL_6357
SK-Mel28	Soengas lab (CNIO)	RRID: CVCL_0526
SK-Mel147	Soengas lab (CNIO)	RRID: CVCL_3876
SK-Mel103	Soengas lab (CNIO)	RRID: CVCL_6069
WM35	Soengas lab (CNIO)	RRID: CVCL_0580
WM164	Soengas lab (CNIO)	RRID: CVCL_7928
Experimental Models: Organisms/strains		
Zebrafish: *Tg(Fli1a:eGFP)*	Peri lab; EMBL zebrafish facility	N/A
Zebrafish: *Tg(mpeg1a:eGFP)*	Lengerke lab; Basel University zebrafish facility	N/A
Zebrafish: *Tg(mpo:eGFP)*	Lengerke lab; Basel University zebrafish facility	N/A
Zebrafish: *Tg(Fli1a:Gal4; UAS:RFP)*	Lengerke lab; Basel University zebrafish facility	N/A
Zebrafish: Casper *Tg(Flk:eGFP; Gata1:RFP)*	Vermot lab; IGBMC zebrafish facility	N/A
Zebrafish: *Tg(mpeg1:mCherry; TNFa:eGFP)*	Djouad lab; IRMB zebrafish facility	N/A
Recombinant DNA		
pSyntenin2-eGFP	Zimmermann lab (CRCM)	N/A
pCS2 Zf-Syntenin2-eGFP	This paper	N/A
pLenti CMV-CD63-AcGFP	This paper	N/A
Software and Algorithms		
Fiji / Image J	NIH	N/A
IMOD	University of Colorado	N/A
Amira for Life Sciences	ThermoFisher Scientific	N/A
GraphPad PRISM	GraphPad Software	N/A
MaxQuant	Max Planck Institute of Biochemistry	N/A
PyCorrFit software	Max Planck Institute of Biochemistry	N/A

(*Continued on next page*)

Continued

REAGENT OR RESOURCE	SOURCE	IDENTIFIER
Other		
Transmitted electron microscope CM12	Philips	N/A
Transmitted electron microscope CM120	Philips	N/A
Biotwin CM120 (FEI) TEM	Philips	
Nanosight NS300	Malvern Instruments	N/A
ZetaView	Particle Metrix	N/A
NanoAcquity UPLC device	Waters	N/A
NanoLC-Ultra 1D+ system	Eksigent	N/A
Cary 400 Scan ultraviolet–visible spectrophotometer	Varian	N/A
FluoroMax-4 spectrofluorometer	Horiba Jobin Yvon	N/A
M205 FA stereomicroscope	Leica	N/A
Inverted TCS SP5 confocal microscope	Leica	N/A
Upright SP8 confocal microscope	Leica	N/A

CONTACT FOR REAGENT AND RESOURCE SHARING

Further information and requests for resources and reagents should be directed to and will be fulfilled by the Lead Contact, Vincent Hyenne (hyenne@unistra.fr).

EXPERIMENTAL MODEL AND SUBJECT DETAILS

Zmel1, Zmel1 tdTomato and Zmel1 Syntenin2-GFP

Zebrafish melanoma Zmel1 and Zmel1 td Tomato Kindly provided by Richard White (Memorial Sloan Kettering Cancer Center, New York) (Heilmann et al., 2015). Zmel1 Syntenin2-GFP generated in the laboratory. Culture condition: 28°C, 5% CO_2. DMEM high glucose (HG), 10% FBS, 1% NEAA-MEM, 1% penicillin-streptomycin.

AB9 Cells

Zebrafish fibroblasts obtained from the caudal fin of an adult AB strain zebrafish (ATCC CRL-2298). Culture condition: 28°C, 5% CO_2. DMEM HG, 10% FBS, 1% NEAA-MEM, 1% Penstrep.

4T1 Cells and 4T1 CD63-GFP

Mouse mammary gland carcinoma (BALB/c female) (CVCL_0125). 4T1 CD63-GFP generated in the laboratory. Culture condition: 37°C, 5%CO_2. RPMI 1640 with 10% FBS, 1% penicillin-streptomycin. Authentication: Injection in the nipple of mammary gland of BALB/c mice lead to mammary tumor.

B16-F0, F1 and F10

Mouse melanoma cell lines, purchased from ATCC (ATCC CRL-6322; ATCC CRL-6323; ATCC CRL-6475). Culture condition: 37°C, 5%CO_2. DMEM supplemented with 10% (v/v) EV-depleted fetal bovine serum (EV-d-FBS), glutamine 2mM and gentamicin

451-LU, SK-Mel28, SK-Mel147, SK-Mel103, WM35 and WM164

Human melanoma cells, kindly provided by Dr. M. Soengas (CNIO, Madrid). Culture condition: 37°C, 5%CO_2. DMEM with 10% EV-d-FBS.

Zebrafish

Zebrafish embryos were obtained from the following strains: *Tg(fli1a:eGFP), Tg(mpeg1:eGFP), Tg(mpo:eGFP), Tg(Fli1:Gal4; UAS:RFP), Casper Tg(Gata1:RFP; flk:GFP), Tg(mpeg:mCherry*; TNF-α:GFP). Embryos were grown in our laboratory or kindly provided by F. Peri's (EMBL, Heidelberg, Germany) and C. Lengerke's laboratories (University Hospital Basel, Switzerland). Embryos were maintained at 28° in Danieau 0.3X medium, supplemented with 1-Phenyl-2-thiourea (Sigma-Aldrich) after 24 h post fertilization (hpf). For all Zebrafish experiments, the offspring of one single cross was selected, based on anatomical/developmental good health. Embryos were split randomly between experimental groups. All injection experiments were carried at 48 hpf and imaged between 48 hpf and 72 hpf. All animal procedures were performed in accordance with French and European Union animal welfare guidelines and supervised by local ethics committee (Animal facility #A6748233; APAFIS #2018092515234191).

Nano-LC-MS/MS Analysis of Zmel1 EVs Protein Content

Nano-LC-MS/MS analysis was performed on a nanoAcquity UPLC device (Waters, Milford, MA) coupled to a Q-Exactive Plus mass spectrometer (Thermo Fisher Scientific, Bremen, Germany). The solvents consisted of 0.1% FA in H_2O (solvent A) and 0.1% in ACN (solvent B). 1 μL of the samples was loaded onto a Symmetry C18 pre-column (20 mm × 180 μm, 5 μm diameter particles; Waters, Milford, MA) over 3 min at 5 μL/min with 1% solvent B. Peptides were eluted on a Acquity UPLC BEH130 C18 column (250 mm × 75 μm, 1.7 μm particles; Waters, Milford, MA) at 450 μL/min with the following gradient of solvent B: linear from 1% to 8 % in 2 min, linear from 8% to 35% in 77 min, linear from 35% to 90% in 1 min, isocratic at 90% for 5 min, down to 1% in 2 min, isocratic at 1% for 2 min.

The Q-Exactive Plus was operated in data-dependent acquisition mode by automatically switching between full MS and consecutive MS/MS acquisitions. Full-scan MS spectra were collected from 300-1,800 m/z at a resolution of 70,000 at 200 m/z with an automatic gain control target fixed at 3×10^6 ions and a maximum injection time of 50 ms. The top 10 precursor ions with an intensity exceeding 2×10^5 ions and charge states ≥ 2 were selected on each MS spectrum for fragmentation by higher-energy collisional dissociation. MS/MS spectra were collected at a resolution of 17,500 at 200 m/z with a fixed first mass at 100 m/z, an automatic gain control target fixed at 1×10^5 ions and a maximum injection time of 100 ms. A dynamic exclusion time was set to 60 s.

Sample Preparation of Mammalian EVs Cargo

Proteins were solubilized using 8 M urea in 100 mM Tris-HCl pH 8.0. Samples (7.5 μg) were digested by means of the standard FASP protocol. Briefly, proteins were reduced (10 mM DTT, 30 min, RT), alkylated (55 mM IA, 20 min in the dark, RT) and sequentially digested with Lys-C (Wako) (protein:enzyme ratio 1:50, o/n at RT) and trypsin (Promega) (protein:enzyme ratio 1:100, 6 h at 37° C). Resulting peptides were desalted using C_{18} stage-tips.

Nano-LC-MS/MS Analysis of Mammalian EVs Cargo

LC-MS/MS was done by coupling a nanoLC-Ultra 1D+ system (Eksigent) to a LTQ Orbitrap Velos mass spectrometer (Thermo Fisher Scientific) via a Nanospray Flex source (Thermo Fisher Scientific). Peptides were loaded into a trap column (NS-MP-10 BioSphere C18 5 μm, 20 mm length, Nanoseparations) for 10 min at a flow rate of 2.5 μl/min in 0.1% FA. Then peptides were transferred to an analytical column (ReproSil Pur C18-AQ 2.4 μm, 500 mm length and 0.075 mm ID) and separated using a 120 min linear gradient (buffer A: 4% ACN, 0.1% FA; buffer B: 100% ACN, 0.1% FA) at a flow rate of 250 nL/min. The gradient used was: 0-2 min 6% B, 2-103 min 30% B, 103-113 min 98% B, 113-120 min 2% B. The peptides were electrosprayed (1.8 kV) into the mass spectrometer with a PicoTip emitter (360/20 Tube OD/ID μm, tip ID 10 μm) (New Objective), a heated capillary temperature of 325°C and S-Lens RF level of 60%. The mass spectrometer was operated in a data-dependent mode, with an automatic switch between MS and MS/MS scans using a top 15 method (threshold signal $\geq$ 800 counts and dynamic exclusion of 60 s). MS spectra (350-1500 m/z) were acquired in the Orbitrap with a resolution of 60,000 FWHM (400 m/z). Peptides were isolated using a 1.5 Th window and fragmented using collision induced dissociation (CID) with linear ion trap read out at a NCE of 35% (0.25 Q-value and 10 ms activation time). The ion target values were 1E6 for MS (500 ms max injection time) and 5000 for MS/MS (100 ms max injection time).

Nano-LC-MS/MS Data Interpretation

Raw files were processed with MaxQuant (versions 1.6.0.16) (Cox et al., 2014) against an in-house concatenated *Danio rerio*-*Bos taurus* (UniProtKB, February 2017, 90,922 entries) supplemented with contaminants for Zmel1 EVs proteins and generated with the database toolbox from MSDA (Carapito et al., 2014), or a human protein database (UniProtKB/Swiss-Prot, August 2014, 20,187 sequences) supplemented with contaminants for mammalian EVs cargo. Label-free quantification was done with the match between runs option activated (match window of 0.7 min and alignment window of 20 min). Carbamidomethylation of cysteines was set as a fixed modification whereas oxidation of methionines and protein N-term acetylation were set as variable modifications. Minimal peptide length was set to 7 amino acids and a maximum of two tryptic missed-cleavages were allowed.

Protein Comparisons

To compare the Zmel1 protein content with mammalian EV content, each protein list was concatenated and duplicate proteins were deleted. Ortholog proteins were searched using the ortholog protein files predicted by the PANTHER classification system (ftp://ftp.pantherdb.org/ortholog/13.0/ (Thomas et al., 2003)). Only proteins referred as "Least diverged ortholog" or "Ortholog" were considered. All comparisons between Zmel1 EVs and mammalian EVs were done using human orthologs and the lists of common proteins was obtained using Venny 2.1 (Oliveros, 2007).

MemBright and PKH Labeling of EVs

Isolated EVs were incubated with MemBright-Cy3 or Cy5 at 200nM (final concentration) in PBS for 30 minutes at room temperature in the dark. They were then rinsed in 15ml of PBS and centrifuged at 100,000g with a SW28 rotor in a Beckman XL-70 centrifuge. Pellets were resuspended in 50 μl PBS and stored at 4°C. For *in vivo* experiments, EVs were used immediately after isolation or stored overnight at 4°C and injected the next day. For PKH-26 labeling EVs were treated according to the manufacturer's instructions (2 μM final concentration). Briefly, EVs in 200 μl of PBS were first mixed with 300 μl of Diluent C, then with 500μl of Diluent C containing 4 μl of PKH and finally incubated for 30 minutes at room temperature in the dark. PKH labeled EVs were then processed as MemBright labeled EVs. As a control, PBS alone was processed similarly to EVs, labeled with MemBright or PKH and analysed by microscopy or spectroscopy.

For photonic microscopy analysis, 3 μl of labeled EV extracts were allowed to settle on poly-L lysine coated coverslips and then imaged on a Zeiss Imager Z2 with a 63X objective (N.A. 1.4) or with a SP5 confocal (Leica) with a 40X objective (N.A. 1.25).

Spectroscopy

EVs labeled with either MemBright-Cy3 or PKH-26, or control MemBright-Cy3 or control PKH (diluted in PBS as described above), as well as the dyes directly diluted in Milli-Q water (Millipore) or ethanol were analyzed by spectroscopy. Absorption and emission spectra were recorded at 20°C in quartz cuvettes on a Cary 400 Scan ultraviolet–visible spectrophotometer (Varian) and a FluoroMax-4 spectrofluorometer (Horiba Jobin Yvon) equipped with a thermostated cell compartment, respectively. For standard recording of fluorescence spectra, excitation was at 520 nm and the emission was collected 10 nm after the excitation wavelength (530 nm to 700 nm). All the spectra were corrected from wavelength-dependent response of the detector. The scattering due to the EVs was corrected with a baseline correction using Origin software. Quantum yields were determined using rhodamine B in water (QY= 0.31) as a reference (Magde et al., 1999).

Fluorescence Correlation Spectroscopy (FCS)

To characterize the size of PKH aggregates, FCS measurements were performed on PKH26 (diluted at 5 μM) using a home-built confocal set-up based on a Nikon inverted microscope with a Nikon 60x 1.2NA water immersion objective. Excitation was provided by a cw laser diode (532 nm, Oxxius) and photons were detected with a fibered Avalanche Photodiode (APD SPCM-AQR-14-FC, Perkin Elmer) connected to an on-line hardware correlator (ALV7000-USB, ALV GmbH, Germany). Typical acquisition time was 5 min (10 × 30 s) with an excitation power of 1.1 μW at the sample level. The data were analyzed using the PyCorrFit software (Müller et al., 2014).

MemBright Labeling of Cells

Sub-confluent cells in 10cm culture dishes were rinsed twice with warm serum free medium and then incubated for 30 minutes at 28°C (Zmel1 cells) or at 37°C (4T1 cells) with MemBright quickly diluted in serum free medium (200nM final). To eliminate all possible traces of unbound MemBright, cells were then rinsed three times with serum free medium, rinsed with EDTA and trypsinated. Cells were then either injected in zebrafish embryos, seeded in a triple flask for EV production, or seeded in glass bottom microwell dishes (MatTek Corporation) pre-coated with fibronectin from bovine plasma at 10μg/ml (Sigma F-1141) for imaging.

Intravascular Injection of Zebrafish Embryo

At 48h post-fertilization (hpf), zebrafish embryos were dechorionated and mounted in 0.8% low melting point agarose pad containing 650 μM of tricaine (ethyl-3-aminobenzoate-methanesulfonate) to immobilize them. Pre-labelled EVs, polystyrene beads (Phosphorex) or tumors cells were injected with a Nanoject microinjector 2 (Drummond) and microforged glass capillaries (25 to 30 μm inner diameter) filled with mineral oil (Sigma). 27,6 nL of a EV, beads or cell suspension (at 100.10^6 cells) per ml were injected into the duct of Cuvier of the embryos under the M205 FA stereomicroscope (Leica), as previously described (Follain et al., 2018b; Stoletov et al., 2010). For the priming experiments, 32hpf embryos were injected with either Zmel1 EVs or 100nm polystyrene beads (together with fluorescent dextran to assess the efficiency of injection). 14h post-injection, embryos were injected in the circulation with Zmel1 tdTomato tumor cells. Larvae were grown for a week and imaged at 7 days post-injection. For late endosome/lysosome labeling, embryos were incubated with Lysotracker Deep Red (Thermo Fisher Scientific) diluted at 5μM in Danieau 0,3X medium for 2 hours at 28°C before injection.

Confocal Imaging and Analysis

Confocal imaging was alternatively performed with an inverted TCS SP5 with HC PL APO 20X/0,7 IMM CORR CS objective (Leica) or an upright SP8 confocal microscope with a HC FLUOTAR L 25X/0,95 W VISIR objective (Leica). For high speed imaging of EVs in the blood flow, embryos were imaged right after injection; acquisitions were done at 80-100 frames per second for 1 minute, using the resonant scanner in a single Z plane, with an opened pinhole of more than 1 airy unit. To identify the cell types uptaking EVs, the caudal plexus region of mpeg1:GFP, mpo:GFP or Fli1a:GFP was imaged 3h post-injection with a z-step of 1 μm. To quantify the proportion of EVs arrested in the dorsal aorta *vs* venous plexus regions, images were acquired similarly in Fli1:GFP embryos. For each case, quantification is described in the next paragraphs. To image the dynamics of macrophage protrusions, short time lapses of mpeg1:GFP embryos were acquired at 5 to 10 Z stacks per minute (z-step of 0,5 μm, stack covering the macrophage). To image the dynamics of macrophages, long time lapses of mpeg1:GFP embryos were acquired at 1 Z stack per minute for one hour in (z-step of 2 μm, stack covering the venous plexus). To image the uptake of EVs by macrophage, mpeg1:GFP embryos short time lapses were generated right after injection at 3 to 8 images per second on single Z planes. Image analysis and processing were performed using Fiji (Schindelin et al., 2012) as described in the following paragraphs.

Semi-automated Method to Determine the Proportion of Internalized EVs

To determine the proportion of EVs internalized by either endothelial or macrophages, we used the Z-stacks obtained from either Fli1:GFP or mpeg1:GFP embryos injected with Zmel1-MemBright EVs. Using Fiji, we split the cell and EVs channels and merged them in a single RGB image. From the merged channel, we made a binary stack followed by a Z-projection with maximal intensity. We used this as a reference image where all the EVs and cells are apparent. After normalizing this image to 1 we multiplied each stack (respectively EVs and Cell) by this projection. In both stacks, we thus kept only the positions that colocalize either with the EV position or the Cells position (all other positions possess a null value). We then made a binary from the Cell stack, applied close and dilated before normalizing it to 1. The multiplication of this stack with the EV one lead to a new stack that keeps only the particle enclosed in

METHOD DETAILS

Cell Line Generation

To generate Zmel1 cells expressing Syntenin2-GFP, Syntenin2 (a gift from P.Zimmerman) was first cloned in pCS2 eGFP Ires Blast vector. Then, 2 millions of Zmel dark cells were transfected with 2 μg of plasmid pCS2 Zf-Syntenin2-eGFP Ires Blast cut with NotI using 4 μl of JetPrime according to manufactory instructions (PolyPlus, Illkirch, France). After 1 week, cells with stable integration of the construct were selected using 4μg/ml of blasticidin (Sigma Aldrich, St. Quentin Fallavier, France). 4T1 cells expressing CD63-GFP were generated as follows. Briefly, human CD63 cDNA was fused to AcGFP cDNA by In-Fusion cloning (Takara, Ozyme, Saint-Quentin-en-Yvelines, France) and introduced in pLenti CMV-MABBXXS mPGK-Blast vector. Lentiviruses were obtained by HEK293T cells (ATCC CRL-3216; cultured in DMEM, 10% FCS, 1% penicillin-streptomycin) transfection (Invitrogen, Life Technologies, Saint Aubin, France) with pLenti CMV-CD63-acGFP mPGK-Blast together with pLP1, pLP2 and pLP/VSVG lentiviral packaging plasmids to obtain lentiviral particles. After 48 hours, conditioned media was collected, filtered through a 0.22 μm filter to remove cell debris, and used to transduce 4T1 cells cultured in DMEM supplemented with 10% fetal calf serum and 1% penicillin-streptomycin (Gibco, USA) in the presence of 5μg/mL polybrene (Sigma Aldrich, Lyon, France), followed by selection with puromycin (1 μg/mL, Sigma Aldrich, Lyon, France). Human blood was collected from healthy donors using 3.8% (v/v) sodium citrate (1:9) as anticoagulant. Human erythrocyte rich pellet was obtained by centrifugation at 250 rpm during 15 minutes at room temperature.

EV Isolation and Analysis

For Zmel1 and 4T1 EVs isolation, cells were cultured in EV depleted medium (obtained by overnight ultracentrifugation at 100,000g, using a Beckman, XL-70 centrifuge with a Ti70 rotor) for 24h before supernatant collection. Extracellular medium was concentrated using a Centricon Plus-70 centrifugal filter (10k; Millipore) and EVs were isolated by successive centrifugation at 4°C: 5 minutes at 300 g, 10 minutes at 2,000 g, 30 minutes at 10,000 g and 70 minutes at 100,000 g (using a Beckman XL-70 centrifuge with a SW28 rotor). EVs pellets were washed in PBS, centrifuged again at 100,000 g for 70 minutes, resuspended in PBS and stored at 4°C. For *in vivo* experiments, EVs were used immediately after isolation or kept 4°C at and used the next day.

For mouse and human melanoma EVs isolation, cells were cultured in media supplemented with 10% EV-depleted FBS (FBS, Hyclone). FBS was depleted of bovine EVs by ultracentrifugation at 100,000xg for 70 min. EVs were isolated from conditioned media collected after 72 h of cell cultures by successive centrifugation at 10°C: 5 minutes at 300 g, 10 minutes at 500 g, 20 minutes at 12,000 g and 70 minutes at 100,000 g (using a Beckman Optima X100 with a Beckman 70Ti rotor). EVs pellets were washed in PBS, centrifuged again at 100,000 g for 70 minutes, and resuspended in PBS. Protein content was measured by bicinchoninic acid assay (BCA assay).

For transmitted electron microscopy analysis, 3 μl of EV extracts were allowed to dry on formvar coated grids for 20 minutes, fixed in 3% PFA for 10 minutes, rinsed in water and contrasted in a uranyl acetate (0,4%)/ methylcellulose (2%) mix for 10 minutes on ice. EVs were observed either with an Orius 100 charge-coupled device camera (Gatan) mounted on a Philips CM12 microscope operated at 80kV or with a Veleta 2kx2k side-mounted TEM CDD Camera (Olympus Soft Imaging Solutions) mounted on a Philips CM120 microscope operated at 120kV.

NTA was performed on Zmel1 EVs diluted 10 times with sterile PBS, using a Nanosight NS300 (Malvern Instruments) or a ZetaView (Particle Metrix). The measurement was repeated three times.

For density gradient analysis, EVs isolated in the 100,000 g pellet were loaded on top of a 5-40% iodixanol (Optiprep) density gradient prepared as previously described (Van Deun et al., 2014). The gradient was centrifuged for 18 hours at 100,000g and 4°C (using a Beckman XL-70 centrifuge with a SW28 rotor). Gradient fractions of 1ml were collected from the top of the gradient. Fractions 1 to 4, 5 to 10 and 11 to 16 were pooled, diluted to 16 ml in PBS and centrifuged for 3 hours at 100,000g and 4°C. The resulting pellet was resuspended in 50 μl of PBS. For western blotting analysis, 10 μl of EV extracts were loaded on 4-20% polyacrylamide gels (Biorad), under denaturing conditions. The following antibodies were used: Alix (BD Biosciences 611621) and TSG101 (GeneTex GTX70255). Acquisitions were done using a PXi system (Syngene).

Shotgun Proteomics

Sample Preparation of Zmel1 EVs Protein Content

After having determined protein concentration (RC-DC™; Bio-Rad, Hercules, CA), 20 μg samples were denaturated at 95°C for 5 min in Laemmli buffer and then concentrated in one stacking band using a 5% SDS-PAGE gel. The gel was fixed with 50% ethanol/3% phosphoric acid and stained with colloidal Coomassie Brilliant Blue. Each band was excised, cut in five pieces, and transferred into a 96-well microtiter plate. Gel slices were washed with 3 cycles of incubations in 100 μL of 50:50 (v/v) 25 mM NH_4HCO_3/ACN for 10 min. Gel bands were then dehydrated with 50 μL 100% ACN and then reduced with 50 μL 10 mM DTT for 30 min at 60°C, followed by 30 min at RT. Proteins were then alkylated with 50 μL 55 mM iodoacetamide for 20 min in the dark at RT, and then 100 μL ACN were added for 5 min. Samples were washed with 50 μL 25 mM NH_4HCO_3 for 10 min, and then 50 μL ACN for 5 min, before being dehydrated with two cycles of incubations in 50 μL ACN for 5 min. Proteins were digested overnight with a modified porcine trypsin (Promega, Madison, WI) solution at a 1:100 (w/w) enzyme/protein ratio at 37°C. Tryptic peptides were extracted under agitation at RT with 60 μL 60% ACN/0.1% FA for 45 min, and then 100% ACN for 10 min. The extraction supernatants were pooled and vacuum-dried, before re-suspension in 40 μL 2% ACN/0.1% FA.

the cellular compartments. Getting back to the Cell stack, we apply an inversion of the intensity values before substracting 254. The resulting stack was then multiplied by the EV stack and the created new stack let only apparent the EVs that did not colocalize with the cells. Further analyses of the intensities from the two stacks allowed us to access the ratiometric values of EVs uptaken by the different cell lines.

Quantification of EVs in Aorta vs Vein Regions

Each region (dorsal aorta and venous plexus) was manually delimited on Z-projections, using vessels visible in Fli1:GFP channels. Total EV intensity was then measured in each region and reported to the area. A ratio of EV fluorescence in the venous plexus over dorsal aorta was then measured for each fish.

Flow Analysis for Red Blood Cells

Flow analysis of red blood cells

We first globally enhanced the contrast of the whole stack. Then we performed a Z-projection with the average intensity and subtracted the obtained image to the stack. The remaining stack exhibits only the moving objects i.e. the red blood cells in this case. Then we applied a binarisation to the stack before applying a bandpass filter with the correct values to remove the background noise and keeping only the flowing blood cells. This stack was then further analyzed with the Mosaic 2D/3D particle tracker plugin. We thus accessed the positions of each blood cell for the different frames and we computed the velocities of each individual track.

Flow Analysis of EVs

Time-lapses of EVs were first thresholded and binarized. We then inverted the stack before running the 2D spot enhancing Filter plugin. We used the resulting stack to perform a second binarisation and then launched the Mosaic 2D/3D particle tracker plugin. We thus accessed the positions of each EV for the different frames and we computed the velocities of each individual track

EVs and RBCs Distance and Velocity from the Endothelial Barrier

In order to access to the distance of the EVs or red blood cells to the endothelial barrier, we first drew the endothelial wall using the transmitted light and extracted its coordinates to a table. From the analysis described in the previous paragraph, we extracted the coordinates and the velocity EVs and red blood cells. We ran a macro where we compared for all the position X_{EV} and Y_{EV} of the EV the closest position X_{endo} and Y_{endo} by comparing all the possible distances d by calculating :

$$d = \sqrt{(x_{EV} - x_{endo})^2 + (y_{EV} - y_{endo})^2}$$

and keeping the smallest distance.

This allowed us to plot the EV or the red blood cells velocities as a function of the distance from the endothelial wall.

Sample Preparation for Correlative Light and Electronic Microscopy of ZF Embryos

Correlative Light and Electron Microscopy was performed as previously described (Goetz et al., 2014; Karreman et al., 2016a). Transgenic mpeg1:GFP embryos were injected with MemBright-Cy3 4T1 EVs and imaged alive with a Leica SP8 confocal microscope (see "Confocal imaging and analysis section"). Z stack was performed on two patrolling macrophages having uptaken EVs. After imaging, the embryo was chemically fixed with 2,5% glutaraldehyde and 4% paraformaldehyde in 0.1 M Cacodylate buffer (the fish tail was cut off in the fixative). The sample was kept in fixative at room temperature for 1-2h and stored in fixative at 4°C overnight or until further processing. The sample was rinsed in 0.1M Cacodylate buffer for 2x5min and post-fixed using 1% OsO4 in 0.1 M Cacodylate buffer, for 1h at 4°C. Then, sample was rinsed for 2x10 min in 0.1M Cacodlyate buffer and secondary post-fixed with 4% water solution of uranyl acetate, 1h at room temperature. Rotation was used at all steps of sample processing. Followed by 5 min wash in MiliQ water, the sample was stepwise dehydrated in Ethanol (25%, 50% each 15min, 95%, 3X100% each 20 min) and infiltrated in a graded series of Epon (Ethanol/Epon 3/1, 1/1, 1/3, each 45 min). Sample was left in absolute Epon (EmBed812) overnight. The following day, sample was placed in a fresh absolute Epon for 1h and polymerized (flat embedded) at 60°C for 24-48h. Once polymerized, most surrounding Epon was cut off using razorblade and sample was mounted on empty Epon blocks (samples flat on the top of the blocks) and left at 60°C for 24h-48h. Samples were attached to an imaging pin with dental wax and mounted into the Brukker Skyscan 1272 for microCT imaging. Data were acquired over 188° with 0.2° angular step and a pixel size of 9 μm. Karreman et al. thoroughly details the process of how the microCT data enables the correlation of fluorescent imaging to 3D EM of voluminous samples (Karreman et al., 2016a). Retrieval of the region of interest is described in Figure S4. The region of interest was targeted by ultramicrotome, sections stained with toluidine blue and compared with the MicroCT and LM datasets. After targeting, serial 70nm sections were collected in formvar coated slot grids. The sections were post stained with uranyl acetate (4%) and lead citrate. The sections were imaged in a Biotwin CM120 Philips (FEI) TEM at 80kV with a SIS 1K KeenView. Stitches of the 70 sections were aligned using the Track EM plugin in Fiji (Cardona et al., 2012). Segmentation and 3D reconstruction were done using the IMOD software package (Boulder Laboratory, University of Colorado) and Amira.

QUANTIFICATION AND STATISTICAL ANALYSIS

Statistical Tests

Statistical analysis of the results was performed using the GraphPad Prism program version 5.04. The Shapiro-Wilk normality test was used to confirm the normality of the data. The statistical difference of Gaussian data sets was analyzed using the Student unpaired two-tailed t test, with Welch's correction in case of unequal variances. For data not following a Gaussian distribution, the Mann-Whitney test was used. Illustrations of these statistical analyses are displayed as the mean +/- standard deviation (SD). p-values smaller than 0.05 were considered as significant. *, $p<0.05$, **, $p < 0.01$, ***, $p < 0.001$, ****, $p < 0.0001$.

Zebrafish Experiments

Measurements of EVs displacement in the dorsal aorta and in the caudal vein of zebrafish embryos (Figures 3B–3E) was performed on four zebrafish embryos. Measurements of EV uptake in aorta versus venous plexus was repeated three times (n=17; Figure 4B). Comparison of the uptake of beads, AB9 EVs and Zmel1 EVs by endothelial cells (n=20, 24 and 11 respectively; Figure 4C) and macrophages (n=28, 21 and 19 respectively; Figure 5C) was repeated three times each. The correlation between Zmel1 uptake intensity and macrophages perimeter was done on 73 macrophages (13 embryos; Figure 5B). The velocity of non-injected macrophages was measured on 35 macrophages (6 embryos; Figure 5E). The colocalization between uptaken EVs and lysotracker in macrophages at 10 min and 3h post-injection was performed on 61 and 54 puncta, respectively (n=6 and 7 fish, respectively; Figure 6D). The dynamics of macrophages injected with either beads or Zmel1 EVs was measured on 27 and 47 macrophages, respectively (5 and 8 embryos; Figure 8A). The activation of M1 macrophages after beads or Zmel1 EVs injection was repeated twice (n=38 and 28 fish, respectively; Figures 8B and 8C). The metastatic outgrowth of Zmel1 cells in zebrafish embryos injected with either beads or Zmel1 EVs was repeated five times (n=55 and 57 fish, respectively; Figure 8D).

EVs Experiments

Measurements of the diameters of Zmel1 EVs (Figure 1B) and Zmel1 EVs labeled with MemBright (Figure 2E) by NTA was repeated three times. Analysis of Zmel1 EVs (Figures 1C and 2D) and Zmel1 EVs labeled with MemBright (Figure 2D) by TEM was repeated each three times (n= 871 and 356, respectively). Spectroscopic analysis of PKH and MemBright labeled EVs (Figure 1B) was performed once, at different concentrations. Measurements of the fluorescence of PKH or MemBright labeled EVs was repeated three times (Figures S2A and S2B). The number of puncta measured is indicated in the graph bars. The density gradient isolation of EVs was repeated twice (Figure S1F). The measurements of the apparent EV diameter Vs beads diameter by confocal was repeated three times *in vitro* and *in vivo* (Figure S2). The number of individual puncta measured is indicated in the graphs. Mass spectrometry of EVs was performed on triplicates (Figure 1E; Table S1).

DATA AND SOFTWARE AVAILABILITY

The proteomics data have been deposited on Exocarta. All relevant data regarding the EVs experiments have been deposited on the EV-TRACK knowledgebase (EV-Track ID:EV180078) (Van Deun et al., 2017).

Developmental Cell, Volume *48*

Supplemental Information

Studying the Fate of Tumor Extracellular Vesicles at High Spatiotemporal Resolution Using the Zebrafish Embryo

Vincent Hyenne, Shima Ghoroghi, Mayeul Collot, Joanna Bons, Gautier Follain, Sébastien Harlepp, Benjamin Mary, Jack Bauer, Luc Mercier, Ignacio Busnelli, Olivier Lefebvre, Nina Fekonja, Maria J. Garcia-Leon, Pedro Machado, François Delalande, Ana Amor López, Susana Garcia Silva, Frederik J. Verweij, Guillaume van Niel, Farida Djouad, Héctor Peinado, Christine Carapito, Andrey S. Klymchenko, and Jacky G. Goetz

Supplementary figure legends

Supplementary Figure 1 (Related to Figure 2): Analysis of MemBright labeled EVs (A) Histograms showing a spectroscopy analysis of MemBright and PKH describing the absorbance (left, y axis) and the fluorescence intensity (right, y axis) versus the wavelength (nm, x axis) of the two probes in water or methanol. The presence of aggregates of PKH in water is visible. Arrows indicate the presence of PKH aggregates in labeled EVs (left) as well as in control PKH alone (right). **(B)** Histograms showing the absorbance (left, y axis) and the normalized absorbance (right, y axis) of Zmel1 or 4T1 EVs labeled with PKH or MemBright versus the wavelength (nm, x axis). PKH aggregates are denoted with an arrow. **(C)** Histograms showing the intensity of the emitted fluorescence (left, y axis) and the normalized fluorescence intensity (right, y axis) of Zmel1 or 4T1 EVs labeled with PKH or MemBright versus the versus the wavelength (nm, x axis). PKH fluorescent aggregates are denoted with an arrow. **(D)** Representative fluorescent images of Zmel1 EVs labeled with PKH (at 2µM) or MemBright (at 200nM) and histogram showing the relative fluorescent intensity of individual puncta (p=0,001; Mann-Whitney test). **(E)** Representative fluorescent images of 4T1 EVs labeled with PKH (at 200nM) or MemBright (at 200nM) and histogram showing a higher fluorescent intensity of Zmel1-MemBright individual puncta compared to Zmel1-PKH puncta (p<0,0001; Mann-Whitney test). **(F)** Western blot on EVs labeled with MembrightCy3, or MemBright alone, separated on a density gradient (Left). It shows the presence of Alix and TSG-101 in the fractions 5-10 exclusively. No signal is observed in the control MemBright alone. Representative fluorescent images at low (upper) and high (lower) magnifications of the same samples than the western blots (right). Fluorescent MemBrightCy3 puncta accumulate in fractions 5-10.

Supplementary Figure 2 (Related to Figure 3): Characterization of MemBright EVs *in vivo*. (A) Representative confocal images of Zmel1 EVs labeled with MemBright-Cy5 and incubated with 100nm red fluorescent polystyrene beads *in vitro*. **(B)** Representative confocal Z projections of *Tg(pu1:GFP)* (lymphoid, monocytes/macrophages) embryos co-injected with Zmel1 EVs labeled with MemBright-Cy5 and with 100nm red fluorescent polystyrene beads imaged 3 hours post-injection. **(C)** Single plane zoom on embryos co-injected with Zmel1 EVs labeled with MemBright-Cy5 and with 100nm red fluorescent polystyrene beads. **(D)** Histogram showing the apparent diameters (left, nm) of MemBright labeled Zmel1 EVs and 100nm beads measured in confocal images *in vitro* and *in vivo* in zebrafish embryos (*in vitro*: p<0,0001; *in vivo*: p=0,6; Mann-Whitney test). **(E)** Confocal images from three different Z planes of Zmel1 EVs labeled with MemBright-Cy5 and incubated with human red blood cells *in vitro* for 10 minutes. **(F)** Confocal images from rapid time-lapses of *Tg(Gata1:RFP; Fli1:GFP)* embryos injected with MemBright-Cy5 labeled Zmel1 EVs, showing examples of EVs far (upper panel) or close (lower panel) from RBCs in the circulation. **(G)** Representative confocal Z projections of *Tg(Fli1:GFP)* embryos co-injected with Zmel1 EVs labeled with MemBright-Cy3 and with 4T1 EVs labeled with MemBright-Cy5. **(H)** Representative confocal single planes from a time-lapse imaged right after injection of *Tg(Fli1:GFP)* embryos co-injected with Zmel1 EVs labeled with MemBright-Cy3 and with 4T1 EVs labeled with MemBright-Cy5. **(I)** Time projection over 10 seconds of a time-lapse

imaged right after injection of *Tg(Fli1:GFP)* embryos co-injected with Zmel1 EVs labeled with MemBright-Cy3 and with 4T1 EVs labeled with MemBright-Cy5.

Supplementary Figure 3 (Related to Figure 4): Control Zebrafish embryo injected with MemBright-labeled EVs or with control MemBright alone. Representative confocal Z-projections of *Tg(mpeg1:GFP)* (macrophages) embryos injected with either 4T1 EVs labeled with MemBright-Cy3 or with MemBright-Cy3 without EVs and imaged 3 hours post injection.

Supplementary Figure 4 (Related to Figure 5): Retrieval of the cells by CLEM and the putative journey of EVs in macrophages by electron microscopy (A) *Tg(mpeg1:GFP)* embryos were injected with 4T1 MemBright-Cy3 labeled EVs and imaged by confocal (upper panels). The upper right panel shows the position of the Region Of Interest (ROI) containing the two target cells, with respect to several embryonic landmarks imaged by confocal at low magnification. The lower left image shows the tail of the embryo after fixation and resin embedding imaged by microCT. The lower right image shows the position of the ROI in an electron microscopy section. **(B)** Higher magnification of the ROI imaged by confocal and electron microscopy. Common features between transmitted light in the living fish and electron microscopy on fixed fish are highlighted to allow a precise positioning of the ROI. The electron microscopy panel is stitched together from several individual images to allow a larger region to be visualized with better resolution. The asterisk points to a dirt speck on the EM section. **(C)** Electron microscopy images of EVs observed in the lumen of the vessel, in the close proximity of protrusions extending from the macrophage plasma membrane, which were identified by CLEM. **(D)** Electron microscopy images of putative EVs present in early endosomes close to the surface of macrophages. **(E)** Electron microscopy images of putative EVs present in MVBs.

Supplementary Figure 5 (Related to Figure 7): 4T1 CD63-GFP cells pre-labeled with MemBright. (A) Representative confocal images of 4T1 CD63-GFP cells labeled with MemBright-Cy3 at different times before and after MemBright addition. **(B)** Zooms on confocal images of 4T1 CD63-GFP cells labeled with MemBright-Cy3 at 3h and 24h after MemBright addition. **(C)** Representative images of EVs isolated from the extracellular medium of 4T1 CD63-GFP cells pre-labeled with MemBright-Cy3.

Supplementary tables

Table 1 (Related to Figure 1): proteins identified in EVs by mass spectrometry (A) proteins identified in EVs isolated from Zmel1 zebrafish melanoma cells (page 1-20); **(B-G)** proteins identified in EVS isolated from human melanoma 451-LU cells (page 21-68) **(B)**, SK-Mel28 cells (page 69-125) **(C)**, SK-Mel147 cells (page 126-167) **(D)**, SK-Mel103 cells (page 168-215) **(E)**, WM35 (page 216-258) **(F)** and WM164 cells (page 259-307) **(G)**; **(H-J)** proteins identified in EVs isolated from mouse melanoma B16-F0 cells (page 308-322) **(H)**, B16-F1 cells (page 323-349) **(I)** and B16-F10 cells (page 350-364) **(J)**; **(K)** proteins common to zebrafish, mouse and human melanoma EVs (page 365-367); **(L)** proteins common to Zmel1 EVs and AB9 EVs (page 368-371); **(M)** proteins common to Zmel1 EVs and YSL CD63-GFP positive EVs (page 372).

Table 2 (Related to Figure 2): Quantum yield of MemBright and PKH labeled EVs.

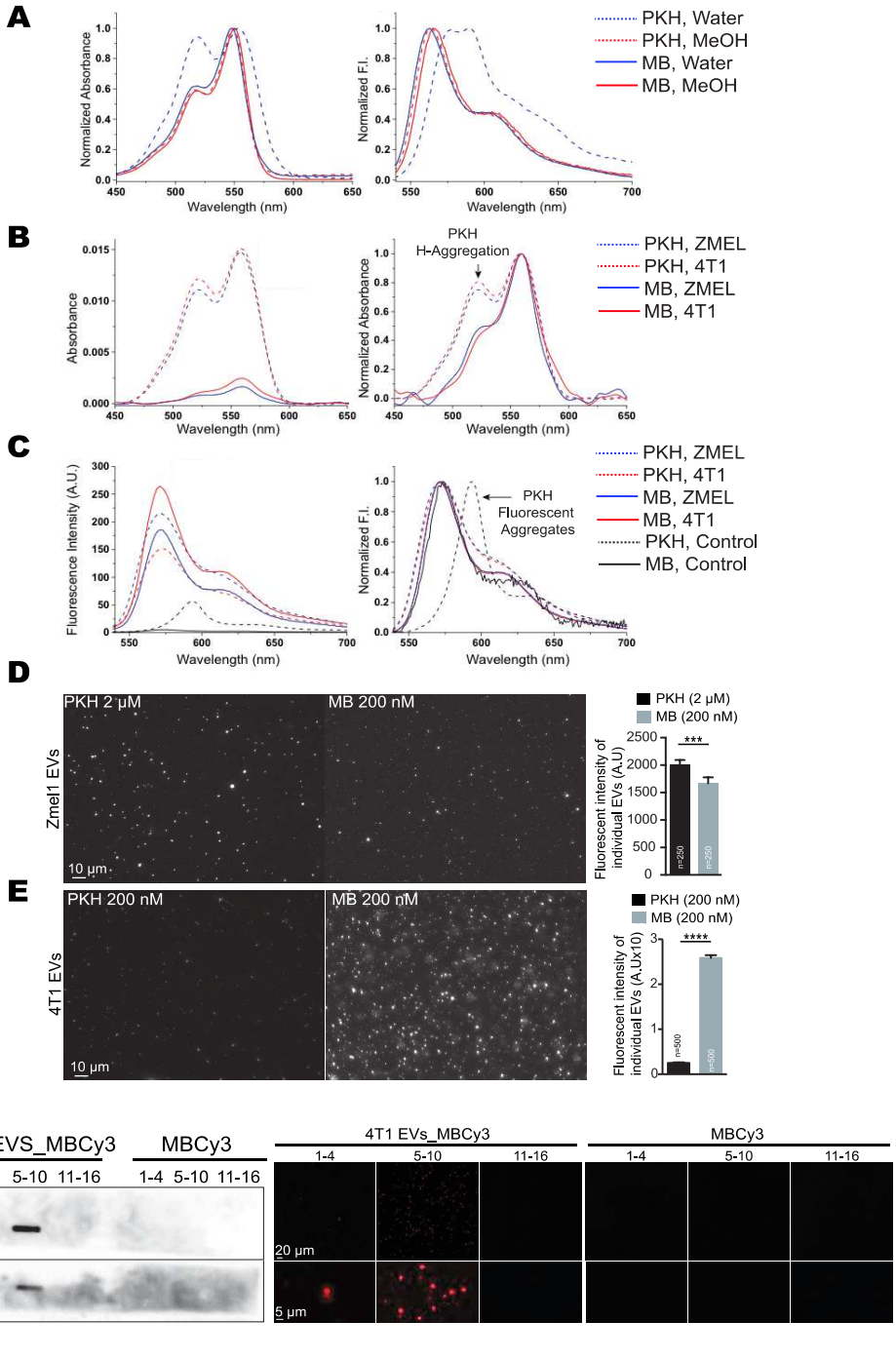

Supplementary Figure 1_Hyenne et al.

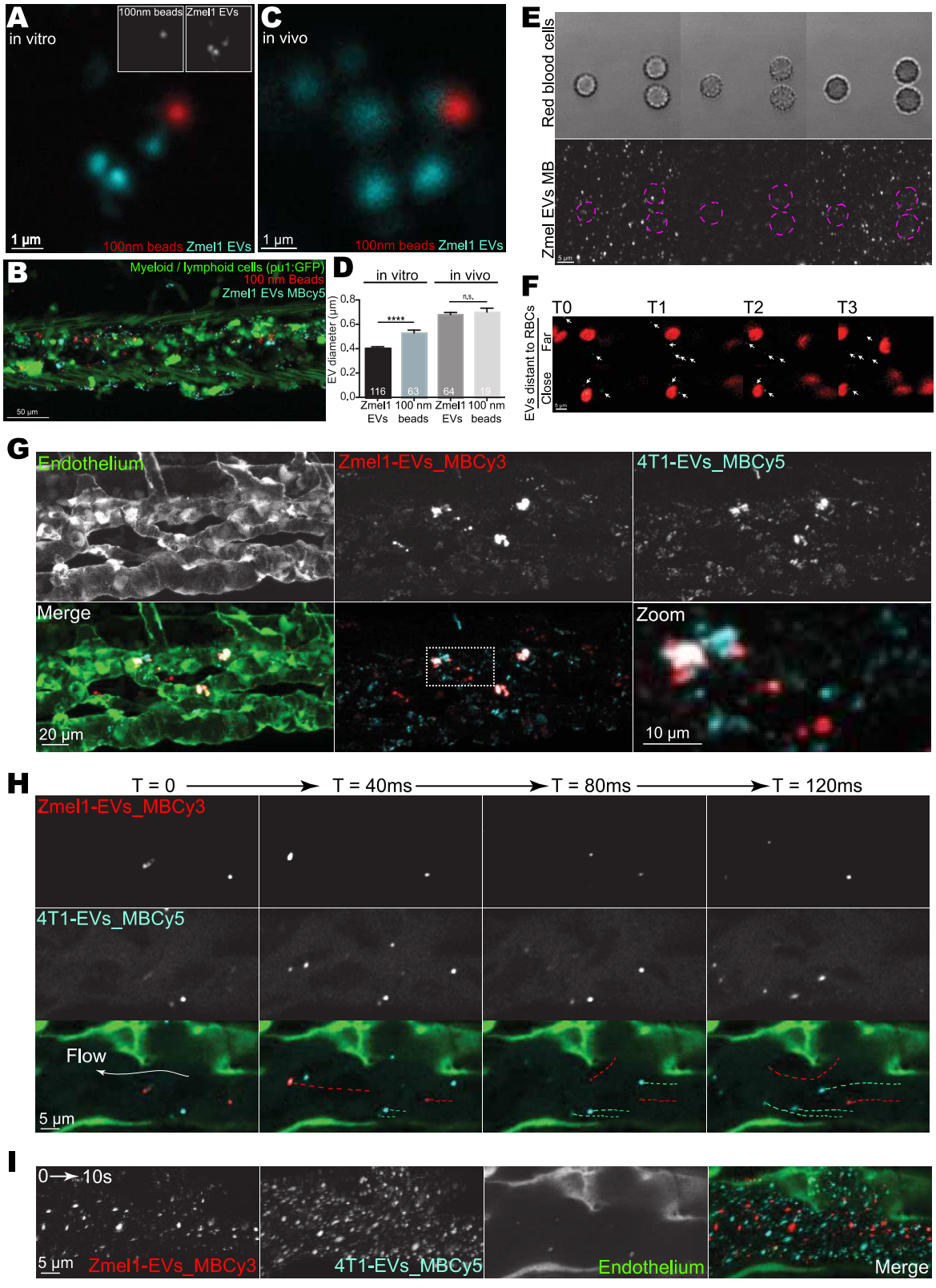

Supplementary Figure 2_Hyenne et al.

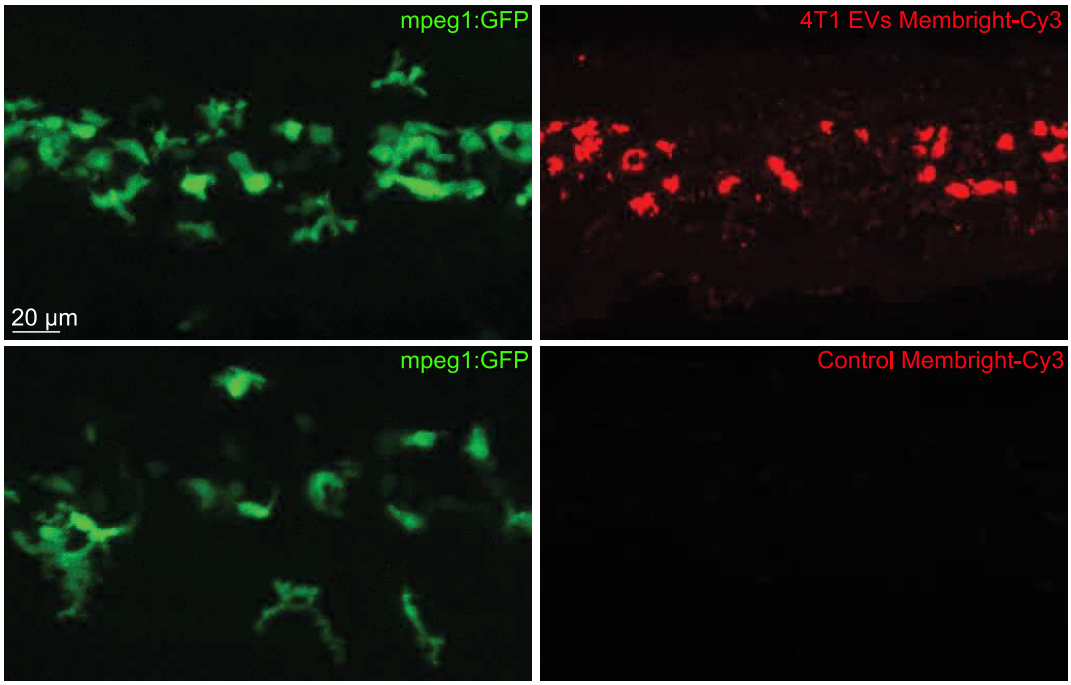

Supplementary Figure 3_Hyenne et al.

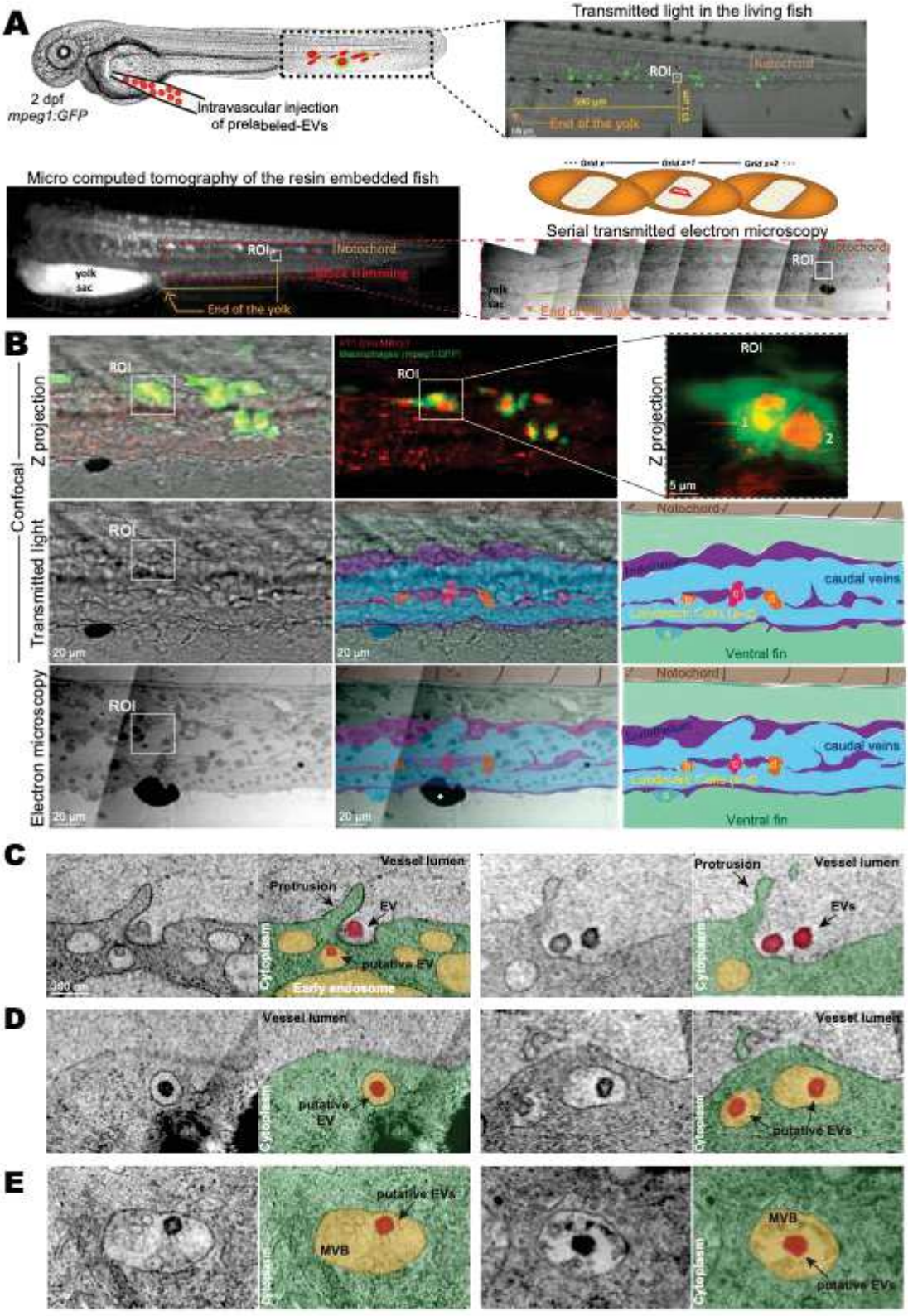

Supplementary Figure 4_Hyenne et al.

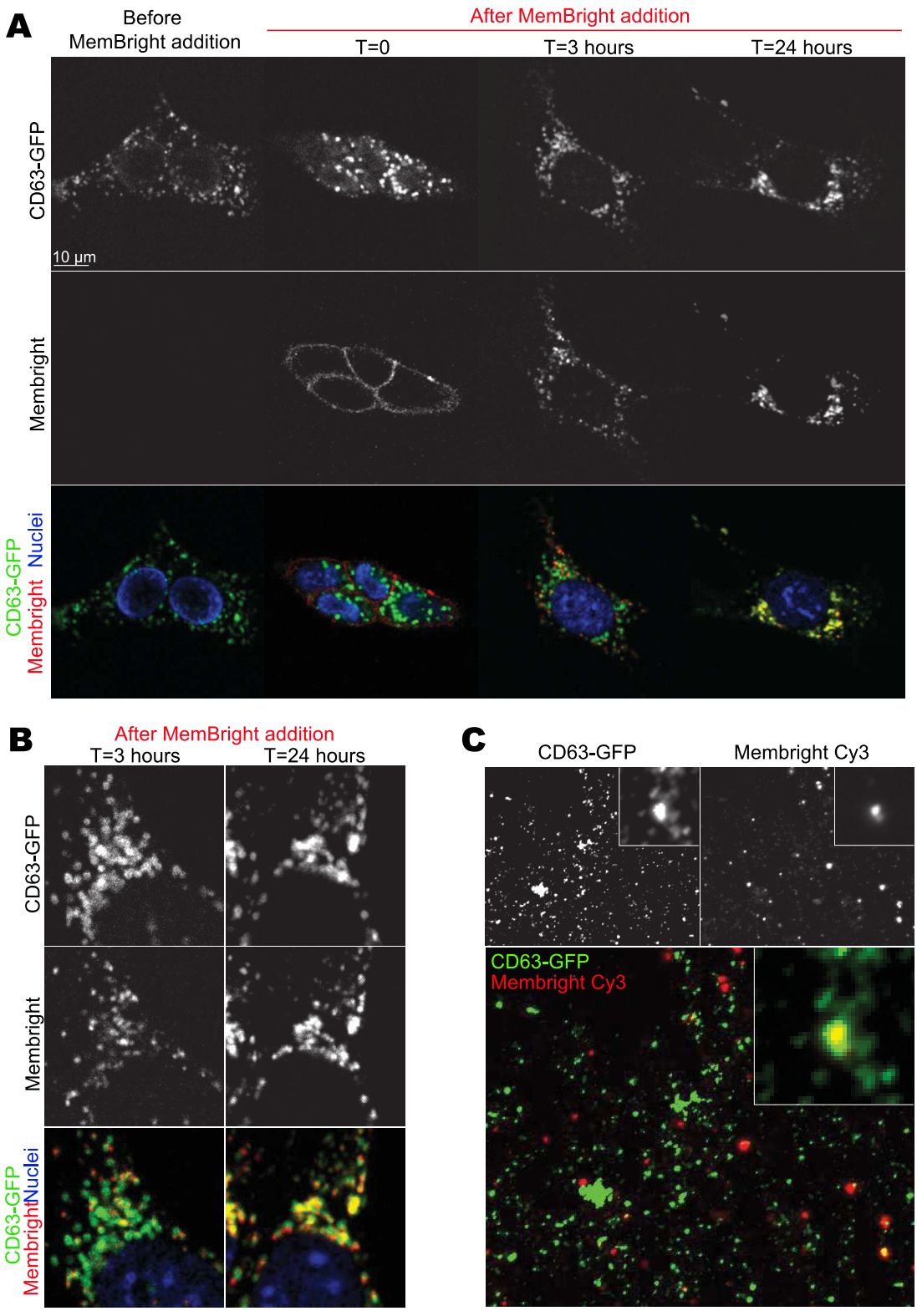

Supplementary Figure 5_Hyenne et al.

Table S2, related to Figure 2 : Photo-physical properties of labelled EVs.

	λ Abs (nm)	FWHM Abs (nm)	λ Em (nm)	FWHM Em (nm)	QY (ϕ)
PKH 4T1	559[a]	72	574	47	0.02
PKH Zmel1	558[a]	71	572	50	0.04
MB 4T1	559	42	572	33	0.42
MB Zmel1	560	42	571	34	0.41

[a] A second H-aggregation peak was observed at 522nm.

CHAPTER FOURTEEN

Live tracking of extracellular vesicles in larval zebrafish

Benjamin Mary[a,b,c,†], **Shima Ghoroghi**[a,b,c,†], **Vincent Hyenne**[a,b,c,d,*], **and Jacky G. Goetz**[a,b,c,*]

[a]INSERM UMR_S1109, Strasbourg, France
[b]Université de Strasbourg, Strasbourg, France
[c]Fédération de Médecine Translationnelle de Strasbourg (FMTS), Strasbourg, France
[d]CNRS, SNC 5055, Strasbourg, France
*Corresponding authors: e-mail address: hyenne@unistra.fr; jacky.goetz@inserm.fr

Contents

Abstract

Formerly considered as insignificant cell debris, extracellular vesicles (EVs) have emerged as potent mediators of cell-cell communication, both in proximity and at distance from the producing cell. EVs are transported in body fluids and can be internalized by specific distant cells to ultimately deliver a functional message. Despite their striking importance in many physiological and pathological contexts, the exact mechanisms by

† These authors contributed equally.

Methods in Enzymology, Volume 645
ISSN 0076-6879
https://doi.org/10.1016/bs.mie.2020.07.013

which EVs impose local and distant modifications of the microenvironment *in vivo* remain to be fully understood. We realized that some conceptual gaps are direct consequences of the difficulty to visualize the shuttling and targeting of EVs in real time *in vivo*. The zebrafish larvae offered attractive features for live tracking of EVs, within circulating fluids. Here, we describe the experimental procedures that we have built for dissecting the dissemination of EVs at high spatio-temporal resolution *in vivo*.

1. Introduction

Over the past 20 years, extracellular vesicles (EVs) became central mediators of cell-cell communication in various physiologic contexts, such as development, reproduction, metabolism or neurology (Yáñez-Mó et al., 2015). They also contribute to the progression of multiple pathologies, such as immune deficiencies, cardiovascular disorders, infectious disease, or cancer. These multi-tasking cellular products can also behave as protecting soldiers from bacterial toxins and thus combat infection (Keller et al., 2020). EVs are heterogeneous vesicles secreted by all cell types with diameters ranging from a few nanometers to several micrometers. They can be found in most, if not all human body fluids (blood, lymph, urine, milk, sweat, saliva, tears and others) (Bakhshandeh, Kamaleddin, & Aalishah, 2016; Yáñez-Mó et al., 2015). Their lipid bilayer ensures protection of their cargo, which is composed of mRNAs, non-coding RNAs, proteins and, in the case of some tumor EVs, DNA (Balaj et al., 2011; Lázaro-Ibáñez et al., 2019). The repertoire of molecules that EVs carry depends on their cellular and sub-cellular origin as well as their species of origin and the physiological state of secreting cells (Karimi et al., 2018; Zhao et al., 2020). EVs are heterogeneous by nature. A single cell can secrete a wide variety of EVs-subpopulations (Kowal et al., 2016) that are likely to convey a functional heterogeneity. EVs act within short, medium and distant ranges. They function as paracrine and autocrine factors and can alter the behavior of cells, and the associated microenvironment, in close proximity. For instance, EVs rearrange the extracellular matrix, thereby promoting invadopodia formation and cell migration, close to the site of secretion (Hoshino et al., 2013). EVs also communicate at the scale of an organ through the dissemination of morphogen factors beyond the reach of diffusion gradient of soluble molecules (Gross, Chaudhary, Bartscherer, & Boutros, 2012; Matusek et al., 2014). Finally, and most interestingly for this protocol, EVs also act within long range. They can disseminate in the organism through body fluids, thereby

contributing to cross-organ communication and ultimately, act as endocrine factors (Butler, Abdelhamed, & Kurre, 2018). The most striking examples probably come from cancer studies suggesting that EVs secreted by a primary tumor can exploit the blood circulation to reach distant organs and locally modify the microenvironment to promote future metastasis (Adem, Vieira, & Melo, 2020; Costa-Silva et al., 2015; Hoshino et al., 2015; Peinado et al., 2012). However, some black boxes remain concerning the origin, shuttling behavior, destination and functional impact of the large amounts of EVs present in our body fluids (ranging around 10^{10} EVs per ml in blood (Johnsen, Gudbergsson, Andresen, & Simonsen, 2019)). EVs found in body fluids have several cellular origins (Flaumenhaft, Mairuhu, & Italiano, 2010; Karimi et al., 2018). In blood, their concentration depends on several parameters, that can be physiological (Whitham et al., 2018) or pathological (*i.e.,* Cancer or cardiovascular diseases Peinado et al., 2012; Boulanger, Loyer, Rautou, & Amabile, 2017), and counter-balanced by rapid clearance (Matsumoto et al., 2020). However, how single EV (or population of EVs) use, respond and exploit body fluids remains to be elucidated. Circulating EVs can now be sampled, isolated and analyzed in multiple ways, revealing their contents and their origin (Nielsen, Beck-Nielsen, Andersen, & Handberg, 2014; Zhao et al., 2020). We reasoned that understanding their fate and their function would greatly benefit from animal models adapted to the imaging of small objects in complex environments like circulatory systems *in vivo*.

Microscopic visualization of circulating EVs in realistic pathophysiological situations *in vivo* still faces major challenges (Verweij, Hyenne, Van Niel, & Goetz, 2019). Imaging nano-sized objects as single particles depend on both subcellular resolution and brightness of the labeling objects (*i.e.,* EVs) so that one can distinguish EVs from the potential autofluorescence background. Furthermore, because some body fluids such as blood circulate at high-speed, high-speed sampling is needed to study the dynamic of circulating EVs with microscopy. Finally, the animal model used should allow deep, non-invasive access to internal organs and be compatible with the expression of fluorescent markers in tissue-specific cell lines in order to identify EVs receiving cells and organs. In rodents, different strategies, based on bioluminescence, lipophilic dyes, or transgenic expression of EVs fluorescent markers have been developed (Hyenne, Lefebvre, & Goetz, 2017). It is now possible to track the biodistribution of labeled EVs injected into the circulation at the whole animal scale (Hoshino et al., 2015; Lai et al., 2014; Wiklander et al., 2015). However, these approaches often require *ex vivo* imaging and do not allow to investigate

the circulating EVs behavior at the high spatio-temporal resolution, towards single EV detection. To overcome these limitations, several groups developed intravital imaging of EVs in mice (Lai et al., 2015; van der Vos et al., 2016; Zomer et al., 2015). Although they provide unique observations of EVs in their natural microenvironment, the complexity of these procedures prevents high-throughput imaging and are often not compatible with a high sampling of EVs shuttling in body fluids. Alternatively, the zebrafish larvae meets all requirements for in-depth, high-speed analysis of circulating EVs.

Indeed, over the past years, zebrafish larvae emerged as a unique animal model to study physiological and pathological circulating EVs at unprecedented spatiotemporal resolution (Verweij, Hyenne, et al., 2019). It offers several advantages for non-invasive analysis *in vivo*. Zebrafish embryos develop a stereotype vasculature (and blood circulation) and a maturing immune system within 48 h. Its translucent body allows simple *in vivo* non-invasive imaging and it is easily amenable to all types of confocal and high-speed microscopy. This model easily tolerates genetic manipulation to express fluorescent proteins in specific cell populations within zebrafish tissues. Overall, zebrafish presents a high level of genetic and physiologic homology with humans and can be used to model a large number of human diseases (cancer, cardiovascular, neurological, *etc*...). More particularly, it reproduces a relevant physiological environment for the study of circulating EVs (Hyenne et al., 2019; Verweij, Hyenne, et al., 2019; Verweij, Revenu, et al., 2019). Detection of fluorescent EVs, labeled with either lipophilic dyes or by transgenic expression of fluorescent markers within secreting cells is favored by transparent larvae. Zebrafish internal organs are easily accessible by confocal microscopy thus, 3D analysis of regions where EVs arrest and accumulate is within reach. Moreover, high-speed imaging allows to follow circulating EVs dynamic at single-particle scale in fish vasculature, and transgenic zebrafish lines are used to visualized EVs/cells interaction *in vivo*. Finally, we exploited this model to perform an extensive analysis of circulating EVs and describe their hemodynamic behavior *in vivo* in both physiological and pathological conditions (Hyenne et al., 2019; Verweij, Revenu, et al., 2019).

In this chapter, we describe a simple but detailed procedure (Hyenne et al., 2019), from isolation and labeling of EVs to intravascular injection and imaging in the zebrafish larvae. The versatility of our experimental approach offers the possibility to study exogenous EVs of different origins and pathological conditions, for instance from human samples, and to compare their respective roles and hemodynamic behavior once they have

reached the circulation. Despite the advantages of using zebrafish for studying tumor EVs, there are some limitations that are important and need to be addressed (such as difference in maintenance temperature and/or molecular and cellular process conservation between species) when studying human pathophysiology. Nevertheless, the zebrafish has proven very useful in different fields of human medical research (tissue regeneration, cardiovascular diseases, cancer progression) and could pave the way for later validation in mammalian models. In particular, it is suitable to study the dissemination of tumor EVs, document their arrest and internalization, as well as their capacity to cross the endothelium and induce local phenotypic changes.

2. EVs isolation and labeling

EVs are generally isolated from conditioned cell culture media or from various body fluids such as blood plasma, urine, saliva, breast milk, semen, and amniotic fluid. There are several methods available to isolate EVs including ultracentrifugation-based methods, size-based techniques, immune affinity, precipitation and microfluidic (Karimi et al., 2018; Willms, Cabañas, Mäger, Wood, & Vader, 2018; Yang et al., 2020). Here, we will describe two approaches that we found suitable for a subsequent labeling approach: differential centrifugation (UC) (Théry, Amigorena, Raposo, & Clayton, 2006) and size exclusion chromatography (SEC). The latter has no deleterious effect on EVs' integrity, and better preserves their functionality (Mol, Goumans, Doevendans, Sluijter, & Vader, 2017; Stranska et al., 2018). A schematic illustration of UC and SEC methods are shown in Fig. 1C. Upon isolation, we characterize EVs to confirm the presence, size and concentration of EVs in the preparation (physical characterization), but also to assess EV purity and content (molecular characterization) (Théry et al., 2018). Isolation is followed by characterization of EVs population. In this chapter, we will describe the basic quantification of EVs size and concentration by nanoparticle tracking analysis (NTA). Finally, we will detail a procedure for EV fluorescent labeling. While several strategies have been developed to fluorescently label EVs (Chuo, Chien, & Lai, 2018), the post-isolation labeling with fluorescent lipophilic dyes remains the most versatile and rapid approach to label EVs. They, such as PKH-26, PKH-67, DiO, DiL, Dir or MemBright, are inserted into EVs lipid bilayer (Collot et al., 2018; Hood, Roman, & Wickline, 2011; Hoshino et al., 2015; Takahashi et al., 2013). Due to their lipophilic nature, these dyes have been shown to have multiple drawbacks, including non-specific labeling, altered biodistribution, and

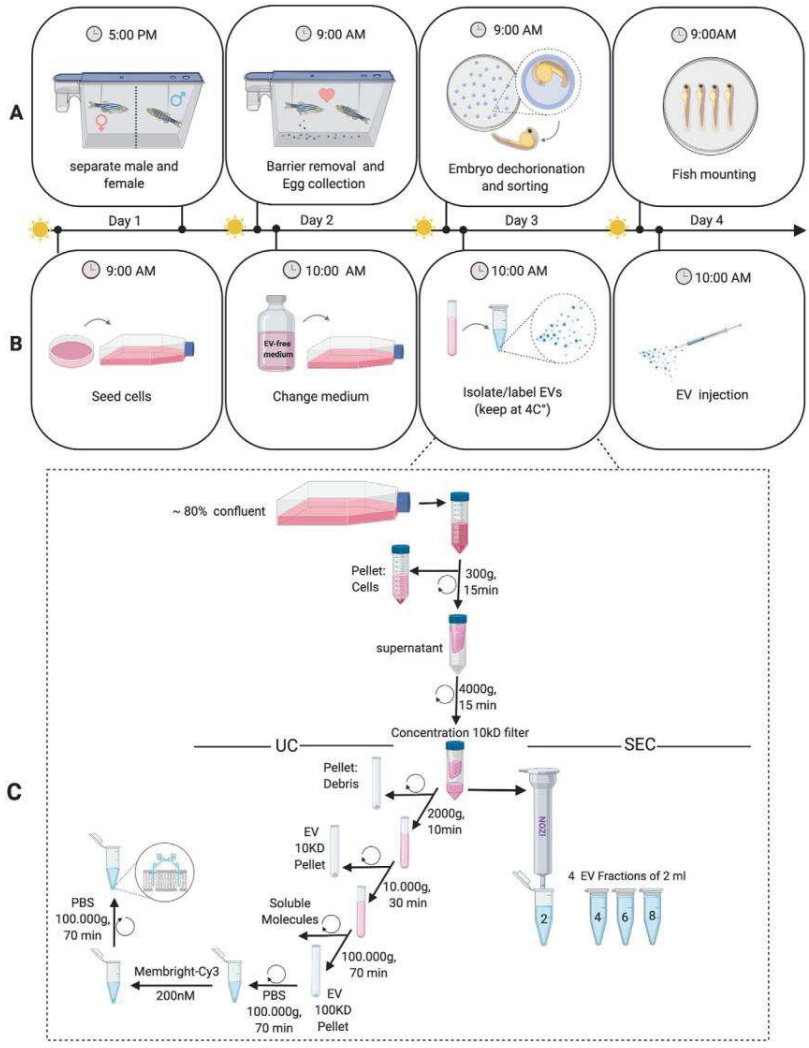

Fig. 1 Parallel zebrafish embryo and EV preparation. A schematic illustration of the parallel workflow timeline required for zebrafish embryo generation (A) and EV isolation and labeling (B and C).

presence of additional artifacts (Takov, Yellon, & Davidson, 2017). However, they remain very useful and unique tools for labeling of EVs from all origins and can be trusted when used with appropriate controls (Simonsen, 2019). As an alternative strategy, EV proteins can be fused to fluorescent proteins and expressed in EV-producing cells (Corso, 2019; Görgens et al., 2019).

This allows to visualize unique subpopulations of EVs and can also be used to track EVs from a genetically engineered cell or zebrafish lines, as we have done for endogenous zebrafish EVs (Verweij, Hyenne, et al., 2019; Verweij, Revenu, et al., 2019). Here, we present both strategies: genetically labeled EVs isolated from zebrafish melanoma cells (Zmel1) expressing syntenin2-GFP and post-isolation labeling of EVs with MemBright. MemBrights are recently developed cyanine-based membrane probes (Cy3, Cy5 or Cy7), bearing alkyl chains and zwitterionic groups (Collot et al., 2018). These probes have unique properties that provide high brightness and specificity to labeled-EVs in addition to preventing fluorescent self-aggregation (Hyenne et al., 2019). In addition, MemBright can be used to co-inject different types of EVs labeled with different colors (Cy3, Cy5), which allows us to compare different EV population (or origin) and track their specific behavior, fate and function. As a control, PBS is incubated with MemBright in a similar way as we labeled EVs, analyzed by NTA and injected into zebrafish larvae.

2.1 Equipment and reagents

- Centricon Plus-70 centrifugal filter (10 k, Millipore).
- Beckman tubes thinwall polypropylene (17 mL).
- Ultracentrifuge (Beckman XL-70, equipped with at SW28 and 70Ti rotors).
- Size exclusion chromatography column (iZon qEV2).
- ZetaView apparatus (Particle Metrix, Meerbusch, Germany) for NTA.
- Alignment suspension for NTA measurement (Particle Metrix, Meerbusch, Germany).
- MemBright-Cy3 or Cy5 (Collot et al., 2018).
- PBS solution (Dutscher X0520-500; 0.2 μm filtered using a pore filtration unit (Stericup Merck)).
- EV free medium, obtained by ultracentrifugation of classical culture media for 20 h at 100000 g during (Beckman XL-70 centrifuge, rotor70Ti) to eliminate EVs present in FBS. The supernatant is collected and filtered at 0.22 μm (Stericup Merck).
- Cells lines. Here, we use Zmel1 melanoma cells (Heilmann et al., 2015) and Zmel1 cells expressing Syntenin2-GFP (Hyenne et al., 2019). Depending on the cell type and the growth rate of EVs producing cells, the number of cells seeded 48 h before EV isolation could differ. Usually, EVs are isolated when cell confluency reaches 80%.

2.2 EV isolation

2.2.1 Isolation by ultracentrifugation

1. Culture cells in the EV free medium for 24 h before collecting conditioned medium (see Fig. 1).
2. Transfer supernatant media from a cell culture flask (~80% confluent) to a 50 mL falcon, and centrifuge at 300 × *g* for 15 min at 4 °C. Keep the supernatant for further processing
3. Concentrate supernatant in 15 mL using a Centricon Plus-70 centrifugal filter (10 k; Millipore)
   - Add supernatant to sample filter cup and spin at up to 4000 × *g* until the desired concentration is achieved.
   - Typical spin time is 15–20 min, depending on solute type and concentration.
4. Centrifuge concentrated medium at 2000 × *g* for 10 min at 4 °C. Keep the supernatant for further processing.
5. Centrifuge supernatant at 10,000 × *g* for 30 min at 4 °C, discard 10 K pellet (large-sized EVs). Keep the supernatant for further processing. Note that in this protocol, large-sized EVs that mainly include micro-vesicles are discarded because we mainly focused on the effect and characterization of small tumor EVs (exosomes).
6. Centrifuge supernatant medium at 100,000 × *g* for 70 min at 4 °C and the 100 K pellet (small-sized EVs) is kept for further processing.
7. Wash pellet with 15 mL of 1 × PBS, centrifuge at 100,000 × *g* for 70 min at 4 °C.
8. Resuspend the EV pellet in 50 μL of 1 × PBS by gentle pipetting.
9. Use isolated EVs immediately or store at 4 °C in the dark to use the next day.

2.2.2 Isolation by size-exclusion chromatography (SEC)

1. Collect and concentrate conditioned medium similarly to Section 2.2.1 (Steps 1–3) but with a final volume of 2 mL.
2. Rinse the SEC columns with 50 mL of PBS, twice.
3. Apply 2 mL of the concentrated extracellular medium on top of qEV column (Izon Science).
4. Fill the column with PBS and collect 2 mL fractions. At this step, the concentration of EVs in each fraction should be analyzed, for instance using NTA analysis. Depending on the experiments, single fractions can be used, or multiple fractions can be pooled.

5. Centrifuge single or pooled fractions for 1 h at 100,000 × *g*, 4 °C.
6. Resuspend the EV pellet in 50 µL of 1 × PBS by gentle pipetting.
7. Alternatively, single or pooled fractions can be concentrated using an Amicon Ultra-4 10 kDa centrifugal filter device (Merck Millipore).
8. Use isolated EVs immediately or store at 4 °C in the dark to use the next day.

2.3 EV labeling

1. Use fresh EVs isolated by ultracentrifugation or SEC (see Section 2.2). As a control, use a similar volume of particle-free PBS (0.2 µm filtered).
2. Incubate isolated EVs, or control PBS with MemBright-Cy3 or Cy5 at 200 nM (final concentration) in PBS.
3. Mix continuously for 30 s by gentle pipetting.
4. Let stand at room temperature in the dark for 30 min.
5. Rinse labeled EVs in 15 mL of PBS and centrifuged at 100,000 × *g* for 70 min at 4 °C.
6. Carefully aspirate the supernatant which contains the excess unbound dye.
7. Resuspend the EV pellet in 50 µL of 1 × PBS by gentle pipetting.
8. To ensure the highest possible fluorescent intensity, use labeled EVs a soon as possible or store at 4 °C in the dark.

2.4 EV quantification and size measurement

1. Dilute EVs samples before analysis in particle-free PBS (0.2 µm filtered) to obtain a concentration within the recommended measurement range ($1–10 \times 10^9$ particles/mL), corresponding to dilutions from 1:100 to 1:100,000 depending on the initial sample concentration.
2. Start the program and flush the cell channel with distilled water prior to measurement.
3. To align the foci of the laser and microscope, inject the alignment suspension, containing polystyrene particles, into the NTA instrument.
4. Inject the EV suspension into the channel and start the measurement.
5. Save the measurement and based on that adjust the EV sample to have the ideal concentrations for zebrafish injections which is between 10^9 and 10^{10} EVs per mL.

Since freezing is sought to alter EVs pellet (Cheng, Zeng, Han, & Xia, 2019) we recommend using only fresh EVs for fish injections. EV pellets are either used right after isolation or the next morning. In any case, EV pellets are never frozen and are kept at 4 °C, protected from the light, for a maximum

duration of 1 week. To coordinate EVs isolation with fish breeding and embryo production, we use an optimized organizational timeline developed to save maximum time for experimentation (Fig. 1B). In this workflow, EV isolation and fish breeding protocols are followed in parallel. Starting from day 1 EVs isolation takes 3 days and zebrafish larvae are ready for injection in the morning of the fourth day of the protocol which corresponds to 2 dpf for zebrafish larvae (Fig. 1).

3. Zebrafish embryo handling and injection

Intravascular injection of EVs in zebrafish larvae is an easy-handling protocol based on a previously described method of tumor cell injection (Follain, Osmani, Fuchs, et al., 2018; Follain, Osmani, Azevedo, et al., 2018). Zebrafish fluorescent transgenic zebrafish strains allow to identify specific cell types and can be adapted to the user's need (see Section 3.3). When EVs are labeled with Membright-Cy5 or Membright-Cy3, these strains offer the possibility to dissect cell types that are targeted by EVs once they reach their final destination within the circulatory system. Once EVs samples are collected, characterized and labeled in particle-free PBS, they are ready to be injected in the larvae. Larvae are anesthetized and immobilized in an agarose drop to facilitate injection of a few nanoliters of EVs solution under the stereomicroscope using a nanoinjector. This methodology (*i.e.,* intravascular injection of EVs) can also be used for educating metastatic niches (Hyenne et al., 2019) as it had been done in murine models (Costa-Silva et al., 2015; Peinado et al., 2012).

3.1 Reagents

- DANIEAU: stock solution 30 ×: H_2O + 1740 mM NaCL, 21 mM KCl, 12 mM $MgSO_4$, 18 mM$Ca(NO_3)_2$, 150 mM HEPES, pH at 7.6
- PTU: 1-phenyl-2-thiourea (Merck KGaA P7629): stock solution (50 ×): 10 mM in DANIEAU (0.3 ×) solution
- Tricain (ethyl-3-aminobenzoate-methanesulfonate): stock solution (25 ×): 16.25 mM in DANIEAU (0,3 ×)/PTU (1 ×) solution
- Low melting point agarose 0.8% (m/v): melt at 80 °C cool down and maintain at 40 °C during the procedure
- Mineral oil

3.2 Equipment

- 10 cm petri dish
- Plastic pipette
- Thin tweezers (Electron Microscopy Sciences 5,SA-78320-5)
- 35 cm glass-bottomed petri dish (ref: 35 mm Dish | No. 1.0 Coverslip | 20 mm Glass 9. Diameter | Uncoated-P35G-1.0-20-C)
- Stereomicroscope: Leica M205 FA equipped with a fluorescent excitation lamp (Mercury short-arc reflector lamp, EL6000), a GFP filter (Ex. 450–490/Em. 500–550), an ET-C filter (Ex. 533–557/Em. 570–640), a plan APO objective 20× (10450028) and a camera (DFC3000 G)
- Capillary glass (Drummond scientific company—Item# 3-000-203-G/X)
- Capillary puller (Sutter Instrument P-1000)
- Nanoinjector (Drummond Scientific Nanoject II Auto-Nanoliter Injector)

3.3 Biological materials

- Labeled EVs in PBS at an ideal concentration of 10^{10} particles/mL (Section 2).
- Basically, any fish line can be used in this model depending on the biology that is tested. We provide a non-exhaustive list of transgenic lines commonly used in our lab (Table 1). This list is non-exhaustive and can be extended depending on the cell type or biological pathway that is studied.
- Zebrafish, *Danio rerio,* fluorescent transgenic lines: in our case, we mostly use the following strains:
  - *Tg(Fli1a::eGFP)* and *Tg(Fli1a::RFP)* stably expressing GFP and RFP proteins respectively in endothelial cells.
  - *Tg(mpeg::GFP)* stably expressing GFP in myeloid cells (macrophages and monocytes are visualized at this stage of development).
  - Double transgenic lines *Tg(Fli1a::Gal4 Uas::RFP, mpeg::GFP)* that express RFP in endothelial cells and GFP in myeloid cells at the same time.

    These transgenes are expressed in fish with a golden background, which are mutated for the gene slc24a5 and present a delayed pigmentation in their early developmental stage (Lamason et al., 2005). Note that we also use these transgenic fish lines in Casper background, which is a mutant fish strain homozygous for two genes, roy$^{-/-}$ and nacre$^{-/-}$, that control pigmentation. These fish lack melanocytes and iridophores and are translucent even in adulthood (White et al., 2008).

Table 1 Zebrafish transgenic lines.

Genetic background	Name of transgenic line	Fluorophore	Tissue/Cell type	References
Golden (Lamason et al., 2005) or Casper (White et al., 2008)	*Tg(Fli1a: eGFP)*	GFP	Endothelial cells	Lawson and Weinstein (2002)
Golden (Lamason et al., 2005) or Casper (White et al., 2008)	*Tg(mpeg: GFP)*	GFP	Myeloid cells (macrophages and monocytes)	Ellett, Pase, Hayman, Andrianopoulos, and Lieschke (2011)
Golden (Lamason et al., 2005) or Casper (White et al., 2008)	*Tg(Fli1a: Gal4, Uas: RFP, mpeg: GFP)*	RFP and GFP	Endothelial cells and myeloid cells (macrophages and monocytes)	Herwig et al. (2011); Ellett et al. (2011); Hyenne et al. (2019)
Golden (Lamason et al., 2005)	*Tg(mpo: eGFP)*	GFP	Neutrophils	Yuan et al. (2011)
Golden (Lamason et al., 2005)	*Tg(mpeg: mcherry/TNF α:eGFP)*	mCherry and GFP	Myeloid cells (Red) and TNFα-secreting macrophages (Green)	Nguyen-Chi et al. (2015)
Casper (White et al., 2008)	*Tg (Flk: eGFP; Gata1: RFP)*	GFP and RFP	Endothelium and red blood cells	Home-made
Casper (White et al., 2008)	*Tg(gata1: dsRed)*	dsRed	Red blood cells	Traver et al. (2003)

- Other fish strains are commonly used like: *Tg(mpo::eGFP)* which expresses GFP in neutrophils, *Tg(mpeg::mcherry/TNFα::eGFP)* which expresses mcherry in macrophages and GFP in TNF α-secreting macrophages (Nguyen-Chi et al., 2015), (Casper) *Tg (Flk::eGFP; Gata1::RFP)* expressing GFP in the endothelium and RFP in red blood cells or *Tg(gata1:dsRed)* expressing dsRed in red blood cells.

All animal procedures were performed in accordance with French and European Union animal welfare guidelines and supervised by the local ethics committee (Animal facility #A6748233; APAFIS #2018092515234191).

3.4 Zebrafish lines handling and embryo preparation

3.4.1 Zebrafish handling

1. Prepare 0.3× DANIEAU solution using the stock solution (Section 3.1.)
2. Collect the fertilized eggs after mating in 10 cm petri dish and kept in DANIEAU (0.3×) solution at 28 °C for the first 24 h post-fertilization (hpf).
3. Sort the positive embryos 24 hpf with a stereomicroscope M205 FA Leica.
4. Put embryos in DANIEAU (0.3×) solution with 200 µM of PTU (1-phenyl-2-thiourea Merck KGaA P7629) to inhibit melanogenesis (Karlsson, von Hofsten, & Olsson, 2001). Embryos remain in this DANIEAU (0.3×)/PTU(1×) solution over the course of the experiment.
5. Mechanically dechorionate embryo with precaution using a thin tweezer before immobilization.

3.4.2 Zebrafish immobilization

1. At 48 hpf, anesthetize zebrafish larvae with DANIEAU(0.3×)/PTU (1×) solution containing 650 µM of tricaine (DANIEAU(0.3×)/PTU (1×)/Tricain(1×) solution).
2. Carefully put larvae in a low melting point 0.8% agarose drop also containing 650 µM of tricaine on a glass-bottomed petri dish compatible with imaging (Fig. 2B). We use 35 mm MatTek microwell petri dish No.1.0 Coverslip, 14 mm glass diameter, uncoated. Larvae are all aligned in the same direction on their flank at the bottom of the agarose drop using tweezers before agarose solidifies. After 5 min agarose should be solidified and the fish immobilized in the petri dish.
3. Add DANIEAU(0.3×)/PTU(1×) solution in the petri dish.

3.4.3 Preparations for larvae injection

1. Pull 0.53 mm diameter glass needles with a capillary puller (Sutter Instrument P-1000) in order to obtain capillaries with a tip of approximately 10 µm of diameter (Fig. 2A).

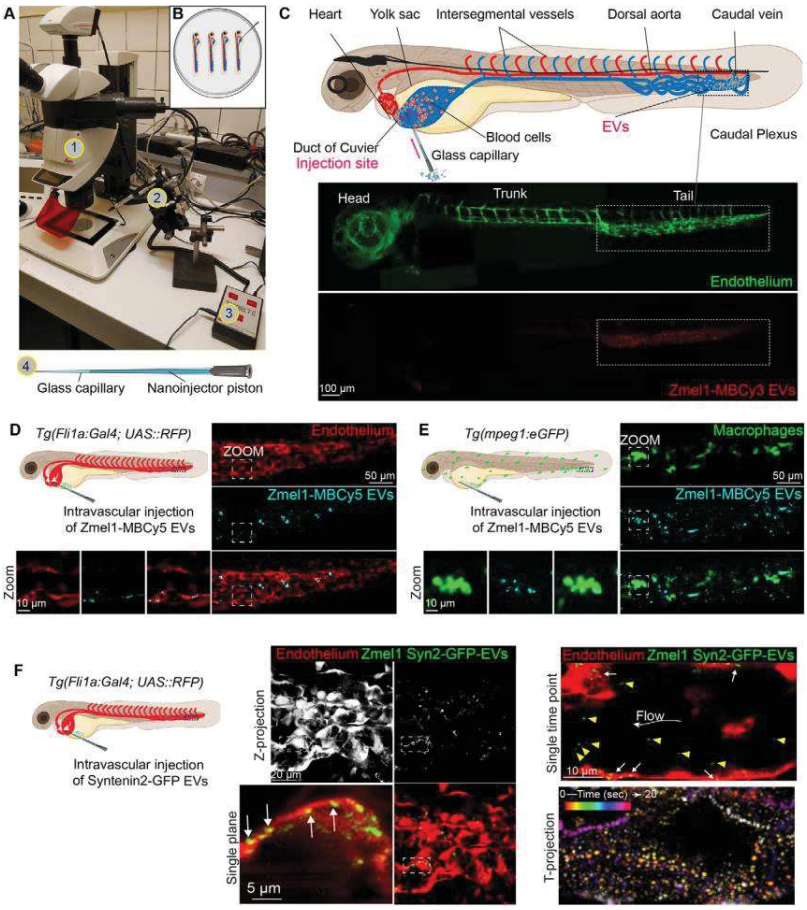

Fig. 2 EV injection and imaging in zebrafish larvae. (A) Equipment required for EVs injection in zebrafish larvae 1: Stereomicroscope, 2: Nanoinjector, 3: Injection control unit, 4: Scheme of glass capillary. (B) Schematic representation of 48 hpf larvae embedded in agarose and mounted in a glass-bottom petri dish. (C) Upper panel: Schematic representation of a 48 hpf zebrafish larvae showing the site of EVs injection (duct of Cuvier) and their main site of arrest (caudal plexus). Bottom panels: Confocal images of Fli1a::eGFP larvae injected with Membright Cy3 labeled Zmel EVs. (D) Schematic representation and confocal images of the caudal plexus of Fli1a::Gal4 UAS::RFP larvae injected with Membright Cy5 Zmel EVs. Large field of view: Z-stack. Zoom: single plane. (E) Schematic representation and confocal images of the caudal plexus of Mpeg::GFP larvae injected with Membright Cy5 Zmel EVs. Large field of view: Z-stack. Zoom: single plane. (F) Schematic representation and confocal images of the caudal plexus of Fli1a::Gal4 UAS::RFP larvae injected with Zmel EVs expressing the fusion protein syntenin2-GFP. Middle panels: Z-projection and single plane images showing arrested and internalized EVs in endothelial cells. Right panels: EVs circulating in the caudal vein at a single time point (upper panel). Temporal projection representing EVs movements (lower panel). *Panel C: from Hyenne, V., Ghoroghi, S., Collot, M., Bons, J., Follain, G., Harlepp, S., Mary, B., Bauer, J., Mercier, L., Busnelli, I., Lefebvre, O., Fekonja, N., Garcia-Leon, M.J., Machado, P., Delalande, F., López, A.A., Silva, S.G., Verweij, F.J., van Niel, G., Djouad, F., Peinado, H., Carapito, C., Klymchenko, A.S., Goetz, J.G., 2019. Studying the fate of tumor extracellular vesicles at high spatiotemporal resolution using the zebrafish embryo. Developmental Cell 48, 554–572.e7. https://doi.org/10.1016/j.devcel.2019.01.014.*

2. Break the tip of the capillary with tweezers to obtain the thinnest capillary tip that can pierce through the yolk sac.
3. Fill the needle with mineral oil using a syringe. It is important to avoid the presence of any bubbles inside the needle as it could affect the quality and reproducibility of the injection. The needle is mounted on a nanoinjector (Drummond Scientific Nanoject II Auto-Nanoliter Injector) (Fig. 2 A2) which allows injecting between 2.3 nL and 69 nL of a solution with a speed of 46 nL/s (fast) or 23 nL/s (slow). The nanoinjector piston is pushed up to two-third of the needle length in order to have enough available volume to aspirate the solution containing the EVs (Fig. 2A).
4. Put 5 µL of fluorescent EVs suspension in 1 × PBS on a parafilm paper placed under the stereomicroscope.
5. Fill the capillary of EV suspension. Avoid air bubbles in the capillary.

3.5 Larvae injection

1. Place the petri dish containing aligned larvae mounted in agarose under the stereomicroscope with their yolk facing the injector and the tip of the needle (Fig. 2B).
2. Gently insert the capillary in the duct of Cuvier, which connects the yolk vasculature to the heart (Fig. 2C). The needle's tip is placed in the vicinity of the circulating blood cell in the blood vessel right under the epidermis that cover the yolk sac.
3. Inject between 23.0 nL and 36.8 nL of EVs, depending on the concentration of EVs and the number of particles you want to inject, in one single injection. Best results are obtained with $5e10^5$ to $1e10^6$ particles per injection. During injection, blood cells that are displaced by the injected volume and pumped by the heartbeat can be visualized under the stereomicroscope (Fig. 2C). These movements are used as readout to control the efficacy of the injection. It is important to ensure that the injected volume is pumped by the heart during injection in order to avoid that the solution of EVs leaks out of the circulatory tract by the wound made by the capillary. Doing so will allow reproducible injections.

4. *In vivo* imaging of circulating EVs in zebrafish larvae: Applications

Once a series of 8–16 larvae are injected, they can be imaged with any microscope allowing fast imaging, ideally with optimal resolution (spinning

disk, single-plane illumination (SPIM), confocal microscopy, etc…). These microscopes should ideally be equipped with a thermostatic chamber heated at 28 °C. Here, we will describe high spatio-temporal imaging of EVs using confocal microscopy (Leica SP5/SP8 equipped with a resonant scanner). Alternatively, spinning disk microscopy proved to be equally efficient (Verweij, Hyenne, et al., 2019; Verweij, Revenu, et al., 2019) and SPIM should in theory also allow non-invasive imaging of circulating EVs over a long period of time (Follain, Mercier, Osmani, Harlepp, & Goetz, 2017). In the next sections, we provide specific microscopy procedures to track: (1) circulating EVs, (2–3) individual EVs right after injection, (4) freshly arrested EVs (5) EVs uptake and (6) the functional consequences of dispersion of tumor EVs. We also show how these procedures can be adapted to the multi-color simultaneous imaging of different EV populations (Hyenne et al., 2019). These imaging sessions are focused on the caudal plexus area of the zebrafish vasculature, which proves to be a perfect region for optimal imaging parameters (speed and resolution). This region is thin and thus easily accessible with single-photon imaging. Furthermore, it is a hotspot for the arrest of circulating tumor cells (Follain, Osmani, Fuchs, et al., 2018; Follain, Osmani, Azevedo, et al., 2018) and EVs (Hyenne et al., 2019).

4.1 Equipment

- Microscope: TCS inverted SP5 with HC PL APO 20 × /0.7 IMM CORR CS objective (Leica) or upright SP8 confocal microscope with an HC FLUOTAR L 25 × /0.95 W VISIR objective (Leica), equipped with a resonant scanner and a thermostatic chamber (28 °C).
- Softwares: SP5/SP8 microscope is equipped with the Leica LAS_AF software version INK 2.7.3.9723. The FIJI/Image J software is used for further image analysis.
- Imaris: Fast tracking of EVs can be performed and rendered using the tracking tool of Imaris.

4.2 Imaging and analysis protocols

4.2.1 High-speed imaging for hemodynamic profiling of circulating EVs

High-speed imaging is mandatory to reveal the accurate hemodynamic profiles of populations of fluorescently labeled EVs in the zebrafish vasculature. Here, we provide examples of how one can reach high-speed

confocal microscopy that is suited for imaging and tracking circulating EVs in the blood flow of zebrafish larvae (as published in Hyenne et al., 2019).

1. Place the glass-bottom petri dish containing zebrafish larvae under the microscope right after injection. Larvae can be either imaged using an inverted or an upright confocal microscope.
2. Use transmitted light and overall fluorescence to focus, if desired, on the caudal plexus region where most of the EVS would accumulate (see Verweij, Hyenne, et al., 2019; Verweij, Revenu, et al., 2019; Hyenne et al., 2019). Such region can be of course adapted to the needs of the study. Imaging at several magnifications is recommended to fully characterize the vascular region of interest with optical sectioning.
3. Lasers are set according to the dyes (Membright, *etc.*) and the transgenic zebrafish strain that are used. We usually use Membright-Cy3 or -Cy5 labeled EVs injected in *Tg(Fli1a::eGFP)*, *Tg(mpeg1::eGFP)* or *Tg(Fli1a::Gal4; UAS::RFP)* fish, respectively, to identify circulating EVs in the vasculature (Fig. 2C–E). Note that the same protocol is used for genetically engineered fluorescent EVs (Fig. 2F). Transmitted light imaging is also used to record and track the displacement of circulating red blood cells (RBCs). Alternatively, one can use the *Tg(gata1::dsRed)* zebrafish line to track circulating RBCs using fluorescence (see Goetz et al., 2014; Hyenne et al., 2019). Finally, two populations of EVs can be imaged simultaneously, for instance, population #1 labeled with MemBright-Cy3, co-injected with population #2 labeled with MemBright-Cy5 in *Tg(Fli1a::eGFP)* fish.
4. Use a resonant scanner (Leica) to reach a frequency of 80–100 frames per second in order to capture the motion of EVs in circulation. This could imply to reduce the image pixel size to 512×32 pixels, for example, focusing on a single arterial or venous vessel. We usually rotate the acquisition region so that a single vessel/vascular region would fit within a 512×32 pixels window (Fig. 3A).
5. Acquire only one Z plane inside the selected vascular region with a pinhole >1 airy unit to capture EVs moving slightly out of the focal plane, for 1 min (Fig. 3A) at optimal scanning speed (to reach 80–100 frames/s, which should allow capturing RBCs and EVs flowing in the dorsal aorta of a 2dpf larvae). RBCs can be imaged at the same time by transmitted light, or by fluorescence using transgenic fish with fluorescent erythrocytes (Gata1::dsRed for instance).

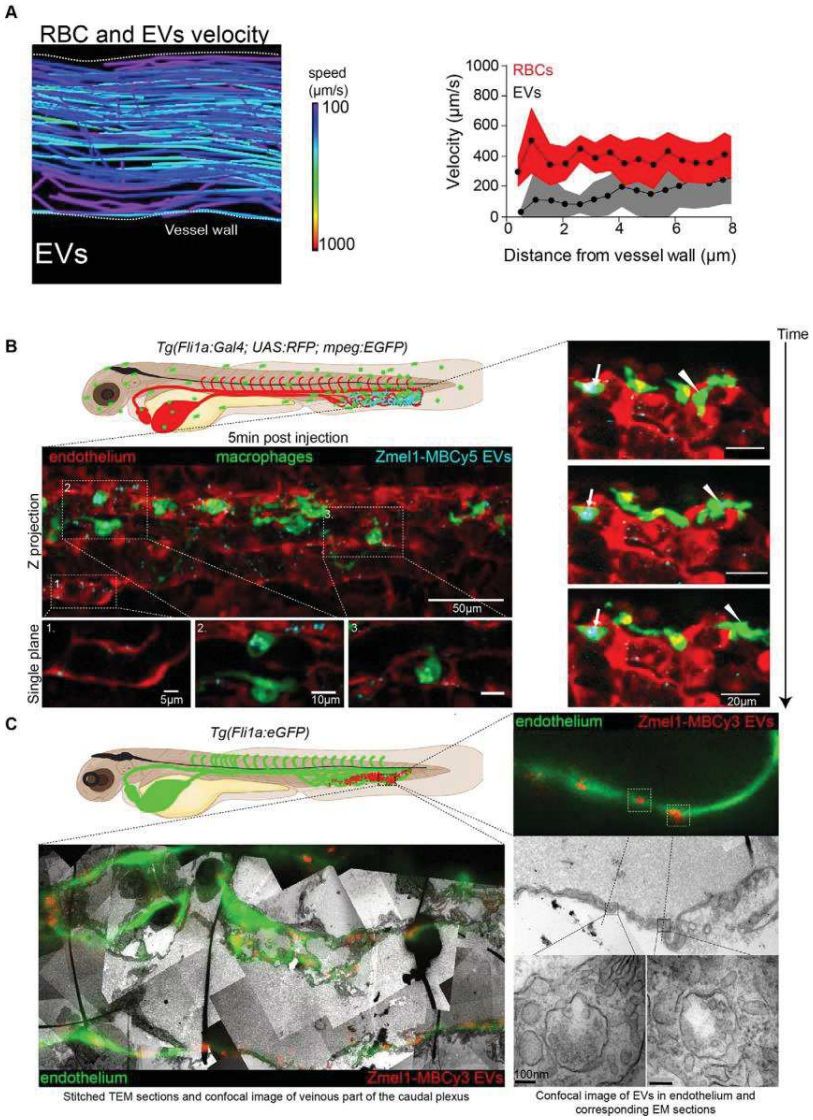

Fig. 3 Dynamic behavior of circulating EVs and fate of internalized EVs. (A) Membright Cy3 4T1 EVs and red blood cells (RBC) tracking in zebrafish caudal plexus: tracking of individual 4T1 EVs in the caudal vein. Right histogram: EVs and RBC velocities (y axis: µm/s) *versus* distance to vessel wall (x axis: µm). (B) Schematic representation and confocal images of double transgenic fish (Fli1a::Gal4 UAS::RFP mpeg::eGFP) injected with Membright Cy5 Zmel EVs. Left panels: 3D stack of caudal plexus region. Zoom: single planes. Right panels: time-lapse showing macrophages (GFP) having internalized

(Continued)

4.2.2 Image analysis

Once movies are recorded, we use FIJI (or Imaris tracking modules) to track RBCs and EVs in motion and process the images. We provide here one possible workflow to analyze these images. We recommend referring to the Imaris tracking modules for optimal tracking parameters and will detail below how we reach accurate tracking of flowing EVs and RBCs using FIJI plugins.

4.2.2.1 Tracking of RBCs

1. Enhance the contrast of the whole stack. Depending on the quality of the image, the Gaussian Blur or Unsharp mask FIJI filters can be used.
2. Execute a Z-projection with average intensity option and subtract the obtained image to the stack. The remaining stack should only display RBCs.
3. Make a binary image of the resulting stack.
4. Apply a bandpass filter with the correct values to remove the background noise and keep only the RBCs.
5. Analyze the obtain stack with the Mosaic 2D/3D particle tracker plugin. For each frame, the position of each blood cell is obtained, and the velocities of each individual track can be visualized (Fig. 3A).

4.2.2.2 Tracking of EVs

1. Use an appropriate threshold to improve the quality of the images (flowing EVs).
2. Make binary images and invert the stack.

Fig. 3—Cont'd Membright Cy5-Zmel EVs (cyan) and moving along the endothelium (red). Arrows: macrophage inside the vasculature. Arrowheads: macrophage carrying EVs and moving outside the vasculature. (C) Schematic representation and illustrative images of a CLEM experiment on a Fli1a:eGFP larvae injected with Membright Cy3-Zmel EVs (Upper left). Lower left panel: superposition of the region of interest imaged with confocal and with electron microscopy. Bottom right panels: Same endothelial region imaged with confocal and with electron microscopy. Magnified areas show that this region contains multivesicular endosomes, which could be the compartments containing internalized EVs. *Panel A: Adapted from Hyenne, V., Ghoroghi, S., Collot, M., Bons, J., Follain, G., Harlepp, S., Mary, B., Bauer, J., Mercier, L., Busnelli, I., Lefebvre, O., Fekonja, N., Garcia-Leon, M.J., Machado, P., Delalande, F., López, A.A., Silva, S.G., Verweij, F.J., van Niel, G., Djouad, F., Peinado, H., Carapito, C., Klymchenko, A.S., Goetz, J.G., 2019. Studying the fate of tumor extracellular vesicles at high spatiotemporal resolution using the zebrafish embryo. Developmental Cell 48, 554–572.e7. https://doi.org/10.1016/j.devcel.2019.01.014.*

3. Use the 2D spot enhancing Filter plugin.
4. Use the stack obtained to make another binarization.
5. Use the Mosaic 2D/3D particle tracker plugin. The position of each EV for each frame is obtained, thus their velocity can be plotted on the image (Fig. 3A).

4.2.2.3 Spatio-temporal analysis of EVs and RBCs within blood vessels

An important parameter to dissect the hemodynamic profiles of EVs is their exact location, and subsequent velocity, within blood vessels when flowing. We previously analyzed the velocity of EVs according to their position within the vessel (Hyenne et al., 2019). Here, we provide a detailed procedure for performing such analysis.

1. Delineate the endothelial wall using the transmitted light (or GFP fluorescence from a *Tg(Fli1a:eGFP)* larvae, and extract the coordinates (into an excel or csv table).
2. Using the temporal analysis of RBCs and EVs velocities (Sections 4.2.2.1 and 4.2.2.2.), extract the coordinates of EVs and RBCs over time.
3. Calculate all the possible distances "d" between EVs (or RBCs) positions (X_{EV} and Y_{EV} or X_{RBC} and Y_{RBC}, respectively) and the closest position of the endothelium (X_{endo} and Y_{endo}).
4. Use these following equations to calculate "d":

$$d = \sqrt{(X_{EV} - X_{endo})^2 + (Y_{EV} - Y_{endo})^2} \text{ or}$$

$$d = \sqrt{(X_{RBC} - X_{endo})^2 + (Y_{RBC} - Y_{endo})^2}$$

5. Keep the smallest distances "d" for each EVs or RBC position.
6. This procedure allows to plot the velocities of RBCs and EVs as a function of the distance from the endothelial wall (Fig. 3A) and thus their position within the vessel.

Such detailed analysis allowed us to make the first hemodynamic profiling of circulating EVs in the zebrafish vasculature (Hyenne et al., 2019). We found that EVs follow a Poiseuille repartition during the circulation in zebrafish vessels. They display high velocity in the middle of the vessel and reduced velocity in the vicinity of endothelial walls, where they drastically slow down and engage rolling and adhesion behaviors. To go further in the analysis of circulating EVs and their interactions with their microenvironment, we complement the dynamic analysis of EVs in movement with fine 3D imaging of arrested EVs in the caudal plexus.

4.2.3 Dissect the mechanisms of EVs arrest with 3D volume imaging

In order to prime metastatic niches (Peinado et al., 2017), circulating EVs are believed to first target specific vascular regions and get internalized by endothelial cells or patrolling macrophages present in the circulation. Whether this is an active or passive process remains to be determined. We provide here means to accurately characterize the intravascular arrest behavior of circulating EVs *in vivo*. Such analysis is based on volume imaging of the zebrafish vasculature concomitantly with arrested EVs. Doing so, we discovered that the vast majority of artificially introduced tumor EVs display a flow-dependent arrest behavior and preferentially stop in low flow venous compartments of the zebrafish vasculature, only 10 min after injection (Hyenne et al., 2019). We also identified the main cell types taking up EVs in zebrafish: endothelial cells and patrolling macrophages. This protocol can also be adapted to image two populations of EVs concomitantly. It could therefore allow comparing simultaneously different profiles of the arrest of natural subpopulations of EVs (*e.g.,* microvesicles and exosomes) or of engineered EVs (*e.g.,* expressing or not an adhesion receptor).

1–3. The three first steps -1. -2. -3. are common with the protocols described in Section 4.2.1.

4. Use a pinhole of 1 airy unit and a z-step of 0.5 µm, acquire an optical confocal section of the entire caudal plexus (Fig. 2D and F, Fig. 3B). Several resolutions can be used and we, for example, apply 512×512 or 1024×1024 pixels imaging (or 512×256, 1024×350 pixels) which are imaging parameters (size) that allow optimal EVs and vasculature imaging (Fig. 2D and E).

5. Perform a maximum intensity Z projection of the stack to visualize the overall distribution of EVs in the caudal plexus. Such analysis allows to attribute EV arrest position with respect to the vessel identity and flow parameters (see Hyenne et al., 2019; Verweij, Hyenne, et al., 2019).

6. Single planes of the stack are selected to confirm the internalization of fluorescent EVs in fish cells (Fig. 2D–F, Fig. 3B).

When combined with imaging acquisition parameters allowing to accurately determine hemodynamic profiles (see Section 3.3), such an analysis allows to correlate hotspots of the arrest of EVs with vascular flow profiles. In addition, this protocol allows to identify the cells internalizing circulating EVs. For example, we routinely inject EVs labeled with Membright dyes in *Tg(Fli1a::eGFP), Tg(mpeg1::eGFP), Tg(Fli1a::Gal4; UAS::RFP)* or *Tg(Fli1a::Gal4; UAS::RFP; mpeg1::GFP)* fish lines (Fig. 2C–F, Fig. 3) as we had identified that patrolling

macrophages, in addition to endothelial cells, are massively engulfing circulating EVs (Hyenne et al., 2019; Verweij, Hyenne, et al., 2019) (Fig. 2D and E, Fig. 3B). Finally, this protocol can be used to compare the preferential arrest sites and target cells of two populations of EVs simultaneously. In this case, two populations of EVs will be labeled with two different dyes in parallel and mixed at the same concentration right before injection in zebrafish larvae (Hyenne et al., 2019).

4.2.4 Visualization of circulating EVs arrest and uptake

Depending on the source of EVs and the identity of the receiving cell, many different mechanisms of EV arrest and uptake have been described. They include direct fusion between EVs and the receiving cell plasma membrane, phagocytosis, macropinocytosis, clathrin-dependent and independent endocytosis and receptor mediated endocytosis. The arrest and internalization of circulating EVs can now be visualized *in vivo* in zebrafish larvae. It can be used to directly test the involvement of a particular EV receptor or to compare the arrest and uptake of different populations of EVs.

1–3. The three first steps -1. -2. -3. are common with the protocols described in Section 4.2.1.

4. Note that for this protocol, it is essential to start imaging right after injection, as quickly as possible, since most of the circulating EVs get internalized in less than 10 min.

5. Make a xyzt time-lapse of the cell of interest. Of note, different settings can be used depending on the dynamic of the internalization. As an example, we previously used the following settings: Short time lapses at 5–10 Z stacks per minute for 1 min with a z-step of 0.5 mm; long time lapses at 1 Z stack per minute for 1 h with a z-step of 2 mm; short time-lapses at 3–8 images per second on single Z planes (Hyenne et al., 2019).

This protocol allowed us to capture events of internalization by endothelial cells and macrophages (Fig. 3B right panel) (Hyenne et al., 2019). Our analysis identified two different mechanisms of EVs uptake by macrophages *in vivo*: endocytosis and a mechanism similar to filopodia surfing (Heusermann et al., 2016; Hyenne et al., 2019). Furthermore, this protocol can be used to track the trafficking of EVs within the receiving cells, from the initial entry of EVs, to their storage compartment.

4.2.5 Identification of the compartments storing internalized EVs

After uptake, EVs are usually trafficked to late endosomes-lysosomes, where they will deliver their cargo or be degraded. Zebrafish larvae are well adapted

to study the fate of circulating EV once they are internalized. Indeed, as zebrafish larvae are permeable, it is possible to visualize the late endosomes-lysosomes by simply adding lysotracker to zebrafish incubating medium.

The following labeling protocol can be added to the protocols Sections 4.2.3 or 4.2.4 described above:

- Add lysoTracker (Thermofisher Scientific) at 5 μM in the DANIEAU medium for 2 h before EVs injection

Another way to study the fate of circulating EVs in zebrafish with the high spatial resolution is to use correlative light electron microscopy (CLEM) (Fig. 3C). Since this protocol has been described elsewhere (Follain, Osmani, Fuchs, et al., 2018; Goetz, Monduc, Schwab, & Vermot, 2015; Hyenne et al., 2019), we will briefly describe the main steps. Living zebrafish larvae are imaged at different magnifications after EVs internalization, with labeling allowing visualization of EVs and a specific cell type (endothelial cells or macrophages for instance) as well as additional anatomical landmarks. Larvae are fixed and processed for serial electron microscopy analysis, using previously described protocols (Follain, Osmani, Fuchs, et al., 2018; Goetz et al., 2015; Hyenne et al., 2019). Using recorded anatomic landmarks, such as the architecture of the vasculature in the caudal plexus, the cell of interest can be retrieved (Fig. 3C). It is then possible to image and reconstruct the 3D volume of the cell of interest at high resolution by serial section electron microscopy or tomography.

These approaches (with their associated protocols described above (in particular Sections 4.2.3 or 4.2.4)) can be instrumental to identify the fate of internalized EVs. In the future, it could contribute to the understanding of the mechanisms of EV cargo transfer.

4.2.6 Functional assay: Priming of metastatic niches

EVs are known to induce phenotypic changes in multiple physiologic and pathologic contexts. The zebrafish larvae can be used to capture these phenotypes in real time and correlate them with the uptake of EVs. While many other possibilities will likely arise in different fields in the coming years, we provide here an example of a functional assay aiming to determine the pro-metastatic potential of tumor EVs. Many studies in mice revealed that intravenous injection of tumor EVs increases the metastatic growth of tumor cells subsequently injected into the circulation (Costa-Silva et al., 2015; Peinado et al., 2012). Here, we detail a protocol allowing to directly image the events occurring after the initial arrival of tumors EVs. In this assay, zebrafish melanoma EVs (Zmel1 EVs) are injected into larvae circulation before the

injection and tracking of Zmel1 td-tomato cells. As a control for EVs, we initially used 100 nm polystyrene beads, but complementary controls should use EVs from non-tumoral cells (*e.g.,* Zebrafish fibroblasts AB9). Afterward, tumor cell growth is monitored over time using longitudinal imaging.

1. Inject a control concentration of (in our case Zmel EVs, 100 nm polystyrene beads (phosphorex) as a control) into the circulation of zebrafish larvae at 32 hpf
2. 14 h after EVs injection, inject tumor cells corresponding to the tEVs secreting cells, in our case, Zmel1 td-Tomato melanoma cells. Tumor cells are prepared as previously described (Follain, Osmani, Fuchs, et al., 2018). Briefly, cells are detached, and a cell suspension is prepared in their culture medium at a 10^8 cells/mL. Between 27.6 and 32 nL of the cell suspension is injected into the fish vasculature.
3. Image the zebrafish caudal plexus with a confocal microscope at different time points to record tumor cells survival and colonization. In our case 24 h, 48 h and 7 days after tumor cell injection (Fig. 4B). Larvae are mounted for imaging and replaced in their growing medium, according to the procedure. Note that in this experiment we use beads as control, in previous work we added a supplemental control injecting EVs coming from zebrafish fibroblasts (AB9 cell line) (Hyenne et al., 2019).

The zebrafish transparency allows to easily visualize the arrest of tumor cells in the circulation at a single cell level (Fig. 4B left panels), to follow extravasation of tumor cells at different time-points (Fig. 4B middle and right panels) and their outgrowth and invasion of surrounding tissues (Fig. 4B right panels).

5. Conclusions

As research in circulating extracellular vesicles grows with developments in diagnosis, biomaterials or fundamental biology, appropriate models are crucial to dissect their behavior in physiologic and pathologic conditions *in vivo*. Unfortunately, a majority of *in vitro* studies have not yet taken into account the hemodynamic environment which circulating EVs use to disseminate and execute their functions. In addition, classical *in vivo* models (such as mice) do not allow to precisely follow EVs dynamics in body fluids. On the contrary, intravascular injection of EVs within the zebrafish larvae allows a non-invasive visualization of individual EVs dispersion, uptake and interactions with cells in the physiological environment of a circulatory system. This methodology is compatible with every type of EVs isolation

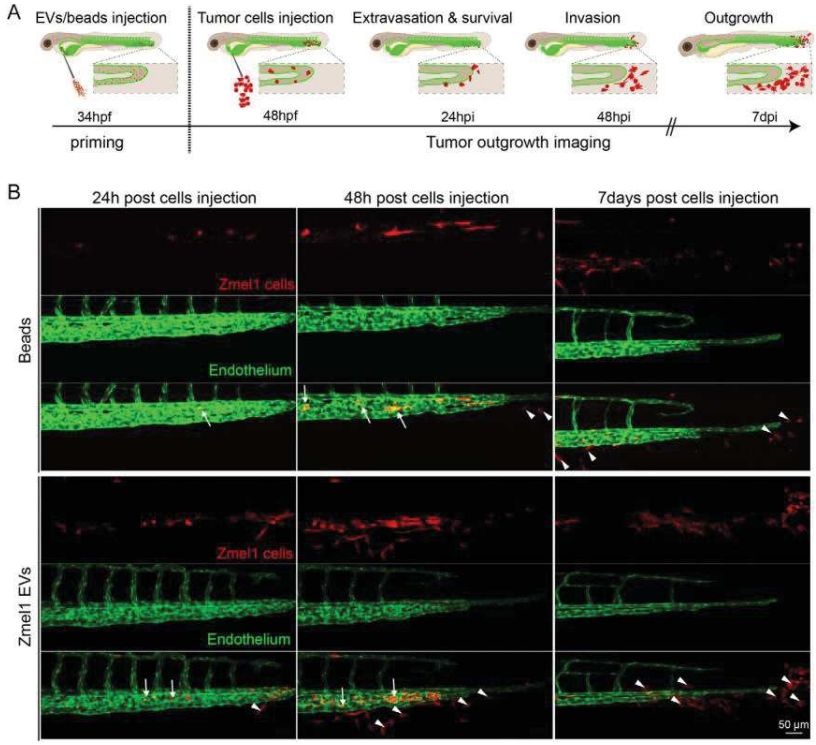

Fig. 4 Example of a functional EVs experiment in zebrafish. (A) Schematic representation a priming experiment protocol in zebrafish. EVs or 100 nm beads are injected in 34 hpf larvae. Tumor cells are injected in 48 hpf larvae. Tumor cell survival and colonization is followed at different time-points. Hptci: hours post tumor cell injection. (B) Confocal images of a representative priming experiment. The growth of Zmel1 tdTomato cells is imaged in Flie1a:eGFP fish at three different time-points after tumor EVs or beads treatments. Arrows: intravascular cells, arrowheads: extravascular cells.

protocol, requires minimum material and basic imaging setup. Ultimately, it is currently the best model to investigate EVs hemodynamics behavior, attachment, uptake and endocytosis by specific cell types *in vivo* (Hyenne et al., 2019; Verweij, Hyenne, et al., 2019).

The methodology described within this chapter is likely to provide fertile grounds for increasing our knowledge and address several important questions:

(1) *How do EVs disseminate through body fluids?* To escape their secreting site and reach distant receiving cells, EVs often need to cross the endothelial barriers. Two processes, transcytosis and endothelial leakage have been

described (Matsumoto et al., 2017; Tominaga et al., 2015). However, the articulation of the two processes and their underlying molecular mechanism remains to be unraveled *in vivo*. In zebrafish, injection of pre-labeled EVs with appropriate dyes, combined with CLEM imaging, could allow to image EVs leaving the blood circulation with high levels of details (Hyenne et al., 2019). High-resolution visualization of EVs inside and outside the zebrafish vasculature will help to understand if EVs reach distant cells as isolated vesicles or if other cells (*e.g.*, macrophages) can help EVs to cross the endothelial barrier (Fig. 3B arrowheads). Furthermore, using CD63-pHLuorin tool (a pH sensitive GFP fused to the CD63 EV marker that is fluorescent only in non-acidic compartments) in zebrafish larvae (Verweij, Hyenne, et al., 2019; Verweij, Revenu, et al., 2019) allows visualizing EVs diffusing from their secreting site and helps to understand how EVs cross the endothelial barrier to reach the circulation. Therefore, zebrafish larvae can be used to track the journey of EVs from their secretion site to their target cells, *via* the blood circulation.

(2) *Which mechanisms control EVs organotropism and uptake?* It is thought that the repertoire of adhesion molecules present on the surface EVs is responsible for specific interactions between EVs and receiving cells, ultimately leading to EVs internalization and cargo delivery. Several molecules, such as integrins (Hoshino et al., 2015), tetraspanins (Nazarenko et al., 2010; Rana, Claas, Kretz, Nazarenko, & Zoeller, 2011; Rana, Yue, Stadel, & Zöller, 2012), heparan sulfate proteoglycans (Purushothaman et al., 2016) and lectins (Barrès et al., 2010; Bruno et al., 2009) have been shown to mediate the interaction between EVs and receiving cells. However, the relative importance and the interplay of these molecules is unknown. Zebrafish model allows comparing and visualizing *in vivo* interaction and internalization of different populations of EVs bearing different membrane proteins. Therefore, it offers the possibility to test the individual or combined role of specific adhesion molecules in circulating EVs arrest and uptake. Furthermore, because pharmacological approaches and genetic manipulation are easily performed in the zebrafish, one can dissect endocytic pathways that control EVs uptake *in vivo* and test pathways previously identified *in vitro* like clathrin-dependent endocytosis or micropinocytosis (Nakase, Kobayashi, Takatani-Nakase, & Yoshida, 2015; Tian et al., 2014). The zebrafish larvae provides a relevant model to test these pathways in realistic physiological environments where hemodynamics forces are taken into account.

(3) *What are the consequences of EVs uptake?* The dynamic of the phenotypic changes induced by EVs uptake on a receiving cell are not fully understood. This is in part due to the lack of appropriate models allowing to visualize the impact of EVs on receiving cells *in vivo*. However, zebrafish larvae offers the possibility to directly correlate the number and timing of EVs uptake to modifications of the phenotype of an individual receiving cell. Various tools could be developed to investigate this question. For instance, we have shown that tumor EVs activate the expression of TNF-α in macrophages in zebrafish (Hyenne et al., 2019). This transgenic line, *Tg(mpeg::mcherry, TNF-α::GFP)* (Nguyen-Chi et al., 2015) can now be used to dissect precisely the consequences of EVs uptake on macrophages phenotypic switch. Similar approaches adapted to other fields of biology could easily be developed in zebrafish. For instance, genetic reporters, such as the Cre-Lox system, which are available in zebrafish (Carney & Mosimann, 2018), could be used to visualize EVs cargo delivery, similarly to what has been done in mice (Zomer et al., 2015).

Finally, we think that the zebrafish model could be a great asset in various fields of EVs research. Indeed, zebrafish models have been developed in several domains (Gut, Reischauer, Stainier, & Arnaout, 2017; Kirchberger, Sturtzel, Pascoal, & Distel, 2017; Torraca & Mostowy, 2018; White, Rose, & Zon, 2013; Xi, Noble, & Ekker, 2011) where circulating tEVs play instrumental roles, such as cancer biology, cardiovascular diseases, neurodegenerative disorders or pathogenic diseases. Therefore, these fields could strongly benefit from studying the role of EVs in zebrafish, which could increase our knowledge on EVs biology in addition to accelerate the development of therapeutic strategies and clinical trials.

Acknowledgments

We thank all members of the Goetz Lab for helpful discussions. We are indebted to Kerstin Richter and Francesca Peri (EMBL, Heidelberg, Germany) as well as to Pauline Hanns and Claudia Lengerke (University Hospital Basel, Switzerland) for supplying zebrafish embryos during the early stages of this work. We are grateful to Camille Hergott and Gregory Khelifi for zebrafish care. We are grateful to R. White (MSKCC, New York, USA) for the Zmel1 (native and tdTomato) cells, as well as to Pascale Zimmerman (CRCM, Marseille, France) for the Syntenin-2 construct. This work was supported by a fellowship from the French Ministry for Research to BM, and by a fellowship from the IDEX (University of Strasbourg) and ARC (Association pour le Recherche sur le Cancer) to SG, by grants from La Ligue contre le Cancer, Cancéropole Grand-Est, INCa (EVRALTIC) and Plan Cancer (VESMATIC) to VH and JGG, and by institutional funds from University of Strasbourg, INSERM to JGG.

References

Adem, B., Vieira, P. F., & Melo, S. A. (2020). Decoding the biology of exosomes in metastasis. *Trends in Cancer*, *6*, 20–30. https://doi.org/10.1016/j.trecan.2019.11.007.

Bakhshandeh, B., Kamaleddin, M., & Aalishah, K. (2016). A comprehensive review on exosomes and microvesicles as epigenetic factors. *CSCR*, *12*, 31–36. https://doi.org/10.2174/1574888X11666160709211528.

Balaj, L., Lessard, R., Dai, L., Cho, Y.-J., Pomeroy, S. L., Breakefield, X. O., et al. (2011). Tumour microvesicles contain retrotransposon elements and amplified oncogene sequences. *Nature Communications*, *2*, 180. https://doi.org/10.1038/ncomms1180.

Barrès, C., Blanc, L., Bette-Bobillo, P., André, S., Mamoun, R., Gabius, H.-J., et al. (2010). Galectin-5 is bound onto the surface of rat reticulocyte exosomes and modulates vesicle uptake by macrophages. *Blood*, *115*, 696–705. https://doi.org/10.1182/blood-2009-07-231449.

Boulanger, C. M., Loyer, X., Rautou, P.-E., & Amabile, N. (2017). Extracellular vesicles in coronary artery disease. *Nature Reviews. Cardiology*, *14*, 259–272. https://doi.org/10.1038/nrcardio.2017.7.

Bruno, S., Grange, C., Deregibus, M. C., Calogero, R. A., Saviozzi, S., Collino, F., et al. (2009). Mesenchymal stem cell-derived microvesicles protect against acute tubular injury. *JASN*, *20*, 1053–1067. https://doi.org/10.1681/ASN.2008070798.

Butler, J. T., Abdelhamed, S., & Kurre, P. (2018). Extracellular vesicles in the hematopoietic microenvironment. *Haematologica*, *103*, 382–394. https://doi.org/10.3324/haematol.2017.183335.

Carney, T. J., & Mosimann, C. (2018). Switch and trace: Recombinase genetics in zebrafish. *Trends in Genetics*, *34*, 362–378. https://doi.org/10.1016/j.tig.2018.01.004.

Cheng, Y., Zeng, Q., Han, Q., & Xia, W. (2019). Effect of pH, temperature and freezing-thawing on quantity changes and cellular uptake of exosomes. *Protein & Cell*, *10*, 295–299. https://doi.org/10.1007/s13238-018-0529-4.

Chuo, S. T.-Y., Chien, J. C.-Y., & Lai, C. P.-K. (2018). Imaging extracellular vesicles: Current and emerging methods. *Journal of Biomedical Science*, *25*, 91. https://doi.org/10.1186/s12929-018-0494-5.

Collot, M., Fam, T. K., Ashokkumar, P., Faklaris, O., Galli, T., Danglot, L., et al. (2018). Ultrabright and Fluorogenic probes for multicolor imaging and tracking of lipid droplets in cells and tissues. *Journal of the American Chemical Society*, *140*, 5401–5411. https://doi.org/10.1021/jacs.7b12817.

Corso, G., Heusermann, W., Trojer, D., Görgens, A., Steib, E., Voshol, J., et al. (2019). Systematic characterization of extracellular vesicle sorting domains and quantification at the single molecule – single vesicle level by fluorescence correlation spectroscopy and single particle imaging. *Journal of Extracellular Vesicles*, *8*(1), 1663043.

Costa-Silva, B., Aiello, N. M., Ocean, A. J., Singh, S., Zhang, H., Thakur, B. K., et al. (2015). Pancreatic cancer exosomes initiate pre-metastatic niche formation in the liver. *Nature Cell Biology*, *17*, 816–826. https://doi.org/10.1038/ncb3169.

Ellett, F., Pase, L., Hayman, J. W., Andrianopoulos, A., & Lieschke, G. J. (2011). mpeg1 promoter transgenes direct macrophage-lineage expression in zebrafish. *Blood*, *117*, e49–e56. https://doi.org/10.1182/blood-2010-10-314120.

Flaumenhaft, R., Mairuhu, A., & Italiano, J. (2010). Platelet- and megakaryocyte-derived microparticles. *Seminars in Thrombosis and Hemostasis*, *36*, 881–887. https://doi.org/10.1055/s-0030-1267042.

Follain, G., Mercier, L., Osmani, N., Harlepp, S., & Goetz, J. G. (2017). Seeing is believing – Multi-scale spatio-temporal imaging towards *in vivo* cell biology. *Journal of Cell Science*, *130*, 23–38. https://doi.org/10.1242/jcs.189001.

Follain, G., Osmani, N., Azevedo, A. S., Allio, G., Mercier, L., Karreman, M. A., et al. (2018). Hemodynamic forces tune the arrest, adhesion, and extravasation of circulating tumor cells. *Developmental Cell*, *45* 33–52.e12. https://doi.org/10.1016/j.devcel.2018.02.015.

Follain, G., Osmani, N., Fuchs, C., Allio, G., Harlepp, S., & Goetz, J. G. (2018). *Using the zebrafish embryo to dissect the early steps of the metastasis Cascade. In A. Gautreau (Ed.), Cell Migration* (pp. 195–211). New York, NY: Methods in Molecular Biology. Springer New York. *https://doi.org/10.1007/978-1-4939-7701-7_15*.

Goetz, J. G., Monduc, F., Schwab, Y., & Vermot, J. (2015). Using correlative light and Electron microscopy to study zebrafish vascular morphogenesis. In C. M. Nelson (Ed.), *Tissue morphogenesis, Methods in Molecular Biology* (pp. 31–46). New York, NY: Springer New York. https://doi.org/10.1007/978-1-4939-1164-6_3.

Goetz, J. G., Steed, E., Ferreira, R. R., Roth, S., Ramspacher, C., Boselli, F., et al. (2014). Endothelial cilia mediate low flow sensing during zebrafish vascular development. *Cell Reports*, *6*, 799–808. https://doi.org/10.1016/j.celrep.2014.01.032.

Görgens, A., Bremer, M., Ferrer-Tur, R., Murke, F., Tertel, T., et al. (2019). Optimisation of imaging flow cytometry for the analysis of single extracellular vesicles by using fluorescence-tagged vesicles as biological reference material. *Journal of Extracellular Vesicles*, *8*(1), 1587567.

Gross, J. C., Chaudhary, V., Bartscherer, K., & Boutros, M. (2012). Active Wnt proteins are secreted on exosomes. *Nature Cell Biology*, *14*, 1036–1045. https://doi.org/10.1038/ncb2574.

Gut, P., Reischauer, S., Stainier, D. Y. R., & Arnaout, R. (2017). Little fish, big data: Zebrafish as a model for cardiovascular and metabolic disease. *Physiological Reviews*, *97*, 889–938. https://doi.org/10.1152/physrev.00038.2016.

Heilmann, S., Ratnakumar, K., Langdon, E. M., Kansler, E. R., Kim, I. S., Campbell, N. R., et al. (2015). A quantitative system for studying metastasis using transparent zebrafish. *Cancer Research*, *75*, 4272–4282. https://doi.org/10.1158/0008-5472.CAN-14-3319.

Herwig, L., Blum, Y., Krudewig, A., Ellertsdottir, E., Lenard, A., Belting, H.-G., et al. (2011). Distinct Cellular Mechanisms of Blood Vessel Fusion in the Zebrafish Embryo. *Current Biology*, *21*, 1942–1948. https://doi.org/10.1016/j.cub.2011.10.016.

Heusermann, W., Hean, J., Trojer, D., Steib, E., von Bueren, S., Graff-Meyer, A., et al. (2016). Exosomes surf on filopodia to enter cells at endocytic hot spots, traffic within endosomes, and are targeted to the ER. *The Journal of Cell Biology*, *213*, 173–184. https://doi.org/10.1083/jcb.201506084.

Hood, J. L., Roman, S. S., & Wickline, S. A. (2011). Exosomes released by melanoma cells prepare sentinel lymph nodes for tumor metastasis. *Cancer Research*, *71*(11), 3792–3801.

Hoshino, A., Costa-Silva, B., Shen, T.-L., Rodrigues, G., Hashimoto, A., Tesic Mark, M., et al. (2015). Tumour exosome integrins determine organotropic metastasis. *Nature*, *527*, 329–335. https://doi.org/10.1038/nature15756.

Hoshino, D., Kirkbride, K. C., Costello, K., Clark, E. S., Sinha, S., Grega-Larson, N., et al. (2013). Exosome secretion is enhanced by invadopodia and drives invasive behavior. *Cell Reports*, *5*, 1159–1168. https://doi.org/10.1016/j.celrep.2013.10.050.

Hyenne, V., Ghoroghi, S., Collot, M., Bons, J., Follain, G., Harlepp, S., et al. (2019). Studying the fate of tumor extracellular vesicles at high spatiotemporal resolution using the zebrafish embryo. *Developmental Cell*, *48*, 554–572.e7. https://doi.org/10.1016/j.devcel.2019.01.014.

Hyenne, V., Lefebvre, O., & Goetz, J. G. (2017). Going live with tumor exosomes and microvesicles. *Cell Adhesion & Migration*, *11*, 173–186. https://doi.org/10.1080/19336918.2016.1276694.

Johnsen, K. B., Gudbergsson, J. M., Andresen, T. L., & Simonsen, J. B. (2019). What is the blood concentration of extracellular vesicles? Implications for the use of extracellular

vesicles as blood-borne biomarkers of cancer. *Biochimica et Biophysica Acta, Reviews on Cancer*, *1871*, 109–116. https://doi.org/10.1016/j.bbcan.2018.11.006.

Karimi, N., Cvjetkovic, A., Jang, S. C., Crescitelli, R., Hosseinpour Feizi, M. A., Nieuwland, R., et al. (2018). Detailed analysis of the plasma extracellular vesicle proteome after separation from lipoproteins. *Cellular and Molecular Life Sciences*, *75*, 2873–2886. https://doi.org/10.1007/s00018-018-2773-4.

Karlsson, J., von Hofsten, J., & Olsson, P.-E. (2001). Generating transparent zebrafish: A refined method to improve detection of gene expression during embryonic development. *Marine Biotechnology*, *3*, 0522–0527. https://doi.org/10.1007/s1012601-0053-4.

Keller, M. D., Ching, K. L., Liang, F.-X., Dhabaria, A., Tam, K., Ueberheide, B. M., et al. (2020). Decoy exosomes provide protection against bacterial toxins. *Nature*, *579*, 260–264. https://doi.org/10.1038/s41586-020-2066-6.

Kirchberger, S., Sturtzel, C., Pascoal, S., & Distel, M. (2017). Quo natas, danio?—recent progress in modeling Cancer in zebrafish. *Frontiers in Oncology*, 7, 186. https://doi.org/10.3389/fonc.2017.00186.

Kowal, J., Arras, G., Colombo, M., Jouve, M., Morath, J. P., Primdal-Bengtson, B., et al. (2016). Proteomic comparison defines novel markers to characterize heterogeneous populations of extracellular vesicle subtypes. *Proceedings National Academy of Sciences United States of America*, *113*, E968–E977. https://doi.org/10.1073/pnas.1521230113.

Lai, C. P., Kim, E. Y., Badr, C. E., Weissleder, R., Mempel, T. R., Tannous, B. A., et al. (2015). Visualization and tracking of tumour extracellular vesicle delivery and RNA translation using multiplexed reporters. *Nature Communications*, *6*, 7029. https://doi.org/10.1038/ncomms8029.

Lai, C. P., Mardini, O., Ericsson, M., Prabhakar, S., Maguire, C. A., Chen, J. W., et al. (2014). Dynamic biodistribution of extracellular vesicles *in Vivo* using a multimodal imaging reporter. *ACS Nano*, *8*, 483–494. https://doi.org/10.1021/nn404945r.

Lamason, R. L., Mohideen, M. A. P. K., Mest, J. R., Wong, A. C., Norton, H. L., Aros, M. C., et al. (2005). SLC24A5, a putative cation exchanger, affects pigmentation in zebrafish and humans. *Science*, *310*, 1782–1786. https://doi.org/10.1126/science.1116238.

Lawson, N. D., & Weinstein, B. M. (2002). In Vivo Imaging of Embryonic Vascular Development Using Transgenic Zebrafish. *Developmental Biology*, *248*, 307–318. https://doi.org/10.1006/dbio.2002.0711.

Lázaro-Ibáñez, E., Lässer, C., Shelke, G. V., Crescitelli, R., Jang, S. C., Cvjetkovic, A., et al. (2019). DNA analysis of low- and high-density fractions defines heterogeneous subpopulations of small extracellular vesicles based on their DNA cargo and topology. *Journal of Extracellular Vesicles*, *8*, 1656993. https://doi.org/10.1080/20013078.2019.1656993.

Matsumoto, J., Stewart, T., Sheng, L., Li, N., Bullock, K., Song, N., et al. (2017). Transmission of α-synuclein-containing erythrocyte-derived extracellular vesicles across the blood-brain barrier via adsorptive mediated transcytosis: Another mechanism for initiation and progression of Parkinson's disease? *Acta Neuropathologica Communications*, *5*, 71. https://doi.org/10.1186/s40478-017-0470-4.

Matsumoto, A., Takahashi, Y., Chang, H. Y., Wu, Y. W., Yamamoto, A., Ishihama, Y., et al. (2020). Blood concentrations of small extracellular vesicles are determined by a balance between abundant secretion and rapid clearance. *Journal of Extracellular Vesicles*, *9*, 1696517. https://doi.org/10.1080/20013078.2019.1696517.

Matusek, T., Wendler, F., Polès, S., Pizette, S., D'Angelo, G., Fürthauer, M., et al. (2014). The ESCRT machinery regulates the secretion and long-range activity of Hedgehog. *Nature*, *516*, 99–103. https://doi.org/10.1038/nature13847.

Mol, E. A., Goumans, M.-J., Doevendans, P. A., Sluijter, J. P. G., & Vader, P. (2017). Higher functionality of extracellular vesicles isolated using size-exclusion chromatography

compared to ultracentrifugation. *Nanomedicine: Nanotechnology, Biology and Medicine*, *13*, 2061–2065. https://doi.org/10.1016/j.nano.2017.03.011.

Nakase, I., Kobayashi, N. B., Takatani-Nakase, T., & Yoshida, T. (2015). Active macropinocytosis induction by stimulation of epidermal growth factor receptor and oncogenic Ras expression potentiates cellular uptake efficacy of exosomes. *Scientific Reports*, *5*, 10300. https://doi.org/10.1038/srep10300.

Nazarenko, I., Rana, S., Baumann, A., McAlear, J., Hellwig, A., Trendelenburg, M., et al. (2010). Cell surface Tetraspanin Tspan8 contributes to molecular pathways of exosome-induced endothelial cell activation. *Cancer Research*, *70*, 1668–1678. https://doi.org/10.1158/0008-5472.CAN-09-2470.

Nguyen-Chi, M., Laplace-Builhe, B., Travnickova, J., Luz-Crawford, P., Tejedor, G., Phan, Q. T., et al. (2015). Identification of polarized macrophage subsets in zebrafish. *eLife*, *4*, e07288 https://doi.org/10.7554/eLife.07288.

Nielsen, M. H., Beck-Nielsen, H., Andersen, M. N., & Handberg, A. (2014). A flow cytometric method for characterization of circulating cell-derived microparticles in plasma. *Journal of Extracellular Vesicles*, *3*, 20795. https://doi.org/10.3402/jev.v3.20795.

Peinado, H., Alečković, M., Lavotshkin, S., Matei, I., Costa-Silva, B., Moreno-Bueno, G., et al. (2012). Melanoma exosomes educate bone marrow progenitor cells toward a pro-metastatic phenotype through MET. *Nature Medicine*, *18*, 883–891. https://doi.org/10.1038/nm.2753.

Peinado, H., Zhang, H., Matei, I. R., Costa-Silva, B., Hoshino, A., Rodrigues, G., et al. (2017). Pre-metastatic niches: Organ-specific homes for metastases. *Nature Reviews Cancer*, *17*, 302–317.

Purushothaman, A., Bandari, S. K., Liu, J., Mobley, J. A., Brown, E. E., & Sanderson, R. D. (2016). Fibronectin on the surface of myeloma cell-derived exosomes mediates exosome-cell interactions. *The Journal of Biological Chemistry*, *291*, 1652–1663. https://doi.org/10.1074/jbc.M115.686295.

Rana, S., Claas, C., Kretz, C. C., Nazarenko, I., & Zoeller, M. (2011). Activation-induced internalization differs for the tetraspanins CD9 and Tspan8: Impact on tumor cell motility. *The International Journal of Biochemistry & Cell Biology*, *43*, 106–119. https://doi.org/10.1016/j.biocel.2010.10.002.

Rana, S., Yue, S., Stadel, D., & Zöller, M. (2012). Toward tailored exosomes: The exosomal tetraspanin web contributes to target cell selection. *The International Journal of Biochemistry & Cell Biology*, *44*, 1574–1584. https://doi.org/10.1016/j.biocel.2012.06.018.

Simonsen, J. B. (2019). Pitfalls associated with lipophilic fluorophore staining of extracellular vesicles for uptake studies. *Journal of Extracellular Vesicles*, *8*, 1582237. https://doi.org/10.1080/20013078.2019.1582237.

Stranska, R., Gysbrechts, L., Wouters, J., Vermeersch, P., Bloch, K., Dierickx, D., et al. (2018). Comparison of membrane affinity-based method with size-exclusion chromatography for isolation of exosome-like vesicles from human plasma. *Journal of Translational Medicine*, *16*, 1. https://doi.org/10.1186/s12967-017-1374-6.

Takahashi, Y., Nishikawa, M., Shinotsuka, H., Matsui, Y., Ohara, S., Imai, T., et al. (2013). Visualization and in vivo tracking of the exosomes of murine melanoma B16-BL6 cells in mice after intravenous injection. *Journal of Biotechnology*, *165*(2), 77–84.

Takov, K., Yellon, D. M., & Davidson, S. M. (2017). Confounding factors in vesicle uptake studies using fluorescent lipophilic membrane dyes. *Journal of Extracellular Vesicles*, *6*(1), 1388731.

Théry, C., Amigorena, S., Raposo, G., & Clayton, A. (2006). Isolation and characterization of exosomes from cell culture supernatants and biological fluids. *Current Protocols in Cell Biology*, *30*, 3.22.1–3.22.29. https://doi.org/10.1002/0471143030.cb0322s30.

Tian, T., Zhu, Y.-L., Zhou, Y.-Y., Liang, G.-F., Wang, Y.-Y., Hu, F.-H., et al. (2014). Exosome uptake through Clathrin-mediated endocytosis and macropinocytosis and mediating miR-21 delivery. *The Journal of Biological Chemistry*, *289*, 22258–22267. https://doi.org/10.1074/jbc.M114.588046.

Tominaga, N., Kosaka, N., Ono, M., Katsuda, T., Yoshioka, Y., Tamura, K., et al. (2015). Brain metastatic cancer cells release microRNA-181c-containing extracellular vesicles capable of destructing blood–brain barrier. *Nature Communications*, *6*, 6716. https://doi.org/10.1038/ncomms7716.

Torraca, V., & Mostowy, S. (2018). Zebrafish infection: From pathogenesis to cell biology. *Trends in Cell Biology*, *28*, 143–156. https://doi.org/10.1016/j.tcb.2017.10.002.

Traver, D., Paw, B. H., Poss, K. D., Penberthy, W. T., Lin, S., & Zon, L. I. (2003). Transplantation and in vivo imaging of multilineage engraftment in zebrafish bloodless mutants. *Nature Immunology*, *4*, 1238–1246. https://doi.org/10.1038/ni1007.

van der Vos, K. E., Abels, E. R., Zhang, X., Lai, C., Carrizosa, E., Oakley, D., et al. (2016). Directly visualized glioblastoma-derived extracellular vesicles transfer RNA to microglia/macrophages in the brain. *Neuro-Oncology*, *18*, 58–69. https://doi.org/10.1093/neuonc/nov244.

Verweij, F. J., Hyenne, V., Van Niel, G., & Goetz, J. G. (2019). Extracellular vesicles: Catching the light in zebrafish. *Trends in Cell Biology*, *29*, 770–776. https://doi.org/10.1016/j.tcb.2019.07.007.

Verweij, F. J., Revenu, C., Arras, G., Dingli, F., Loew, D., Pegtel, D. M., et al. (2019). Live tracking of inter-organ communication by endogenous exosomes in vivo. *Developmental Cell*, *48* 573–589.e4. https://doi.org/10.1016/j.devcel.2019.01.004.

White, R., Rose, K., & Zon, L. (2013). Zebrafish cancer: The state of the art and the path forward. *Nature Reviews Cancer*, *13*, 624–636. https://doi.org/10.1038/nrc3589.

White, R. M., Sessa, A., Burke, C., Bowman, T., LeBlanc, J., Ceol, C., et al. (2008). Transparent adult zebrafish as a tool for in vivo transplantation analysis. *Cell Stem Cell*, *2*, 183–189. https://doi.org/10.1016/j.stem.2007.11.002.

Whitham, M., Parker, B. L., Friedrichsen, M., Hingst, J. R., Hjorth, M., Hughes, W. E., et al. (2018). Extracellular vesicles provide a means for tissue crosstalk during exercise. *Cell Metabolism*, *27* 237–251.e4. https://doi.org/10.1016/j.cmet.2017.12.001.

Wiklander, O. P. B., Nordin, J. Z., O'Loughlin, A., Gustafsson, Y., Corso, G., Mäger, I., et al. (2015). Extracellular vesicle in vivo biodistribution is determined by cell source, route of administration and targeting. *Journal of Extracellular Vesicles*, *4*, 26316. https://doi.org/10.3402/jev.v4.26316.

Willms, E., Cabañas, C., Mäger, I., Wood, M. J. A., & Vader, P. (2018). Extracellular vesicle heterogeneity: Subpopulations, isolation techniques, and diverse functions in Cancer progression. *Frontiers in Immunology*, *9*, 738. https://doi.org/10.3389/fimmu.2018.00738.

Xi, Y., Noble, S., & Ekker, M. (2011). Modeling Neurodegeneration in Zebrafish. *Current Neurology and Neuroscience Reports*, *11*, 274–282. https://doi.org/10.1007/s11910-011-0182-2.

Yáñez-Mó, M., Siljander, P. R.-M., Andreu, Z., Zavec, A. B., Borràs, F. E., Buzas, E. I., et al. (2015). Biological properties of extracellular vesicles and their physiological functions. *Journal of Extracellular Vesicles*, *4*, 27066. https://doi.org/10.3402/jev.v4.27066.

Yang, D., Zhang, W., Zhang, H., Zhang, F., Chen, L., Ma, L., et al. (2020). Progress, opportunity, and perspective on exosome isolation - efforts for efficient exosome-based theranostics. *Theranostics*, *10*, 3684–3707. https://doi.org/10.7150/thno.41580.

Yuan, H., Zhou, J., Deng, M., Zhang, Y., Chen, Y., Jin, Y., et al. (2011). Sumoylation of CCAAT/enhancer–binding protein α promotes the biased primitive hematopoiesis of zebrafish. *Blood*, *117*, 7014–7020. https://doi.org/10.1182/blood-2010-12-325712.

Zhao, F., Cheng, L., Shao, Q., Chen, Z., Lv, X., Li, J., et al. (2020). Characterization of serum small extracellular vesicles and their small RNA contents across humans, rats, and mice. *Scientific Reports*, *10*, 4197. https://doi.org/10.1038/s41598-020-61098-9.

Zomer, A., Maynard, C., Verweij, F. J., Kamermans, A., Schäfer, R., Beerling, E., et al. (2015). In vivo imaging reveals extracellular vesicle-mediated Phenocopying of metastatic behavior. *Cell*, *161*, 1046–1057. https://doi.org/10.1016/j.cell.2015.04.042.

DISCUSSION

Between 20%-30% of women with breast cancer will develop metastasis which is the main reason for patient mortality (Harbeck et al. 2019). The therapeutic limitations of breast cancer metastasis warrant a deeper understanding of its molecular machinery. This is the reason why a large amount of research is currently focused on improving the knowledge on the biological and molecular mechanisms underlying the metastatic processes in breast cancer. Tumor EVs (Graça Raposo and Stahl 2019) have been shown as essential players in the initiation, progression and metastatic cascade in breast cancer (Adem, Vieira, and Melo 2020). The levels of tumor secreted EVs correlate with tumor aggressiveness, however, the link between EV secretion mechanisms and their capacity to form pre-metastatic niches remains unknown. Thus, it's crucial to focus on how the EV secretion machinery regulates the pro-metastatic properties of tEVs. During my PhD, the main goal of my project was to understand the mechanisms by which two GTPases (RalA/B) control exosome secretion and to determine how this affects breast cancer progression and metastasis. The main results from my project are illustrated in Figure. 13:

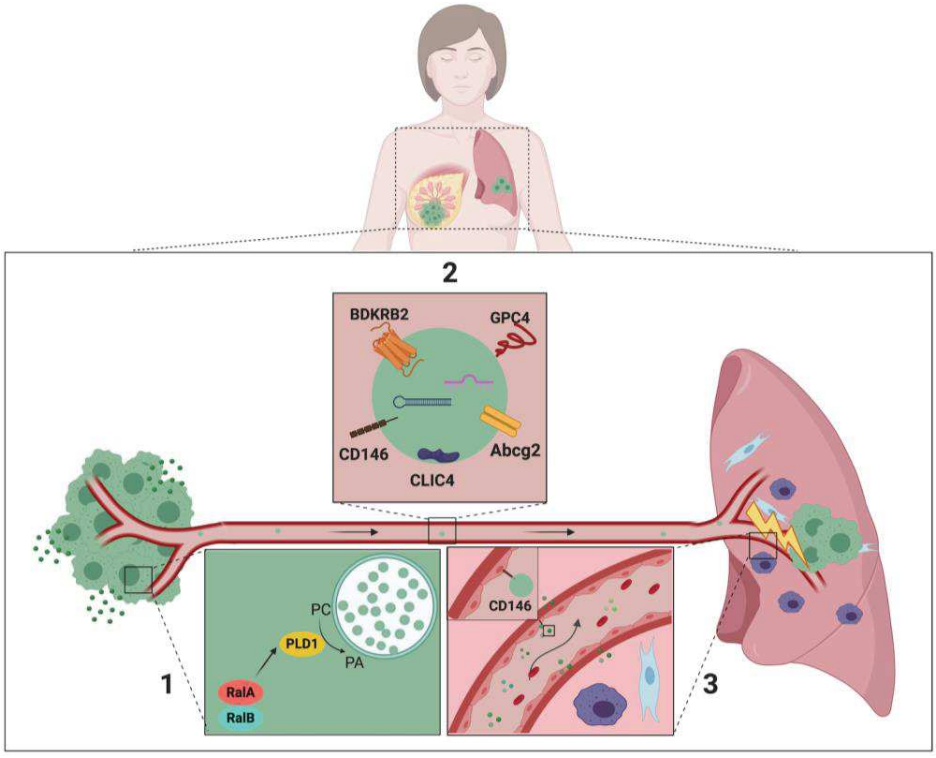

Figure 13. Model describing the role of RalA/B dependent EVs in metastatic formation. 1) Ral GTPases control PLD1 localization on MVBs, which is required for MVB homeostasis and exosome secretion, 2) Ral GTPases control the pro-metastatic function of EVs by modulating their content, 3) Ral GTPases promote the secretion CD146-enriched EVs, whose lung tropism sustains efficient metastasis. Created with BioRender.com

In the following section, I will discuss my major findings in relation to the existing literature. I will also discuss the possible limitations of my study, and potential perspectives to be explored.

Ral GTPases control PLD1 localization on MVBs, which is required for MVB homeostasis and exosome secretion

We observed **Ral depleted cells secrete much less EVs** in 4T1 cells and using chemical inhibitors of Ral (RBC8 and BQU57) we also showed a decrease in EV secretion with other cancer cell types. Theodorescu's group identified these small compounds that could bind to a site in the GDP-bound form of Ral GTPases and lock them in their inactive GDP-bound state. Both of these inhibitors target Ral-GDP to make it unavailable to its effectors(C. Yan et al. 2014). Then, we also found that **depletion of either RalA or RalB significantly reduces the number of MVBs** in the cytoplasm, suggesting that these genes are controlling MVB homeostasis in breast mammary tumor cells. Recently, other studies also suggested that chemical or electric stimulation of MVB biogenesis results in increased EV secretion (D. Yang et al. 2020; Kanemoto et al. 2016). Another study showed, leptin treatment (a well-known adipokine implicated in mammary tumorigenesis) promoted the number of MVBs in the cytoplasm of breast cancer cells and lead to an increased EV secretion(Giordano et al. 2020). Overall, this suggests that there is a direct correlation between MVB density and levels of secreted EVs. To test whether RalA/B were acting on exosome secretion by controlling PLD activities, we showed **Ral and PLD1 localized to the similar endosomal compartment. On the contrary, PLD2 mostly localizes to the plasma membrane**. In general, PLD1 localizes at intracellular compartments, such as the endosome, the Golgi complex, lysosome, and exocytotic vesicles (Jenkins and Frohman 2005), whereas PLD2 was shown to be mainly localized at the plasma membrane (Jenkins and Frohman 2005). Then, using specific chemical inhibitors we showed that either **inhibition of PLD1 or inhibition of PLD2 reduces EV secretion** levels in 4T1 cells. Interestingly, while PLD2 inhibition was found to impact EVs secretion in a cell line model of human mammary carcinoma (MCF-7) (Ghossoub et al. 2014), our data rather suggest that PLD1 or PLD2 controls EVs secretion in 4T1 cells. However, the electron microscopy analysis of these cells revealed that **inhibition of PLD1, but not of PLD2,**

induces a 40% decrease in the number of MVBs per cytoplasmic surface. **Thus, the question is: do PLD isoforms regulate EV secretion potentially through distinct mechanisms?** PLD2 mostly localize to the plasma membrane, we could imagine it affect EV secretion from the plasma membrane by controlling MVs secretion. Due to heterogeneity in EV population, lack of ability to purify EV subtypes to 100% homogeneity, and absence of specific protein markers for identification of different EVs subtypes; we don't have a clear answer to this question yet. The other possibility could be that drugs at high concentration (10 μM) may not be specific to one PLD, but target both PLD1 and PLD2. To solve non-specific action of drug we can either use specific siRNA against each gene, or a lower concentration to inhibit PLD1 or PLD2. Next, we observed that in **40% of shRalA or shRalB cells, PLD1 is uniformly cytoplasmic instead of being endosomal.** This shows that RalA/B are required for PLD1 localization on endosomes. In the similar experiment, we also looked into PLD2 localization and observed PLD2 mostly appeared on the plasma membrane and sometimes as cytoplasmic puncta. However, in the cells that were depleted for RalA/B we observed an increased accumulation of cytoplasmic puncta. We can conclude RalA/B control localization of PLD1 on MVB and it seems they could also affect PLD2 trafficking to the plasma membrane. However, how does RalA/B affect the dynamic of PLD2 need more analysis. Altogether, we showed RalA/B control PLD1 localization on MVBs, which could be required for local phosphatidic acid (PA) accumulation. We failed to detect PA in the living 4T1 cell by testing biosensor constructs (Nicolas Vitale) that specifically binds to PA (data not shown). Then, we quantified EVs lipids and found that **RalA/B depletion significantly reduces the PA/PC ratio of secreted EVs**. As mentioned previously, ILV formation requires enzymatic modification of lipids on the MVB membrane thus underline the important role of specific lipids and lipid-related enzymes in this process (Scott, Vacca, and Gruenberg 2014). Specific lipid classes involved in ILV formation are ceramide, lysophospholipids and PA, whose accumulation in membranes promote the formation of lipid microdomain and membrane invagination (Record et al. 2018). PA is a phospholipid characterized by a small and negative polar head. PA increased level during membrane rearrangement generates negative membrane curvature. In addition to PLD, diacylglycerol kinase α (DGKα) is also responsible for PA synthesis and seems to function antagonistically to PLDs, as it negatively regulates the formation of mature MVBs and the secretion of exosomes in T lymphocytes (Roberto Alonso et al. 2005; R. Alonso et al. 2011). PA

is a pleiotropic bioactive lipid, which can activate or locally recruit specific proteins (Kooijman et al. 2003; 2005). Because it interacts with cytosolic proteins, PA could also work as an anchor for their sorting into exosome. For example, it has been shown that PA directly binds syntenin and induce negative membrane curvature, thereby favoring ILV budding and exosome secretion (Ghossoub et al. 2014; Kooijman et al. 2005). Thus, further work is required to determine how the Ral-PLD1-PA axis is connected to other known machineries of ILV biogenesis. In addition, there is evidence that RAS mediates the activation of PLD (Jiang et al. 1995) but whether RAS might function in exosome biogenesis and cargo-loading by acting on the Ral-PLD-PA axis is important to be determined. Ral could also function through other effectors; one appealing candidate could be Cortactin. Ral activity regulates the tyrosine phosphorylation of cortactin (Goi et al. 2000), which has been known to promote exosome secretion as an actin-binding protein by controlling branched actin dynamics (Sinha et al. 2016), it would also be interesting to know how cortactin controls EV secretion in the absence of Ral. Altogether identification of Ral GTPase and other small GTPases, in the regulation of exosome biogenesis and secretion raises many questions. How d**o Ral GTPase and other molecular machineries for exosome biogenesis act together and coordinate in the same cell type or even within the same MVB? And how do these different molecular machineries link to heterogeneous populations of EVs?** we can address these questions by a combination of different strategies such as genetic co-depletion of parallel pathways, immunodetection of specific cargo and morphological analysis of MVBs by electron microscopy, as well as molecular and physical characterization of secreted EVs.

Ral GTPases control the pro-metastatic function of EVs, likely by modulating their content

Having identified RalA and RalB as important regulators of EV secretion in breast cancer cells, we next wondered whether such a function could impact metastasis. Thus, using orthotopic tumor cell injection in syngeneic mice, we observed that **RalA depletion significantly increased tumor growth, while RalB depletion induced the opposite effect when compared to control tumors**. According to the literature, in the absence of either RalA or RalB, there is no effect or a decrease in the growth of primary tumor (C. Yan and Theodorescu 2018; Moghadam et al. 2017). There is only one study where the loss of RalA leads to an increase in the proliferation *in vitro*, in mouse embryonic fibroblasts (MEFs) (Peschard et al. 2012). It seems that the role of different Ral proteins is tumor-type specific, but how exactly RalA and RalB contribute to tumor growth

downstream of Ras activation need further investigation. In contrast, depletion of RalA and RalB increased the growth rate of 4T1 cells *in vitro*, while a similar increase in proliferation rates was observed *in vivo* in the absence of RalA. We should also consider that cell proliferation *in vitro* does not necessarily represent normal physiologic behavior and may lead to different cellular behavior *in vivo*. Therefore, while depletion of RalA favors *in vivo* tumor growth by enhancing 4T1 proliferation potential, it is likely that additional non-cell autonomous factors are responsible for the decreased tumor growth observed upon RalB depletion. We obtained the most remarkable result when carefully assessing the lung metastasis burden of these mice after 41 days. Compared to other subtypes of breast cancer, triple-negative is highly associated with lung metastasis (D. Gao et al. 2009). Our 4T1 native cells also mimic human triple-negative subtype. We thus decided to assess lung metastasis **from both shRalA and shRalB orthotopic tumors. We observed a reduced lung metastatic burden from Ral-depleted cells compared to the control**. In contrast to our study, it has been shown that knockdown of neither RalA nor RalB affects bone metastasis of a human breast cancer cell line (MDA-MB-231) in athymic nude mice (Yin et al. 2007). This different result could be attributed to the cell type and the model, which are not similar to those of our study; suggesting the role of RalA or RalB in metastasis might be tumor-type specific and dedicating specific functions to either Ral protein in cancer should be done carefully.

Performing 2D and 3D *in vitro* invasion assays, we observed no effect of RalA or RalB expression levels on motility potential of 4T1 cells. Therefore, RalA/B seem to promote metastasis non-cell autonomously, likely by inducing pro-metastatic microenvironmental changes. This result prompted us to further dissect whether RalA or RalB could tune the priming of pre-metastatic niches and observed that **control EVs significantly enhances lung metastasis when compared to PBS. In contrast, priming of mouse lungs with a similar number of EVs from Ral-depleted cells did not promote metastasis.** Precisely dissecting the mechanisms by which tEVs reach specific organs would allow to understand the priming of premetastatic niches. **However, further studies are also needed to understand how the lungs are changed after priming with 4T1 EVs?** to address this question we should check the composition of the pre-metastatic niche compared to normal lungs such as immune cells, ECM component, stromal and endothelial cells since they have a key role in pre-metastatic niche formation.

To unravel why EVs from Ral-depleted cells are unable to promote metastasis, we first determined their capacity to efficiently reach lungs and tracked the dissemination of fluorescently labeled EVs that were injected in the blood circulation of Balb/C mice. Due to EVs short half-life in the circulation (~2 min) (Morishita et al. 2015; Saunderson et al. 2014), one hour after injection we checked and **found 4T1 EVs mostly accumulate in the lungs. Importantly, EVs from RalA/B knockdown cells failed to efficiently reach the lungs**, even though a similar amount were injected in all conditions. Similarly, upon tracking of fluorescent EVs injected in the circulation of zebrafish embryos, we observed that endothelial arrest of EVs from RalA/B knockdown cells is significantly hampered suggesting that RalA/B knockdown reduced the adhesive properties of EVs, to the endothelium, establishing a potential link with their failure to accumulate in mice lungs. Through a careful analysis of cell types that internalize EVs in these conditions, we observed that 4T1 EVs mostly accumulate in endothelial cells, macrophages and fibroblasts of the lung parenchyma. **Now the question is how can fibroblasts and other cells take up EVs, while they are not in contact with the circulation?** how tEV pass the endothelial barrier is not very well known yet. However, recently it has been shown that tEVs could reach cells distant from blood vessels by mechanisms such as transcytosis or vascular leakiness (Morad et al. 2019; Adem, Vieira, and Melo 2020). We have tested the capacity of RalA/B dependent EVs to promote vascular leakiness *in vitro* by exposing endothelial cells to similar amounts of EVs derived from 4T1 cells expressing or not RalA/B. Interestingly, endothelial monolayers became less permeable when treated with a similar amount of EVs from shRalA or shRalB cells compare to the shControl. However, this test needs to be done *in vivo* as well to provide a better understanding of EVs behavior in circulation. **Another question is what could be the fate of EVs that failed to accumulate in the lung especially EVs from RalA/B knockdown cells?** based on the previous finding we can imagine the clearance of these EVs from the circulation could depend on myeloid cells — particularly macrophages in zebrafish (Hyenne et al. 2019) and neutrophils in mice (Chennakrishnaiah et al. 2018) — that are present in blood vessels and on endothelial cells. In addition, like synthetic nanoparticles, the small size of EVs also favours their margination close to the endothelium walls (Toy et al. 2011; Müller, Fedosov, and Gompper 2014), increasing their probability of being ingested by phagocytic cells (Hyenne et al. 2019). Moreover, EVs that are not rapidly taken up might be subjected to the high shear characteristic of arteries and destroyed,

as shown for breast, ovarian and lung CTCs and for leukaemia cells in a microfluidics system(Regmi, Fu, and Luo 2017). In mice, tEVs are also rapidly transported in lymphatics(Srinivasan, Vannberg, and Dixon 2016), where they end up in metastasis- free lymph nodes and can be internalized by resident macrophages of the subcapsular sinus (Hood, San, and Wickline 2011; Pucci et al. 2016).

Our results further showed that in addition to promoting EV secretion, **RalA/B GTPases control the pro-metastatic function of these EVs, likely by modulating their content.** We analyzed RNA and protein content and showed that depletion of either RalA or RalB deeply affects the EV RNA loading and changes the levels of several key proteins. **It is also important to investigate whether EVs content reflects cargo sorting or cell expression levels?** To answer this question one way is to do RNA-seq and MS for the whole cell using cell lysate and compare the changes. If the same RNA and protein are going up and down in both EVs and cells, we can imagine EV is reflecting the changes in transcription or translation which could be explained by a bigger level of regulation since among the Ral effectors there are some transcription factors. Since Ral is localized at the site of ILV biogenesis, we can imagine it could also control the sorting of EV cargo. Moreover, Ras, which is known to activate RalA/B (Gentry et al. 2014), also controls the protein and RNA cargo of tumor EVs(Demory Beckler et al. 2013; McKenzie et al. 2016). As McKenzie and collaborators identified a MEK-ERK-Ago2 pathway downstream of Ras(McKenzie et al. 2016), it would be interesting to determine how this pathway connects with the Ral-PLD-PA axis.

Ral GTPases promote the secretion CD146-enriched EVs, whose lung tropism sustains efficient metastasis

We hypothesized CD146, as an adhesion receptor could be responsible, at least in part for the seeding potential defects observed with EVs from Ral-depleted cells. CD146 functions as an adhesion molecule involved in homophilic and heterophilic interactions(Z. Wang and Yan 2013), promoting for instance monocyte transmigration(Bardin et al. 2009). CD146 can perform trans-homophilic interactions via its immunoglobulin-like extracellular domain (Taira et al. 1994; 2005). It also binds to extracellular matrix proteins or other transmembrane proteins, such as VEGFR2 (Z. Wang and Yan 2013). Up to now, a total of 13 molecules or complexes have been known as ligands for CD146. These ligands can be categorized into components of the ECM, pro-angiogenic

factor receptors, and growth factors. All these ligands directly interact with CD146 and have been shown to be involved in the promotion of CD146-mediated angiogenesis and tumor metastasis (Z. Wang et al. 2020, 14). Previously, CD146 has been shown to affect melanoma cell extravasation to the lung during dissemination, by interacting with endothelial cells and regulating VEGF-induced vessel permeability (Jouve et al. 2015). Later, another group suggested CD146 enhance melanoma cell extravasation and interaction with resident mesenchymal stem cells and pericytes to prepare the pre-metastatic niche formation(Correa et al. 2016). We showed that **EVs pre-treated with CD146 blocking antibody failed to successfully arrest on endothelial walls of zebrafish embryos and inefficiently reached the lungs in the mouse.** Therefore, we speculate that CD146 affects the biodistribution and organ targeting efficiency of circulating tEVs by mediating their interaction with specific ligands present on the luminal side of endothelial cells of metastatic organs. Other adhesion molecules, such as integrins and tetraspanins were shown to affect the biodistribution of tEVs and ultimately the formation of metastasis (Hoshino et al. 2015; Yue et al. 2015). Therefore, it is likely that the combination of these receptors at the surface of tEVs, combined with the differential expression of their ligands on endothelial cells throughout the organism will dictate their homing. **Now the question is how EV-loaded CD146 mechanistically determine such specificity?** In addition to organ-dependent enrichment of adhesion molecules such as CD146 ligands in specific regions of the vasculature, such organotropism could also be explained by (i) the site of EV injection, (ii) vascular architecture and hemodynamic patterns (Follain et al. 2020; Hyenne et al. 2019), (iii) presence of other cell types in the circulation, such as patrolling monocytes (Hyenne et al. 2019; Plebanek 2017) and/or (iv) the permeable nature of the target tissue (Verweij, Hyenne, et al. 2019). Next, we wondered how does **EV-loaded CD146** affect the priming of pre-metastatic niche. This experiment is still ongoing but our preliminary result shows that we have less formation of pre-metastatic niche when we block CD146 on 4T1 EVs. These results suggest that CD146, whose presence at the surface of EVs is tuned by RalA/B, is partially responsible for the adhesion and lung tropism of 4T1 EVs and its reduced levels lead to failure of reaching thus priming the PMN in the lungs efficiently. **Another question is, other than lung tropism effect of CD146-enriched EVs, what are other pro-metastatic function of these EVs on priming the PMN?** Most of the study in the EV field including ours is based on doing priming experiments with a large amount of EVs. We basically

treat the recipient cells with these EVs which is not what happened physiologically. Thus, there will be a need for more studies trying to balance the dose of EVs to the physiological concentration so we can really understand the precise function of these EVs. It is also difficult to imagine one single protein such as CD146 play the whole functional results we observe in the given scenario. Therefore, it is also necessary to carefully study the functional role of other proteins we found in our pro-metastatic EVs including Clic4, Glypican 4, BDKRB2 and Abcg2.

Overall, our study identifies RalA/B GTPases as a novel molecular machinery that regulates the formation and shedding of pro-metastatic EVs and offers new potential targets (RalA/B and CD146) for developing new therapeutic strategies to impact the progression of metastatic breast cancer. Since there is no drug developed successfully to directly targeting Ras proteins or acting on Ras-driven effectors (Gysin et al. 2011), it seems that Ral GTPases could be considered as therapeutic targets in cancer. For example, it has been shown RBC8 and BQU57 effectively inhibit anchorage-independent and xenograft growth in some, but not all, human cancer cells (C. Yan et al. 2014). However, RBC8 and BQU57 are first generation tools and their effectiveness in clinical trials has not been investigated yet. Therefore, in addition to targeting Ral for use as a cancer therapy, it is also possible that Ral may be used as a biomarker since we found both RalA and RalB in 4T1 EVs by mass spectrometry. We also detected RalA and RalB in EVs from blood samples of 4T1 tumor-bearing mice. This represents the promising option to probe expression levels of RalA and RalB concomitantly in primary tumors and liquid biopsies as novel markers of bad prognosis since EVs constitute novel targets for early cancer diagnosis or longitudinal monitoring of anticancer treatment response (Hoshino et al. 2020; Moravec, Divi, and Verma 2017). However, all these requiring further investigation.

BIBLIOGRAPHY

Aaronson, S., U. Behrens, R. Orner, and T. H. Haines. 1971. “Ultrastructure of Intracellular and Extracellular Vesicles, Membranes, and Myelin Figures Produced by Ochromonas Danica.” *Journal of Ultrastructure Research* 35 (5): 418–30. https://doi.org/10.1016/s0022-5320(71)80003-5.

Aceto, Nicola, Aditya Bardia, David T. Miyamoto, Maria C. Donaldson, Ben S. Wittner, Joel A. Spencer, Min Yu, et al. 2014. “Circulating Tumor Cell Clusters Are Oligoclonal Precursors of Breast Cancer Metastasis.” *Cell* 158 (5): 1110–22. https://doi.org/10.1016/j.cell.2014.07.013.

Adachi, Eri, Katsuya Sakai, Takumi Nishiuchi, Ryu Imamura, Hiroki Sato, and Kunio Matsumoto. 2016. “Different Growth and Metastatic Phenotypes Associated with a Cell-Intrinsic Change of Met in Metastatic Melanoma.” *Oncotarget* 7 (43): 70779–93. https://doi.org/10.18632/oncotarget.12221.

Adem, Bárbara, Patricia F. Vieira, and Sonia A. Melo. 2020. “Decoding the Biology of Exosomes in Metastasis.” *Trends in Cancer* 6 (1): 20–30. https://doi.org/10.1016/j.trecan.2019.11.007.

Admyre, Charlotte, Sara M. Johansson, Khaleda Rahman Qazi, Jan-Jonas Filén, Riitta Lahesmaa, Mikael Norman, Etienne P. A. Neve, Annika Scheynius, and Susanne Gabrielsson. 2007. “Exosomes with Immune Modulatory Features Are Present in Human Breast Milk.” *The Journal of Immunology* 179 (3): 1969–78. https://doi.org/10.4049/jimmunol.179.3.1969.

Aga, M., G. L. Bentz, S. Raffa, M. R. Torrisi, S. Kondo, N. Wakisaka, T. Yoshizaki, J. S. Pagano, and J. Shackelford. 2014. “Exosomal HIF1α Supports Invasive Potential of Nasopharyngeal Carcinoma-Associated LMP1-Positive Exosomes.” *Oncogene* 33 (37): 4613–22. https://doi.org/10.1038/onc.2014.66.

Aird, W. C. 2007. “Vascular Bed-Specific Thrombosis.” *Journal of Thrombosis and Haemostasis* 5 (s1): 283–91. https://doi.org/10.1111/j.1538-7836.2007.02515.x.

Allison, Kimberly H. 2012. “Molecular Pathology of Breast Cancer: What a Pathologist Needs to Know.” *American Journal of Clinical Pathology* 138 (6): 770–80. https://doi.org/10.1309/AJCPIV9IQ1MRQMOO.

Al-Nedawi, Khalid, Brian Meehan, Johann Micallef, Vladimir Lhotak, Linda May, Abhijit Guha, and Janusz Rak. 2008. “Intercellular Transfer of the Oncogenic Receptor EGFRvIII by Microvesicles Derived from Tumour Cells.” *Nature Cell Biology* 10 (5): 619–24. https://doi.org/10.1038/ncb1725.

Alonso, R., C. Mazzeo, M. C. Rodriguez, M. Marsh, A. Fraile-Ramos, V. Calvo, A. Avila-Flores, I. Merida, and M. Izquierdo. 2011. “Diacylglycerol Kinase α Regulates the Formation and Polarisation of Mature Multivesicular Bodies Involved in the Secretion of Fas Ligand-Containing Exosomes in T Lymphocytes.” *Cell Death & Differentiation* 18 (7): 1161–73. https://doi.org/10.1038/cdd.2010.184.

Alonso, Roberto, M. Carmen Rodríguez, Jose Pindado, Ernesto Merino, Isabel Mérida, and Manuel Izquierdo. 2005. “Diacylglycerol Kinase α Regulates the Secretion of Lethal Exosomes Bearing Fas Ligand during Activation-Induced Cell Death of T

Lymphocytes." *Journal of Biological Chemistry* 280 (31): 28439–50. https://doi.org/10.1074/jbc.M501112200.
Anand, Sushma, Monisha Samuel, Sharad Kumar, and Suresh Mathivanan. 2019. "Ticket to a Bubble Ride: Cargo Sorting into Exosomes and Extracellular Vesicles." *Biochimica et Biophysica Acta (BBA) - Proteins and Proteomics* 1867 (12): 140203. https://doi.org/10.1016/j.bbapap.2019.02.005.
Andreu, Zoraida, and María Yáñez-Mó. 2014. "Tetraspanins in Extracellular Vesicle Formation and Function." *Frontiers in Immunology* 5 (September). https://doi.org/10.3389/fimmu.2014.00442.
Antonyak, Marc A., and Richard A. Cerione. 2014. "Microvesicles as Mediators of Intercellular Communication in Cancer." *Methods in Molecular Biology (Clifton, N.J.)* 1165: 147–73. https://doi.org/10.1007/978-1-4939-0856-1_11.
Aponte, Pedro M., and Andrés Caicedo. 2017. "Stemness in Cancer: Stem Cells, Cancer Stem Cells, and Their Microenvironment." *Stem Cells International* 2017: 1–17. https://doi.org/10.1155/2017/5619472.
Armulik, Annika, Guillem Genové, and Christer Betsholtz. 2011. "Pericytes: Developmental, Physiological, and Pathological Perspectives, Problems, and Promises." *Developmental Cell* 21 (2): 193–215. https://doi.org/10.1016/j.devcel.2011.07.001.
Asea, Alexzander, Claudel Jean-Pierre, Punit Kaur, Preethi Rao, Iara M. Linhares, Daniel Skupski, and Steven S. Witkin. 2008. "Heat Shock Protein-Containing Exosomes in Mid-Trimester Amniotic Fluids." *Journal of Reproductive Immunology* 79 (1): 12–17. https://doi.org/10.1016/j.jri.2008.06.001.
Auguste, Patrick, Lucia Fallavollita, Ni Wang, Julia Burnier, Andreas Bikfalvi, and Pnina Brodt. 2007. "The Host Inflammatory Response Promotes Liver Metastasis by Increasing Tumor Cell Arrest and Extravasation." *The American Journal of Pathology* 170 (5): 1781–92. https://doi.org/10.2353/ajpath.2007.060886.
Azevedo, Ana Sofia, Gautier Follain, Shankar Patthabhiraman, Sébastien Harlepp, and Jacky G. Goetz. 2015. "Metastasis of Circulating Tumor Cells: Favorable Soil or Suitable Biomechanics, or Both?" *Cell Adhesion & Migration* 9 (5): 345–56. https://doi.org/10.1080/19336918.2015.1059563.
Baccelli, Irène, Andreas Schneeweiss, Sabine Riethdorf, Albrecht Stenzinger, Anja Schillert, Vanessa Vogel, Corinna Klein, et al. 2013. "Identification of a Population of Blood Circulating Tumor Cells from Breast Cancer Patients That Initiates Metastasis in a Xenograft Assay." *Nature Biotechnology* 31 (6): 539–44. https://doi.org/10.1038/nbt.2576.
Baeriswyl, Vanessa, and Gerhard Christofori. 2009. "The Angiogenic Switch in Carcinogenesis." *Seminars in Cancer Biology* 19 (5): 329–37. https://doi.org/10.1016/j.semcancer.2009.05.003.
Baietti, Maria Francesca, Zhe Zhang, Eva Mortier, Aurélie Melchior, Gisèle Degeest, Annelies Geeraerts, Ylva Ivarsson, et al. 2012. "Syndecan–Syntenin–ALIX Regulates the Biogenesis of Exosomes." *Nature Cell Biology* 14 (7): 677–85. https://doi.org/10.1038/ncb2502.
Balaj, Leonora, Ryan Lessard, Lixin Dai, Yoon-Jae Cho, Scott L. Pomeroy, Xandra O. Breakefield, and Johan Skog. 2011. "Tumour Microvesicles Contain Retrotransposon

Elements and Amplified Oncogene Sequences." *Nature Communications* 2 (February): 180. https://doi.org/10.1038/ncomms1180.
Balakireva, Maria, Carine Rossé, Johanna Langevin, Yu-chen Chien, Michel Gho, Geneviève Gonzy-Treboul, Stéphanie Voegeling-Lemaire, et al. 2006. "The Ral/Exocyst Effector Complex Counters c-Jun N-Terminal Kinase-Dependent Apoptosis in Drosophila Melanogaster." *Molecular and Cellular Biology* 26 (23): 8953–63. https://doi.org/10.1128/MCB.00506-06.
Bardin, Nathalie, Marcel Blot-Chabaud, Nicolas Despoix, Abdeldjalil Kebir, Karim Harhouri, Jean-Pierre Arsanto, Leon Espinosa, et al. 2009. "CD146 and Its Soluble Form Regulate Monocyte Transendothelial Migration." *Arteriosclerosis, Thrombosis, and Vascular Biology* 29 (5): 746–53. https://doi.org/10.1161/ATVBAHA.108.183251.
Barthel, Steven R., Danielle L. Hays, Erika M. Yazawa, Matthew Opperman, Kempland C. Walley, Leonardo Nimrichter, Monica M. Burdick, et al. 2013. "Definition of Molecular Determinants of Prostate Cancer Cell Bone Extravasation." *Cancer Research* 73 (2): 942–52. https://doi.org/10.1158/0008-5472.CAN-12-3264.
Baylin, Stephen B., and Peter A. Jones. 2016. "Epigenetic Determinants of Cancer." *Cold Spring Harbor Perspectives in Biology* 8 (9): a019505. https://doi.org/10.1101/cshperspect.a019505.
Becker, Annette, Basant Kumar Thakur, Joshua Mitchell Weiss, Han Sang Kim, Héctor Peinado, and David Lyden. 2016. "Extracellular Vesicles in Cancer: Cell-to-Cell Mediators of Metastasis." *Cancer Cell* 30 (6): 836–48. https://doi.org/10.1016/j.ccell.2016.10.009.
Belaiche, Yohanns. 2014. "RalGTPase Controls Cell Polarity Organization during Epithelial Tissue Remodeling." *Cell & Developmental Biology* 03 (01). https://doi.org/10.4172/2168-9296.1000134.
Bellingham, Shayne A., Belinda B. Guo, Bradley M. Coleman, and Andrew F. Hill. 2012. "Exosomes: Vehicles for the Transfer of Toxic Proteins Associated with Neurodegenerative Diseases?" *Frontiers in Physiology* 3 (May). https://doi.org/10.3389/fphys.2012.00124.
Berditchevski, F, M M Zutter, and M E Hemler. 1996. "Characterization of Novel Complexes on the Cell Surface between Integrins and Proteins with 4 Transmembrane Domains (TM4 Proteins)." *Molecular Biology of the Cell* 7 (2): 193–207. https://doi.org/10.1091/mbc.7.2.193.
Bidwell, Bradley N, Clare Y Slaney, Nimali P Withana, Sam Forster, Yuan Cao, Sherene Loi, Daniel Andrews, et al. 2012. "Silencing of Irf7 Pathways in Breast Cancer Cells Promotes Bone Metastasis through Immune Escape." *Nature Medicine* 18 (8): 1224–31. https://doi.org/10.1038/nm.2830.
Biswas, Subhra K., and Alberto Mantovani. 2010. "Macrophage Plasticity and Interaction with Lymphocyte Subsets: Cancer as a Paradigm." *Nature Immunology* 11 (10): 889–96. https://doi.org/10.1038/ni.1937.
Bobrie, A., S. Krumeich, F. Reyal, C. Recchi, L. F. Moita, M. C. Seabra, M. Ostrowski, and C. Thery. 2012. "Rab27a Supports Exosome-Dependent and -Independent Mechanisms That Modify the Tumor Microenvironment and Can Promote Tumor Progression." *Cancer Research* 72 (19): 4920–30. https://doi.org/10.1158/0008-5472.CAN-12-0925.

Bodemann, Brian O., and Michael A. White. 2008. “Ral GTPases and Cancer: Linchpin Support of the Tumorigenic Platform.” *Nature Reviews Cancer* 8 (2): 133–40. https://doi.org/10.1038/nrc2296.

Boelens, Mirjam C., Tony J. Wu, Barzin Y. Nabet, Bihui Xu, Yu Qiu, Taewon Yoon, Diana J. Azzam, et al. 2014. “Exosome Transfer from Stromal to Breast Cancer Cells Regulates Therapy Resistance Pathways.” *Cell* 159 (3): 499–513. https://doi.org/10.1016/j.cell.2014.09.051.

Bolukbasi, Mehmet Fatih, Arda Mizrak, Gokhan Baris Ozdener, Sibylle Madlener, Thomas Ströbel, Erdogan Pekcan Erkan, Jian-Bing Fan, Xandra O Breakefield, and Okay Saydam. 2012. “MiR-1289 and ‘Zipcode’-like Sequence Enrich MRNAs in Microvesicles.” *Molecular Therapy. Nucleic Acids* 1 (2): e10. https://doi.org/10.1038/mtna.2011.2.

Bos, Paula D., Xiang H.-F. Zhang, Cristina Nadal, Weiping Shu, Roger R. Gomis, Don X. Nguyen, Andy J. Minn, et al. 2009. “Genes That Mediate Breast Cancer Metastasis to the Brain.” *Nature* 459 (7249): 1005–9. https://doi.org/10.1038/nature08021.

Brassart-Pasco, Sylvie, Karine Sénéchal, Jessica Thevenard, Laurent Ramont, Jérome Devy, Ludivine Di Stefano, Aurélie Dupont-Deshorgue, et al. 2012. “Tetrastatin, the NC1 Domain of the A4(IV) Collagen Chain: A Novel Potent Anti-Tumor Matrikine.” Edited by Jingwu Xie. *PLoS ONE* 7 (4): e29587. https://doi.org/10.1371/journal.pone.0029587.

Bray, Freddie, Jacques Ferlay, Isabelle Soerjomataram, Rebecca L. Siegel, Lindsey A. Torre, and Ahmedin Jemal. 2018. “Global Cancer Statistics 2018: GLOBOCAN Estimates of Incidence and Mortality Worldwide for 36 Cancers in 185 Countries.” *CA: A Cancer Journal for Clinicians* 68 (6): 394–424. https://doi.org/10.3322/caac.21492.

Bruno, Stefania, Cristina Grange, Maria Chiara Deregibus, Raffaele A. Calogero, Silvia Saviozzi, Federica Collino, Laura Morando, et al. 2009. “Mesenchymal Stem Cell-Derived Microvesicles Protect Against Acute Tubular Injury.” *Journal of the American Society of Nephrology : JASN* 20 (5): 1053–67. https://doi.org/10.1681/ASN.2008070798.

Budczies, Jan, Moritz von Winterfeld, Frederick Klauschen, Michael Bockmayr, Jochen K. Lennerz, Carsten Denkert, Thomas Wolf, et al. 2014. “The Landscape of Metastatic Progression Patterns across Major Human Cancers.” *Oncotarget* 6 (1): 570–83. https://www.ncbi.nlm.nih.gov/pmc/articles/PMC4381616/.

Buschow, Sonja I., Jolanda M. P. Liefhebber, Richard Wubbolts, and Willem Stoorvogel. 2005. “Exosomes Contain Ubiquitinated Proteins.” *Blood Cells, Molecules, and Diseases* 35 (3): 398–403. https://doi.org/10.1016/j.bcmd.2005.08.005.

Caby, Marie-Pierre, Danielle Lankar, Claude Vincendeau-Scherrer, Graça Raposo, and Christian Bonnerot. 2005. “Exosomal-like Vesicles Are Present in Human Blood Plasma.” *International Immunology* 17 (7): 879–87. https://doi.org/10.1093/intimm/dxh267.

Campbell, Louise J., Maria Peppa, Michael D. Crabtree, Arooj Shafiq, Nicholas F. McGough, Helen R. Mott, and Darerca Owen. 2015. “Thermodynamic Mapping of Effector Protein Interfaces with RalA and RalB.” *Biochemistry* 54 (6): 1380–89. https://doi.org/10.1021/bi501530u.

Carmeliet, Peter, and Rakesh K. Jain. 2011. “Molecular Mechanisms and Clinical Applications of Angiogenesis.” *Nature* 473 (7347): 298–307. https://doi.org/10.1038/nature10144.

Cascone, Ilaria, Rasim Selimoglu, Cafer Ozdemir, Elaine Del Nery, Charles Yeaman, Michael White, and Jacques Camonis. 2008. "Distinct Roles of RalA and RalB in the Progression of Cytokinesis Are Supported by Distinct RalGEFs." *The EMBO Journal* 27 (18): 2375–87. https://doi.org/10.1038/emboj.2008.166.

Chairoungdua, Arthit, Danielle L. Smith, Pierre Pochard, Michael Hull, and Michael J. Caplan. 2010. "Exosome Release of β-Catenin: A Novel Mechanism That Antagonizes Wnt Signaling." *Journal of Cell Biology* 190 (6): 1079–91. https://doi.org/10.1083/jcb.201002049.

Chambers, Ann F., Alan C. Groom, and Ian C. MacDonald. 2002. "Dissemination and Growth of Cancer Cells in Metastatic Sites." *Nature Reviews. Cancer* 2 (8): 563–72. https://doi.org/10.1038/nrc865.

Chandler, E M, M P Saunders, C J Yoon, D Gourdon, and C Fischbach. 2011. "Adipose Progenitor Cells Increase Fibronectin Matrix Strain and Unfolding in Breast Tumors." *Physical Biology* 8 (1): 015008. https://doi.org/10.1088/1478-3975/8/1/015008.

Chanteloup, Gaëtan, Marine Cordonnier, Nicolas Isambert, Aurélie Bertaut, Alice Hervieu, Audrey Hennequin, Maxime Luu, et al. 2020. "Monitoring HSP70 Exosomes in Cancer Patients' Follow up: A Clinical Prospective Pilot Study." *Journal of Extracellular Vesicles* 9 (1): 1766192. https://doi.org/10.1080/20013078.2020.1766192.

Chaudhary, Pankaj, Lee D. Gibbs, Sayantan Maji, Cheryl M. Lewis, Sumihiro Suzuki, and Jamboor K. Vishwanatha. 2020. "Correction to: Serum Exosomal-Annexin A2 Is Associated with African-American Triple-Negative Breast Cancer and Promotes Angiogenesis." *Breast Cancer Research : BCR* 22. https://doi.org/10.1186/s13058-020-01268-9.

Chen, Gang, Alexander C. Huang, Wei Zhang, Gao Zhang, Min Wu, Wei Xu, Zili Yu, et al. 2018. "Exosomal PD-L1 Contributes to Immunosuppression and Is Associated with Anti-PD-1 Response." *Nature* 560 (7718): 382–86. https://doi.org/10.1038/s41586-018-0392-8.

Chen, Wenjing, Andrew D. Hoffmann, Huiping Liu, and Xia Liu. 2018. "Organotropism: New Insights into Molecular Mechanisms of Breast Cancer Metastasis." *Npj Precision Oncology* 2 (1): 4. https://doi.org/10.1038/s41698-018-0047-0.

Chen, Xiao-Wei, Dara Leto, Tingting Xiong, Genggeng Yu, Alan Cheng, Stuart Decker, and Alan R. Saltiel. 2010. "A Ral GAP Complex Links PI 3-Kinase/Akt Signaling to RalA Activation in Insulin Action." *Molecular Biology of the Cell* 22 (1): 141–52. https://doi.org/10.1091/mbc.e10-08-0665.

Chennakrishnaiah, S., B. Meehan, E. D'Asti, L. Montermini, T.-H. Lee, N. Karatzas, M. Buchanan, et al. 2018. "Leukocytes as a Reservoir of Circulating Oncogenic DNA and Regulatory Targets of Tumor-Derived Extracellular Vesicles." *Journal of Thrombosis and Haemostasis: JTH* 16 (9): 1800–1813. https://doi.org/10.1111/jth.14222.

Chevillet, John R., Qing Kang, Ingrid K. Ruf, Hilary A. Briggs, Lucia N. Vojtech, Sean M. Hughes, Heather H. Cheng, et al. 2014. "Quantitative and Stoichiometric Analysis of the MicroRNA Content of Exosomes." *Proceedings of the National Academy of Sciences* 111 (41): 14888–93. https://doi.org/10.1073/pnas.1408301111.

Chiaruttini, Nicolas, Lorena Redondo-Morata, Adai Colom, Frédéric Humbert, Martin Lenz, Simon Scheuring, and Aurélien Roux. 2015. "Relaxation of Loaded ESCRT-III Spiral

Springs Drives Membrane Deformation." *Cell* 163 (4): 866–79. https://doi.org/10.1016/j.cell.2015.10.017.
Chien, Yuchen, and Michael A. White. 2003. "RAL GTPases Are Linchpin Modulators of Human Tumour-Cell Proliferation and Survival." *EMBO Reports* 4 (8): 800–806. https://doi.org/10.1038/sj.embor.embor899.
Chow, Amy, Weiying Zhou, Liang Liu, Miranda Y. Fong, Jackson Champer, Desiree Van Haute, Andrew R. Chin, et al. 2014. "Macrophage Immunomodulation by Breast Cancer-Derived Exosomes Requires Toll-like Receptor 2-Mediated Activation of NF-KB." *Scientific Reports* 4 (July): 5750. https://doi.org/10.1038/srep05750.
Clark, Emily S., Brandee Brown, Amy S. Whigham, Avtandyl Kochaishvili, Wendell G. Yarbrough, and Alissa M. Weaver. 2009. "Aggressiveness of HNSCC Tumors Depends on Expression Levels of Cortactin, a Gene in the 11q13 Amplicon." *Oncogene* 28 (3): 431–44. https://doi.org/10.1038/onc.2008.389.
Clever, David, Rahul Roychoudhuri, Michael G. Constantinides, Michael H. Askenase, Madhusudhanan Sukumar, Christopher A. Klebanoff, Robert L. Eil, et al. 2016. "Oxygen Sensing by T Cells Establishes an Immunologically Tolerant Metastatic Niche." *Cell* 166 (5): 1117-1131.e14. https://doi.org/10.1016/j.cell.2016.07.032.
Colditz, Graham A., and Kari Bohlke. 2014. "Priorities for the Primary Prevention of Breast Cancer." *CA: A Cancer Journal for Clinicians* 64 (3): 186–94. https://doi.org/10.3322/caac.21225.
Collot, Mayeul, Pichandi Ashokkumar, Halina Anton, Emmanuel Boutant, Orestis Faklaris, Thierry Galli, Yves Mély, Lydia Danglot, and Andrey S. Klymchenko. 2019. "MemBright: A Family of Fluorescent Membrane Probes for Advanced Cellular Imaging and Neuroscience." *Cell Chemical Biology* 26 (4): 600-614.e7. https://doi.org/10.1016/j.chembiol.2019.01.009.
Colombo, Marina, Catarina Moita, Guillaume van Niel, Joanna Kowal, James Vigneron, Philippe Benaroch, Nicolas Manel, Luis F. Moita, Clotilde Théry, and Graça Raposo. 2013. "Analysis of ESCRT Functions in Exosome Biogenesis, Composition and Secretion Highlights the Heterogeneity of Extracellular Vesicles." *Journal of Cell Science* 126 (24): 5553–65. https://doi.org/10.1242/jcs.128868.
Colombo, Marina, Graça Raposo, and Clotilde Théry. 2014. "Biogenesis, Secretion, and Intercellular Interactions of Exosomes and Other Extracellular Vesicles." *Annual Review of Cell and Developmental Biology* 30 (1): 255–89. https://doi.org/10.1146/annurev-cellbio-101512-122326.
Conde, Ian del, Corie N. Shrimpton, Perumal Thiagarajan, and José A. López. 2005. "Tissue-Factor–Bearing Microvesicles Arise from Lipid Rafts and Fuse with Activated Platelets to Initiate Coagulation." *Blood* 106 (5): 1604–11. https://doi.org/10.1182/blood-2004-03-1095.
Conner, Sean D., and Sandra L. Schmid. 2003. "Regulated Portals of Entry into the Cell." *Nature* 422 (6927): 37–44. https://doi.org/10.1038/nature01451.
Cooke, Vesselina G., Valerie S. LeBleu, Doruk Keskin, Zainab Khan, Joyce T. O'Connell, Yingqi Teng, Michael B. Duncan, et al. 2012. "Pericyte Depletion Results in Hypoxia-Associated Epithelial-to-Mesenchymal Transition and Metastasis Mediated by Met Signaling Pathway." *Cancer Cell* 21 (1): 66–81. https://doi.org/10.1016/j.ccr.2011.11.024.

Cordonnier, Marine, Gaëtan Chanteloup, Nicolas Isambert, Renaud Seigneuric, Pierre Fumoleau, Carmen Garrido, and Jessica Gobbo. 2017. "Exosomes in Cancer Theranostic: Diamonds in the Rough." *Cell Adhesion & Migration* 11 (2): 151–63. https://doi.org/10.1080/19336918.2016.1250999.

Cordonnier, Marine, Charlée Nardin, Gaëtan Chanteloup, Valentin Derangere, Marie-Paule Algros, Laurent Arnould, Carmen Garrido, François Aubin, and Jessica Gobbo. 2020. "Tracking the Evolution of Circulating Exosomal-PD-L1 to Monitor Melanoma Patients." *Journal of Extracellular Vesicles* 9 (1): 1710899. https://doi.org/10.1080/20013078.2019.1710899.

Cornelison, R. Chase, Caroline E. Brennan, Kathryn M. Kingsmore, and Jennifer M. Munson. 2018. "Convective Forces Increase CXCR4-Dependent Glioblastoma Cell Invasion in GL261 Murine Model." *Scientific Reports* 8 (1): 17057. https://doi.org/10.1038/s41598-018-35141-9.

Coronella, J. A., P. Telleman, G. A. Kingsbury, T. D. Truong, S. Hays, and R. P. Junghans. 2001. "Evidence for an Antigen-Driven Humoral Immune Response in Medullary Ductal Breast Cancer." *Cancer Research* 61 (21): 7889–99. https://cancerres.aacrjournals.org/content/61/21/7889.

Coronella, J A, P Telleman, G A Kingsbury, T D Truong, S Hays, and R P Junghans. n.d. "Evidence for an Antigen-Driven Humoral Immune Response in Medullary Ductal Breast Cancer," 11.

Correa, Diego, Rodrigo A. Somoza, Paul Lin, William P. Schiemann, and Arnold I. Caplan. 2016. "Mesenchymal Stem Cells Regulate Melanoma Cancer Cells Extravasation to Bone and Liver at Their Perivascular Niche." *International Journal of Cancer* 138 (2): 417–27. https://doi.org/10.1002/ijc.29709.

Corso, Giulia, Wolf Heusermann, Dominic Trojer, André Görgens, Emmanuelle Steib, Johannes Voshol, Alexandra Graff, et al. 2019. "Systematic Characterization of Extracellular Vesicle Sorting Domains and Quantification at the Single Molecule – Single Vesicle Level by Fluorescence Correlation Spectroscopy and Single Particle Imaging." *Journal of Extracellular Vesicles* 8 (1). https://doi.org/10.1080/20013078.2019.1663043.

Costa Verdera, Helena, Jerney J. Gitz-Francois, Raymond M. Schiffelers, and Pieter Vader. 2017. "Cellular Uptake of Extracellular Vesicles Is Mediated by Clathrin-Independent Endocytosis and Macropinocytosis." *Journal of Controlled Release: Official Journal of the Controlled Release Society* 266 (November): 100–108. https://doi.org/10.1016/j.jconrel.2017.09.019.

Costa-Silva, Bruno, Nicole M. Aiello, Allyson J. Ocean, Swarnima Singh, Haiying Zhang, Basant Kumar Thakur, Annette Becker, et al. 2015. "Pancreatic Cancer Exosomes Initiate Pre-Metastatic Niche Formation in the Liver." *Nature Cell Biology* 17 (6): 816–26. https://doi.org/10.1038/ncb3169.

Cox, Adrienne D., Stephen W. Fesik, Alec C. Kimmelman, Ji Luo, and Channing J. Der. 2014. "Drugging the Undruggable RAS: Mission Possible?" *Nature Reviews. Drug Discovery* 13 (11): 828–51. https://doi.org/10.1038/nrd4389.

D, Skokos, Le Panse S, Villa I, Rousselle Jc, Peronet R, David B, Namane A, and Mécheri S. 2001. "Mast Cell-Dependent B and T Lymphocyte Activation Is Mediated by the Secretion of Immunologically Active Exosomes." Journal of Immunology (Baltimore, Md. : 1950). J Immunol. January 15, 2001. https://doi.org/10.4049/jimmunol.166.2.868.

Dai, Jie, Yangzhou Su, Suye Zhong, Li Cong, Bang Liu, Junjun Yang, Yongguang Tao, Zuping He, Chao Chen, and Yiqun Jiang. 2020. "Exosomes: Key Players in Cancer and Potential Therapeutic Strategy." *Signal Transduction and Targeted Therapy* 5 (1): 1–10. https://doi.org/10.1038/s41392-020-00261-0.

D'Aloia, A., G. Berruti, B. Costa, C. Schiller, R. Ambrosini, V. Pastori, E. Martegani, and M. Ceriani. 2018. "RalGPS2 Is Involved in Tunneling Nanotubes Formation in 5637 Bladder Cancer Cells." *Experimental Cell Research* 362 (2): 349–61. https://doi.org/10.1016/j.yexcr.2017.11.036.

DeBerardinis, Ralph J., Julian J. Lum, Georgia Hatzivassiliou, and Craig B. Thompson. 2008. "The Biology of Cancer: Metabolic Reprogramming Fuels Cell Growth and Proliferation." *Cell Metabolism* 7 (1): 11–20. https://doi.org/10.1016/j.cmet.2007.10.002.

Demory Beckler, Michelle, James N. Higginbotham, Jeffrey L. Franklin, Amy-Joan Ham, Patrick J. Halvey, Imade E. Imasuen, Corbin Whitwell, Ming Li, Daniel C. Liebler, and Robert J. Coffey. 2013. "Proteomic Analysis of Exosomes from Mutant KRAS Colon Cancer Cells Identifies Intercellular Transfer of Mutant KRAS." *Molecular & Cellular Proteomics: MCP* 12 (2): 343–55. https://doi.org/10.1074/mcp.M112.022806.

Denève, Eric, Sabine Riethdorf, Jeanne Ramos, David Nocca, Amandine Coffy, Jean-Pierre Daurès, Thierry Maudelonde, Jean-Michel Fabre, Klaus Pantel, and Catherine Alix-Panabières. 2013. "Capture of Viable Circulating Tumor Cells in the Liver of Colorectal Cancer Patients." *Clinical Chemistry* 59 (9): 1384–92. https://doi.org/10.1373/clinchem.2013.202846.

Dhanasekaran, Danny N., and E. Premkumar Reddy. 2008. "JNK Signaling in Apoptosis." *Oncogene* 27 (48): 6245–51. https://doi.org/10.1038/onc.2008.301.

Dominiak, Agnieszka, Beata Chełstowska, Wioletta Olejarz, and Grażyna Nowicka. 2020. "Communication in the Cancer Microenvironment as a Target for Therapeutic Interventions." *Cancers* 12 (5): 1232. https://doi.org/10.3390/cancers12051232.

Doyle, Laura M., and Michael Zhuo Wang. 2019. "Overview of Extracellular Vesicles, Their Origin, Composition, Purpose, and Methods for Exosome Isolation and Analysis." *Cells* 8 (7). https://doi.org/10.3390/cells8070727.

Dragovic, Rebecca A., Christopher Gardiner, Alexandra S. Brooks, Dionne S. Tannetta, David J.P. Ferguson, Patrick Hole, Bob Carr, et al. 2011. "Sizing and Phenotyping of Cellular Vesicles Using Nanoparticle Tracking Analysis." *Nanomedicine: Nanotechnology, Biology and Medicine* 7 (6): 780–88. https://doi.org/10.1016/j.nano.2011.04.003.

Edgar, James R., Emily R. Eden, and Clare E. Futter. 2014. "Hrs- and CD63-Dependent Competing Mechanisms Make Different Sized Endosomal Intraluminal Vesicles." *Traffic* 15 (2): 197–211. https://doi.org/10.1111/tra.12139.

Edgar, James R, Paul T Manna, Shinichi Nishimura, George Banting, and Margaret S Robinson. 2016. "Tetherin Is an Exosomal Tether." Edited by Randy Schekman. *ELife* 5 (September): e17180. https://doi.org/10.7554/eLife.17180.

Egea-Jimenez, Antonio Luis, and Pascale Zimmermann. 2018. "Phospholipase D and Phosphatidic Acid in the Biogenesis and Cargo Loading of Extracellular Vesicles." *Journal of Lipid Research* 59 (9): 1554–60. https://doi.org/10.1194/jlr.R083964.

Eichbaum, Christine, Anne-Sophie Meyer, Ni Wang, Esther Bischofs, Andrea Steinborn, Thomas Bruckner, Pnina Brodt, Christof Sohn, and Michael H R Eichbaum. 2011.

"Breast Cancer Cell-Derived Cytokines, Macrophages and Cell Adhesion: Implications for Metastasis." *ANTICANCER RESEARCH*, 9.

Eitan, Erez, Caitlin Suire, Shi Zhang, and Mark P. Mattson. 2016. "Impact of Lysosome Status on Extracellular Vesicle Content and Release." *Ageing Research Reviews* 32: 65–74. https://doi.org/10.1016/j.arr.2016.05.001.

Engblom, Camilla, Christina Pfirschke, Rapolas Zilionis, Janaina Da Silva Martins, Stijn A. Bos, Gabriel Courties, Steffen Rickelt, et al. 2017. "Osteoblasts Remotely Supply Lung Tumors with Cancer-Promoting SiglecF ^{high} Neutrophils." *Science* 358 (6367): eaal5081. https://doi.org/10.1126/science.aal5081.

Epelman, Slava, Kory J. Lavine, Anna E. Beaudin, Dorothy K. Sojka, Javier A. Carrero, Boris Calderon, Thaddeus Brija, et al. 2014. "Embryonic and Adult-Derived Resident Cardiac Macrophages Are Maintained through Distinct Mechanisms at Steady State and during Inflammation." *Immunity* 40 (1): 91–104. https://doi.org/10.1016/j.immuni.2013.11.019.

Erez, Neta, Morgan Truitt, Peter Olson, and Douglas Hanahan. 2010. "Cancer-Associated Fibroblasts Are Activated in Incipient Neoplasia to Orchestrate Tumor-Promoting Inflammation in an NF-KB-Dependent Manner." *Cancer Cell* 17 (2): 135–47. https://doi.org/10.1016/j.ccr.2009.12.041.

Ewing, James. 1928. "Neoplastic Diseases: A Treatise on Tumours." *British Journal of Surgery* 16 (61): 174–75. https://doi.org/10.1002/bjs.1800166126.

Fares, Jawad, Mohamad Y. Fares, Hussein H. Khachfe, Hamza A. Salhab, and Youssef Fares. 2020. "Molecular Principles of Metastasis: A Hallmark of Cancer Revisited." *Signal Transduction and Targeted Therapy* 5 (1): 28. https://doi.org/10.1038/s41392-020-0134-x.

Feng, Yixiao, Mia Spezia, Shifeng Huang, Chengfu Yuan, Zongyue Zeng, Linghuan Zhang, Xiaojuan Ji, et al. 2018. "Breast Cancer Development and Progression: Risk Factors, Cancer Stem Cells, Signaling Pathways, Genomics, and Molecular Pathogenesis." *Genes & Diseases* 5 (2): 77–106. https://doi.org/10.1016/j.gendis.2018.05.001.

Fenwick, R. Brynmor, Louise J. Campbell, Karthik Rajasekar, Sunil Prasannan, Daniel Nietlispach, Jacques Camonis, Darerca Owen, and Helen R. Mott. 2010. "The RalB-RLIP76 Complex Reveals a Novel Mode of Ral-Effector Interaction." *Structure (London, England: 1993)* 18 (8): 985–95. https://doi.org/10.1016/j.str.2010.05.013.

Ferlay, Jacques, Isabelle Soerjomataram, Rajesh Dikshit, Sultan Eser, Colin Mathers, Marise Rebelo, Donald Maxwell Parkin, David Forman, and Freddie Bray. 2015. "Cancer Incidence and Mortality Worldwide: Sources, Methods and Major Patterns in GLOBOCAN 2012: Globocan 2012." *International Journal of Cancer* 136 (5): E359–86. https://doi.org/10.1002/ijc.29210.

Follain, Gautier, David Herrmann, Sébastien Harlepp, Vincent Hyenne, Naël Osmani, Sean C. Warren, Paul Timpson, and Jacky G. Goetz. 2020. "Fluids and Their Mechanics in Tumour Transit: Shaping Metastasis." *Nature Reviews Cancer* 20 (2): 107–24. https://doi.org/10.1038/s41568-019-0221-x.

Follain, Gautier, Naël Osmani, Ana Sofia Azevedo, Guillaume Allio, Luc Mercier, Matthia A. Karreman, Gergely Solecki, et al. 2018. "Hemodynamic Forces Tune the Arrest, Adhesion, and Extravasation of Circulating Tumor Cells." *Developmental Cell* 45 (1): 33-52.e12. https://doi.org/10.1016/j.devcel.2018.02.015.

Frankel, Paul, Ami Aronheim, Emma Kavanagh, Maria S Balda, Karl Matter, Tom D Bunney, and Christopher J Marshall. 2005. “RalA Interacts with ZONAB in a Cell Density-Dependent Manner and Regulates Its Transcriptional Activity.” *The EMBO Journal* 24 (1): 54–62. https://doi.org/10.1038/sj.emboj.7600497.

Fridman, Wolf Herman, Franck Pagès, Catherine Sautès-Fridman, and Jérôme Galon. 2012. “The Immune Contexture in Human Tumours: Impact on Clinical Outcome.” *Nature Reviews Cancer* 12 (4): 298–306. https://doi.org/10.1038/nrc3245.

Fukai, Shuya, Hugo T. Matern, Junutula R. Jagath, Richard H. Scheller, and Axel T. Brunger. 2003. “Structural Basis of the Interaction between RalA and Sec5, a Subunit of the Sec6/8 Complex.” *The EMBO Journal* 22 (13): 3267–78. https://doi.org/10.1093/emboj/cdg329.

Gabrilovich, Dmitry I., Suzanne Ostrand-Rosenberg, and Vincenzo Bronte. 2012. “Coordinated Regulation of Myeloid Cells by Tumours.” *Nature Reviews Immunology* 12 (4): 253–68. https://doi.org/10.1038/nri3175.

Galdiero, Maria Rosaria, Gianni Marone, and Alberto Mantovani. 2018. “Cancer Inflammation and Cytokines.” *Cold Spring Harbor Perspectives in Biology* 10 (8): a028662. https://doi.org/10.1101/cshperspect.a028662.

Gámez-Valero, Ana, Marta Monguió-Tortajada, Laura Carreras-Planella, Marcel·la Franquesa, Katrin Beyer, and Francesc E. Borràs. 2016. “Size-Exclusion Chromatography-Based Isolation Minimally Alters Extracellular Vesicles’ Characteristics Compared to Precipitating Agents.” *Scientific Reports* 6 (September). https://doi.org/10.1038/srep33641.

Gao, Dongwei, Jiajun Du, Lei Cong, and Qi Liu. 2009. “Risk Factors for Initial Lung Metastasis from Breast Invasive Ductal Carcinoma in Stages I–III of Operable Patients.” *Japanese Journal of Clinical Oncology* 39 (2): 97–104. https://doi.org/10.1093/jjco/hyn133.

Gao, Yang, Igor Bado, Hai Wang, Weijie Zhang, Jeffrey M. Rosen, and Xiang H.-F. Zhang. 2019. “Metastasis Organotropism: Redefining the Congenial Soil.” *Developmental Cell* 49 (3): 375–91. https://doi.org/10.1016/j.devcel.2019.04.012.

Gardiner, Chris, Dolores Di Vizio, Susmita Sahoo, Clotilde Théry, Kenneth W. Witwer, Marca Wauben, and Andrew F. Hill. 2016. “Techniques Used for the Isolation and Characterization of Extracellular Vesicles: Results of a Worldwide Survey.” *Journal of Extracellular Vesicles* 5 (October). https://doi.org/10.3402/jev.v5.32945.

Gauvreau, Marie-Élaine, Marie-Hélène Côté, Marie-Claude Bourgeois-Daigneault, Louis-David Rivard, Fangming Xiu, Alexandre Brunet, Andrew Shaw, Viktor Steimle, and Jacques Thibodeau. 2009. “Sorting of MHC Class II Molecules into Exosomes through a Ubiquitin-Independent Pathway.” *Traffic* 10 (10): 1518–27. https://doi.org/10.1111/j.1600-0854.2009.00948.x.

Gentry, Leanna R., Timothy D. Martin, David J. Reiner, and Channing J. Der. 2014. “Ral Small GTPase Signaling and Oncogenesis: More than Just 15minutes of Fame.” *Biochimica et Biophysica Acta (BBA) - Molecular Cell Research* 1843 (12): 2976–88. https://doi.org/10.1016/j.bbamcr.2014.09.004.

Gentry, Leanna R., Akiyuki Nishimura, Adrienne D. Cox, Timothy D. Martin, Denis Tsygankov, Motohiro Nishida, Timothy C. Elston, and Channing J. Der. 2015. “Divergent Roles of CAAX Motif-Signaled Posttranslational Modifications in the Regulation and Subcellular

Localization of Ral GTPases." *The Journal of Biological Chemistry* 290 (37): 22851–61. https://doi.org/10.1074/jbc.M115.656710.

Ghajar, Cyrus M., Héctor Peinado, Hidetoshi Mori, Irina R. Matei, Kimberley J. Evason, Hélène Brazier, Dena Almeida, et al. 2013. "The Perivascular Niche Regulates Breast Tumor Dormancy." *Nature Cell Biology* 15 (7): 807–17. https://doi.org/10.1038/ncb2767.

Ghossoub, Rania, Frédérique Lembo, Aude Rubio, Carole Baron Gaillard, Jérôme Bouchet, Nicolas Vitale, Josef Slavík, Miroslav Machala, and Pascale Zimmermann. 2014. "Syntenin-ALIX Exosome Biogenesis and Budding into Multivesicular Bodies Are Controlled by ARF6 and PLD2." *Nature Communications* 5 (1): 3477. https://doi.org/10.1038/ncomms4477.

Gil-Bernabé, Ana M., Špela Ferjančič, Monika Tlalka, Lei Zhao, Philip D. Allen, Jae Hong Im, Karla Watson, et al. 2012. "Recruitment of Monocytes/Macrophages by Tissue Factor-Mediated Coagulation Is Essential for Metastatic Cell Survival and Premetastatic Niche Establishment in Mice." *Blood* 119 (13): 3164–75. https://doi.org/10.1182/blood-2011-08-376426.

Giordano, Cinzia, Giusi La Camera, Luca Gelsomino, Ines Barone, Daniela Bonofiglio, Sebastiano Andò, and Stefania Catalano. 2020. "The Biology of Exosomes in Breast Cancer Progression: Dissemination, Immune Evasion and Metastatic Colonization." *Cancers* 12 (8): 2179. https://doi.org/10.3390/cancers12082179.

Glasner, Ariella, Assi Levi, Jonatan Enk, Batya Isaacson, Sergey Viukov, Shari Orlanski, Alon Scope, et al. 2018. "NKp46 Receptor-Mediated Interferon-γ Production by Natural Killer Cells Increases Fibronectin 1 to Alter Tumor Architecture and Control Metastasis." *Immunity* 48 (1): 107-119.e4. https://doi.org/10.1016/j.immuni.2017.12.007.

Goi, Takanori, Michail Shipitsin, Zhimin Lu, David A. Foster, Stephan G. Klinz, and Larry A. Feig. 2000. "An EGF Receptor/Ral-GTPase Signaling Cascade Regulates c–Src Activity and Substrate Specificity." *The EMBO Journal* 19 (4): 623–30. https://doi.org/10.1093/emboj/19.4.623.

Gonda, Amber, Janviere Kabagwira, Girish N. Senthil, and Nathan R. Wall. 2019. "Internalization of Exosomes through Receptor-Mediated Endocytosis." *Molecular Cancer Research* 17 (2): 337–47. https://doi.org/10.1158/1541-7786.MCR-18-0891.

Görgens, André. 2016. "Webinar | Analysis of Extracellular Vesicles Including Exosomes by Imaging Flow Cytometry." *Science* 352 (6290): 1238–1238. https://doi.org/10.1126/science.352.6290.1238-b.

Grange, C., M. Tapparo, F. Collino, L. Vitillo, C. Damasco, M. C. Deregibus, C. Tetta, B. Bussolati, and G. Camussi. 2011. "Microvesicles Released from Human Renal Cancer Stem Cells Stimulate Angiogenesis and Formation of Lung Premetastatic Niche." *Cancer Research* 71 (15): 5346–56. https://doi.org/10.1158/0008-5472.CAN-11-0241.

Granger, Elizabeth, Gavin McNee, Victoria Allan, and Philip Woodman. 2014. "The Role of the Cytoskeleton and Molecular Motors in Endosomal Dynamics." *Seminars in Cell & Developmental Biology*, Endosome dynamics & Tubulogenesis, 31 (July): 20–29. https://doi.org/10.1016/j.semcdb.2014.04.011.

Groza, Monica, Alina-Andreea Zimta, Alexandru Irimie, Patriciu Achimas-Cadariu, Diana Cenariu, Giorgio Stanta, and Ioana Berindan-Neagoe. 2020. "Recent Advancements in the Study of Breast Cancer Exosomes as Mediators of Intratumoral Communication." *Journal of Cellular Physiology* 235 (2): 691–705. https://doi.org/10.1002/jcp.29096.

Gu, Jianmei, Hui Qian, Li Shen, Xu Zhang, Wei Zhu, Ling Huang, Yongmin Yan, et al. 2012. "Gastric Cancer Exosomes Trigger Differentiation of Umbilical Cord Derived Mesenchymal Stem Cells to Carcinoma-Associated Fibroblasts through TGF-β/Smad Pathway." *PloS One* 7 (12): e52465. https://doi.org/10.1371/journal.pone.0052465.

Gupta, Gaorav P., and Joan Massagué. 2006. "Cancer Metastasis: Building a Framework." *Cell* 127 (4): 679–95. https://doi.org/10.1016/j.cell.2006.11.001.

Gusterson, Barry A, Michael J Warburton, Diana Mitchell, Morag Ellison, and A Munro Neville. 1982. "Distribution of Myoepithelial Cells and Basement Membrane Proteins in the Normal Breast and in Benign and Malignant Breast Diseases" 42: 10.

Gysin, Stephan, Megan Salt, Amy Young, and Frank McCormick. 2011. "Therapeutic Strategies for Targeting Ras Proteins." *Genes & Cancer* 2 (3): 359–72. https://doi.org/10.1177/1947601911412376.

Hamad, Nesrin M., Joel H. Elconin, Antoine E. Karnoub, Wenli Bai, Jeremy N. Rich, Robert T. Abraham, Channing J. Der, and Christopher M. Counter. 2002. "Distinct Requirements for Ras Oncogenesis in Human versus Mouse Cells." *Genes & Development* 16 (16): 2045–57. https://doi.org/10.1101/gad.993902.

Hanahan, Douglas, and Robert A Weinberg. 2000. "The Hallmarks of Cancer." *Cell* 100 (1): 57–70. https://doi.org/10.1016/S0092-8674(00)81683-9.

Hanahan, Douglas, and Robert A. Weinberg. 2011. "Hallmarks of Cancer: The Next Generation." *Cell* 144 (5): 646–74. https://doi.org/10.1016/j.cell.2011.02.013.

Hand, P. Horan, A. Thor, J. Schlom, C. N. Rao, and L. Liotta. 1985. "Expression of Laminin Receptor in Normal and Carcinomatous Human Tissues as Defined by a Monoclonal Antibody." *Cancer Research* 45 (6): 2713–19. https://cancerres.aacrjournals.org/content/45/6/2713.

Hanna, Richard N., Caglar Cekic, Duygu Sag, Robert Tacke, Graham D. Thomas, Heba Nowyhed, Erica Herrley, et al. 2015. "Patrolling Monocytes Control Tumor Metastasis to the Lung." *Science (New York, N.Y.)* 350 (6263): 985–90. https://doi.org/10.1126/science.aac9407.

Hansen, M T, B Forst, N Cremers, L Quagliata, N Ambartsumian, B Grum-Schwensen, J Klingelhöfer, et al. 2015. "A Link between Inflammation and Metastasis: Serum Amyloid A1 and A3 Induce Metastasis, and Are Targets of Metastasis-Inducing S100A4." *Oncogene* 34 (4): 424–35. https://doi.org/10.1038/onc.2013.568.

Haraszti, Reka A., Marie-Cecile Didiot, Ellen Sapp, John Leszyk, Scott A. Shaffer, Hannah E. Rockwell, Fei Gao, et al. 2016. "High-Resolution Proteomic and Lipidomic Analysis of Exosomes and Microvesicles from Different Cell Sources." *Journal of Extracellular Vesicles* 5 (November). https://doi.org/10.3402/jev.v5.32570.

Harbeck, Nadia, Frédérique Penault-Llorca, Javier Cortes, Michael Gnant, Nehmat Houssami, Philip Poortmans, Kathryn Ruddy, Janice Tsang, and Fatima Cardoso. 2019. "Breast Cancer." *Nature Reviews Disease Primers* 5 (1): 66. https://doi.org/10.1038/s41572-019-0111-2.

Harding, CLIFFORD, JOHN Heuser, and PHILIP Stahl. 1983. "Receptor-Mediated Endocytosis of Transferrin and Recycling of the Transferrin Receptor in Rat Reticulocytes." *The Journal of Cell Biology* 97 (2): 329–39. https://www.ncbi.nlm.nih.gov/pmc/articles/PMC2112509/.

Hartjes, Thomas A., Serhii Mytnyk, Guido W. Jenster, Volkert van Steijn, and Martin E. van Royen. 2019. “Extracellular Vesicle Quantification and Characterization: Common Methods and Emerging Approaches.” *Bioengineering* 6 (1). https://doi.org/10.3390/bioengineering6010007.

Headley, Mark B., Adriaan Bins, Alyssa Nip, Edward W. Roberts, Mark R. Looney, Audrey Gerard, and Matthew F. Krummel. 2016. “Visualization of Immediate Immune Responses to Pioneer Metastatic Cells in the Lung.” *Nature* 531 (7595): 513–17. https://doi.org/10.1038/nature16985.

Heilmann, Silja, Kajan Ratnakumar, Erin Langdon, Emily Kansler, Isabella Kim, Nathaniel R. Campbell, Elizabeth Perry, et al. 2015. “A Quantitative System for Studying Metastasis Using Transparent Zebrafish.” *Cancer Research* 75 (20): 4272–82. https://doi.org/10.1158/0008-5472.CAN-14-3319.

Hemler, Martin E. 2005. “Tetraspanin Functions and Associated Microdomains.” *Nature Reviews Molecular Cell Biology* 6 (10): 801–11. https://doi.org/10.1038/nrm1736.

Hendrix, An, Dawn Maynard, Patrick Pauwels, Geert Braems, Hannelore Denys, Rudy Van den Broecke, Jo Lambert, et al. 2010. “Effect of the Secretory Small GTPase Rab27B on Breast Cancer Growth, Invasion, and Metastasis.” *Journal of the National Cancer Institute* 102 (12): 866–80. https://doi.org/10.1093/jnci/djq153.

Henke, Erik, Rajender Nandigama, and Süleyman Ergün. 2020. “Extracellular Matrix in the Tumor Microenvironment and Its Impact on Cancer Therapy.” *Frontiers in Molecular Biosciences* 6 (January): 160. https://doi.org/10.3389/fmolb.2019.00160.

Hiratsuka, Sachie, Dan G. Duda, Yuhui Huang, Shom Goel, Tatsuki Sugiyama, Takashi Nagasawa, Dai Fukumura, and Rakesh K. Jain. 2011. “C-X-C Receptor Type 4 Promotes Metastasis by Activating P38 Mitogen-Activated Protein Kinase in Myeloid Differentiation Antigen (Gr-1)-Positive Cells.” *Proceedings of the National Academy of Sciences* 108 (1): 302–7. https://doi.org/10.1073/pnas.1016917108.

Hood, Joshua L., Roman Susana San, and Samuel A. Wickline. 2011. “Exosomes Released by Melanoma Cells Prepare Sentinel Lymph Nodes for Tumor Metastasis.” *Cancer Research* 71 (11): 3792–3801. https://doi.org/10.1158/0008-5472.CAN-10-4455.

Hoshino, Ayuko, Bruno Costa-Silva, Tang-Long Shen, Goncalo Rodrigues, Ayako Hashimoto, Milica Tesic Mark, Henrik Molina, et al. 2015. “Tumour Exosome Integrins Determine Organotropic Metastasis.” *Nature* 527 (7578): 329–35. https://doi.org/10.1038/nature15756.

Hoshino, Ayuko, Han Sang Kim, Linda Bojmar, Kofi Ennu Gyan, Michele Cioffi, Jonathan Hernandez, Constantinos P. Zambirinis, et al. 2020. “Extracellular Vesicle and Particle Biomarkers Define Multiple Human Cancers.” *Cell* 182 (4): 1044-1061.e18. https://doi.org/10.1016/j.cell.2020.07.009.

Houali, K., X. Wang, Y. Shimizu, D. Djennaoui, J. Nicholls, S. Fiorini, A. Bouguermouh, and T. Ooka. 2007. “A New Diagnostic Marker for Secreted Epstein-Barr Virus Encoded LMP1 and BARF1 Oncoproteins in the Serum and Saliva of Patients with Nasopharyngeal Carcinoma.” *Clinical Cancer Research* 13 (17): 4993–5000. https://doi.org/10.1158/1078-0432.CCR-06-2945.

Hsieh, Chyi-Song, Yuqiong Liang, Aaron J. Tyznik, Steven G. Self, Denny Liggitt, and Alexander Y. Rudensky. 2004. “Recognition of the Peripheral Self by Naturally Arising

CD25+ CD4+ T Cell Receptors." *Immunity* 21 (2): 267–77. https://doi.org/10.1016/j.immuni.2004.07.009.
Hsu, Chieh, Yuichi Morohashi, Shin-ichiro Yoshimura, Natalia Manrique-Hoyos, SangYong Jung, Marcel A. Lauterbach, Mostafa Bakhti, et al. 2010. "Regulation of Exosome Secretion by Rab35 and Its GTPase-Activating Proteins TBC1D10A–C." *Journal of Cell Biology* 189 (2): 223–32. https://doi.org/10.1083/jcb.200911018.
Hu, Y.-B., C. Yan, L. Mu, Y.-L. Mi, H. Zhao, H. Hu, X.-L. Li, et al. 2019. "Exosomal Wnt-Induced Dedifferentiation of Colorectal Cancer Cells Contributes to Chemotherapy Resistance." *Oncogene* 38 (11): 1951–65. https://doi.org/10.1038/s41388-018-0557-9.
Huang, Po-Hsun, Yung-Hsiang Chen, Chao-Hung Wang, Jia-Shiong Chen, Hsiao-Ya Tsai, Feng-Yen Lin, Wei-Yuh Lo, et al. 2009. "Matrix Metalloproteinase-9 Is Essential for Ischemia-Induced Neovascularization by Modulating Bone Marrow–Derived Endothelial Progenitor Cells." *Arteriosclerosis, Thrombosis, and Vascular Biology* 29 (8): 1179–84. https://doi.org/10.1161/ATVBAHA.109.189175.
Huang, Tu-Xiong, Xin-Yuan Guan, and Li Fu. 2019. "Therapeutic Targeting of the Crosstalk between Cancer-Associated Fibroblasts and Cancer Stem Cells." *American Journal of Cancer Research* 9 (9): 1889–1904. https://www.ncbi.nlm.nih.gov/pmc/articles/PMC6780671/.
Hurley, James H. 2015. "ESCRT s Are Everywhere." *The EMBO Journal* 34 (19): 2398–2407. https://doi.org/10.15252/embj.201592484.
Hyenne, Vincent, Ahmet Apaydin, David Rodriguez, Coralie Spiegelhalter, Sarah Hoff-Yoessle, Maxime Diem, Saurabh Tak, et al. 2015. "RAL-1 Controls Multivesicular Body Biogenesis and Exosome Secretion." *Journal of Cell Biology* 211 (1): 27–37. https://doi.org/10.1083/jcb.201504136.
Hyenne, Vincent, Shima Ghoroghi, Mayeul Collot, Joanna Bons, Gautier Follain, Sébastien Harlepp, Benjamin Mary, et al. 2019. "Studying the Fate of Tumor Extracellular Vesicles at High Spatiotemporal Resolution Using the Zebrafish Embryo." *Developmental Cell* 48 (4): 554-572.e7. https://doi.org/10.1016/j.devcel.2019.01.014.
Hyenne, Vincent, Olivier Lefebvre, and Jacky G. Goetz. 2017. "Going Live with Tumor Exosomes and Microvesicles." *Cell Adhesion & Migration* 11 (2): 173–86. https://doi.org/10.1080/19336918.2016.1276694.
J, Fauré, Lachenal G, Court M, Hirrlinger J, Chatellard-Causse C, Blot B, Grange J, et al. 2006. "Exosomes Are Released by Cultured Cortical Neurones." Molecular and Cellular Neurosciences. Mol Cell Neurosci. April 2006. https://doi.org/10.1016/j.mcn.2005.12.003.
Jacob, Abitha, and Rytis Prekeris. 2015. "The Regulation of MMP Targeting to Invadopodia during Cancer Metastasis." *Frontiers in Cell and Developmental Biology* 3 (February). https://doi.org/10.3389/fcell.2015.00004.
Jahn, Reinhard, and Richard H. Scheller. 2006. "SNAREs — Engines for Membrane Fusion." *Nature Reviews Molecular Cell Biology* 7 (9): 631–43. https://doi.org/10.1038/nrm2002.
Jan, Arif Tasleem, Safikur Rahman, Shahanavaj Khan, Sheikh Abdullah Tasduq, and Inho Choi. 2019. "Biology, Pathophysiological Role, and Clinical Implications of Exosomes: A Critical Appraisal." *Cells* 8 (2). https://doi.org/10.3390/cells8020099.

Jenkins, G. M., and M. A. Frohman. 2005. “Phospholipase D: A Lipid Centric Review.” *Cellular and Molecular Life Sciences: CMLS* 62 (19–20): 2305–16. https://doi.org/10.1007/s00018-005-5195-z.

Jeppesen, Dennis K., Aidan M. Fenix, Jeffrey L. Franklin, James N. Higginbotham, Qin Zhang, Lisa J. Zimmerman, Daniel C. Liebler, et al. 2019. “Reassessment of Exosome Composition.” *Cell* 177 (2): 428-445.e18. https://doi.org/10.1016/j.cell.2019.02.029.

Jeppesen, Dennis K., Michael L. Hvam, Bjarke Primdahl-Bengtson, Anders T. Boysen, Bradley Whitehead, Lars Dyrskjøt, Torben F. Ørntoft, Kenneth A. Howard, and Marie S. Ostenfeld. 2014. “Comparative Analysis of Discrete Exosome Fractions Obtained by Differential Centrifugation.” *Journal of Extracellular Vesicles* 3 (1): 25011. https://doi.org/10.3402/jev.v3.25011.

Jiang, Hong, Zhimin Lu, Jing-Qing Luo, Alan Wolfman, and David A. Foster. 1995. “Ras Mediates the Activation of Phospholipase D by V-Src.” *Journal of Biological Chemistry* 270 (11): 6006–9. https://doi.org/10.1074/jbc.270.11.6006.

Johnstone, R. M., M. Adam, J. R. Hammond, L. Orr, and C. Turbide. 1987. “Vesicle Formation during Reticulocyte Maturation. Association of Plasma Membrane Activities with Released Vesicles (Exosomes).” *Journal of Biological Chemistry* 262 (19): 9412–20. http://www.jbc.org/content/262/19/9412.

Jouve, Nathalie, Richard Bachelier, Nicolas Despoix, Muriel G. Blin, Maryam Khalili Matinzadeh, Stéphane Poitevin, Michel Aurrand-Lions, et al. 2015. “CD146 Mediates VEGF-Induced Melanoma Cell Extravasation through FAK Activation.” *International Journal of Cancer* 137 (1): 50–60. https://doi.org/10.1002/ijc.29370.

Joyce, Johanna A., and Jeffrey W. Pollard. 2009. “Microenvironmental Regulation of Metastasis.” *Nature Reviews Cancer* 9 (4): 239–52. https://doi.org/10.1038/nrc2618.

Js, Bonifacino, and Glick Bs. 2004. “The Mechanisms of Vesicle Budding and Fusion.” *Cell* 116 (2): 153–66. https://doi.org/10.1016/s0092-8674(03)01079-1.

Jullien-Flores, V., Y. Mahe, G. Mirey, C. Leprince, B. Meunier-Bisceuil, A. Sorkin, and J.H. Camonis. 2000. “RLIP76, an Effector of the GTPase Ral, Interacts with the AP2 Complex: Involvement of the Ral Pathway in Receptor Endocytosis.” *Journal of Cell Science* 113 (16): 2837. http://jcs.biologists.org/content/113/16/2837.abstract.

Kahlert, Christoph, Sonia A. Melo, Alexei Protopopov, Jiabin Tang, Sahil Seth, Moritz Koch, Jianhua Zhang, et al. 2014. “Identification of Double-Stranded Genomic DNA Spanning All Chromosomes with Mutated KRAS and P53 DNA in the Serum Exosomes of Patients with Pancreatic Cancer.” *The Journal of Biological Chemistry* 289 (7): 3869–75. https://doi.org/10.1074/jbc.C113.532267.

Kajimoto, Taketoshi, Taro Okada, Satoshi Miya, Lifang Zhang, and Shun-ichi Nakamura. 2013. “Ongoing Activation of Sphingosine 1-Phosphate Receptors Mediates Maturation of Exosomal Multivesicular Endosomes.” *Nature Communications* 4: 2712. https://doi.org/10.1038/ncomms3712.

Kalani, Anuradha, Alka Tyagi, and Neetu Tyagi. 2014. “Exosomes: Mediators of Neurodegeneration, Neuroprotection and Therapeutics.” *Molecular Neurobiology* 49 (1): 590–600. https://doi.org/10.1007/s12035-013-8544-1.

Kalra, Hina, Richard J. Simpson, Hong Ji, Elena Aikawa, Peter Altevogt, Philip Askenase, Vincent C. Bond, et al. 2012. “Vesiclepedia: A Compendium for Extracellular Vesicles

with Continuous Community Annotation." *PLoS Biology* 10 (12): e1001450. https://doi.org/10.1371/journal.pbio.1001450.

Kanemoto, Soshi, Ryota Nitani, Tatsuhiko Murakami, Masayuki Kaneko, Rie Asada, Koji Matsuhisa, Atsushi Saito, and Kazunori Imaizumi. 2016. "Multivesicular Body Formation Enhancement and Exosome Release during Endoplasmic Reticulum Stress." *Biochemical and Biophysical Research Communications* 480 (2): 166–72. https://doi.org/10.1016/j.bbrc.2016.10.019.

Kaplan, Rosandra N., Rebecca D. Riba, Stergios Zacharoulis, Anna H. Bramley, Loïc Vincent, Carla Costa, Daniel D. MacDonald, et al. 2005. "VEGFR1-Positive Haematopoietic Bone Marrow Progenitors Initiate the Pre-Metastatic Niche." *Nature* 438 (7069): 820–27. https://doi.org/10.1038/nature04186.

Kashatus, David F., Kian-Huat Lim, Donita C. Brady, Nicole L. K. Pershing, Adrienne D. Cox, and Christopher M. Counter. 2011. "RALA and RALBP1 Regulate Mitochondrial Fission at Mitosis." *Nature Cell Biology* 13 (9): 1108–15. https://doi.org/10.1038/ncb2310.

Kaur, Punit, Ganachari M Nagaraja, Hongying Zheng, Dawit Gizachew, Moses Galukande, Sunil Krishnan, and Alexzander Asea. 2012. "A Mouse Model for Triple-Negative Breast Cancer Tumor-Initiating Cells (TNBC-TICs) Exhibits Similar Aggressive Phenotype to the Human Disease." *BMC Cancer* 12 (March): 120. https://doi.org/10.1186/1471-2407-12-120.

Kaur, Sukhbir, Abdel G. Elkahloun, Anush Arakelyan, Lynn Young, Timothy G. Myers, Francisco Otaizo-Carrasquero, Weiwei Wu, Leonid Margolis, and David D. Roberts. 2018. "CD63, MHC Class 1, and CD47 Identify Subsets of Extracellular Vesicles Containing Distinct Populations of Noncoding RNAs." *Scientific Reports* 8 (1): 2577. https://doi.org/10.1038/s41598-018-20936-7.

Kim, J. H., S. D. Lee, J. M. Han, T. G. Lee, Y. Kim, J. B. Park, J. D. Lambeth, P. G. Suh, and S. H. Ryu. 1998. "Activation of Phospholipase D1 by Direct Interaction with ADP-Ribosylation Factor 1 and RalA." *FEBS Letters* 430 (3): 231–35. https://doi.org/10.1016/s0014-5793(98)00661-9.

Kim, Sunhwa, Hiroyuki Takahashi, Wan-Wan Lin, Pascal Descargues, Sergei Grivennikov, Youngjun Kim, Jun-Li Luo, and Michael Karin. 2009. "Carcinoma Produced Factors Activate Myeloid Cells via TLR2 to Stimulate Metastasis." *Nature* 457 (7225): 102–6. https://doi.org/10.1038/nature07623.

King, Hamish W., Michael Z. Michael, and Jonathan M. Gleadle. 2012. "Hypoxic Enhancement of Exosome Release by Breast Cancer Cells." *BMC Cancer* 12 (September): 421. https://doi.org/10.1186/1471-2407-12-421.

Klumperman, Judith, and Graça Raposo. 2014. "The Complex Ultrastructure of the Endolysosomal System." *Cold Spring Harbor Perspectives in Biology* 6 (10). https://doi.org/10.1101/cshperspect.a016857.

Kooijman, Edgar E., Vladimir Chupin, Nola L. Fuller, Michael M. Kozlov, Ben de Kruijff, Koert N. J. Burger, and Peter R. Rand. 2005. "Spontaneous Curvature of Phosphatidic Acid and Lysophosphatidic Acid." *Biochemistry* 44 (6): 2097–2102. https://doi.org/10.1021/bi0478502.

Kooijman, Edgar E., Vladimir Chupin, Ben de Kruijff, and Koert N. J. Burger. 2003. "Modulation of Membrane Curvature by Phosphatidic Acid and Lysophosphatidic Acid."

Traffic (Copenhagen, Denmark) 4 (3): 162–74. https://doi.org/10.1034/j.1600-0854.2003.00086.x.

Kosaka, Nobuyoshi, Haruhisa Iguchi, Keitaro Hagiwara, Yusuke Yoshioka, Fumitaka Takeshita, and Takahiro Ochiya. 2013. "Neutral Sphingomyelinase 2 (NSMase2)-Dependent Exosomal Transfer of Angiogenic MicroRNAs Regulate Cancer Cell Metastasis." *The Journal of Biological Chemistry* 288 (15): 10849–59. https://doi.org/10.1074/jbc.M112.446831.

Kosaka, Nobuyoshi, Haruhisa Iguchi, Yusuke Yoshioka, Fumitaka Takeshita, Yasushi Matsuki, and Takahiro Ochiya. 2010. "Secretory Mechanisms and Intercellular Transfer of MicroRNAs in Living Cells♦." *The Journal of Biological Chemistry* 285 (23): 17442–52. https://doi.org/10.1074/jbc.M110.107821.

Kosaka, Nobuyoshi, Yusuke Yoshioka, Keitaro Hagiwara, Naoomi Tominaga, and Takahiro Ochiya. 2013. "Functional Analysis of Exosomal MicroRNA in Cell–Cell Communication Research." In *Circulating MicroRNAs: Methods and Protocols*, edited by Nobuyoshi Kosaka, 1–10. Methods in Molecular Biology. Totowa, NJ: Humana Press. https://doi.org/10.1007/978-1-62703-453-1_1.

Kowal, Joanna, Guillaume Arras, Marina Colombo, Mabel Jouve, Jakob Paul Morath, Bjarke Primdal-Bengtson, Florent Dingli, Damarys Loew, Mercedes Tkach, and Clotilde Théry. 2016. "Proteomic Comparison Defines Novel Markers to Characterize Heterogeneous Populations of Extracellular Vesicle Subtypes." *Proceedings of the National Academy of Sciences* 113 (8): E968–77. https://doi.org/10.1073/pnas.1521230113.

Kucharzewska, Paulina, Helena C. Christianson, Johanna E. Welch, Katrin J. Svensson, Erik Fredlund, Markus Ringnér, Matthias Mörgelin, Erika Bourseau-Guilmain, Johan Bengzon, and Mattias Belting. 2013. "Exosomes Reflect the Hypoxic Status of Glioma Cells and Mediate Hypoxia-Dependent Activation of Vascular Cells during Tumor Development." *Proceedings of the National Academy of Sciences of the United States of America* 110 (18): 7312–17. https://doi.org/10.1073/pnas.1220998110.

Kuderer, Nicole M., Thomas L. Ortel, and Charles W. Francis. 2009. "Impact of Venous Thromboembolism and Anticoagulation on Cancer and Cancer Survival." *Journal of Clinical Oncology: Official Journal of the American Society of Clinical Oncology* 27 (29): 4902–11. https://doi.org/10.1200/JCO.2009.22.4584.

Kzhyshkowska, Julia, Ilja Ovsiy, and Alexei Gratchev. 2014. "Novel Biomarkers of Hidden Inflammation and Implantation." *EPMA Journal* 5 (S1): A116, 1878-5085-5-S1-A116. https://doi.org/10.1186/1878-5085-5-S1-A116.

Labelle, M., S. Begum, and R. O. Hynes. 2014. "Platelets Guide the Formation of Early Metastatic Niches." *Proceedings of the National Academy of Sciences* 111 (30): E3053–61. https://doi.org/10.1073/pnas.1411082111.

Lahmar, Qods, Jiri Keirsse, Damya Laoui, Kiavash Movahedi, Eva Van Overmeire, and Jo A. Van Ginderachter. 2016. "Tissue-Resident versus Monocyte-Derived Macrophages in the Tumor Microenvironment." *Biochimica et Biophysica Acta (BBA) - Reviews on Cancer* 1865 (1): 23–34. https://doi.org/10.1016/j.bbcan.2015.06.009.

Lai, Charles P., Edward Y. Kim, Christian E. Badr, Ralph Weissleder, Thorsten R. Mempel, Bakhos A. Tannous, and Xandra O. Breakefield. 2015. "Visualization and Tracking of Tumour Extracellular Vesicle Delivery and RNA Translation Using Multiplexed Reporters." *Nature Communications* 6 (May). https://doi.org/10.1038/ncomms8029.

Lai, Ruenn Chai, Fatih Arslan, May May Lee, Newman Siu Kwan Sze, Andre Choo, Tian Sheng Chen, Manuel Salto-Tellez, et al. 2010. “Exosome Secreted by MSC Reduces Myocardial Ischemia/Reperfusion Injury.” *Stem Cell Research* 4 (3): 214–22. https://doi.org/10.1016/j.scr.2009.12.003.

Lambert, Arthur W., Diwakar R. Pattabiraman, and Robert A. Weinberg. 2017. “Emerging Biological Principles of Metastasis.” *Cell* 168 (4): 670–91. https://doi.org/10.1016/j.cell.2016.11.037.

Larios, Jorge, Vincent Mercier, Aurélien Roux, and Jean Gruenberg. 2020. “ALIX- and ESCRT-III–Dependent Sorting of Tetraspanins to Exosomes.” *Journal of Cell Biology* 219 (3). https://doi.org/10.1083/jcb.201904113.

Lata, Suman, Guy Schoehn, Ankur Jain, Ricardo Pires, Jacob Piehler, Heinrich G. Göttlinger, and Winfried Weissenhorn. 2008. “Helical Structures of ESCRT-III Are Disassembled by VPS4.” *Science* 321 (5894): 1354–57. https://doi.org/10.1126/science.1161070.

Latysheva, Nadya, Gairat Muratov, Sundaresan Rajesh, Matthew Padgett, Neil A. Hotchin, Michael Overduin, and Fedor Berditchevski. 2006. “Syntenin-1 Is a New Component of Tetraspanin-Enriched Microdomains: Mechanisms and Consequences of the Interaction of Syntenin-1 with CD63.” *Molecular and Cellular Biology* 26 (20): 7707–18. https://doi.org/10.1128/MCB.00849-06.

Lawrence, Toby, and Gioacchino Natoli. 2011. “Transcriptional Regulation of Macrophage Polarization: Enabling Diversity with Identity.” *Nature Reviews Immunology* 11 (11): 750–61. https://doi.org/10.1038/nri3088.

Lee, M.-H. 2004. “Matrix Metalloproteinases at a Glance.” *Journal of Cell Science* 117 (18): 4015–16. https://doi.org/10.1242/jcs.01223.

Leidal, Andrew M., and Jayanta Debnath. 2020. “LC3-Dependent Extracellular Vesicle Loading and Secretion (LDELS).” *Autophagy* 16 (6): 1162–63. https://doi.org/10.1080/15548627.2020.1756557.

Leiss, Michael, Karsten Beckmann, Amparo Girós, Mercedes Costell, and Reinhard Fässler. 2008. “The Role of Integrin Binding Sites in Fibronectin Matrix Assembly in Vivo.” *Current Opinion in Cell Biology* 20 (5): 502–7. https://doi.org/10.1016/j.ceb.2008.06.001.

Levental, Kandice R., Hongmei Yu, Laura Kass, Johnathon N. Lakins, Mikala Egeblad, Janine T. Erler, Sheri F.T. Fong, et al. 2009. “Matrix Crosslinking Forces Tumor Progression by Enhancing Integrin Signaling.” *Cell* 139 (5): 891–906. https://doi.org/10.1016/j.cell.2009.10.027.

Li, Irene, and Barzin Y. Nabet. 2019. “Exosomes in the Tumor Microenvironment as Mediators of Cancer Therapy Resistance.” *Molecular Cancer* 18 (1): 32. https://doi.org/10.1186/s12943-019-0975-5.

Li, Mu, Emily Zeringer, Timothy Barta, Jeoffrey Schageman, Angie Cheng, and Alexander V. Vlassov. 2014. “Analysis of the RNA Content of the Exosomes Derived from Blood Serum and Urine and Its Potential as Biomarkers.” *Philosophical Transactions of the Royal Society B: Biological Sciences* 369 (1652): 20130502. https://doi.org/10.1098/rstb.2013.0502.

Li, Timothy T., Mistre Alemayehu, Adel I. Aziziyeh, Cynthia Pape, Macarena Pampillo, Lynne-Marie Postovit, Gordon B. Mills, Andy V. Babwah, and Moshmi Bhattacharya. 2009. “β-Arrestin/Ral Signaling Regulates Lysophosphatidic Acid–Mediated Migration and

Invasion of Human Breast Tumor Cells." *Molecular Cancer Research* 7 (7): 1064–77. https://doi.org/10.1158/1541-7786.MCR-08-0578.
Lim, Kian-Huat, Antonio T. Baines, James J. Fiordalisi, Michail Shipitsin, Larry A. Feig, Adrienne D. Cox, Channing J. Der, and Christopher M. Counter. 2005. "Activation of RalA Is Critical for Ras-Induced Tumorigenesis of Human Cells." *Cancer Cell* 7 (6): 533–45. https://doi.org/10.1016/j.ccr.2005.04.030.
Lim, Kian-Huat, Donita C. Brady, David F. Kashatus, Brooke B. Ancrile, Channing J. Der, Adrienne D. Cox, and Christopher M. Counter. 2010. "Aurora-A Phosphorylates, Activates, and Relocalizes the Small GTPase RalA." *Molecular and Cellular Biology* 30 (2): 508–23. https://doi.org/10.1128/MCB.00916-08.
Lim, Kian-Huat, Kevin O'Hayer, Stacey J. Adam, S. DiSean Kendall, Paul M. Campbell, Channing J. Der, and Christopher M. Counter. 2006. "Divergent Roles for RalA and RalB in Malignant Growth of Human Pancreatic Carcinoma Cells." *Current Biology* 16 (24): 2385–94. https://doi.org/10.1016/j.cub.2006.10.023.
Lingwood, Daniel, and Kai Simons. 2010. "Lipid Rafts As a Membrane-Organizing Principle." *Science* 327 (5961): 46–50. https://doi.org/10.1126/science.1174621.
Liu, Yanfang, Yan Gu, Yanmei Han, Qian Zhang, Zhengping Jiang, Xiang Zhang, Bo Huang, Xiaoqing Xu, Jianming Zheng, and Xuetao Cao. 2016. "Tumor Exosomal RNAs Promote Lung Pre-Metastatic Niche Formation by Activating Alveolar Epithelial TLR3 to Recruit Neutrophils." *Cancer Cell* 30 (2): 243–56. https://doi.org/10.1016/j.ccell.2016.06.021.
Liu, Yang, and Xuetao Cao. 2016. "Characteristics and Significance of the Pre-Metastatic Niche." *Cancer Cell* 30 (5): 668–81. https://doi.org/10.1016/j.ccell.2016.09.011.
Llorente, Alicia, Tore Skotland, Tuulia Sylvänne, Dimple Kauhanen, Tomasz Róg, Adam Orłowski, Ilpo Vattulainen, Kim Ekroos, and Kirsten Sandvig. 2013. "Molecular Lipidomics of Exosomes Released by PC-3 Prostate Cancer Cells." *Biochimica et Biophysica Acta (BBA) - Molecular and Cell Biology of Lipids* 1831 (7): 1302–9. https://doi.org/10.1016/j.bbalip.2013.04.011.
Lopez-Verrilli, María Alejandra, Frederic Picou, and Felipe A. Court. 2013. "Schwann Cell-Derived Exosomes Enhance Axonal Regeneration in the Peripheral Nervous System." *Glia* 61 (11): 1795–1806. https://doi.org/10.1002/glia.22558.
Lötvall, Jan, Andrew F. Hill, Fred Hochberg, Edit I. Buzás, Dolores Di Vizio, Christopher Gardiner, Yong Song Gho, et al. 2014. "Minimal Experimental Requirements for Definition of Extracellular Vesicles and Their Functions: A Position Statement from the International Society for Extracellular Vesicles." *Journal of Extracellular Vesicles* 3 (December). https://doi.org/10.3402/jev.v3.26913.
Luga, Valbona, Liang Zhang, Alicia M. Viloria-Petit, Abiodun A. Ogunjimi, Mohammad R. Inanlou, Elaine Chiu, Marguerite Buchanan, Abdel Nasser Hosein, Mark Basik, and Jeffrey L. Wrana. 2012. "Exosomes Mediate Stromal Mobilization of Autocrine Wnt-PCP Signaling in Breast Cancer Cell Migration." *Cell* 151 (7): 1542–56. https://doi.org/10.1016/j.cell.2012.11.024.
Lukanidin, Eugene, and Jonathan P. Sleeman. 2012. "Building the Niche: The Role of the S100 Proteins in Metastatic Growth." *Seminars in Cancer Biology* 22 (3): 216–25. https://doi.org/10.1016/j.semcancer.2012.02.006.
Luo, Jing-Qing, Xin Liu, Paul Frankel, Thuy Rotunda, Miguel Ramos, Judith Flom, Hong Jiang, et al. 1998. "Functional Association between Arf and RalA in Active Phospholipase D

Complex." *Proceedings of the National Academy of Sciences* 95 (7): 3632–37. https://doi.org/10.1073/pnas.95.7.3632.
Maas, Sybren L.N., Xandra O. Breakefield, and Alissa M. Weaver. 2017. "Extracellular Vesicles: Unique Intercellular Delivery Vehicles." *Trends in Cell Biology* 27 (3): 172–88. https://doi.org/10.1016/j.tcb.2016.11.003.
Malanchi, Ilaria, Albert Santamaria-Martínez, Evelyn Susanto, Hong Peng, Hans-Anton Lehr, Jean-Francois Delaloye, and Joerg Huelsken. 2012. "Interactions between Cancer Stem Cells and Their Niche Govern Metastatic Colonization." *Nature* 481 (7379): 85–89. https://doi.org/10.1038/nature10694.
Male, Heather, Vijay Patel, Mark A. Jacob, Emma Borrego-Diaz, Kun Wang, Derek A. Young, Amanda L. Wise, et al. 2012. "Inhibition of RalA Signaling Pathway in Treatment of Non-Small Cell Lung Cancer." *Lung Cancer (Amsterdam, Netherlands)* 77 (2): 252–59. https://doi.org/10.1016/j.lungcan.2012.03.007.
Mallegol, Julia, Guillaume Van Niel, Corinne Lebreton, Yves Lepelletier, Céline Candalh, Christophe Dugave, Joan K. Heath, Graça Raposo, Nadine Cerf-Bensussan, and Martine Heyman. 2007. "T84-Intestinal Epithelial Exosomes Bear MHC Class II/Peptide Complexes Potentiating Antigen Presentation by Dendritic Cells." *Gastroenterology* 132 (5): 1866–76. https://doi.org/10.1053/j.gastro.2007.02.043.
Martin, Timothy D., Natalia Mitin, Adrienne D. Cox, Jen Jen Yeh, and Channing J. Der. 2012. "Phosphorylation by Protein Kinase Cα Regulates RalB Small GTPase Protein Activation, Subcellular Localization, and Effector Utilization." *The Journal of Biological Chemistry* 287 (18): 14827–36. https://doi.org/10.1074/jbc.M112.344986.
Martin, Timothy D., Jonathan C. Samuel, Elizabeth D. Routh, Channing J. Der, and Jen Jen Yeh. 2011. "Activation and Involvement of Ral GTPases in Colorectal Cancer." *Cancer Research* 71 (1): 206–15. https://doi.org/10.1158/0008-5472.CAN-10-1517.
Mateescu, Bogdan, Emma J. K. Kowal, Bas W. M. van Balkom, Sabine Bartel, Suvendra N. Bhattacharyya, Edit I. Buzás, Amy H. Buck, et al. 2017. "Obstacles and Opportunities in the Functional Analysis of Extracellular Vesicle RNA – an ISEV Position Paper." *Journal of Extracellular Vesicles* 6 (1). https://doi.org/10.1080/20013078.2017.1286095.
Mathieu, Mathilde, Lorena Martin-Jaular, Grégory Lavieu, and Clotilde Théry. 2019. "Specificities of Secretion and Uptake of Exosomes and Other Extracellular Vesicles for Cell-to-Cell Communication." *Nature Cell Biology* 21 (1): 9–17. https://doi.org/10.1038/s41556-018-0250-9.
Mauri, Claudia, and Anneleen Bosma. 2012. "Immune Regulatory Function of B Cells." *Annual Review of Immunology* 30 (1): 221–41. https://doi.org/10.1146/annurev-immunol-020711-074934.
Maus, Rachel L. G., James W. Jakub, Wendy K. Nevala, Trace A. Christensen, Klara Noble-Orcutt, Zohar Sachs, Tina J. Hieken, and Svetomir N. Markovic. 2017. "Human Melanoma-Derived Extracellular Vesicles Regulate Dendritic Cell Maturation." *Frontiers in Immunology* 8. https://doi.org/10.3389/fimmu.2017.00358.
Mauti, Laetitia A., Marie-Aude Le Bitoux, Karine Baumer, Jean-Christophe Stehle, Dela Golshayan, Paolo Provero, and Ivan Stamenkovic. 2011. "Myeloid-Derived Suppressor Cells Are Implicated in Regulating Permissiveness for Tumor Metastasis during Mouse Gestation." *The Journal of Clinical Investigation* 121 (7): 2794–2807. https://doi.org/10.1172/JCI41936.

McAllister, Sandra S., and Robert A. Weinberg. 2014. “The Tumour-Induced Systemic Environment as a Critical Regulator of Cancer Progression and Metastasis.” *Nature Cell Biology* 16 (8): 717–27. https://doi.org/10.1038/ncb3015.

McGranahan, Nicholas, and Charles Swanton. 2017. “Clonal Heterogeneity and Tumor Evolution: Past, Present, and the Future.” *Cell* 168 (4): 613–28. https://doi.org/10.1016/j.cell.2017.01.018.

McKee, Karen K., David Harrison, Stephanie Capizzi, and Peter D. Yurchenco. 2007. “Role of Laminin Terminal Globular Domains in Basement Membrane Assembly.” *Journal of Biological Chemistry* 282 (29): 21437–47. https://doi.org/10.1074/jbc.M702963200.

McKenzie, Andrew J., Daisuke Hoshino, Nan Hyung Hong, Diana J. Cha, Jeffrey L. Franklin, Robert J. Coffey, James G. Patton, and Alissa M. Weaver. 2016. “KRAS-MEK Signaling Controls Ago2 Sorting into Exosomes.” *Cell Reports* 15 (5): 978–87. https://doi.org/10.1016/j.celrep.2016.03.085.

Melo, Sonia A., Linda B. Luecke, Christoph Kahlert, Agustin F. Fernandez, Seth T. Gammon, Judith Kaye, Valerie S. LeBleu, et al. 2015. “Glypican-1 Identifies Cancer Exosomes and Detects Early Pancreatic Cancer.” *Nature* 523 (7559): 177–82. https://doi.org/10.1038/nature14581.

Meredith, Matthew M., Kang Liu, Guillaume Darrasse-Jeze, Alice O. Kamphorst, Heidi A. Schreiber, Pierre Guermonprez, Juliana Idoyaga, et al. 2012. “Expression of the Zinc Finger Transcription Factor ZDC (Zbtb46, Btbd4) Defines the Classical Dendritic Cell Lineage.” *The Journal of Experimental Medicine* 209 (6): 1153–65. https://doi.org/10.1084/jem.20112675.

Mierzwa, Beata E., Nicolas Chiaruttini, Lorena Redondo-Morata, Joachim Moser von Filseck, Julia König, Jorge Larios, Ina Poser, et al. 2017. “Dynamic Subunit Turnover in ESCRT-III Assemblies Is Regulated by Vps4 to Mediate Membrane Remodelling during Cytokinesis.” *Nature Cell Biology* 19 (7): 787–98. https://doi.org/10.1038/ncb3559.

Milne, Katy, Martin Köbel, Steven E. Kalloger, Rebecca O. Barnes, Dongxia Gao, C. Blake Gilks, Peter H. Watson, and Brad H. Nelson. 2009. “Systematic Analysis of Immune Infiltrates in High-Grade Serous Ovarian Cancer Reveals CD20, FoxP3 and TIA-1 as Positive Prognostic Factors.” Edited by Derya Unutmaz. *PLoS ONE* 4 (7): e6412. https://doi.org/10.1371/journal.pone.0006412.

Minciacchi, Valentina R., Michael R. Freeman, and Dolores Di Vizio. 2015. “Extracellular Vesicles in Cancer: Exosomes, Microvesicles and the Emerging Role of Large Oncosomes.” *Seminars in Cell & Developmental Biology* 40 (April): 41–51. https://doi.org/10.1016/j.semcdb.2015.02.010.

Mishra, P. J., L. Ha, J. Rieker, E. V. Sviderskaya, D. C. Bennett, M. D. Oberst, K. Kelly, and G. Merlino. 2010. “Dissection of RAS Downstream Pathways in Melanomagenesis: A Role for Ral in Transformation.” *Oncogene* 29 (16): 2449–56. https://doi.org/10.1038/onc.2009.521.

Mitchell, P., E. Petfalski, A. Shevchenko, M. Mann, and D. Tollervey. 1997. “The Exosome: A Conserved Eukaryotic RNA Processing Complex Containing Multiple 3’-->5’ Exoribonucleases.” *Cell* 91 (4): 457–66. https://doi.org/10.1016/s0092-8674(00)80432-8.

Moghadam, Adel Rezaei, Elham Patrad, Elham Tafsiri, Warner Peng, Benjamin Fangman, Timothy J Pluard, Anthony Accurso, et al. 2017. “Ral Signaling Pathway in Health and Cancer.” *Cancer Medicine* 6 (12): 2998–3013. https://doi.org/10.1002/cam4.1105.

Möller, Andreas, and Richard J. Lobb. 2020. “The Evolving Translational Potential of Small Extracellular Vesicles in Cancer.” *Nature Reviews Cancer*, September. https://doi.org/10.1038/s41568-020-00299-w.

Morad, Golnaz, Christopher V. Carman, Elliott J. Hagedorn, Julie R. Perlin, Leonard I. Zon, Nur Mustafaoglu, Tae-Eun Park, Donald E. Ingber, Cassandra C. Daisy, and Marsha A. Moses. 2019. “Tumor-Derived Extracellular Vesicles Breach the Intact Blood-Brain Barrier via Transcytosis.” *ACS Nano* 13 (12): 13853–65. https://doi.org/10.1021/acsnano.9b04397.

Moravec, Radim, Rao Divi, and Mukesh Verma. 2017. “Detecting Circulating Tumor Material and Digital Pathology Imaging during Pancreatic Cancer Progression.” *World Journal of Gastrointestinal Oncology* 9 (6): 235–50. https://doi.org/10.4251/wjgo.v9.i6.235.

Morelli, Adrian E., Adriana T. Larregina, William J. Shufesky, Mara L. G. Sullivan, Donna Beer Stolz, Glenn D. Papworth, Alan F. Zahorchak, et al. 2004. “Endocytosis, Intracellular Sorting, and Processing of Exosomes by Dendritic Cells.” *Blood* 104 (10): 3257–66. https://doi.org/10.1182/blood-2004-03-0824.

Moreno-Gonzalo, Olga, Carolina Villarroya-Beltri, and Francisco Sánchez-Madrid. 2014. “Post-Translational Modifications of Exosomal Proteins.” *Frontiers in Immunology* 5 (August). https://doi.org/10.3389/fimmu.2014.00383.

Morishita, Masaki, Yuki Takahashi, Makiya Nishikawa, Kohei Sano, Kana Kato, Takuma Yamashita, Takafumi Imai, Hideo Saji, and Yoshinobu Takakura. 2015. “Quantitative Analysis of Tissue Distribution of the B16BL6-Derived Exosomes Using a Streptavidin-Lactadherin Fusion Protein and Iodine-125-Labeled Biotin Derivative after Intravenous Injection in Mice.” *Journal of Pharmaceutical Sciences* 104 (2): 705–13. https://doi.org/10.1002/jps.24251.

Mosser, David M., and Xia Zhang. 2008. “Activation of Murine Macrophages.” *Current Protocols in Immunology* 83 (1): 14.2.1-14.2.8. https://doi.org/10.1002/0471142735.im1402s83.

Mulcahy, Laura Ann, Ryan Charles Pink, and David Raul Francisco Carter. 2014. “Routes and Mechanisms of Extracellular Vesicle Uptake.” *Journal of Extracellular Vesicles* 3. https://doi.org/10.3402/jev.v3.24641.

Müller, Kathrin, Dmitry A. Fedosov, and Gerhard Gompper. 2014. “Margination of Micro- and Nano-Particles in Blood Flow and Its Effect on Drug Delivery.” *Scientific Reports* 4 (1): 4871. https://doi.org/10.1038/srep04871.

Muralidharan-Chari, V., J. W. Clancy, A. Sedgwick, and C. D’Souza-Schorey. 2010. “Microvesicles: Mediators of Extracellular Communication during Cancer Progression.” *Journal of Cell Science* 123 (10): 1603–11. https://doi.org/10.1242/jcs.064386.

Murray, Rachael Zoe, and Jennifer Lea Stow. 2014. “Cytokine Secretion in Macrophages: SNAREs, Rabs, and Membrane Trafficking.” *Frontiers in Immunology* 5. https://doi.org/10.3389/fimmu.2014.00538.

Nabhan, J. F., R. Hu, R. S. Oh, S. N. Cohen, and Q. Lu. 2012. “Formation and Release of Arrestin Domain-Containing Protein 1-Mediated Microvesicles (ARMMs) at Plasma Membrane by Recruitment of TSG101 Protein.” *Proceedings of the National Academy of Sciences* 109 (11): 4146–51. https://doi.org/10.1073/pnas.1200448109.

Nakase, Ikuhiko, Kosuke Noguchi, Ikuo Fujii, and Shiroh Futaki. 2016. “Vectorization of Biomacromolecules into Cells Using Extracellular Vesicles with Enhanced

Internalization Induced by Macropinocytosis." *Scientific Reports* 6 (1): 34937. https://doi.org/10.1038/srep34937.
Nakashima, Shintaro, Kenji Morinaka, Shinya Koyama, Masahiro Ikeda, Michiko Kishida, Katsuya Okawa, Akihiro Iwamatsu, Shosei Kishida, and Akira Kikuchi. 1999. "Small G Protein Ral and Its Downstream Molecules Regulate Endocytosis of EGF and Insulin Receptors." *The EMBO Journal* 18 (13): 3629–42. https://doi.org/10.1093/emboj/18.13.3629.
Nazarenko, Irina, Sanyukta Rana, Alexandra Baumann, Jessica McAlear, Andrea Hellwig, Michael Trendelenburg, Günter Lochnit, Klaus T. Preissner, and Margot Zöller. 2010. "Cell Surface Tetraspanin Tspan8 Contributes to Molecular Pathways of Exosome-Induced Endothelial Cell Activation." *Cancer Research* 70 (4): 1668–78. https://doi.org/10.1158/0008-5472.CAN-09-2470.
Nguyen, Michael O, Manisha Jalan, Carl A Morrow, Fekret Osman, and Matthew C Whitby. 2015. "Recombination Occurs within Minutes of Replication Blockage by RTS1 Producing Restarted Forks That Are Prone to Collapse." Edited by Stephen C Kowalczykowski. *ELife* 4 (March): e04539. https://doi.org/10.7554/eLife.04539.
Nguyen-Ngoc, K.-V., K. J. Cheung, A. Brenot, E. R. Shamir, R. S. Gray, W. C. Hines, P. Yaswen, Z. Werb, and A. J. Ewald. 2012. "ECM Microenvironment Regulates Collective Migration and Local Dissemination in Normal and Malignant Mammary Epithelium." *Proceedings of the National Academy of Sciences* 109 (39): E2595–2604. https://doi.org/10.1073/pnas.1212834109.
Niel, Guillaume van, Gisela D'Angelo, and Graça Raposo. 2018. "Shedding Light on the Cell Biology of Extracellular Vesicles." *Nature Reviews Molecular Cell Biology* 19 (4): 213–28. https://doi.org/10.1038/nrm.2017.125.
Nordin, Joel Z., Yi Lee, Pieter Vader, Imre Mäger, Henrik J. Johansson, Wolf Heusermann, Oscar P.B. Wiklander, et al. 2015. "Ultrafiltration with Size-Exclusion Liquid Chromatography for High Yield Isolation of Extracellular Vesicles Preserving Intact Biophysical and Functional Properties." *Nanomedicine: Nanotechnology, Biology and Medicine* 11 (4): 879–83. https://doi.org/10.1016/j.nano.2015.01.003.
Obenauf, Anna C., and Joan Massagué. 2015. "Surviving at a Distance: Organ Specific Metastasis." *Trends in Cancer* 1 (1): 76–91. https://doi.org/10.1016/j.trecan.2015.07.009.
O'Brien, Killian, Koen Breyne, Stefano Ughetto, Louise C. Laurent, and Xandra O. Breakefield. 2020. "RNA Delivery by Extracellular Vesicles in Mammalian Cells and Its Applications." *Nature Reviews Molecular Cell Biology* 21 (10): 585–606. https://doi.org/10.1038/s41580-020-0251-y.
Orimo, Akira, Piyush B. Gupta, Dennis C. Sgroi, Fernando Arenzana-Seisdedos, Thierry Delaunay, Rizwan Naeem, Vincent J. Carey, Andrea L. Richardson, and Robert A. Weinberg. 2005. "Stromal Fibroblasts Present in Invasive Human Breast Carcinomas Promote Tumor Growth and Angiogenesis through Elevated SDF-1/CXCL12 Secretion." *Cell* 121 (3): 335–48. https://doi.org/10.1016/j.cell.2005.02.034.
Oskarsson, Thordur, Swarnali Acharyya, Xiang H-F Zhang, Sakari Vanharanta, Sohail F Tavazoie, Patrick G Morris, Robert J Downey, Katia Manova-Todorova, Edi Brogi, and Joan Massagué. 2011. "Breast Cancer Cells Produce Tenascin C as a Metastatic Niche Component to Colonize the Lungs." *Nature Medicine* 17 (7): 867–74. https://doi.org/10.1038/nm.2379.

Ostrowski, Matias, Nuno B. Carmo, Sophie Krumeich, Isabelle Fanget, Graça Raposo, Ariel Savina, Catarina F. Moita, et al. 2010. "Rab27a and Rab27b Control Different Steps of the Exosome Secretion Pathway." *Nature Cell Biology* 12 (1): 19–30. https://doi.org/10.1038/ncb2000.

Oxford, Gary, Charles R. Owens, Brian J. Titus, Tonia L. Foreman, Mikael C. Herlevsen, Steven C. Smith, and Dan Theodorescu. 2005. "RalA and RalB: Antagonistic Relatives in Cancer Cell Migration." *Cancer Research* 65 (16): 7111–20. https://doi.org/10.1158/0008-5472.CAN-04-1957.

Padua, David, Xiang H-F. Zhang, Qiongqing Wang, Cristina Nadal, William L. Gerald, Roger R. Gomis, and Joan Massagué. 2008. "TGFβ Primes Breast Tumors for Lung Metastasis Seeding through Angiopoietin-like 4." *Cell* 133 (1): 66–77. https://doi.org/10.1016/j.cell.2008.01.046.

Paget, S. 1989. "The Distribution of Secondary Growths in Cancer of the Breast. 1889." *Cancer Metastasis Reviews* 8 (2): 98–101.

Palmulli, Roberta, and Guillaume van Niel. 2018. "To Be or Not to Be... Secreted as Exosomes, a Balance Finely Tuned by the Mechanisms of Biogenesis." Edited by Philip Stahl and Graça Raposo. *Essays in Biochemistry* 62 (2): 177–91. https://doi.org/10.1042/EBC20170076.

Pan, Bin-Tao, and Rose M. Johnstone. 1983. "Fate of the Transferrin Receptor during Maturation of Sheep Reticulocytes in Vitro: Selective Externalization of the Receptor." *Cell* 33 (3): 967–78. https://doi.org/10.1016/0092-8674(83)90040-5.

Parrini, Maria Carla, Amel Sadou-Dubourgnoux, Kazuhiro Aoki, Katsuyuki Kunida, Marco Biondini, Anastassia Hatzoglou, Patrick Poullet, et al. 2011. "SH3BP1, an Exocyst-Associated RhoGAP, Inactivates Rac1 at the Front to Drive Cell Motility." *Molecular Cell* 42 (5): 650–61. https://doi.org/10.1016/j.molcel.2011.03.032.

Pascucci, Luisa, Valentina Coccè, Arianna Bonomi, Diletta Ami, Piero Ceccarelli, Emilio Ciusani, Lucia Viganò, et al. 2014. "Paclitaxel Is Incorporated by Mesenchymal Stromal Cells and Released in Exosomes That Inhibit in Vitro Tumor Growth: A New Approach for Drug Delivery." *Journal of Controlled Release* 192 (October): 262–70. https://doi.org/10.1016/j.jconrel.2014.07.042.

Paszek, Matthew J., Nastaran Zahir, Kandice R. Johnson, Johnathon N. Lakins, Gabriela I. Rozenberg, Amit Gefen, Cynthia A. Reinhart-King, et al. 2005. "Tensional Homeostasis and the Malignant Phenotype." *Cancer Cell* 8 (3): 241–54. https://doi.org/10.1016/j.ccr.2005.08.010.

Pavlyukov, Marat S., Hai Yu, Soniya Bastola, Mutsuko Minata, Victoria O. Shender, Yeri Lee, Suojun Zhang, et al. 2018. "Apoptotic Cell-Derived Extracellular Vesicles Promote Malignancy of Glioblastoma via Intercellular Transfer of Splicing Factors." *Cancer Cell* 34 (1): 119-135.e10. https://doi.org/10.1016/j.ccell.2018.05.012.

Paz, Dante J., and Ariel G. Sánchez. 2015. "Improving the Precision Matrix for Precision Cosmology." *Monthly Notices of the Royal Astronomical Society* 454 (4): 4326–34. https://doi.org/10.1093/mnras/stv2259.

Peinado, Héctor, Maša Alečković, Simon Lavotshkin, Irina Matei, Bruno Costa-Silva, Gema Moreno-Bueno, Marta Hergueta-Redondo, et al. 2012. "Melanoma Exosomes Educate Bone Marrow Progenitor Cells toward a Pro-Metastatic Phenotype through MET." *Nature Medicine* 18 (6): 883–91. https://doi.org/10.1038/nm.2753.

Peinado, Héctor, Haiying Zhang, Irina R. Matei, Bruno Costa-Silva, Ayuko Hoshino, Goncalo Rodrigues, Bethan Psaila, et al. 2017. "Pre-Metastatic Niches: Organ-Specific Homes for Metastases." *Nature Reviews Cancer* 17 (5): 302–17. https://doi.org/10.1038/nrc.2017.6.
Pereira, Ethel R., Dmitriy Kedrin, Giorgio Seano, Olivia Gautier, Eelco F. J. Meijer, Dennis Jones, Shan-Min Chin, et al. 2018. "Lymph Node Metastases Can Invade Local Blood Vessels, Exit the Node, and Colonize Distant Organs in Mice." *Science* 359 (6382): 1403–7. https://doi.org/10.1126/science.aal3622.
Peschard, Pascal, Afshan McCarthy, Valérie Leblanc-Dominguez, Maggie Yeo, Sabrina Guichard, Gordon Stamp, and Christopher J. Marshall. 2012. "Genetic Deletion of RALA and RALB Small GTPases Reveals Redundant Functions in Development and Tumorigenesis." *Current Biology* 22 (21): 2063–68. https://doi.org/10.1016/j.cub.2012.09.013.
Pfeffer, Suzanne R. 2010. "Two Rabs for Exosome Release." *Nature Cell Biology* 12 (1): 3–4. https://doi.org/10.1038/ncb0110-3.
Pisitkun, T., R.-F. Shen, and M. A. Knepper. 2004. "Identification and Proteomic Profiling of Exosomes in Human Urine." *Proceedings of the National Academy of Sciences* 101 (36): 13368–73. https://doi.org/10.1073/pnas.0403453101.
Piskounova, Elena, Michalis Agathocleous, Malea M. Murphy, Zeping Hu, Sara E. Huddlestun, Zhiyu Zhao, A. Marilyn Leitch, Timothy M. Johnson, Ralph J. DeBerardinis, and Sean J. Morrison. 2015. "Oxidative Stress Inhibits Distant Metastasis by Human Melanoma Cells." *Nature* 527 (7577): 186–91. https://doi.org/10.1038/nature15726.
Plebanek, Michael P. 2017. "Pre-Metastatic Cancer Exosomes Induce Immune Surveillance by Patrolling Monocytes at the Metastatic Niche." *NATURE COMMUNICATIONS*, 12.
Poh, Luting, Sung-Wook Kang, Sang-Ha Baik, Gavin Yong Quan Ng, David T. She, Priyanka Balaganapathy, S. Thameem Dheen, et al. 2019. "Evidence That NLRC4 Inflammasome Mediates Apoptotic and Pyroptotic Microglial Death Following Ischemic Stroke." *Brain, Behavior, and Immunity* 75 (January): 34–47. https://doi.org/10.1016/j.bbi.2018.09.001.
Poliakov, Anton, Michael Spilman, Terje Dokland, Christopher L. Amling, and James A. Mobley. 2009. "Structural Heterogeneity and Protein Composition of Exosome-like Vesicles (Prostasomes) in Human Semen." *The Prostate* 69 (2): 159–67. https://doi.org/10.1002/pros.20860.
Polyak, Kornelia. 2007. "Breast Cancer: Origins and Evolution." *The Journal of Clinical Investigation* 117 (11): 3155–63. https://doi.org/10.1172/JCI33295.
Psaila, Bethan, and David Lyden. 2009. "The Metastatic Niche: Adapting the Foreign Soil." *Nature Reviews Cancer* 9 (4): 285–93. https://doi.org/10.1038/nrc2621.
Pucci, Ferdinando, Christopher Garris, Charles P. Lai, Andita Newton, Christina Pfirschke, Camilla Engblom, David Alvarez, et al. 2016. "SCS Macrophages Suppress Melanoma by Restricting Tumor-Derived Vesicle-B Cell Interactions." *Science (New York, N.Y.)* 352 (6282): 242–46. https://doi.org/10.1126/science.aaf1328.
Purushothaman, Anurag, Shyam Kumar Bandari, Jian Liu, James A. Mobley, Elizabeth E. Brown, and Ralph D. Sanderson. 2016. "Fibronectin on the Surface of Myeloma Cell-Derived Exosomes Mediates Exosome-Cell Interactions." *The Journal of Biological Chemistry* 291 (4): 1652–63. https://doi.org/10.1074/jbc.M115.686295.
Qi, Jianfei, Ning Chen, Junfu Wang, and Chi-Hung Siu. 2005. "Transendothelial Migration of Melanoma Cells Involves N-Cadherin-Mediated Adhesion and Activation of the β-

Catenin Signaling Pathway." *Molecular Biology of the Cell* 16 (9): 4386–97. https://doi.org/10.1091/mbc.E05-03-0186.
Qian, Bin-Zhi, Jiufeng Li, Hui Zhang, Takanori Kitamura, Jinghang Zhang, Liam R. Campion, Elizabeth A. Kaiser, Linda A. Snyder, and Jeffrey W. Pollard. 2011. "CCL2 Recruits Inflammatory Monocytes to Facilitate Breast-Tumour Metastasis." *Nature* 475 (7355): 222–25. https://doi.org/10.1038/nature10138.
Qiu, Xia, Haosheng Tan, Deyuan Fu, Yuxiang Zhu, and Jiaxin Zhang. 2018. "Laminin Is over Expressed in Breast Cancer and Facilitate Cancer Cell Metastasis." *Journal of Cancer Research and Therapeutics* 14 (Supplement): S1170–72. https://doi.org/10.4103/0973-1482.191035.
Quail, Daniela F, and Johanna A Joyce. 2013. "Microenvironmental Regulation of Tumor Progression and Metastasis." *Nature Medicine* 19 (11): 1423–37. https://doi.org/10.1038/nm.3394.
Rahn, Jennifer J., Jeffrey W. Chow, Garnet J. Horne, Brian K. Mah, Joanne T. Emerman, Pat Hoffman, and Judith C. Hugh. 2005. "MUC1 Mediates Transendothelial Migration in Vitro by Ligating Endothelial Cell ICAM-1." *Clinical & Experimental Metastasis* 22 (6): 475–83. https://doi.org/10.1007/s10585-005-3098-x.
Rajendran, Lawrence, Masanori Honsho, Tobias R. Zahn, Patrick Keller, Kathrin D. Geiger, Paul Verkade, and Kai Simons. 2006. "Alzheimer's Disease Beta-Amyloid Peptides Are Released in Association with Exosomes." *Proceedings of the National Academy of Sciences of the United States of America* 103 (30): 11172–77. https://doi.org/10.1073/pnas.0603838103.
Ramos-Zayas, Yareellys, Moisés Armides Franco-Molina, Alex Jesús Hernádez-Granados, Diana Ginette Zárate-Triviño, Erika Evangelina Coronado-Cerda, Edgar Mendoza-Gamboa, Pablo Zapata-Benavides, et al. 2019. "Immunotherapy for the Treatment of Canine Transmissible Venereal Tumor Based in Dendritic Cells Pulsed with Tumoral Exosomes." *Immunopharmacology and Immunotoxicology* 41 (1): 48–54. https://doi.org/10.1080/08923973.2018.1533969.
Rankin, E. B., and A. J. Giaccia. 2016. "Hypoxic Control of Metastasis." *Science* 352 (6282): 175–80. https://doi.org/10.1126/science.aaf4405.
Raposo, Graca. 1996. "B Lymphocytes Secrete Antigen-Presenting Vesicles." *The Journal of Experimental Medicine* 183 (3): 1161–72. https://www.ncbi.nlm.nih.gov/pmc/articles/PMC2192324/.
Raposo, Graça, and Philip D. Stahl. 2019. "Extracellular Vesicles: A New Communication Paradigm?" *Nature Reviews Molecular Cell Biology* 20 (9): 509–10. https://doi.org/10.1038/s41580-019-0158-7.
Raynaud, Christophe M., Juana Hernandez, Frédérique P. Llorca, Paolo Nuciforo, Marie-Christine Mathieu, Frederic Commo, Suzette Delaloge, Laure Sabatier, Fabrice André, and Jean-Charles Soria. 2010. "DNA Damage Repair and Telomere Length in Normal Breast, Preneoplastic Lesions, and Invasive Cancer." *American Journal of Clinical Oncology* 33 (4): 341–345. https://doi.org/10.1097/COC.0b013e3181b0c4c2.
Rebbeck, Timothy R., Tara M. Friebel, Nandita Mitra, Fei Wan, Stephanie Chen, Irene L. Andrulis, Paraskevi Apostolou, et al. 2016. "Inheritance of Deleterious Mutations at Both BRCA1 and BRCA2 in an International Sample of 32,295 Women." *Breast Cancer Research : BCR* 18. https://doi.org/10.1186/s13058-016-0768-3.

Record, Michel, Sandrine Silvente-Poirot, Marc Poirot, and Michael J. O. Wakelam. 2018. "Extracellular Vesicles: Lipids as Key Components of Their Biogenesis and Functions." *Journal of Lipid Research* 59 (8): 1316–24. https://doi.org/10.1194/jlr.E086173.

Regmi, Sagar, Afu Fu, and Kathy Qian Luo. 2017. "High Shear Stresses under Exercise Condition Destroy Circulating Tumor Cells in a Microfluidic System." *Scientific Reports* 7 (1): 39975. https://doi.org/10.1038/srep39975.

Remec Pavlin, Mark, and James H. Hurley. 2020. "The ESCRTs – Converging on Mechanism." *Journal of Cell Science* 133 (18): jcs240333. https://doi.org/10.1242/jcs.240333.

Ricklefs, Franz L., Quazim Alayo, Harald Krenzlin, Ahmad B. Mahmoud, Maria C. Speranza, Hiroshi Nakashima, Josie L. Hayes, et al. 2018. "Immune Evasion Mediated by PD-L1 on Glioblastoma-Derived Extracellular Vesicles." *Science Advances* 4 (3): eaar2766. https://doi.org/10.1126/sciadv.aar2766.

Roberts, P J, and C J Der. 2007. "Targeting the Raf-MEK-ERK Mitogen-Activated Protein Kinase Cascade for the Treatment of Cancer." *Oncogene* 26 (22): 3291–3310. https://doi.org/10.1038/sj.onc.1210422.

Roefs, Marieke T., Joost P.G. Sluijter, and Pieter Vader. 2020. "Extracellular Vesicle-Associated Proteins in Tissue Repair." *Trends in Cell Biology*, October, S0962892420301896. https://doi.org/10.1016/j.tcb.2020.09.009.

Rossé, Carine, Anastassia Hatzoglou, Maria-Carla Parrini, Michael A. White, Philippe Chavrier, and Jacques Camonis. 2006. "RalB Mobilizes the Exocyst To Drive Cell Migration." *Molecular and Cellular Biology* 26 (2): 727–34. https://doi.org/10.1128/MCB.26.2.727-734.2006.

Russo, Isabella, Luigi Bubacco, and Elisa Greggio. 2012. "Exosomes-Associated Neurodegeneration and Progression of Parkinson's Disease." *American Journal of Neurodegenerative Disease* 1 (3): 217–25. https://www.ncbi.nlm.nih.gov/pmc/articles/PMC3560468/.

Sansone, Pasquale, Claudia Savini, Ivana Kurelac, Qing Chang, Laura Benedetta Amato, Antonio Strillacci, Anna Stepanova, et al. 2017. "Packaging and Transfer of Mitochondrial DNA via Exosomes Regulate Escape from Dormancy in Hormonal Therapy-Resistant Breast Cancer." *Proceedings of the National Academy of Sciences* 114 (43): E9066–75. https://doi.org/10.1073/pnas.1704862114.

Satpathy, Ansuman T, Xiaodi Wu, Jörn C Albring, and Kenneth M Murphy. 2012. "Re(de)Fining the Dendritic Cell Lineage." *Nature Immunology* 13 (12): 1145–54. https://doi.org/10.1038/ni.2467.

Saunderson, Sarah C., Amy C. Dunn, Paul R. Crocker, and Alexander D. McLellan. 2014. "CD169 Mediates the Capture of Exosomes in Spleen and Lymph Node." *Blood* 123 (2): 208–16. https://doi.org/10.1182/blood-2013-03-489732.

Savardashtaki, Amir, Zahra Shabaninejad, Ahmad Movahedpour, Roxana Sahebnasagh, Hamed Mirzaei, and Michael R. Hamblin. 2019. "MiRNAs Derived from Cancer-Associated Fibroblasts in Colorectal Cancer." *Epigenomics* 11 (14): 1627–45. https://doi.org/10.2217/epi-2019-0110.

Savina, Ariel, Claudio M. Fader, María T. Damiani, and María Isabel Colombo. 2005. "Rab11 Promotes Docking and Fusion of Multivesicular Bodies in a Calcium-Dependent Manner." *Traffic* 6 (2): 131–43. https://doi.org/10.1111/j.1600-0854.2004.00257.x.

Schey, Kevin L., J. Matthew Luther, and Kristie L. Rose. 2015. “Proteomics Characterization of Exosome Cargo.” *Methods (San Diego, Calif.)* 87 (October): 75–82. https://doi.org/10.1016/j.ymeth.2015.03.018.
Schöneberg, Johannes, Il-Hyung Lee, Janet H. Iwasa, and James H. Hurley. 2017. “Reverse-Topology Membrane Scission by the ESCRT Complexes.” *Nature Reviews. Molecular Cell Biology* 18 (1): 5–17. https://doi.org/10.1038/nrm.2016.121.
Schreiber, Robert D., Lloyd J. Old, and Mark J. Smyth. 2011. “Cancer Immunoediting: Integrating Immunity’s Roles in Cancer Suppression and Promotion.” *Science* 331 (6024): 1565–70. https://doi.org/10.1126/science.1203486.
Scott, Cameron C., Fabrizio Vacca, and Jean Gruenberg. 2014. “Endosome Maturation, Transport and Functions.” *Seminars in Cell & Developmental Biology* 31 (July): 2–10. https://doi.org/10.1016/j.semcdb.2014.03.034.
Segura, Elodie, Carole Nicco, Bérangère Lombard, Philippe Véron, Graça Raposo, Frédéric Batteux, Sebastian Amigorena, and Clotilde Théry. 2005. “ICAM-1 on Exosomes from Mature Dendritic Cells Is Critical for Efficient Naive T-Cell Priming.” *Blood* 106 (1): 216–23. https://doi.org/10.1182/blood-2005-01-0220.
Sell, Stewart. 2005. “Leukemia: Stem Cells, Maturation Arrest, and Differentiation Therapy.” *Stem Cell Reviews* 1 (3): 197–205. https://doi.org/10.1385/SCR:1:3:197.
Sevenich, Lisa, and Johanna A. Joyce. 2014. “Pericellular Proteolysis in Cancer.” *Genes & Development* 28 (21): 2331–47. https://doi.org/10.1101/gad.250647.114.
Sharma, Aman. 2018. “Role of Stem Cell Derived Exosomes in Tumor Biology.” *International Journal of Cancer* 142 (6): 1086–92. https://doi.org/10.1002/ijc.31089.
Sharma, Padmanee, and James P. Allison. 2015. “The Future of Immune Checkpoint Therapy.” *Science* 348 (6230): 56–61. https://doi.org/10.1126/science.aaa8172.
Shen, Yingjie, Lizhong Xu, and David A. Foster. 2001. “Role for Phospholipase D in Receptor-Mediated Endocytosis.” *Molecular and Cellular Biology* 21 (2): 595–602. https://doi.org/10.1128/MCB.21.2.595-602.2001.
Shields, J. D., I. C. Kourtis, A. A. Tomei, J. M. Roberts, and M. A. Swartz. 2010. “Induction of Lymphoidlike Stroma and Immune Escape by Tumors That Express the Chemokine CCL21.” *Science* 328 (5979): 749–52. https://doi.org/10.1126/science.1185837.
Shirakawa, Ryutaro, Shuya Fukai, Mitsunori Kawato, Tomohito Higashi, Hirokazu Kondo, Tomoyuki Ikeda, Ei Nakayama, et al. 2009. “Tuberous Sclerosis Tumor Suppressor Complex-like Complexes Act as GTPase-Activating Proteins for Ral GTPases.” *The Journal of Biological Chemistry* 284 (32): 21580–88. https://doi.org/10.1074/jbc.M109.012112.
Shurtleff, Matthew J., Jun Yao, Yidan Qin, Ryan M. Nottingham, Morayma M. Temoche-Diaz, Randy Schekman, and Alan M. Lambowitz. 2017. “Broad Role for YBX1 in Defining the Small Noncoding RNA Composition of Exosomes.” *Proceedings of the National Academy of Sciences* 114 (43): E8987–95. https://doi.org/10.1073/pnas.1712108114.
Sica, Antonio, and Vincenzo Bronte. 2007. “Altered Macrophage Differentiation and Immune Dysfunction in Tumor Development.” *Journal of Clinical Investigation* 117 (5): 1155–66. https://doi.org/10.1172/JCI31422.
Siegel, Rebecca L., Kimberly D. Miller, and Ahmedin Jemal. 2018. “Cancer Statistics, 2018.” *CA: A Cancer Journal for Clinicians* 68 (1): 7–30. https://doi.org/10.3322/caac.21442.

Simpson, Richard J., Hina Kalra, and Suresh Mathivanan. 2012. “ExoCarta as a Resource for Exosomal Research.” *Journal of Extracellular Vesicles* 1 (1): 18374. https://doi.org/10.3402/jev.v1i0.18374.

Sinha, Seema, Daisuke Hoshino, Nan Hyung Hong, Kellye C. Kirkbride, Nathan E. Grega-Larson, Motoharu Seiki, Matthew J. Tyska, and Alissa M. Weaver. 2016. “Cortactin Promotes Exosome Secretion by Controlling Branched Actin Dynamics.” *The Journal of Cell Biology* 214 (2): 197–213. https://doi.org/10.1083/jcb.201601025.

Skotland, Tore, Nina P. Hessvik, Kirsten Sandvig, and Alicia Llorente. 2019. “Exosomal Lipid Composition and the Role of Ether Lipids and Phosphoinositides in Exosome Biology.” *Journal of Lipid Research* 60 (1): 9–18. https://doi.org/10.1194/jlr.R084343.

Skotland, Tore, Krizia Sagini, Kirsten Sandvig, and Alicia Llorente. 2020. “An Emerging Focus on Lipids in Extracellular Vesicles.” *Advanced Drug Delivery Reviews*, March, S0169409X20300144. https://doi.org/10.1016/j.addr.2020.03.002.

Sleeman, Jonathan P. 2012. “The Metastatic Niche and Stromal Progression.” *Cancer Metastasis Reviews* 31 (3–4): 429–40. https://doi.org/10.1007/s10555-012-9373-9.

Smith, S. C., A. S. Baras, C. R. Owens, G. Dancik, and D. Theodorescu. 2012. “Transcriptional Signatures of Ral GTPase Are Associated with Aggressive Clinicopathologic Characteristics in Human Cancer.” *Cancer Research* 72 (14): 3480–91. https://doi.org/10.1158/0008-5472.CAN-11-3966.

Smith, S. C., G. Oxford, A. S. Baras, C. Owens, D. Havaleshko, D. L. Brautigan, M. K. Safo, and D. Theodorescu. 2007. “Expression of Ral GTPases, Their Effectors, and Activators in Human Bladder Cancer.” *Clinical Cancer Research* 13 (13): 3803–13. https://doi.org/10.1158/1078-0432.CCR-06-2419.

Spaderna, Simone, Otto Schmalhofer, Falk Hlubek, Geert Berx, Andreas Eger, Susanne Merkel, Andreas Jung, Thomas Kirchner, and Thomas Brabletz. 2006. “A Transient, EMT-Linked Loss of Basement Membranes Indicates Metastasis and Poor Survival in Colorectal Cancer.” *Gastroenterology* 131 (3): 830–40. https://doi.org/10.1053/j.gastro.2006.06.016.

Srinivasan, Swetha, Fredrik O. Vannberg, and J. Brandon Dixon. 2016. “Lymphatic Transport of Exosomes as a Rapid Route of Information Dissemination to the Lymph Node.” *Scientific Reports* 6 (1): 24436. https://doi.org/10.1038/srep24436.

Stranska, Ruzena, Laurens Gysbrechts, Jens Wouters, Pieter Vermeersch, Katarzyna Bloch, Daan Dierickx, Graciela Andrei, and Robert Snoeck. 2018. “Comparison of Membrane Affinity-Based Method with Size-Exclusion Chromatography for Isolation of Exosome-like Vesicles from Human Plasma.” *Journal of Translational Medicine* 16 (January). https://doi.org/10.1186/s12967-017-1374-6.

Strauss, Katrin, Cornelia Goebel, Heiko Runz, Wiebke Möbius, Sievert Weiss, Ivo Feussner, Mikael Simons, and Anja Schneider. 2010. “Exosome Secretion Ameliorates Lysosomal Storage of Cholesterol in Niemann-Pick Type C Disease.” *The Journal of Biological Chemistry* 285 (34): 26279–88. https://doi.org/10.1074/jbc.M110.134775.

Strilic, Boris, and Stefan Offermanns. 2017. “Intravascular Survival and Extravasation of Tumor Cells.” *Cancer Cell* 32 (3): 282–93. https://doi.org/10.1016/j.ccell.2017.07.001.

Stuffers, Susanne, Catherine Sem Wegner, Harald Stenmark, and Andreas Brech. 2009. “Multivesicular Endosome Biogenesis in the Absence of ESCRTs.” *Traffic* 10 (7): 925–37. https://doi.org/10.1111/j.1600-0854.2009.00920.x.

Stylianopoulos, Triantafyllos, John D. Martin, Vikash P. Chauhan, Saloni R. Jain, Benjamin Diop-Frimpong, Nabeel Bardeesy, Barbara L. Smith, et al. 2012. "Causes, Consequences, and Remedies for Growth-Induced Solid Stress in Murine and Human Tumors." *Proceedings of the National Academy of Sciences* 109 (38): 15101–8. https://doi.org/10.1073/pnas.1213353109.

Sugimoto, Hikaru, Thomas M Mundel, Mark W. Kieran, and Raghu Kalluri. 2006. "Identification of Fibroblast Heterogeneity in the Tumor Microenvironment." *Cancer Biology & Therapy* 5 (12): 1640–46. https://doi.org/10.4161/cbt.5.12.3354.

Sung, Bong Hwan, Tatiana Ketova, Daisuke Hoshino, Andries Zijlstra, and Alissa M. Weaver. 2015. "Directional Cell Movement through Tissues Is Controlled by Exosome Secretion." *Nature Communications* 6 (1): 7164. https://doi.org/10.1038/ncomms8164.

Sung, Bong Hwan, and Alissa M. Weaver. 2017. "Exosome Secretion Promotes Chemotaxis of Cancer Cells." *Cell Adhesion & Migration* 11 (2): 187–95. https://doi.org/10.1080/19336918.2016.1273307.

Sungur, Can M., and William J. Murphy. 2014. "Positive and Negative Regulation by NK Cells in Cancer." *Critical Reviews in Oncogenesis* 19 (1–2): 57–66. https://doi.org/10.1615/CritRevOncog.2014010805.

Swartz, Melody A., and Amanda W. Lund. 2012. "Lymphatic and Interstitial Flow in the Tumour Microenvironment: Linking Mechanobiology with Immunity." *Nature Reviews Cancer* 12 (3): 210–19. https://doi.org/10.1038/nrc3186.

Syn, Nicholas, Lingzhi Wang, Gautam Sethi, Jean-Paul Thiery, and Boon-Cher Goh. 2016. "Exosome-Mediated Metastasis: From Epithelial–Mesenchymal Transition to Escape from Immunosurveillance." *Trends in Pharmacological Sciences* 37 (7): 606–17. https://doi.org/10.1016/j.tips.2016.04.006.

Tabariès, Sébastien, Fanny Dupuy, Zhifeng Dong, Anie Monast, Matthew G. Annis, Jonathan Spicer, Lorenzo E. Ferri, et al. 2012. "Claudin-2 Promotes Breast Cancer Liver Metastasis by Facilitating Tumor Cell Interactions with Hepatocytes." *Molecular and Cellular Biology* 32 (15): 2979–91. https://doi.org/10.1128/MCB.00299-12.

Taira, Eiichi, Keiko Kohama, Yasuhiro Tsukamoto, Shigeki Okumura, and Naomasa Miki. 2005. "Gicerin/CD146 Is Involved in Neurite Extension of NGF-Treated PC12 Cells." *Journal of Cellular Physiology* 204 (2): 632–37. https://doi.org/10.1002/jcp.20365.

Taira, Eiichi, Natsuki Takaha, Hideo Taniura, Cheol-Hee Kim, and Naomasa Miki. 1994. "Molecular Cloning and Functional Expression of Gicerin, a Novel Cell Adhesion Molecule That Binds to Neurite Outgrowth Factor." *Neuron* 12 (4): 861–72. https://doi.org/10.1016/0896-6273(94)90338-7.

Tang, Yanyan, Ping Zhang, Yumin Wang, Jinpeng Wang, Min Su, Ying Wang, Lianqing Zhou, et al. 2020. "The Biogenesis, Biology, and Clinical Significance of Exosomal PD-L1 in Cancer." *Frontiers in Immunology* 11 (April). https://doi.org/10.3389/fimmu.2020.00604.

Tauro, Bow J., David W. Greening, Rommel A. Mathias, Suresh Mathivanan, Hong Ji, and Richard J. Simpson. 2013. "Two Distinct Populations of Exosomes Are Released from LIM1863 Colon Carcinoma Cell-Derived Organoids." *Molecular & Cellular Proteomics : MCP* 12 (3): 587–98. https://doi.org/10.1074/mcp.M112.021303.

Thakur, Basant Kumar, Haiying Zhang, Annette Becker, Irina Matei, Yujie Huang, Bruno Costa-Silva, Yan Zheng, et al. 2014. "Double-Stranded DNA in Exosomes: A Novel Biomarker in Cancer Detection." *Cell Research* 24 (6): 766–69. https://doi.org/10.1038/cr.2014.44.

Théry, Clotilde, Sebastian Amigorena, Graça Raposo, and Aled Clayton. 2006. “Isolation and Characterization of Exosomes from Cell Culture Supernatants and Biological Fluids.” *Current Protocols in Cell Biology* 30 (1): 3.22.1-3.22.29. https://doi.org/10.1002/0471143030.cb0322s30.

Théry, Clotilde, Kenneth W Witwer, Elena Aikawa, Maria Jose Alcaraz, Johnathon D Anderson, Ramaroson Andriantsitohaina, Anna Antoniou, et al. 2018. “Minimal Information for Studies of Extracellular Vesicles 2018 (MISEV2018): A Position Statement of the International Society for Extracellular Vesicles and Update of the MISEV2014 Guidelines.” *Journal of Extracellular Vesicles* 7 (1): 1535750. https://doi.org/10.1080/20013078.2018.1535750.

Théry, Clotilde, Laurence Zitvogel, and Sebastian Amigorena. 2002. “Exosomes: Composition, Biogenesis and Function.” *Nature Reviews Immunology* 2 (8): 569–79. https://doi.org/10.1038/nri855.

Thomas, Stacy K., Jesse Lee, and Gregory L. Beatty. 2020. “Paracrine and Cell Autonomous Signalling in Pancreatic Cancer Progression and Metastasis.” *EBioMedicine* 53 (March): 102662. https://doi.org/10.1016/j.ebiom.2020.102662.

Tichet, Mélanie, Virginie Prod’Homme, Nina Fenouille, Damien Ambrosetti, Aude Mallavialle, Michael Cerezo, Mickaël Ohanna, et al. 2015. “Tumour-Derived SPARC Drives Vascular Permeability and Extravasation through Endothelial VCAM1 Signalling to Promote Metastasis.” *Nature Communications* 6 (1): 6993. https://doi.org/10.1038/ncomms7993.

Tominaga, Naoomi, Nobuyoshi Kosaka, Makiko Ono, Takeshi Katsuda, Yusuke Yoshioka, Kenji Tamura, Jan Lotvall, Hitoshi Nakagama, and Takahiro Ochiya. 2015. “Brain Metastatic Cancer Cells Release MicroRNA- 181c-Containing Extracellular Vesicles Capable of Destructing Blood–Brain Barrier.” *NATURE COMMUNICATIONS*, 12.

Toy, Randall, Elliott Hayden, Christopher Shoup, Harihara Baskaran, and Efstathios Karathanasis. 2011. “The Effects of Particle Size, Density and Shape on Margination of Nanoparticles in Microcirculation.” *Nanotechnology* 22 (11): 115101. https://doi.org/10.1088/0957-4484/22/11/115101.

Trajkovic, Katarina, Chieh Hsu, Salvatore Chiantia, Lawrence Rajendran, Dirk Wenzel, Felix Wieland, Petra Schwille, Britta Brügger, and Mikael Simons. 2008. “Ceramide Triggers Budding of Exosome Vesicles into Multivesicular Endosomes.” *Science* 319 (5867): 1244–47. https://doi.org/10.1126/science.1153124.

Trams, Eberhard G., Carl J. Lauter, Jr. Norman Salem, and Ursula Heine. 1981. “Exfoliation of Membrane Ecto-Enzymes in the Form of Micro-Vesicles.” *Biochimica et Biophysica Acta (BBA) - Biomembranes* 645 (1): 63–70. https://doi.org/10.1016/0005-2736(81)90512-5.

Tricarico, Christopher, James Clancy, and Crislyn D’Souza-Schorey. 2016. “Biology and Biogenesis of Shed Microvesicles.” *Small GTPases* 8 (4): 220–32. https://doi.org/10.1080/21541248.2016.1215283.

Umezu, Tomohiro, Hiroko Tadokoro, Kenko Azuma, Seiichiro Yoshizawa, Kazuma Ohyashiki, and Junko H. Ohyashiki. 2014. “Exosomal MiR-135b Shed from Hypoxic Multiple Myeloma Cells Enhances Angiogenesis by Targeting Factor-Inhibiting HIF-1.” *Blood* 124 (25): 3748–57. https://doi.org/10.1182/blood-2014-05-576116.

Urano, T., R. Emkey, and L. A. Feig. 1996. “Ral-GTPases Mediate a Distinct Downstream Signaling Pathway from Ras That Facilitates Cellular Transformation.” *The EMBO Journal* 15 (4): 810–16.

Valadi, Hadi, Karin Ekström, Apostolos Bossios, Margareta Sjöstrand, James J Lee, and Jan O Lötvall. 2007. “Exosome-Mediated Transfer of MRNAs and MicroRNAs Is a Novel Mechanism of Genetic Exchange between Cells.” *Nature Cell Biology* 9 (6): 654–59. https://doi.org/10.1038/ncb1596.

Valapala, Mallika, and Jamboor K. Vishwanatha. 2011. “Lipid Raft Endocytosis and Exosomal Transport Facilitate Extracellular Trafficking of Annexin A2.” *The Journal of Biological Chemistry* 286 (35): 30911–25. https://doi.org/10.1074/jbc.M111.271155.

Valastyan, Scott, and Robert A. Weinberg. 2011. “Tumor Metastasis: Molecular Insights and Evolving Paradigms.” *Cell* 147 (2): 275–92. https://doi.org/10.1016/j.cell.2011.09.024.

Valencia, Karmele, Diego Luis-Ravelo, Nicolas Bovy, Iker Antón, Susana Martínez-Canarias, Carolina Zandueta, Cristina Ormazábal, et al. 2014. “MiRNA Cargo within Exosome-like Vesicle Transfer Influences Metastatic Bone Colonization.” *Molecular Oncology* 8 (3): 689–703. https://doi.org/10.1016/j.molonc.2014.01.012.

van Niel, Guillaume, Stéphanie Charrin, Sabrina Simoes, Maryse Romao, Leila Rochin, Paul Saftig, Michael S. Marks, Eric Rubinstein, and Graça Raposo. 2011. “The Tetraspanin CD63 Regulates ESCRT-Independent and -Dependent Endosomal Sorting during Melanogenesis.” *Developmental Cell* 21 (4): 708–21. https://doi.org/10.1016/j.devcel.2011.08.019.

Verweij, Frederik J, Monique A J van Eijndhoven, Erik S Hopmans, Tineke Vendrig, Tom Wurdinger, Ellen Cahir-McFarland, Elliott Kieff, et al. 2011. “LMP1 Association with CD63 in Endosomes and Secretion via Exosomes Limits Constitutive NF-KB Activation.” *The EMBO Journal* 30 (11): 2115–29. https://doi.org/10.1038/emboj.2011.123.

Verweij, Frederik J., Vincent Hyenne, Guillaume Van Niel, and Jacky G. Goetz. 2019. “Extracellular Vesicles: Catching the Light in Zebrafish.” *Trends in Cell Biology* 29 (10): 770–76. https://doi.org/10.1016/j.tcb.2019.07.007.

Verweij, Frederik J., Celine Revenu, Guillaume Arras, Florent Dingli, Damarys Loew, D. Michiel Pegtel, Gautier Follain, et al. 2019. “Live Tracking of Inter-Organ Communication by Endogenous Exosomes In Vivo.” *Developmental Cell* 48 (4): 573-589.e4. https://doi.org/10.1016/j.devcel.2019.01.004.

Viaud, Sophie, Magali Terme, Caroline Flament, Julien Taieb, Fabrice André, Sophie Novault, Bernard Escudier, et al. 2009. “Dendritic Cell-Derived Exosomes Promote Natural Killer Cell Activation and Proliferation: A Role for NKG2D Ligands and IL-15Rα.” *PLoS ONE* 4 (3). https://doi.org/10.1371/journal.pone.0004942.

Vidal, M., P. Mangeat, and D. Hoekstra. 1997. “Aggregation Reroutes Molecules from a Recycling to a Vesicle-Mediated Secretion Pathway during Reticulocyte Maturation.” *Journal of Cell Science* 110 (16): 1867–77. https://jcs.biologists.org/content/110/16/1867.

Villarroya-Beltri, Carolina, Cristina Gutiérrez-Vázquez, Fátima Sánchez-Cabo, Daniel Pérez-Hernández, Jesús Vázquez, Noa Martin-Cofreces, Dannys Jorge Martinez-Herrera, Alberto Pascual-Montano, María Mittelbrunn, and Francisco Sánchez-Madrid. 2013. “Sumoylated HnRNPA2B1 Controls the Sorting of MiRNAs into Exosomes through

Binding to Specific Motifs." *Nature Communications* 4 (1): 2980. https://doi.org/10.1038/ncomms3980.
Visvader, J. E., and J. Stingl. 2014. "Mammary Stem Cells and the Differentiation Hierarchy: Current Status and Perspectives." *Genes & Development* 28 (11): 1143–58. https://doi.org/10.1101/gad.242511.114.
Vitale, Nicolas, Sylvette Chasserot-Golaz, Yannick Bailly, Naoko Morinaga, Michael A. Frohman, and Marie-France Bader. 2002. "Calcium-Regulated Exocytosis of Dense-Core Vesicles Requires the Activation of ADP-Ribosylation Factor (ARF)6 by ARF Nucleotide Binding Site Opener at the Plasma Membrane." *Journal of Cell Biology* 159 (1): 79–89. https://doi.org/10.1083/jcb.200203027.
Voduc, K. David, Maggie C.U. Cheang, Scott Tyldesley, Karen Gelmon, Torsten O. Nielsen, and Hagen Kennecke. 2010. "Breast Cancer Subtypes and the Risk of Local and Regional Relapse." *Journal of Clinical Oncology* 28 (10): 1684–91. https://doi.org/10.1200/JCO.2009.24.9284.
Vogel, Robert, Frank A. W. Coumans, Raluca G. Maltesen, Anita N. Böing, Katherine E. Bonnington, Marike L. Broekman, Murray F. Broom, et al. 2016. "A Standardized Method to Determine the Concentration of Extracellular Vesicles Using Tunable Resistive Pulse Sensing." *Journal of Extracellular Vesicles* 5: 31242. https://doi.org/10.3402/jev.v5.31242.
Vos, Kristan E. van der, Erik R. Abels, Xuan Zhang, Charles Lai, Esteban Carrizosa, Derek Oakley, Shilpa Prabhakar, et al. 2016. "Directly Visualized Glioblastoma-Derived Extracellular Vesicles Transfer RNA to Microglia/Macrophages in the Brain." *Neuro-Oncology* 18 (1): 58–69. https://doi.org/10.1093/neuonc/nov244.
Walker, Cameron, Elijah Mojares, and Armando del Río Hernández. 2018. "Role of Extracellular Matrix in Development and Cancer Progression." *International Journal of Molecular Sciences* 19 (10): 3028. https://doi.org/10.3390/ijms19103028.
Wan, Liling, Klaus Pantel, and Yibin Kang. 2013. "Tumor Metastasis: Moving New Biological Insights into the Clinic." *Nature Medicine* 19 (11): 1450–64. https://doi.org/10.1038/nm.3391.
Wang, Jie, Yue Dong, Yiwei Li, Wei Li, Kai Cheng, Yuan Qian, Guoqiang Xu, et al. 2018. "Designer Exosomes for Active Targeted Chemo-Photothermal Synergistic Tumor Therapy." *Advanced Functional Materials* 28 (18): 1707360. https://doi.org/10.1002/adfm.201707360.
Wang, Karin, Bo Ri Seo, Claudia Fischbach, and Delphine Gourdon. 2016. "Fibronectin Mechanobiology Regulates Tumorigenesis." *Cellular and Molecular Bioengineering* 9 (1): 1–11. https://doi.org/10.1007/s12195-015-0417-4.
Wang, Qingqing, Qichao Ni, Xudong Wang, Huijun Zhu, Zhiwei Wang, and Jianfei Huang. 2015. "High Expression of RAB27A and TP53 in Pancreatic Cancer Predicts Poor Survival." *Medical Oncology* 32 (1): 372. https://doi.org/10.1007/s12032-014-0372-2.
Wang, Ting, Daniele M. Gilkes, Naoharu Takano, Lisha Xiang, Weibo Luo, Corey J. Bishop, Pallavi Chaturvedi, Jordan J. Green, and Gregg L. Semenza. 2014. "Hypoxia-Inducible Factors and RAB22A Mediate Formation of Microvesicles That Stimulate Breast Cancer Invasion and Metastasis." *Proceedings of the National Academy of Sciences of the United States of America* 111 (31): E3234-3242. https://doi.org/10.1073/pnas.1410041111.

Wang, Tuanlao, Zhang Ming, Wu Xiaochun, and Wanjin Hong. 2011. “Rab7: Role of Its Protein Interaction Cascades in Endo-Lysosomal Traffic.” *Cellular Signalling* 23 (3): 516–21. https://doi.org/10.1016/j.cellsig.2010.09.012.

Wang, Zhaoqing, Qingji Xu, Nengwei Zhang, Xuemei Du, Guangzhong Xu, and Xiyun Yan. 2020. “CD146, from a Melanoma Cell Adhesion Molecule to a Signaling Receptor.” *Signal Transduction and Targeted Therapy* 5 (1): 148. https://doi.org/10.1038/s41392-020-00259-8.

Wang, Zhaoqing, and Xiyun Yan. 2013. “CD146, a Multi-Functional Molecule beyond Adhesion.” *Cancer Letters* 330 (2): 150–62. https://doi.org/10.1016/j.canlet.2012.11.049.

Webber, Jason, and Aled Clayton. 2013. “How Pure Are Your Vesicles?” *Journal of Extracellular Vesicles* 2 (January). https://doi.org/10.3402/jev.v2i0.19861.

Wei, Zhiyun, Arsen O. Batagov, Sergio Schinelli, Jintu Wang, Yang Wang, Rachid El Fatimy, Rosalia Rabinovsky, et al. 2017. “Coding and Noncoding Landscape of Extracellular RNA Released by Human Glioma Stem Cells.” *Nature Communications* 8 (1): 1145. https://doi.org/10.1038/s41467-017-01196-x.

Wen, Shu Wen, Jaclyn Sceneay, Luize Goncalves Lima, Christina S.F. Wong, Melanie Becker, Sophie Krumeich, Richard J. Lobb, et al. 2016. “The Biodistribution and Immune Suppressive Effects of Breast Cancer–Derived Exosomes.” *Cancer Research* 76 (23): 6816–27. https://doi.org/10.1158/0008-5472.CAN-16-0868.

Wenzel, Eva Maria, Sebastian Wolfgang Schultz, Kay Oliver Schink, Nina Marie Pedersen, Viola Nähse, Andreas Carlson, Andreas Brech, Harald Stenmark, and Camilla Raiborg. 2018. “Concerted ESCRT and Clathrin Recruitment Waves Define the Timing and Morphology of Intraluminal Vesicle Formation.” *Nature Communications* 9 (1): 2932. https://doi.org/10.1038/s41467-018-05345-8.

White, E., and R. S. DiPaola. 2009. “The Double-Edged Sword of Autophagy Modulation in Cancer.” *Clinical Cancer Research* 15 (17): 5308–16. https://doi.org/10.1158/1078-0432.CCR-07-5023.

Willms, Eduard, Carlos Cabañas, Imre Mäger, Matthew J. A. Wood, and Pieter Vader. 2018. “Extracellular Vesicle Heterogeneity: Subpopulations, Isolation Techniques, and Diverse Functions in Cancer Progression.” *Frontiers in Immunology* 9 (April). https://doi.org/10.3389/fimmu.2018.00738.

Willms, Eduard, Henrik J. Johansson, Imre Mäger, Yi Lee, K. Emelie M. Blomberg, Mariam Sadik, Amr Alaarg, et al. 2016. “Cells Release Subpopulations of Exosomes with Distinct Molecular and Biological Properties.” *Scientific Reports* 6 (March). https://doi.org/10.1038/srep22519.

Wisdom, Katrina M., Kolade Adebowale, Julie Chang, Joanna Y. Lee, Sungmin Nam, Rajiv Desai, Ninna Struck Rossen, et al. 2018. “Matrix Mechanical Plasticity Regulates Cancer Cell Migration through Confining Microenvironments.” *Nature Communications* 9 (1): 4144. https://doi.org/10.1038/s41467-018-06641-z.

Witwer, Kenneth W., and Clotilde Théry. 2019. “Extracellular Vesicles or Exosomes? On Primacy, Precision, and Popularity Influencing a Choice of Nomenclature.” *Journal of Extracellular Vesicles* 8 (1): 1648167. https://doi.org/10.1080/20013078.2019.1648167.

Wolf, Erika J., Kelly M. Harrington, Shaunna L. Clark, and Mark W. Miller. 2013. “Sample Size Requirements for Structural Equation Models: An Evaluation of Power, Bias, and

Solution Propriety." *Educational and Psychological Measurement* 73 (6): 913–34. https://doi.org/10.1177/0013164413495237.
Wolf, Peter. 1967. "The Nature and Significance of Platelet Products in Human Plasma." *British Journal of Haematology* 13 (3): 269–88. https://doi.org/10.1111/j.1365-2141.1967.tb08741.x.
Wu, Yueting, Wentao Deng, and David J. Klinke. 2015. "Exosomes: Improved Methods to Characterize Their Morphology, RNA Content, and Surface Protein Biomarkers." *The Analyst* 140 (19): 6631–42. https://doi.org/10.1039/c5an00688k.
Yan, Chao, Degang Liu, Liwei Li, Michael F. Wempe, Sunny Guin, May Khanna, Jeremy Meier, et al. 2014. "Discovery and Characterization of Small Molecules That Target the GTPase Ral." *Nature* 515 (7527): 443–47. https://doi.org/10.1038/nature13713.
Yan, Chao, and Dan Theodorescu. 2018. "RAL GTPases: Biology and Potential as Therapeutic Targets in Cancer." *Pharmacological Reviews* 70 (1): 1–11. https://doi.org/10.1124/pr.117.014415.
Yan, H. H., M. Pickup, Y. Pang, A. E. Gorska, Z. Li, A. Chytil, Y. Geng, J. W. Gray, H. L. Moses, and L. Yang. 2010. "Gr-1+CD11b+ Myeloid Cells Tip the Balance of Immune Protection to Tumor Promotion in the Premetastatic Lung." *Cancer Research* 70 (15): 6139–49. https://doi.org/10.1158/0008-5472.CAN-10-0706.
Yáñez-Mó, María, Maria Dolores Gutiérrez-López, and Carlos Cabañas. 2011. "Functional Interplay between Tetraspanins and Proteases." *Cellular and Molecular Life Sciences* 68 (20): 3323–35. https://doi.org/10.1007/s00018-011-0746-y.
Yang, Dongbin, Weihong Zhang, Huanyun Zhang, Fengqiu Zhang, Lanmei Chen, Lixia Ma, Leon M. Larcher, et al. 2020. "Progress, Opportunity, and Perspective on Exosome Isolation - Efforts for Efficient Exosome-Based Theranostics." *Theranostics* 10 (8): 3684–3707. https://doi.org/10.7150/thno.41580.
Yang, Jian, Wei Liu, Xin'an Lu, Yan Fu, Lin Li, and Yongzhang Luo. 2015. "High Expression of Small GTPase Rab3D Promotes Cancer Progression and Metastasis." *Oncotarget* 6 (13): 11125–38. https://www.ncbi.nlm.nih.gov/pmc/articles/PMC4484444/.
Yang, Yi, Chia-Wei Li, Li-Chuan Chan, Yongkun Wei, Jung-Mao Hsu, Weiya Xia, Jong-Ho Cha, et al. 2018. "Exosomal PD-L1 Harbors Active Defense Function to Suppress T Cell Killing of Breast Cancer Cells and Promote Tumor Growth." *Cell Research* 28 (8): 862–64. https://doi.org/10.1038/s41422-018-0060-4.
Yao, Yuanfa, Xinyi Wang, Hanbing Li, Jiannan Fan, Xiaohan Qian, Hong Li, and Yingke Xu. 2020. "Phospholipase D as a Key Modulator of Cancer Progression." *Biological Reviews* 95 (4): 911–35. https://doi.org/10.1111/brv.12592.
Yap, Timothy A, Michelle D Garrett, Mike I Walton, Florence Raynaud, Johann S de Bono, and Paul Workman. 2008. "Targeting the PI3K–AKT–MTOR Pathway: Progress, Pitfalls, and Promises." *Current Opinion in Pharmacology*, Cancer/Immunomodulation, 8 (4): 393–412. https://doi.org/10.1016/j.coph.2008.08.004.
Yin, JuanJuan, Claire Pollock, Kirsten Tracy, Monika Chock, Philip Martin, Michael Oberst, and Kathleen Kelly. 2007. "Activation of the RalGEF/Ral Pathway Promotes Prostate Cancer Metastasis to Bone." *Molecular and Cellular Biology* 27 (21): 7538–50. https://doi.org/10.1128/MCB.00955-07.
Yoshizaki, Tomokazu, Satoru Kondo, Naohiro Wakisaka, Shigeyuki Murono, Kazuhira Endo, Hisashi Sugimoto, Sayaka Nakanishi, Akira Tsuji, and Makoto Ito. 2013. "Pathogenic

Role of Epstein–Barr Virus Latent Membrane Protein-1 in the Development of Nasopharyngeal Carcinoma." *Cancer Letters* 337 (1): 1–7. https://doi.org/10.1016/j.canlet.2013.05.018.
Yu, Yi, and Larry A. Feig. 2002. "Involvement of R-Ras and Ral GTPases in Estrogen-Independent Proliferation of Breast Cancer Cells." *Oncogene* 21 (49): 7557–68. https://doi.org/10.1038/sj.onc.1205961.
Yue, Shijing, Wei Mu, Ulrike Erb, and Margot Zöller. 2014. "The Tetraspanins CD151 and Tspan8 Are Essential Exosome Components for the Crosstalk between Cancer Initiating Cells and Their Surrounding." *Oncotarget* 6 (4): 2366–84. https://doi.org/10.18632/oncotarget.2958.
———. 2015. "The Tetraspanins CD151 and Tspan8 Are Essential Exosome Components for the Crosstalk between Cancer Initiating Cells and Their Surrounding." *Oncotarget* 6 (4): 2366–84. https://doi.org/10.18632/oncotarget.2958.
Zago, Giulia, Marco Biondini, Jacques Camonis, and Maria Carla Parrini. 2019. "A Family Affair: A Ral-Exocyst-Centered Network Links Ras, Rac, Rho Signaling to Control Cell Migration." *Small GTPases* 10 (5): 323–30. https://doi.org/10.1080/21541248.2017.1310649.
Zarovni, Natasa, Antonietta Corrado, Paolo Guazzi, Davide Zocco, Elisa Lari, Giorgia Radano, Jekatarina Muhhina, Costanza Fondelli, Julia Gavrilova, and Antonio Chiesi. 2015. "Integrated Isolation and Quantitative Analysis of Exosome Shuttled Proteins and Nucleic Acids Using Immunocapture Approaches." *Methods* 87 (October): 46–58. https://doi.org/10.1016/j.ymeth.2015.05.028.
Zeng, Zhicheng. 2018. "Cancer-Derived Exosomal MiR-25-3p Promotes Pre-Metastatic Niche Formation by Inducing Vascular Permeability and Angiogenesis," 14.
Zhang, Haiying, Daniela Freitas, Han Sang Kim, Kristina Fabijanic, Zhong Li, Haiyan Chen, Milica Tesic Mark, et al. 2018. "Identification of Distinct Nanoparticles and Subsets of Extracellular Vesicles by Asymmetric Flow Field-Flow Fractionation." *Nature Cell Biology* 20 (3): 332–43. https://doi.org/10.1038/s41556-018-0040-4.
Zhang, Shipin, Shang Jiunn Chuah, Ruenn Chai Lai, James Hoi Po Hui, Sai Kiang Lim, and Wei Seong Toh. 2018. "MSC Exosomes Mediate Cartilage Repair by Enhancing Proliferation, Attenuating Apoptosis and Modulating Immune Reactivity." *Biomaterials* 156 (February): 16–27. https://doi.org/10.1016/j.biomaterials.2017.11.028.
Zhao, Hongyun, Lifeng Yang, Joelle Baddour, Abhinav Achreja, Vincent Bernard, Tyler Moss, Juan C Marini, et al. 2016. "Tumor Microenvironment Derived Exosomes Pleiotropically Modulate Cancer Cell Metabolism." *ELife* 5. https://doi.org/10.7554/eLife.10250.
Zhou, Biting, Kailun Xu, Xi Zheng, Ting Chen, Jian Wang, Yongmao Song, Yingkuan Shao, and Shu Zheng. 2020. "Application of Exosomes as Liquid Biopsy in Clinical Diagnosis." *Signal Transduction and Targeted Therapy* 5 (1): 1–14. https://doi.org/10.1038/s41392-020-00258-9.
Zhou, Weiying, Miranda Y. Fong, Yongfen Min, George Somlo, Liang Liu, Melanie R. Palomares, Yang Yu, et al. 2014. "Cancer-Secreted MiR-105 Destroys Vascular Endothelial Barriers to Promote Metastasis." *Cancer Cell* 25 (4): 501–15. https://doi.org/10.1016/j.ccr.2014.03.007.
Zhou, Zejun, Lumin Zhang, Miao Ding, Zhenwu Luo, Shao Yuan, Meena B. Bansal, Gary Gilkeson, Ren Lang, and Wei Jiang. 2017. "Estrogen Decreases Tight Junction Protein

ZO-1 Expression in Human Primary Gut Tissues." *Clinical Immunology (Orlando, Fla.)* 183 (October): 174–80. https://doi.org/10.1016/j.clim.2017.08.019.
Zhu, Hong, Sara Guariglia, Raymond Y. L. Yu, Wenjing Li, Deborah Brancho, Hector Peinado, David Lyden, James Salzer, Craig Bennett, and Chi-Wing Chow. 2013. "Mutation of SIMPLE in Charcot-Marie-Tooth 1C Alters Production of Exosomes." *Molecular Biology of the Cell* 24 (11): 1619–37, S1-3. https://doi.org/10.1091/mbc.E12-07-0544.
Zipfel, P A, D C Brady, D F Kashatus, B D Ancrile, D S Tyler, and C M Counter. 2010. "Ral Activation Promotes Melanomagenesis." *Oncogene* 29 (34): 4859–64. https://doi.org/10.1038/onc.2010.224.
Zitvogel, Laurence, Armelle Regnault, Anne Lozier, Joseph Wolfers, Caroline Flament, Danielle Tenza, Paola Ricciardi-Castagnoli, Graça Raposo, and Sebastian Amigorena. 1998. "Eradication of Established Murine Tumors Using a Novel Cell-Free Vaccine: Dendritic Cell Derived Exosomes." *Nature Medicine* 4 (5): 594–600. https://doi.org/10.1038/nm0598-594.
Zomer, Anoek, Carrie Maynard, Frederik Johannes Verweij, Alwin Kamermans, Ronny Schäfer, Evelyne Beerling, Raymond Michel Schiffelers, et al. 2015. "In Vivo Imaging Reveals Extracellular Vesicle-Mediated Phenocopying of Metastatic Behavior." *Cell* 161 (5): 1046–57. https://doi.org/10.1016/j.cell.2015.04.042.

Étude du rôle des GTPases Ral dans la sécrétion des exosomes et la progression métastatique

De plus en plus de preuves suggèrent que les VE dérivées des tumeurs participent aux étapes cruciales de la propagation métastatique d'une tumeur primaire, principalement en exerçant des fonctions pro-tumorales et en modifiant les phénotypes des cellules stromales au profit de la croissance tumorale et des métastases (Becker et al. 2016). Ils font la navette vers des organes distants et favorisent les métastases en conditionnant la niche pré-métastatique (Peinado et al. 2017). Les niveaux de sécrétion des EVs tumoraux sont corrélés avec l'agressivité tumorale, cependant, le lien entre les mécanismes de sécrétion des EVs et leur capacité à former des niches pré-métastatiques reste obscur. Au cours de mon doctorat, l'objectif de mon projet était de comprendre les mécanismes par lesquels deux GTPases (RalA/B) récemment identifiées dans notre laboratoire contrôlent la sécrétion des exosomes et de déterminer comment cela affecte la progression du cancer du sein et les métastases. Ma principale découverte a d'abord démontré une dissection détaillée de l'impact des GTPases Ral sur les niveaux de sécrétion des VE. Nous avons montré que les GTPases de la famille Ral contrôlent, par l'intermédiaire de la phospholipase D1, l'homéostasie des corps multivésiculaires (MVBs) et règlent ainsi la biogenèse et la sécrétion des EVs. Nous avons également démontré que RalA et RalB favorisent les métastases pulmonaires dans un modèle de souris syngénique sans affecter le potentiel invasif du carcinome mammaire. Un autre résultat important est que les VE provenant de cellules dépourvues de RalA ou de RalB ont des capacités organotropiques limitées in vivo et, par conséquent, sont moins efficaces pour promouvoir les métastases pulmonaires. Enfin, nous avons identifié la protéine d'adhésion CD146/MCAM comme une cargaison EV clé contrôlée par RalA et RalB et démontré qu'elle transmet, en partie, la fonction pro-métastatique aux EVs en contrôlant le tropisme pulmonaire des EVs du cancer du sein. Dans l'ensemble, nous avons identifié les GTPases RalA/B comme une nouvelle machinerie moléculaire qui régule la formation et la sécrétion des VE pro-métastatiques et nous avons démêlé RalA/B et CD146 comme de nouvelles cibles thérapeutiques pour les métastases du cancer du sein - voir annexe 1 : Les GTPases Ral favorisent les métastases en contrôlant la biogenèse et la colonisation des organes des exosomes.

Au cours de mon doctorat, j'ai contribué à établir l'embryon de poisson zèbre comme un nouveau modèle animal pour suivre les TEV circulants in vivo (Hyenne et al. 2019). Les outils et les méthodes développés dans ces études ont également été utilisés dans une partie de mon projet principal également.

L'embryon de poisson zèbre comme modèle pour suivre les EVs circulants in vivo

In vivo, très peu de choses sont connues sur le comportement des EVs dans la circulation. L'une des principales limites dans ce domaine est la capacité de suivre ces petites particules in vivo. La visualisation microscopique des VE circulantes in vivo, qui dépend à la fois de la résolution subcellulaire et de la luminosité des VE marquées, est encore confrontée à des défis majeurs (Verweij, Hyenne, et al. 2019). En outre, les modèles appropriés sont cruciaux pour avoir un accès profond et non invasif aux organes internes afin d'identifier les cellules et les organes récepteurs d'EVs. Dans le modèle murin, différentes stratégies, basées sur la bioluminescence, les colorants lipophiles ou l'expression transgénique de marqueurs fluorescents des EVs ont été développées (Hyenne, Lefebvre, et Goetz 2017). Cependant, ces approches impliquent souvent une imagerie ex vivo et ne permettent pas de suivre précisément la dynamique des EVs dans les fluides corporels. Pour surmonter ces limitations, plusieurs groupes ont développé l'imagerie intravitale des VE chez la souris ; cependant, en raison de la complexité de ces procédures, l'imagerie à haut débit et ne sont souvent pas compatibles avec un échantillonnage élevé de VE faisant la navette dans les fluides corporels (van der Vos et al. 2016 ; Zomer et al. 2015 ; C. P. Lai et al. 2015). Par ailleurs, l'embryon de poisson zèbre est apparu comme un modèle animal unique pour étudier les VE circulantes physiologiques et pathologiques à une résolution spatio-temporelle sans précédent (Verweij, Hyenne, et al. 2019). Les embryons de poisson zèbre offrent plusieurs avantages pour une analyse non invasive in vivo, notamment une vascularisation (et une circulation sanguine) stéréotypée, un système immunitaire en maturation dans les 48h, un corps translucide et facilement accessible à tous les types de microscopie confocale et à haute vitesse. Globalement, le poisson zèbre présente un haut niveau d'homologie génétique et physiologique avec l'homme et plus particulièrement, il reproduit un environnement physiologique pertinent pour l'étude des EVs circulants (Verweij, Revenu, et al. 2019 ; Hyenne et al. 2019). La détection des EVs fluorescents, marqués soit par des colorants lipophiles, soit par l'expression transgénique de marqueurs

fluorescents au sein des cellules sécrétrices est favorisée par la transparence des embryons. Le modèle du poisson zèbre permet également de réaliser une analyse approfondie des VE circulants et de décrire leur comportement hémodynamique in vivo (Verweij, Revenu, et al. 2019 ; Hyenne et al. 2019). Comme stratégie alternative, les protéines des VE peuvent être fusionnées à des protéines fluorescentes et exprimées dans des cellules productrices de VE (Corso et al. 2019 ; Görgens 2016). Cela permet de visualiser des sous-populations uniques d'EVs et peut également être utilisé pour suivre les EVs de la cellule génétiquement modifiée (Verweij, Revenu, et al. 2019). En outre, MemBright est une sonde membranaire à base de cyanine récemment développée (Cy3, Cy5 ou Cy7) (Collot et al. 2019) avec des propriétés uniques qui fournissent une luminosité élevée et une spécificité aux VE marqués ainsi que la prévention de l'auto-agrégation fluorescente (Hyenne et al. 2019). MemBright peut également être utilisé pour co-injecter différents types de VE marqués avec différentes couleurs (Cy3, Cy5), ce qui nous permet de comparer différentes populations de VE (ou leur origine) et de suivre leur comportement, leur destin et leur fonction spécifiques. Dans notre projet, nous avons voulu suivre et évaluer la fonction des VEs tumorales circulantes in vivo en utilisant l'embryon de poisson zèbre et fournir une description à haute résolution de leur dissémination et de leur absorption. Tout d'abord, nous avons injecté dans des embryons de poisson-zèbre des VE marquées par des membranes à partir de cellules de mélanome de poisson (zmel) (Heilmann et al. 2015) et nous avons suivi les VE dans le flux sanguin. Nous avons ensuite caractérisé leur absorption par les cellules endothéliales et les monocytes en patrouille. Dans ces cellules, nous avons démontré que la majorité des EVs se concentrent dans les compartiments lysosomaux. Nous avons également réalisé un test fonctionnel sur différents embryons transgéniques montrant une activation et une production de TNF-a (Nguyen et al. 2015), qui correspondent à la transition M2-M1, souvent associée à la transformation de macrophages normaux (M2) en macrophages associés au cancer (M1) (Biswas et Mantovani 2010). Enfin, nous avons effectué une pré-injection de VE (appelée priming), suivie d'une injection de cellules tumorales pour démontrer l'induction de niches pré-métastatiques par les VE. Nous avons montré que les cellules tumorales envahissent plus efficacement le stroma du poisson et développent des micro-métastases plus importantes dans le cas de l'amorçage par les EVs (Hyenne et al. 2019) - voir annexe 2 : Etude du devenir des vésicules extracellulaires tumorales à haute résolution spatio-temporelle en utilisant l'embryon de poisson zèbre. Sur l'autre projet, nous nous sommes

principalement concentrés sur les détails expérimentaux du modèle de poisson zèbre et avons écrit un chapitre sur-voir annexe 3 : Live tracking of extracellular vesicles in larval zebrafish.